Supplementary information for

A Late Devonian coelacanth reconfigures actinistian phylogeny, disparity, and evolutionary dynamics

Alice M. Clement[1]*!, Richard Cloutier[1,2,3]*, Michael S. Y. Lee[1,4], Benedict King[5], Olivia Vanhaesebroucke[2], Corey J. A. Bradshaw[6], Hugo Dutel[7], Kate Trinajstic[8,9] & John A. Long[1]*

[1]College of Science and Engineering, Flinders University, Adelaide 5042, AUSTRALIA.

[2]Université du Québec à Rimouski, Rimouski, Rimouski G5L 3A1, CANADA.

[3]Excellence Center in Evolution of Life, Basin Studies and Applied Paleontology, Palaeontological Research and Education Centre, Mahasarakham University, Maha Sarakham 44150, THAILAND.

[4]Earth Sciences Section, South Australian Museum, North Terrace, Adelaide 5000, AUSTRALIA.

[5]Max Planck Institute for Evolutionary Anthropology, Deutscher Platz 6 04103 Leipzig, GERMANY.

[6]Global Ecology | *Partuyarta Ngadluku Wardli Kuu*, College of Science and Engineering, Flinders University, Adelaide 5001, AUSTRALIA.

[7]University of Bristol, School of Earth Sciences, Bristol, UNITED KINGDOM.

[8]School of Molecular and Life Sciences, Faculty of Science and Engineering, Curtin University, Perth 6845, AUSTRALIA.

[9]Earth and Planetary Sciences, Western Australian Museum, 49 Kew Street, Welshpool, 6106, AUSTRALIA.

SUPPLEMENTARY DATA:

Supplementary Methods

1. Morphological and stratigraphic data
   a. Taxonomic sampling, stratigraphic dates and sources of information
   b. Character descriptions for discrete, meristic and continuous characters
      i. Discrete characters
      ii. Meristic characters
      iii. Continuous characters
   c. Coding modifications from original matrices and new data
2. Disparity and geometric morphometrics
3. Correlation analyses
   a. Data collecting
4. Supplementary figures

Supplementary References

1. Morphological and stratigraphic data

1a. Taxonomic sampling, stratigraphic dates and sources of information

The list of 87 taxa included in our phylogenetic analyses provides stratigraphical bibliographic references from the primary literature, geological period, epoch and age, geographical locality, province and country as well as the first appearance dates in time bin ages (FAD) and the last appearance dates in time bin ages (LAD). All taxa are species, with the exception of *Heptanema paradoxum* where we used information from the holotype figured by Renesto & Stockar (2018)[1] as well as material identified as *Heptanema* sp. by Renesto & Stockar (2018, figs. 10-12)[1]. Recently, Brownstein & Bissell (2022)[2] divided *Diplurus newarki* into a second species names *D. enigmaticus*; in our analysis, our coding did not take into consideration this difference. Bold-faced taxa correspond to taxa for which original material has been observed by at least one of the co-authors. The numerical age of stages is taken from the limits provided in the most recent version (2022) of the International Chronostratigraphic Chart[3]. We calculated the numerical age of stage subdivisions (early, middle, and late) as three equal subdivisions of the stage duration.

Taxa	Age and locality	FAD	LAD
Onychodontida (5 outgroups)			
Onychodus jandemarrai[4]	Upper Devonian (early Frasnian)	382.7	379.2
	Gogo Fm, Western Australia, Australia		
Strunius rolandi[5-7]	Upper Devonian (earliest Frasnian)	382.7	379.2
	Upper Plattenkalk, Heiligenstock quarry, Bergisch-Gladbach, Nordrhein-Westfalen, Germany		
Strunius walteri[5-7]	Upper Devonian (earliest Frasnian)	382.7	379.2
	Upper Plattenkalk, Heiligenstock quarry, Bergisch-Gladbach, Nordrhein-Westfalen, Germany		
Qingmenodus yui[8]	Lower Devonian (late Pragian)	408.67	407.6
	Posongchong Fm, Yunnan, China		
Grossius aragonensis[9]	Middle Devonian (middle Eifelian)	391.43	389.57
	Moyuela Fm, Spain		
Actinistia (82 ingroups)			
Alcoveria brevis[10-12]	Middle Triassic (Ladinian)	242	237
	Tarragona Province, Spain		
Allenypterus montanus[13,14]	Lower Carboniferous (Serpukhovian)	330.9	323.2
	Heath Fm, Bear Gulch Limestone Mbr, Montana, USA		
Atacamaia solitaria[15]	Lower Jurassic (lower-to-middle Sinemurian)	199.3	193.63
	Vaquillas Altas, Atacama Desert, Chile		
Axelia robusta[16,17]	Lower Triassic [Olenekian (Smithian)]	251.2	249.2
	Sticky Keep Fm (Lusitaniadalen Mbr), West Spitsbergen		
Axelrodichthys araripensis[18,19]	Lower Cretaceous (late Aptian)	117	113
	Santana Gr, Romualdo Fm, Chapada do Araripe, Ceara, Brazil		
Axelrodichthys lavocati[20-22]	Upper Cretaceous (early-middle Cenomanian)	100.5	96.1
	Kem-Kem Beds, Morocco		
Axelrodichthys maiseyi[23]	Lower Cretaceous (middle-late Albian)	108.83	100.5
	Codó Fm, Grajaú Basin, Northeastern Brazil		
Axelrodichthys megadromos[24]	Upper Cretaceous (lower Campanian)	83.6	79.77
	Valdonian-Fuvelian local stages, Bouches-du-Rhône, France		
Belemnocerca prolata[25]	Lower Triassic (early Olenekian)	251.2	249.87
	Sulphur Mountain Fm, Wapiti Lake, British Columbia, Canada		
Caridosuctor populosum[13,14]	Lower Carboniferous (Serpukhovian)	330.9	323.2
	Heath Fm, Bear Gulch Limestone Mbr, Montana, USA		
Changxingia aspratilis[26,27]	Upper Permian (Changhsingian)	254.14	252.28
	Changhsing Fm, Meishan Mbr, Zhejiang, China		
Changxingia weii[27,28]	Upper Permian (Changhsingian)	254.14	252.28

Taxon	Age / Formation / Locality	Max	Min
	Changhsing Fm, Meishan Mbr, Zhejiang, China		
Chaohuichthys majiashanensis[29]	Lower Triassic (Olenekian)	251.2	247.2
	Helongshan Fm, Anhui Province, Chaohu, China		
Chinlea sorenseni[12,14,30]	Upper Triassic (Carnian)	237	227
	Chinle Fm, Little Valley, Utah, USA; Colorado, New Mexico and Texas		
Coccoderma suevicum[31-33]	Upper Jurassic (late Kimmeridgian-early Tithonian)	153.83	149.73
	Solnhofen and Nusplingen (W of Solnhofen) Baden-Württemberg, Bavaria, Germany		
Coelacanthus granulatus[12,34]	Upper Permian (Guadaloupian)	272.95	259.1
	Marl Slate, Durham and Northumberland, England, UK; Kuperschiefer, Germany		
Diplocercides heiligenstockiensis[6,7]	Upper Devonian (earliest Frasnian)	382.7	379.2
	Upper Plattenkalk, Heiligenstock quarry, Bergisch-Gladbach, Nordrhein-Westfalen, Germany		
Diplocercides kayseri[6]	Upper Devonian (late Frasnian)	375.7	372.2
	Bad Wildungen, Germany		
Diplurus newarki[12,35,36]	Lower Jurassic (Sinemurian)	199.3	190.8
	New Jersey, USA		
Dobrogeria aegyssensis[37]	Lower Triassic (early Spathian; =late Olenekian)	248.53	247.2
	Tulcea Veche Limestone, North Dobrogea, Romania		
Eoactinistia foreyi[38]	Lower Devonian (mid-Late Pragian)	409.73	407.6
	Fairy Fm, Buchan, Victoria, Australia		
Euporosteus eifeliensis[6,39]	Middle Devonian (late Givetian)	384.37	382.7
	Gerolstein, Germany		
Euporosteus yunnanensis[40]	Lower Devonian (late Pragian)	408.67	407.6
	Posongchong Fm, Zhaotong, Yunnan Province, China		
Foreyia maxkuhni[41,42]	Middle Triassic (early Ladinian)	242	240.33
	Prosanto Fm, Switzerland		
Garnbergia ommata[42,43]	Middle Triassic (late Anisian)	243.73	242
	Baden-Württemberg, Germany		
Gavinia syntrips[44]	Middle Devonian (uppermost Givetian)	384.37	382.7
	Avon River Gr, Mount Howitt, Victoria, Australia		
Guizhoucoelacanthus guanlingensis[45]	Mid-Upper Triassic (Ladinian-Carnian)	242	227
	Falang Fm, Wayao and Zhuganpo Mbrs, Guizhou and Yunnan provinces, China		
Hadronector donbairdi[13,14]	Lower Carboniferous (Serpukhovian)	330.9	323.2
	Heath Fm, Bear Gulch Limestone Mbr, Montana, USA		
Hainbergia granulata[42,46]	Middle Triassic (late Anisian)	243.73	242
	Upper Muschelkalk, Gottingem, Germany		
Heptanema paradoxum[1]	Middle Triassic (Ladinian)	242	239.51
	Meride and Besano Fms, Monte San Giorgio, Canton Ticino, Switzerland		
Holophagus gulo[12]	Lower Jurassic (Sinemurian)	199.3	190.8
	Dorset, England, UK		
Holopterygius nudus[47,48]	Upper Devonian (early Frasnian)	382.7	379.2
	Upper Plattenkalk, Heiligenstock quarry, Bergisch-Gladbach, Nordrhein-Westfalen, Germany		
Indocoelacanthus robustus[49,50]	Lower Jurassic (Toarcian)	182.7	174.1
	Kota Fm, Kota, India		
Latimeria chalumnae[51]	extant	13	0
	Comoros Islands, Mozambique Channel, South Africa		
Latimeria menadoensis[51]	extant	13	0
	Manado, Sulawesi		
Laugia groenlandica[12,52,53]	Lower Triassic (Griesbachian)	251.55	251.2
	Wordie Creek Gr (Kap Stosch Fm), Kap Stosch, East Greenland		
Libys polypterus[12,31,33]	Upper Jurassic (early Tithonian)	152.1	149.73
	Solnhofen, Bavaria, Germany		
Lochmocercus aciculodontus[13,14]	Lower Carboniferous (Serpukhovian)	330.9	323.2
	Heath Fm, Bear Gulch Limestone Mbr, Montana, USA		
Lualabaea lerichei[12,14]	Upper Jurassic (?Kimmeridgian)	157.3	152.1
	Lualabaea Series, Maosaosa, Republic of Zaire		
Luopingcoelacanthus eurylacrimalis[54]	Middle Triassic (late Pelsonian, middle–late Anisian)	245.47	242
	Nicoraella kockeli Zone, Guanling Fm, Mbr II, China		
Macropoma lewesiensis[12]	Upper Cretaceous (Cenomanian)	100.5	93.9
	Sussex, England, UK		

Taxon	Age / Locality		
Macropoma precursor[12]	Upper Cretaceous (Cenomanian) Kent, England, UK	100.5	93.9
Macropoma willemoesii[31,33]	Upper Jurassic (early Tithonian) Solnhofen, Bavaria, Germany	152.1	149.73
Macropomoides orientalis[12]	Upper Cretaceous (middle Cenomanian) Hajula, Lebanon	98.3	96.1
Mawsonia brasiliensis[19,55]	Lower Cretaceous (late Aptian) Santana Gr, Romualdo Fm, Chapada do Araripe, Ceara, Brazil	117	113
Mawsonia gigas[14,18]	Upper Jurassic-Lower Cretaceous (Kimmeridgian-Cenomanian) Marfim and Tacuarembo Fms, Brazil, Uruguay, Democratic Republic of Congo	157.3	93.9
Mawsonia soba[14,56]	Lower Cretaceous (Barriasian-Barremian) Babouri Figuil Basin, Northern Cameroon	145	125
Mawsonia tegamensis[57,58]	Lower Cretaceous (limit Aptian-Albian) Tégama Series, Elrhaz Fm, Gadoufaoua, Niger	117	108.83
Megalocoelacanthus dobiei[59,60]	Upper Cretaceous (late Santonian - early Maastrichian) Eutaw and Blufftown Fms, New Jersey, Alabama, Mississippi, Kansas and Georgia, USA	84.5	70.07
Miguashaia bureaui[61,62]	Upper Devonian (middle Frasnian) Escuminac Fm, Quebec, Canada	379.2	375.7
Miguashaia grossi[63]	Middle Devonian (late Givetian) Gauja and Lode Fms, Latvia	384.37	382.7
Moenkopia wellesi[64]	Middle Triassic (late Anisian) Moenkopi Fm, Holbrook Mbr, Arizona, USA	243.73	242
Ngamugawi wirngarri[65]	Upper Devonian (early Frasnian) Gogo Fm, Western Australia, Australia	382.7	379.2
Parnaibaia maranhaoensis[66,67]	Late Jurassic (Oxfordian to Kimmeridgian) Pastos Bons Fm, Maranhão, Brazil	163.5	152.1
Piveteauia madagascariensis[12,68,69]	Lower Triassic (Induan) Middle Sakamena Gr, Ambilote, northwestern Madagascar	251.90	251.2
Polyosteorhynchus simplex[13,14]	Lower Carboniferous (Serpukhovian) Heath Fm, Bear Gulch Limestone Mbr, Montana, USA	330.9	323.2
Rebellatrix divaricerca[70]	Lower Triassic (late Induan-early Olenekian) Sulphur Mountain Fm, Vega-Phroso Mbr, British Columbia, Canada	251.43	249.87
Reidus hilli[71]	Lower Cretaceous (Albian) Duck Creek Fm, Texas, USA	113	100.5
Rhabdoderma elegans[12,72,73]	Upper Carboniferous (Namurian A - Westphalian D) wide distribution	330.9	303.7
Rhabdoderma exiguum[74]	Upper Carboniferous (upper part of the Moscovian) Francis Creek Shale, Mazon Creek, Illinois, USA	311	306
Rhabdoderma (?) newelli[75,76]	Upper Carboniferous (Stephanian B; Kasimovian) Stanton Fm, Rock Lake Shale Mbr, Garnett, Kansas, USA	307	303.7
Sassenia groenlandica[12,52,53]	Lower Triassic (Griesbachian) Wordie Creek Gr (Kap Stosch Fm), Kap Stosch, East Greenland	251.55	251.2
Sassenia tuberculata[16,77]	Lower Triassic [Olenekian (Smithian)] Sticky Keep Fm, Lusitaniadalen Mbr, West Spitsbergen	251.2	249.2
Serenichthys kowiensis[78]	Upper Devonian (Late Famennian) Witpoort Fm, South Africa	363.33	358.9
Shoshonia arctopteryx[79]	Mid–Late Devonian (Givetian-Frasnian) Jefferson Fm, Wyoming, USA	387.7	372.2
Sinocoelacanthus fengshanensis[80-82]	Lower Triassic (Spathian) Luolou Gr, Kwangsi Province, China	249.2	246.83
Spermatodus pustulosus[12,83]	Lower Permian (Artinskian; ?Kazanian) Wichita Gr, ?Admiral Fm, Texas, USA	290.1	283.5
Styloichthys changae[79,84,85]	Lower Devonian (late Lochkovian) Xitun Fm, Qujing, East Yunnan, China	413.6	410.8
Swenzia latimerae[12,86]	Lower Upper Jurassic (late Oxfordian) Charnay Commune, Burgundy, France	159.37	157.3
Ticinepomis peyeri[87,88]	Middle Triassic (Ladinian) Grenzbitumen Horizon, Monte San Giorgio, Kanton Tessin, Switzerland	242	237
Trachymetopon liassicum[88,89]	Lower Jurassic (Lower Toarcian) Ohmden, Baden-Wuttemberg, Germany	182.7	179.83

Undina penicillata[31,33]	Upper Jurassic (late Kimmeridgian-early Tithonian) 153.83 149.73		
	Solnhofen, Wattendorf and Nusplingen (W of Solnhofen), Bavaria and Baden-Württemberg, Germany		
Undina cirinensis[90]	Upper Jurassic (late Kimmeridgian)	153.83	152.1
	Cerin, Ain, France		
Whitea durabilis[91]	Lower Triassic (early Olenekian)	251.2	249.87
	Sulphur Mountain Fm, Wapiti Lake, British Columbia, Canada		
Whitea lepta[91]	Lower Triassic (early Olenekian)	251.2	249.87
	Sulphur Mountain Fm, Wapiti Lake, British Columbia, Canada		
Whiteia nielseni[12,52,53]	Lower Triassic (Griesbachian)	251.55	251.2
	Wordie Creek Gr, Kap Stosch Fm, Kap Stosch, East Greenland		
Whiteia oishoii[92]	Upper Triassic (earliest Carnian to late Norian)	237	208.5
	Noe Bihati, West Timor, Indonesia		
Whiteia uyenoteruya[12,68,69,93]	Lower Triassic (Induan)	251.90	251.2
	Middle Sakamena Gr, Ambilote, northwestern Madagascar		
Whiteia woodwardi[12,68,69,93]	Lower Triassic (Induan)	251.90	251.2
	Middle Sakamena Gr, Ambilote, northwestern Madagascar		
Wimania sinuosa[16,77]	Lower Triassic [Olenekian (Smithian)]	251.2	249.2
	Sticky Keep Fm, Lusitaniadalen Mb, West Spitsbergen		
Youngichthys xinghuainsis[26,27]	Upper Permian (Changhsingian)	254.14	252.28
	Changhsing Fm, Meishan Mbr, Zhejiang, China		
Yunnancoelacanthus acrotuberculatus[54]	Middle Triassic (late Pelsonian, middle–late Anisian)	245.47	242
	Guanling Fm, Mbr II, Yunnan, China		

1b. Character descriptions for discrete, meristic and continuous characters

To determine the phylogenetic position of *Ngamugawi* among coelacanths, we created a new morphological matrix including 268 discrete characters coded for 87 species. In 1998, Peter Forey[12] published "*History of the Coelacanth Fishes*", a landmark in coelacanth morphology and phylogeny. Subsequently, 22 phylogenetic analyses addressed partial or complete phylogeny of this clade, 20 of which were strictly built on minor modifications of Forey's matrix (30 genera, 108 characters)[12]. Over a period of 25 years, 18 genera and 2 new characters have been added without major revision of the original coding. We first compiled a primary list of characters and character-states from the literature keeping track of the original authors for each character. Characters were split in order to reduce ambiguity in the definition and the coding; for example, when a character included character-states with absence and two states pertaining an attribute of the character itself. Original characters and character-states were rephrased when needed to clarify their definition. Characteristics provided in the diagnosis of taxa were also included; we used most diagnoses revised by Forey (1998)[12]. Many characteristics used in morphological comparisons provided by previous authors were rephrased in terms of phylogenetic characters. We made a special effort to avoid the problematic types of character construction identified by Simões et al. (2017)[94]. The clarity of the definition and the respect of most of Simões et al.'s (2017)[94] categories were revised and discussed by six of us (A.M. Clement, R. Cloutier, H. Dutel, M.Y.S. Lee, J.A. Long, and K. Trinajstic). Characters were subsequently numbered and listed in an anatomical order. 83 new characters have been used.

The coding by species was originally divided among five of us (R. Cloutier, J.A. Long, A.M. Clement, H. Dutel and B. King). Coding was subsequently double-checked by three of us (R. Cloutier, A.M. Clement and H. Dutel). Coding was subsequently validated by character in order to see that the coding was congruent among taxa for a given character (R. Cloutier). Mapping of character-states per character on the tree topology (using Mesquite) was used to identify aberrant coding. Finally, differences of coding between the matrix provided by Toriño et al. (2021)[14] and Forey (1998)[12] and our own matrix were discussed and justified.

The full character-by-taxon matrices for discrete, meristic and continuous characters are available in the Github repository, as excel files (CoelacanthEvolution/data) and as plain text BEAST and TNT executables

(CoelacanthEvolution/scripts/phylogenetics). The discrete matrix is also available on morphobank.org (project number 3471).

1b.i Discrete characters

The list of discrete characters and character-states provides the reference to character numbers used in previous publications: Ca, Cloutier (1991a)[95], Cb, Cloutier (1991b)[96], Fa, Forey (1991)[97], Fb, Forey (1998)[12], C, Clément (2005)[86], F&C, Friedman & Coates (2006)[47], FR, Friedman (2007)[98], Y, Yabumoto (2008)[66], G, Geng et al. (2009)[45], L&Z, Lu & Zhu (2009)[8], W, Wendruff (2011)[91], W&W, Wendruff & Wilson (2012)[70], Da, Dutel et al. (2012)[60], Z, Zhu et al. (2012)[40], GR, Graf (2012)[71], WE, Wen et al. (2013)[54], CAa, Cavin et al. (2013)[87], C&G, Cavin & Grădinaru (2014)[37], A&S, Arratia & Schultze (2015)[15], G&C, Gess & Coates (2015)[78], Db, Dutel et al. (2015)[99], CAb, Cavin et al. (2017)[41], R&S, Renesto & Stockar (2018)[1], CAc, Cavin et al. (2019)[100], CAd, Cavin et al. (2020)[101], T, Toriño et al. (2021)[14]. Characters from previous analyses are either unchanged (refered number), rephrased, modified, or divided (identified as "in part"). Polarity changes are also identified.

Multistate characters were treated as unordered unless they formed clear morphoclines, in which case they were ordered (characters 7, 10, 20, 34, 42, 63, 73, 78, 84, 98, 100, 107, 130, 139, 162, 198, 199 and 201). All characters are weighted equally.

We used MorphoBank[102] version 3.0 to code and document our discrete matrix.

1. **Snout bones** [Fb2, C2, F&C2, Y2, G2, W2, W&W2, Da2, Z2, GR2, WE2, CAa2, C&G2, A&S2, G&C2, Db2, CAb2 modified, R&S2, CAc2 modified, CAd2 modified, T2 modified]: separate from one another (0), consolidated edentulous (1), consolidated toothed (2). Character 1 was originally defined by Forey (1998, char. 2)[12]. Subsequently, Cavin et al. (2017, char. 2)[41] considered an additional character-state for the consolidated condition of snout bones. The three character-states form a morphocline.

2. **Ethmoid commissure, trajectory of** [Ca6 in part, Cb6 in part]: middle portion through median rostral (0), sutural course (1), through bone center of premaxilla (2); The three character-states form a morphocline.

3. **Rostral tubuli** [FR136]: present (0), absent (1)

4. **Rostral organ pores** [Ca, FR145]: absent (0), present (1). Character 4 is linked to characters 5, 6 and 7.

5. **Anterior opening of rostral organ** [Cb55, Fa34, Fb6, C6, F&C6, Y6, G6, W6, W&W6, Da6, Z6, GR6, WE6, CAa6, C&G6, A&S6, G&C6, Db6, CAb6, R&S6, T6]: within premaxilla (0), within separate rostral ossicles (1). Character 5 is linked to character 4.

6. **Posterior openings of rostral organ** [Fa35]: widely separated close to anterior and posterior margins of preorbital (0), separated only by a narrow bridge of bone (1), confluent (2). Forey (1991, char. 35)[97] defined a character to consider the condition in which the posterior openings of the rostral organ were confluent. We subdivided the original plesiomorphic condition into two conditions reflecting the relative distance separating the two pores on the preorbital. Forey (1980)[103] mentioned that this character was linked with the presence of the preorbital (character 57); when the preorbital is absent it is not possible to code for the condition of the posterior openings of the rostral organ. The three character-states form a morphocline. Character 6 is linked to characters 4 and 57.

7. **Posterior openings of rostral organ** [new]: anterior and posterior pores aligned horizontally (0), posterior pore offset posterodorsally to anterior pore (1). Character 7 is linked to characters 4, 6 and 57.

8. **Premaxillae** [Ca4, Cb4, Fb4, C4, F&C4, Y4, G4, W4, W&W4, Da4, Z4, GR4, WE4, CAa4, C&G4, A&S4, G&C4, Db4, CAb4, R&S4, CAc4, CAd4, T4]: fragmented (0), paired (1), fused (2). The character-states of Char. 8 have been reorganized to obtain a morphocline. The condition observed in the out-group is paired premaxillae. The fragmented condition corresponds to a series of small elements located at the position of the premaxillae. The fused condition of Character 8 is partially linked with Character 1.

9. **Dorsal lamina of premaxillae** [Fb5, C5, F&C5, Y5, G5, W5, W&W5, Da5, Z5, GR5, WE5, CAa5, C&G5, A&S5, G&C5, Db5, CAb5, R&S5, T5]: present (0), absent (1). Forey (1998, char. 5)[12] coded for the presence or absence of the dorsal laminae of the premaxillae. It seems that some taxa were originally coded as "?" by Forey (1998)[12] when the dorsal lamina was reduced (e.g., *Allenypterus*, *Lochmocercus*). The extent of the dorsal laminae is taken into consideration in our character 10.

10. **Dorsal lamina of premaxilla, completeness of** [Fa10 in part]: complete (0), invaginated (1), reduced (2). The three character-states form a morphocline. Character 10 is linked with character 9.

11. **Dorsal lamina of premaxilla, perforation of** [Ca6, Cb6]: perforated by ethmoid commissure (0), not perforated by ethmoid commissure (1). Character 11 is linked to character 9.

12. **Premaxilla ventral margin, shape of** [L&Z19 modified]: arched (0), not arched (1). Lu & Zhu (2009, char. 19)[8] used the presence of anteriorly arched premaxilla (their "premaxillary") in order to address interrelationships among onychodontiforms and out-groups including *Diplocercides* and *Styloichthys*. *Diplocercides*, *Styloichthys* and *Psarolepis* were coded as having anteriorly arched premaxillae, whereas *Onychodus*, *Strunius* and Bukkanodus lack anteriorly arched premaxillae. However, the condition of the premaxillae is unknown in *Diplocercides kayseri* and *D. heiligenstockiensis*. In *Styloichthys* the premaxillae are unknown, but the zone of articulation of the premaxillae are preserved.

13. **Median rostral, number of** [Fb3, C3, F&C3, Y3, G3, W3, W&W3, Da3, Z3, GR3, WE3, CAa3, C&G3, A&S3, G&C3, Db3, Cab3, R&S3, CAc3, CAd3, T3]: single median rostral or internasal (0), multiple median rostrals or internasals (1)

14. **Median rostral** [FR143, L&Z3]: without teeth (0), with teeth (1). Lu & Zhu (2009, char. 3)[8] coded for the presence of a tooth-bearing median rostral to determine the relationships among onychodontiforms and potential outgroups including *Diplocercides*. The condition of *Diplocercides* was coded as unknown, and solely *Psarolepis* was coded as having this condition.

15. **Parietal shield, profile of** [CAc52, CAd52]: convex (0), flat (1), concave (2). Fragoso et al. (2018, p. 12)[104] noticed a difference of profile for the parietal shield (their "frontoparietal shield") in terms of its curvature among species of *Axelrodichthys*. Cavin et al. (2020, char. 52)[101] define a character as the dorsal outline of the ethmoid portion in lateral view. Two character-states were used by Cavin et al. (2020, char. 52)[101]: straight or convex (0) and concave (1). We divide the conditions into three character-states that form a morphocline.

16. **Preparietal, size of** [Ca10, Cb10, Fa12 in part, Fb2 rephrased, C2 rephrased, F&C2 rephrased, Y2 rephrased, G2 rephrased, W2 rephrased, W&W2 rephrased, Da2 rephrased, Z2 rephrased, GR2 rephrased, WE2 rephrased, CAa2 rephrased, C&G2 rephrased, A&S2 rephrased, G&C2 rephrased, Db2 rephrased, CAb2 rephrased, R&S2 rephrased, CAc2 rephrased, CAd2 rephrased, T2 rephrased]: parietal longer than posterior preparietal (0), parietal equal in length to posterior preparietal (1), parietal shorter than posterior preparietal (2). Forey (1998, char. 7)[12] coded for the presence of one pair (0) or two pairs (1) of parietals; however, in his matrix (and that of subsequent analyses by most authors they used the coding of one pair (1) or two pairs (2) omitting a coding of "0". In addition, Forey (1998, char.

8)[12] coded for the relative size of the anterior and posterior parietals. Cloutier (1991a, char. 10)[95] named the pair(s) of medial bones anterior to the parietals as the preparietals. Herein, we define the character-states in terms of the length of the posterior preparietals and parietals rather than the size. The three character-states form a morphocline relative to the size proportion between the parietal and preparietal. Morphometric character 9 provides the ratio of the median length of the posteriormost preparietal divided by the median parietal length; a ratio close to a value of one is considered as a condition where the parietal is equal in length to the posteriormost preparietal. In our analysis, the number of preparietals per row is taken into account in our meristic matrix.

17. **Supraorbital canal, course of** [FR31]: straight (0), lyre shaped (1). Friedman (2007, char. 31)[98] mentioned that the trajectory of the supraorbital canals resembles a lyre in dorsal view in *Styloichthys*, *Euporosteus*, *Latimeria* and numerous coelacanths and sarcopterygians. It is considered to be a derived condition shared by *Styloichthys*, Dipnomorpha and Tetrapodomorpha (Friedman, 2007)[98]. The lyre-shape is owing to a medial curvature followed by a lateral trajectory of the supraorbital canal at the most anterior level of the snout.

18. **Supraorbital sensory canals, trajectory of** [Fb19, C19, F&C19, Y19, G19, W19, W&W19, Da19, Z19, GR19, WE19, CAa19, C&G19, A&S19, G&C19, Db19, CAb19, R&S19, CAc19, CAd19, T19]: passing through ossification centers (0), following sutural course (1)

19. **Supraorbital sensory canals opening through bones, condition of** [Ca3 in part, Ca9 in part, Cb3, Fb23, C23, F&C23, Y23, G23, W23, W&W23, Da23 modified, Z23, GR23, WE23, CAa23, C&G23 modified, A&S23 modified, G&C23, Db23, CAb23 modified, R&S23 modified, CAc23, CAd23, T23 modified]: single large pores (0), bifurcating pores (1), many tiny pores (2), large and continuous groove crossed by pillars (3), large and continuous groove without pillars (4). Forey (1998, char. 23)[12] used a character to describe the condition of the pores of the supraorbital sensory canal. Three conditions were originally described: canals opening through bones as single large pores (0), bifurcating pores (1), and many tiny pores (2). These conditions refer to the relation between the main canals and the canaliculi linking the pores at the surface of the bone and the main canal. In a few species, a few pores are present at the surface of a supraorbital but since the relationship between the pore and the canal is simple it is coded as single large pores (e.g., *Guizhoucoelacanthus*). Dutel et al. (2012, char. 23)[60] and Cavin et al. (2017, char. 23)[41] added one additional character-state, respectively: a large, continuous groove crossed by pillars (3) and a large, continuous groove without pillars (4). Based on the onychodontiform outgroups, the plesiomorphic condition corresponds to the presence of many tiny pores.

20. **Lateral bones alongside postparietal, number of** [FR8]: one (0), two or more (1)

21. **Intertemporal** [Ca17, Cb17, Fa15, Fb12, C12, F&C12, FR17, Y12, G12, W12, W&W12, Da12, Z12, GR12, WE12, CAa12, C&G12, A&S12, G&C12, Db12, CAb12, R&S12, T12]: absent (0), present (1)

22. **Supratemporal** [Ca18, Cb18]: present (0), absent (1)

23. **Posterior margin of tabulars** [Cb56, L&Z9]: anterior to posterior margin of postparietals (0), level with posterior margin of postparietals (1), extending beyond posterior margin of postparietals (2). The three character-states for a morphocline.

24. **Tabular descending process** [Ca19, Cb19, Fa17 homology, Fb14 rephrased, C14 rephrased, F&C14 rephrased, Y14 rephrased, G14 rephrased, W&W14 rephrased, Da14 rephrased, Z14 rephrased, GR14 rephrased, WE14 rephrased, CAa14 rephrased, C&G14 rephrased, A&S14 rephrased, G&C14 rephrased, Db14 rephrased, CAb14 rephrased, R&S14 rephrased, CAc7, CAd7, T14 rephrased]: absent

(0), present (1). As defined by Forey (1981, char. 8)[105], the posterolateral margin of the tabular (his "supratemporal") may bear an external descending process. This process articulates against the prootic region of the braincase immediately in front of the hyomandibular facet (e.g., *Coelacanthus granulatus*, *Laugia*) (Cloutier, 1991a, char. 19)[95].

25. **Otic canal** [new]: running through skull roof (0), following edge of skull roof (1)

26. **Otic canal, trajectory of** [Ca20, Cb20, L&Z30 in part]: running through the lateral series of bones (tabular and/or supratemporal and/or intertemporal) (0), running between postparietal and lateral series of bones (tabular and supratemporal and/or intertemporal) (1), running through tabular and postparietal (2). Cloutier (1991a, char. 20)[95] defined a character to describe the trajectory of the otic canal either passing through the lateral series (intertemporal and/or supratemporal) or passing between the postparietal and the lateral series. We redefine the character to encompass the disparity of the trajectory of the otic canal among actinistians and onychodontiforms (out-group). We considered that the lateral series primarily includes the tabular and supratemporal in actinistians with the exception of *Miguashaia* that also includes the intertemporal; the number of bones suturing laterally with the postparietal is taken into account in characters 20, 21 and 22. Character-state 2 corresponds to the condition where the otic canal runs at the suture between the postparietal and the lateral series of bones. In order to take into account, the condition observed in *Coelacanthus granulatus*, character-state 2 has been added to the original character description of Cloutier (1991a, char. 20)[95]. The three character-states form a morphocline.

27. **Medial branch of otic canal** [Ca16, Cb16, Fa37, Fb20, C20, F&C20, Y20, G20, L&Z30 in part, W20, W&W20, Da20, Z20, GR20, WE20, CAa20, C&G20, A&S20, G&C20, Db20, CAb20, R&S20, T20]: absent (0), present (1)

28. **Otic canal joining supratemporal canal** [Fa36, Fb21, C21, F&C21, Y21, G21, W21, W&W21, Da21, Z21, GR21, WE21, CAa21, C&G21, A&S21, G&C21, Db21, CAb21, R&S21, T21]: in lateral extrascapular (0), in tabular (1)

29. **Tabular and postparietal** [Cb57]: separated (0), fused (1)

30. **Lateral process of parietal** [Cb58]: absent (0), present (1). The lateral process of the parietal is formed from the posterolateral margin of the parietal and is directed ventrolaterally toward the dorsal part of the postorbital (Cloutier, 1991b, char. 58)[96]. The process could either be in contact with the postorbital (e.g., *Latimeria*), extends towards the postorbital (e.g., *Swenzia*) or be separated from the postorbital by a supraorbital (e.g., *Laugia, Macropoma, Yunnancoelacanthus*). This process has been coded as present in *Coelacanthus, Axelia, Wimania* and *Latimeria* by Cloutier (1991b, char. 58)[96]. The posterior lateral process of the parietal could carry a segment of the infraorbital canal that connects to the supraorbital canal [e.g., *Axelia* (Stensiö, 1921, fig. 25)[16], *Coelacanthus* (Schaumberg, 1978, figs. 5, 6)[34], *Wimania* (Stensiö, 1921, fig. 43)[16]].

31. **Descending process of parietal** [Ca11, Cb11, Fa13, Fb11, C11, F&C11, Y11, G11, W11, W&W11, Da11, Z11, GR11, WE11, CAa11, C&G11, A&S11, G&C11, Db11, CAb11, R&S11, T11]: absent (0), present (1). The descending process ("ventral process" of Forey (1998)[12]) of the parietal articulates with the dorsal side of the ethmosphenoid (Cloutier, 1991a, char. 11)[95]. Forey (1981, char. 10)[105] mentioned that this posteroventral process braces against the basisphenoid.

32. **Parietals and postparietals, ornament of** [Fa56 in part, Fb27, C27, F&C27, Y27, G27, W27, W&W27, Da27, Z27, GR27, WE27, CAa27, C&G27, A&S27, G&C27, Db27, CAb27, R&S27,

CAc13, CAd13, T27]: enamel capped ridges or tubercles (0), unornamented (1), marked by coarse tuberosities (2)

33. **Pineal foramen** [FR14, L&Z2]: present (0), absent (1)

34. **Parietals and postparietals** [Fb28, C28, F&C28, Y28, G28, W28, W&W28, Da28, Z28, GR28, WE28, CAa28, C&G28, A&S28, G&C28, Db28, CAb28, R&S28, CAc14, CAd14, T28]: without raised or depressed areas (0), with raised areas (1), with depressed areas (2). Forey (1998, char. 28)[12] recognized the presence of a raised area at the anterior margin of the postparietals and posterior margin of the parietals (as seen in *Latimeria chalumnae*) as an apomorphic condition. We recognize a second apomorphic state to take into account the condition observed in *Swenzia latimerae* where there is an anterior depression on the postparietals in the same area.

35. **Anterior margin of parietals** [FR13, L&Z1]: between or in front of orbits (0), slightly posterior to orbits (1)

36. **Parietal and supraorbitals, contact of** [CAc51, CAd51]: parietal contacts more than three supraorbitals (0), parietal contacts three supraorbitals (1), parietal contacts two supraorbitals (2). Cavin et al. (2020, char. 51)[101] defined a character to identify the number of supraorbitals articulating with the parietal (their "posterior parietal"). This multistate character forms a morphocline.

37. **Margin of dermal intracranial joint** [Fb1, C1, F&C1 modified, FR147 in part, Y1, G1, W1, W&W1, Da1, Z1, GR1, WE1, CAa1, C&G1, A&S1 modified, G&C1, Db1, Cab1, R&S1, CAc1 modified, CAd1 modified, T1 modified]: straight (0), deeply notched (1), undulated (2). Forey (1998)[12] defined the apomorphic state as "strongly interdigitate", while Friedman & Coates (2006)[47] and subsequent authors defined the apomorphic state as "deeply notched". Arratia & Schultze (2015)[15] used a second apomorphic character-state defined as "undulated or excavated"; only used for *Atacamaia*.

38. **Postparietal descending process** [Ca13, Cb13, Fa16, Fb13, C13, F&C13, Y13, G13, W13, W&W13, Da13, Z13, GR13, WE13, CAa13, C&G13, A&S13, G&C13, Db13, CAb13, R&S13, T13]: absent (0), present (1). The descending process of the postparietal is located on the posteroventral surface of the postparietal articulating with the oticoccipital part of the neurocranium.

39. **Postparietal, shape of** [Ca12, Cb12]: L shaped (0), rectangular (1), inverted L shaped (2). The shape of the postparietal takes into consideration the dorsal view of the element. In the inverted L shape, the small process forms the anterolateral component of the postparietal. The numbering of character-states has been modified from Cloutier (1991a, char. 12)[95].

40. **Postparietal** [L&Z7]: not narrowing posteriorly (0), narrowing posteriorly (1). Lu and Zhu (2009, char. 7)[8] defined a character about the posterior narrowing of the postparietals in order to investigate the interrelationships among onychodontiforms. The posterior narrowing of the postparietals was coded as present in *Onychodus*, *Qingmenodus* and *Grossius*. The posterior margin of the postparietal is considered to be narrowing when the posterior margin is clearly much narrower than the main body as well as the anteriormost margin of the postparietal. This character is partly linked with the inverted L shape of the postparietal [char. 39(2)].

41. **Postparietal postorbital, contact of** [Ca14, Cb14]: absent (0), present (1). The absence of contact between the anterolateral part of the postparietal and the postorbital could be owing either to the presence of intertemporal and/or supratemporal (e.g., *Miguashaia*), the presence of a gap between the elements (e.g., *Allenypterus*) or the presence of an elongated posterolateral process of the parietal (e.g., *Coelacanthus*).

42. **Postparietal and lateral extrascapular, contact of** [Ca15, Cb15]: present (0), absent (1)

43. **Pit lines on postparietals** [Fb26, C26, F&C26, Y26, G26, W26, W&W26, Da26, Z26, GR26, WE26, CAa26, C&G26, A&S26, G&C26, Db26, CAb26, R&S26, T26]: marking postparietals (0), not marking postparietals (1)

44. **Anterior pit line** [Fb24, C24, F&C24, Y24, G24, W24, W&W24, Da24, Z24, GR24, WE24, CAa24, C&G24, A&S24, G&C24, Db24, CAb24, R&S24, T24]: absent (0), present (1)

45. **Anterior pit line, position of** [FR36]: on postparietal (0), on parietal (1). Character 45 is linked to character 44.

46. **Middle pit line** [L&Z28]: in line with tabular pit line (0), not in line with tabular pit line (1). Character 46 is linked to character 43.

47. **Middle and posterior pit lines, position of** [Fb25, C25, F&C25, Y25, G25, L&Z27, W25, W&W25, Da25, Z25, GR25, WE25, CAa25, C&G25, A&S25, G&C25, Db25, CAb25, R&S25, T25]: within posterior half of postparietals (0), within anterior third of postparietals (1). Character 47 is linked to characters 43 and 46.

48. **Complete fusion of postparietal shield** [new]: no (0), yes (1)

49. **Extratemporal** [FR16, L&Z10]: absent (0), present (1)

50. **Extrascapulars, sutures of** [Fa19, Fb15, C15, F&C15, Y15, G15, W15, W&W15, Da15, Z15, GR15, WE15, CAa15, C&G15, A&S15, G&C15, Db15, CAb15, R&S15, CAc8, CAd8, T15]: sutured with postparietals-parietals (0), free (1). Character 50 is in part link with character 42.

51. **Extrascapulars, position of** [Cb59, Fa19, Fb16, C16, F&C16, Y16, G16, W16, W&W16, Da16, Z16, GR16, WE16, CAa16, C&G16, A&S16, G&C16, Db16, CAb16, R&S16, CAc9, CAd9, T16]: behind level of neurocranium (0), part of skull roof (1)

52. **Median extrascapular** [new]: present (0), absent (1)

53. **Lateral extrascapulars, size of** [new]: less than the width of median extrascapular (0), approximately the same width as median extrascapular (1), more than the width of median extrascapular (2). In species coded for lateral extrascapulars being less than the width of median extrascapular, the median extrascapular could reach up to twice the width of the lateral extrascapular (e.g., *Miguashaia bureaui*). On the other hand, species coded as having lateral extrascapular more than the width of median extrascapular, the lateral extrascapular could reach up to twice the width of the median extrascapular (e.g., *Hadronector donbairdi*). Morphometric character 13 provides the ratio between the lateral extrascapular width and the median extrascapular width. For those species allowing us to measure the ratio, the plesiomorphic condition corresponds to a ratio smaller than 0.9, whereas apomorphic state 2 corresponds to a ratio greater than 1.1. Meristic character 2 provides the number of extrascapulars. Character 53 is linked with the presence of a median extrascapular (Char. 52). The three character-states form a morphocline.

54. **Posterior margin of skull roof** [Fb18, C18, F&C18, Y18, G18, W18, W&W18, Da18, Z18, GR18, WE18, CAa18, C&G18, A&S18, G&C18, Db18, CAb18, R&S18, T18]: straight (0), embayed (1). Forey (1998, char. 18)[12] defined a character concerning the posterior margin of the skull roof as either

straight or embayed. Forey (1998, p. 58)[12] mentioned that the posterior margin of the tabulars (his "supratemporals") with the postparietals is straight in *Diplocercides* thus not taking into account the posterior limit of the lateral and median extrascapulars. In contrast, Forey (1998, p. 91)[12] mentioned that the fusion of the lateral extrascapular with the tabular (his "extratemporal") results in the posterior profile of the skull roof being embayed with the remaining extrascapulars lying in between in *Coelacanthus*. We considered the posterior margin of the skull roof to be interpreted as the posterior margin of the tabulars and postparietals even in species in which lateral and median extrascapulars are present and attached the postparietals and tabulars. Character 54 is in part link with the condition in which the posterior margin of the tabular extends posteriorly to the posterior margin of the postparietal (char. 23.2).

55. **Anterior branches of occipital commissure** [Cb60, Fa40, Fb22, C22, F&C22, Y22, G22, W22, W&W22, Da22, Z22, GR22, WE22, CAa22, C&G22, A&S22, G&C22, Db22, CAb22, R&S22, CAc11, CAd11, T22]: absent (0), present (1). Occipital commissure [= "supratemporal commissural canal" of Schaeffer (1952)[35]; "supratemporal commissure" of Forey (1981)[105]]. Anterior branches (ramifications) of the occipital commissure extending to the anterior part of the extrascapulars and/or the posterior part of the postparietals are found in some actinistian species (Cloutier, 1991b)[96].

56. **Sensory pores, size of** [Fa38]: pores on ethmosphenoid shield similar to parietal shield pores (0), pores on ethmosphenoid shield larger than parietal shield pores (1)

57. **Preorbital** [Ca22, Cb22, Fa20, Fa19, Fb10, C10, F&C10, FR8, Y10, G10, W10, W&W10, Da10, Z10, GR10, WE10, CAa10, C&G10, A&S10, G&C10, Db10, CAb10, R&S10, T10]: present (0), absent (1). The preorbital is a bone forming part of the anterior margin of the orbit in basal coelacanths. A posterior tectal occupies a similar position in onychodontiforms and some tetrapodomorphs. Forey (1998, char. 10)[12] used the opposite polarity of the character-states. We coded the preorbital present in onychodontiforms although this element is referred to as the posterior tectal. This character is linked with characters 6 and 7.

58. **Lateral rostral** [Ca]: without ventral process (0), with ventral process (1). The ventral process of the lateral rostral is located anteriorly, it could be relatively broad and shallow (e.g., *Rhabdoderma elegans*) or narrow and longer (e.g., *Macropoma lewesiensis*).

59. **Lateral rostral** [L&Z4]: forming part of orbit (0), not forming part of orbit (1)

60. **Lateral rostral, shape of** [new]: rectangular (length/height ratio between 1.1 and 2.5) (0), elongated (length/height ratio between 2.6 and 5) (1), highly elongated (length/height ratio greater than 5) (2). The shape of the lateral rostral is defined in terms of a ratio between the length of the element and the height (without taking into consideration the extend of the anterodorsal, anteroventral, and posterodorsal processes). Most coelacanths (more than 15 species out of 38 species including the outgroup *Onychodus*) have a length/height ratio of the lateral rostral around 3. The extreme values for our sample vary between 1.3 (*Onychodus jandemarrai*) and 10.7 (*Axelrodichthys araripensis*). The three character-states are defined in terms of the length/height ratio: rectangular (length/height ratio between 1.1 and 2.5) (0), elongated (length/height ratio between 2.6 and 5) (1), and highly elongated (length/height ratio greater than 5) (2). The three character-states have been ordered to form a morphocline.

61. **Posterodorsal process of lateral rostral** [L&Z5]: absent (0), present (1). The posterodorsal process of the lateral rostral is also referred to as the "lachrymal process" (de Carvalho et al., 2013)[23]. It is a well-developed and well-defined process that extends towards the midline of the skull roof [see *Axelrodichthys maiseyi*, de Carvalho et al. (2013, fig. 3B)[23]].

62. **Cheek bones, contact of** [Ca23 in part, Cb23, Fa22, Fb29, C29, F&C29, Y29, G29, W29, W&W29, Da29, Z29, GR29, WE29, CAa29, C&G29, A&S29, G&C29, Db29, CAb29, R&S29, T29]: in contact or overlapping (0), separated (1). Cloutier (1991a, b, char. 23)[95,96] recognized three conditions for the contact of cheek bones: complete suture among cheek bones (0), loose articulation of the postspiracular (1), and loose articulation of the postspiracular and postorbital (3). Forey (1998, char. 29)[12] defined the contact among cheek bones either as sutured to one another (0) or separated from one another (1). The condition takes into account the relationships primarily among the principal cheek bones, meaning the postorbital, squamosal, preoperculum and quadratojugal.

63. **Contact between lacrimojugal and preorbital and/or supraorbital series** [Fb51, C51, F&C51, Y51, G51, W51, W&W51, Da51, Z51, GR51, WE51, CAa51, C&G51, A&S51, G&C51, Db51, CAb51, R&S51, T51]: present (0), absent (1). Character 63 is in part linked with character 57.

64. **Spiracular** [Ca24, Cb24, Fa21, Fb30 polarity, C30 polarity, F&C30 polarity, Y30 polarity, G30 polarity, W30 polarity, W&W30 polarity, Da30 polarity, Z30 polarity, GR30 polarity, WE30 polarity, CAa30 polarity, C&G30 polarity, A&S30 polarity, G&C30 polarity, Db30 polarity, CAb30 polarity, R&S30 polarity, CAc15, CAd15, T30 polarity]: present (0), absent (1). Schaeffer (1952)[35] [=postspiracular of Lund & Lund (1985)[13]].

65. **Preoperculum** [Fa23, Fb31 polarity, C31 modified, F&C31, Y31, G31, W31, W&W31, Da31 polarity, Z31, GR31 polarity, WE31, CAa31, C&G31 polarity, A&S31 polarity, G&C31, Db31, CAb31 polarity, R&S31 polarity, T31 polarity]: present (0), absent (1)

66. **Preoperculum, size of** [Fb38, C38, F&C38, Y38, G38, W38, W&W38, Da38, Z38, GR38, WE38, CAa38, C&G38, A&S38, G&C38, Db38, CAb38, R&S38, CAc18, CAd18, T38]: large bone (0), reduced to narrow tube (1). Character 66 is linked to character 65.

67. **Preoperculum** [Fb39, C39, F&C39, Y39, G39, W39, W&W39, Da39, Z39, GR39, WE39, CAa39, C&G39, G&C39, Db39, CAb39, R&S39, CAc19, CAd19, T39]: undifferentiated (0), developed as a posterior tube-like canal-bearing portion and an anterior blade-like portion (1). Character 67 is linked to character 65.

68. **Squamosal** [L&Z22]: present (0), absent (1)

69. **Squamosal, position of** [Fb34, C34, F&C34, Y34, G34, W34, W&W34, Da34, Z34, GR34, WE34, CAa34, C&G34, A&S34, G&C34, Db34, CAb34, R&S34, T34]: limited to the midlevel of the cheek (0), extending behind the postorbital to reach skull roof (1). Character 69 is linked with character 68.

70. **Squamosal, position of** [new]: posterior to postorbital (0), ventral to postorbital (1). Character 70 is linked with character 68.

71. **Squamosal, position of** [new]: forming part of upper jaw margin (0), not forming part of upper jaw margin (1). Character 71 is linked with character 68, and partly linked with character 69.

72. **Squamosal, size of** [Cb25 in part, Fb37, C37, F&C37, Y37, G37, W37, W&W37, Da37, Z37, GR37, WE37, CAa37, C&G37, A&S37, G&C37, Db37, CAb37, R&S37, T37]: large bone (0), reduced to a narrow tube (1). Character 72 is linked with character 68.

73. **Squamosal, shape of** [Ca25]: pentagonal (0), quadrilateral (1), triangular (2), irregular (3). Character 73 is linked with character 68.

74. **Lacrimal** [new]: not fused with jugal (0), fused with jugal (1), fused with jugal and squamosal (2). The three character-states form a morphocline.

75. **Stud shaped ossicles near lacrimojugal** [new]: absent (0), present (1). Forey (1998, p. 307)[12] wrote in the diagnosis of *Coelacanthus* that the lacrimojugal is associated with small stud-shaped ossicles which must have lain free in the skin, a condition similar to those of *Spermatodus*.

76. **Lacrimojugal, shape of** [Cb65, Fb35 rephrased, C35 rephrased, F&C35 rephrased, Y35 rephrased, G35, W35, W&W35, Da35 rephrased, Z35 rephrased, GR35 rephrased, WE35 rephrased, CAa35, C&G35 rephrased, A&S35 rephrased, G&C35 rephrased, Db35 rephrased, CAb35 rephrased, R&S35 rephrased, T35 rephrased]: tapering anteriorly (0), not expanded anteriorly (1) expanded anteriorly (2). Forey (1998, char 35)[12] recognized two conditions dealing with the anterior shape of the lacrimojugal: not expanded anteriorly (0) and expanded anteriorly (1). He associated the anterior expansion solely to the loss of the preorbital. Herein, we recognized an additional apomorphic condition of the anterior shape of the lacrimojugal which is "tapering anteriorly". The lacrimojugal expands anteriorly in genera such as *Axelrodichthys*, *Chinlea, Libys*, and *Macropoma*, it tapers anteriorly in *Atacamaia*, *Coelacanthus, Luopingcoelacanthus* and Wimania, while it is not expanded anteriorly in *Hadronector, Polyosteorhynchus, Ticinepomis*, and *Yunnancoelacanthus*. The three character-states form a morphocline. Character 76 is linked with character 74.

77. **Lacrimojugal, sensory pores of** [new]: relatively small size pores through the length of the lacrimojugal (0), anterior pore(s) expanded or forming a groove (1). Character 77 is linked with character 74.

78. **Lacrimojugal, shape of** [Fb36 rephrased, C36 rephrased, F&C36 rephrased, Y36 rephrased, G36, W36, W&W36, Da36 rephrased, Z36 rephrased, GR36 rephrased, WE36 rephrased, CAa36, C&G36 rephrased, A&S36 rephrased, G&C36 rephrased, Db36 rephrased, CAb36 rephrased, R&S36 rephrased, CAc17 modified, CAd17 modified, T36 rephrased]: not angled anteriorly (0), angled anteriorly (1). Forey (1998, char. 36)[12] reported that the lacrimojugal ends anteriorly without or with an anterior angle. This downward angle is present in some species (e.g., *Whiteia woodwardi*, *Atacamaia solitaria*, *Coelacanthus granulatus*) in which the lacrimojugal extends more anteriorly than the anterior limit of the orbit. This angle is distinct from the angle that could be observed at mid-length of the ventral margin of the lacrimojugal (e.g., *Diplocercides*, *Ticinepomis*). Character 78 is linked with character 74.

79. **Lacrimojugal ventral margin** [G&C110 modified]: without a posteroventral extension (0), with a posteroventral extension (1). Gess & Coates (2015, char. 110)[78] defined the shape of the lacrimojugal as elbow-like with a ventral extension. They coded this condition as present in *Serenichthys* and *Diplocercides* among the 28 actinistian taxa they coded for. Character 79 is linked with character 74.

80. **Lacrimojugal ventral margin** [G&C110 in part]: linear (0), V-shaped (1), curvilinear (2), sinusoidal (3). Cavin et al. (2020, char. 48)[101] defined a lacrimojugal character to reflect differences among derived coelacanths. The lacrimojugal was considered either as being curved (0) or straight (1) in its mid-region. We redefine this character in terms of the ventral margin of the lacrimojugal to consider the disparity of all coelacanths. We are using four character-states to describe the shape of the ventral margin of the lacrimojugal: linear (0) (e.g., *Miguashaia bureaui*), V-shaped (1) (e.g., *Diplocercides kayseri*, *Foreyia maxkuhni*), curvilinear (2) (e.g., *Caridosuctor populosum*, *Coccoderma suevicum*), and sinusoidal (3) (e.g., *Hadronector donbairdi*). The V-shaped condition of the ventral margin of the lacrimojugal is in part associated with the presence of the posteroventral expansion of the margin (Character 79). Character 80 is linked with character 74.

81. **Lacrimojugal, position of** [Cb64]: extending only to anterior of orbit (0), extending to snout (1). Cloutier (1991b, char. 64)[96] defined a character to reflect the anterior extent of the lacrimojugal which was suggested to be characteristic of advanced coelacanths by Stensiö (1921)[16]. However, Cloutier (1991b)[96] only coded *Mawsonia gigas* as having a lacrimojugal extending to the anterior part of the snout. We redefined the apomorphic condition as extending to the snout, rather than the anterior part of the snout. Character 81 is linked with character 74.

82. **Lacrimojugal postorbital limb** [new]: absent (0), present (1). Character 82 takes into account the condition of the lacrimojugal. Therefore, the outgroups are coded as "-". Nevertheless, in *Grossius aragonensis*, *Onychodus jandemarrai* and *Strunius walteri*, the jugal lacks a postorbital limb. Character 82 is linked to character 74.

83. **Lacrimojugal postorbital limb, extent of** [new]: above midorbit level or at midorbit level (0), below midorbit level (1). Character 83 is linked with characters 74 and 82.

84. **Preopercular and lacrimojugal (jugal), contact of** [G&C114]: separated (0), abutting (1)

85. **Anterodorsal excavation in postorbital** [Fb40, C40, F&C40, Y40, G40, W40, W&W40, Da40, Z40, GR40, WE40, CAa40, C&G40, A&S40, G&C40, Db40, CAb40, R&S40, CAc20, CAd20, T40]: absent (0), present (1). Forey (1998, char. 40)[12] considered the presence of an anterodorsal excavation in the postorbital to be an apomorphic condition. As described in *Latimeria chalumnae*, this excavation receives a tough ligamentous connection with the posteriormost supraorbitals (Forey, 1998, p. 98, fig. 4.1)[12].

86. **Postorbital** [Cb62, Fb41, C41, F&C41, Y41, G41, W41, W&W41, Da41, Z41, GR41, WE41, CAa41, C&G41, A&S41, G&C41, Db41, CAb41, R&S41, CAc21, CAd21, T41]: without anterior process (0), with anterior process (1). Cloutier (1991b, char. 62)[96] defined this anterior process of the postorbital as the anteroventral corner of the postorbital that extends anteriorly beyond the posteroventral margin of the orbit as seen in *Mawsonia* (e.g., *Mawsonia brasiliensis* (Yabumoto, 2002, fig. 4)[55].

87. **Postorbital, size of** [Cb63, Fb42, C42, F&C42, Y42, G42, W42, W&W42, Da42, Z42, GR42, WE42, CAa42, C&G42, A&S42, G&C42, Db42, CAb42, R&S42, CAc22, CAd22, T42]: large bone (0), reduced to narrow tube (1)

88. **Postorbital, position of** [Fb43, C43, F&C43, Y43, G43, W43, W&W43, Da43, Z43, GR43, WE43, CAa43, C&G43, A&S43, G&C43, Db43, CAb43, R&S43, CAc23, CAd23, T43]: lying wholly behind intracranial joint (0), spanning intracranial joint (1)

89. **Infraorbital canal, trajectory of** [Fb44, C44, F&C44, Y44, G44, W44, W&W44, Da44, Z44, GR44, WE44, CAa44, C&G44, A&S44, G&C44, Db44, CAb44, R&S44, CAc24, CAd24, T44]: within postorbital with simple pores opening directly from main canal (0), anterior and posterior branches within postorbital (1)

90. **Infraorbital canal, trajectory of** [Fb45, C45, F&C45, Y45, G45, W45, W&W45, Da45, Z45, GR45, WE45, CAa45, C&G45, A&S45, G&C45, Db45, CAb45, R&S45, CAc25, CAd25, T45]: running through center of postorbital (0), running along anterior margin of postorbital (1)

91. **Jugal canal** [Fb46, C46, F&C46, Y46, G46, W46, W&W46, Da46, Z46, GR46, WE46, CAa46, C&G46, A&S46, G&C46, Db46, CAb46, R&S46, CAc26, CAd26, T46]: simple (0), prominent branches (1). Forey (1998, char. 46)[12] described the apomorphic condition in which large pores are

lying separate from the main trajectory canal of the jugal canal in the squamosal (e.g., *Rhabdoderma*, *Latimeria*).

92. **Jugal canal, trajectory of** [Fb47, C47, F&C47, Y47, G47, W47, W&W47, Da47, Z47, GR47, WE47, CAa47, C&G47, A&S47, G&C47, Db47, CAb47, R&S47, CAc27, CAd27, T47]: running through center of bone (0), running along ventral margin of squamosal (1)

93. **Pit lines** [Fb48, C48, F&C48, Y48, G48, W48, W&W48, Da48, Z48, GR48, WE48, CAa48, C&G48, A&S48, G&C48, Db48, CAb48, R&S48, T48]: marking cheek bones (0), not marking cheek bones (1)

94. **Preopercular canal** [L&Z29]: preopercular canal ends at dorsal margin of preopercular (0), does not end at dorsal margin of preopercular (1). Character 93 is linked with character 65.

95. **Maxilla** [FR38]: absent (0), present (1)

96. **Ventral margin of maxilla** [L&Z21]: straight (0), curved (1). Character 96 is linked to character 95.

97. **Posterior expansion of the maxilla** [FR39, L&Z20 polarity]: absent (0), small expansion (posterodorsal process) (1), large expansion (cleaver-shaped) (2). The three character-states form a morphocline. Character 97 is linked to character 95.

98. **Contribution by maxilla to posterior margin of cheek** [new]: present (0), absent (1). Character 98 is linked to character 95.

99. **Cheek bones, ornament of** [Fa56 in part, Fb49, C49, F&C49, Y49, G49, W49, W&W49, Da49, Z49, GR49, WE49, CAa49, C&G49, A&S49, G&C49 in part, Db49, CAb49, R&S49, CAc28, CAd28, T49]: absent or with very fine tuberculation (0), tubercular (1), represented as a coarse superficial rugosity (2), ridged (3). Forey (1998, char. 49)[12] considered three character-states to describe the cheek bone ornamentation: tubercular (1), absent (0), and with coarse superficial rugosity (2); in his character description (p. 128), the numbering of these character-states has been mislabeled where only state 1 and 2 have been written. In order to take into account the disparity of the cheek bone ornamentation in coelacanths, we used four character-states that better represent the disparity. In addition, some taxa are coded as a polymorphic condition to include both the tubercular and ridged ornamentation. We are limiting the coding of the cheek bones ornamentation to the condition observed on the postorbital, squamosal, preoperculum, and spiracular; in contrast to some previous papers, we are not taking into consideration the ornamentation of the operculum. Some of the polymorphic conditions correspond to different conditions observed on the preoperculum (frequently with ridges) and the remaining cheek bones (frequently tubercular) of a species.

100. **Openings for infraorbital jugal and preopercular sensory canals** [Fb50 modified, C50 modified, F&C50, Y50, G50, W50, W&W50, Da50 modified, Z50, GR50 modified, WE50, CAa50, C&G50 modified, A&S50 modified, G&C50, Db50, CAb50 modified, R&S50 modified, CAc29, CAd29, T50 modified]: many small pores (0), few large pores (1), large and continuous grooves crossed by pillars (2). Forey (1998, char. 50)[12] described two character-states for the sensory openings for the infraorbital, jugal and preopercular canals: many tiny pores (0) and a few large pores (1). Dutel et al. (2012, char. 50)[60] added a third character-states taking into account a condition in which there is a large continuous groove crossed by pillars. The three character-states form a morphocline.

101. **Squamosal and preopercular** [Ca26 in part, Cb26]: unfused (0), fused (1). Character 101 is linked to character 65.

102. **Foramina similar to infradentary foramina on cheek bones** [L&Z16]: absent (0), present (1). Among actinistians, Friedman (2007, char. 47; fig. 4C)[98] and Lu & Zhu (2009, char. 16)[8] reported the presence of large foramina distinct from the sensory line pores and pit lines on the cheek solely in *Styloichthys*.

103. **Suboperculum** [Ca29, Cb29, Fa24, Fb32 polarity, C32 polarity, F&C32 polarity, Y32 polarity, G32 polarity, W32 polarity, W&W32 polarity, Da32 polarity, Z32 polarity, GR32 polarity, WE32 polarity, CAa32 polarity, C&G32 polarity, A&S32 polarity, G&C32 polarity, Db32 polarity, CAb32 polarity, R&S32 polarity, CAc16, CAd16, T32 polarity]: present (0), absent (1). Forey (1998)[12] defined his character 32 as follows: (0) suboperculum absent, (1) suboperculum present. By out-group comparison (including actinopterygians, onychodontiforms, dipnomorphs and tetrapodomorphs), the presence of a suboperculum is the plesiomorphic condition. Thus, most of the coding that we are using differs from what has been provided by Forey (1998, char. 32)[12] and subsequent analyses (up to Toriño et al., 2021, char. 32)[14] because of the different polarity of the character.

104. **Suboperculum, position of** [Ca30, Cb30]: suturing with both the preoperculum and operculum (0), suturing only with preoperculum (1), suturing only with operculum (2), isolated (3). Character 104 is linked to characters 65 and 103.

105. **Suboperculum, size of** [Ca31, Cb31]: longer than deep (0), deeper than long (1). Character 105 is linked to character 103.

106. **Suboperculum, shape of** [Ca32, Cb32]: quadrilateral (0), triangular (1), ovoid (2). Character 106 is linked to character 103.

107. **Operculum** [new]: without sensory pores (0), with sensory pores (1)

108. **Operculum, shape of** [Ca28, Cb28]: quadrilateral (0), triangular (1), ovoid (2). Cloutier (1991a, char 28)[95] defined a character to describe the shape of the operculum among Palaeozoic coelacanths, either as quadrilateral (including rectangular, square and trapezoidal) (e.g., *Miguashaia*, *Hadronector*) and triangular (e.g., *Coelacanthus, Rhabdoderma*). Cloutier (1991b, p. 406)[96] mentioned that the distinction between the two shapes was generally clear with the exception of species having operculum with strongly asymmetrical, diamond-shape (e.g., *Diplocercides jaekeli*). Instead of coding for the global shape of the operculum, Cavin et al. (2020, char. 55)[101] characterized the posteroventral edge of the operculum: marks an angle (or posterior margin rounded) (0) (e.g., *Macropoma, Latimeria*), straight (1) (e.g., *Trachymetopon, Mawsonia*), and regularly curved (2) (e.g., *Axelrodichthys, Chinlea*). We redefine the shape of the operculum using three character-states; we add the ovoid shape in contrast to the original description of Cloutier (1991a, b, char. 28)[95,96]. The ovoid shape takes into account some of the species that could have been coded as a regularly curved margin by Cavin et al. (2020, char. 55)[101].

109. **Dentary, shape of** [Cb66, Fa30, Fb57, C57, F&C57, Y57, G57, W57, W&W57, Da57, Z57, GR57, WE57, CAa57, C&G57, A&S57, G&C57, Db57, CAb57, R&S57, CAc31 modified, CAd31 modified, T57]: absence of hook-shape process posteriorly oriented on the dentary (0), presence of hook-shape process posteriorly oriented on the dentary (1). Cloutier (1991b, char. 66)[96] described this character as absence (0) or presence (1) of posterodorsal hook on the dentary. Forey (1998, char. 57)[12] used a character to describe the shape of the dentary as simple (0) and hook-shaped (1). Forey (1998)[12] associated this feature with the elaboration of the muscular lip fold as present in *Latimeria* chalumnae. This hook-shape is present in a few derived actinistians such as *Chinlea, Heptanema, Foreyia, Luopingcoelacanthus, Macropoma, Macropomoides, Undina, Swenzia* and *Whiteia*.

110.   **Dentary relative, size of** [new]: dentary much bigger than the splenial (0), dentary approximately the same size as the splenial (1), dentary much smaller than the splenial (2). The relative size of the dentary and splenial considers the general surface of these bones in lateral view. The three character-states form a morphocline. Character 110 is linked with character 133.

111.   **Posterior margin of dentary** [new]: relatively at right angle with the dorsal margin (0), dorsally beveled (1), ventrally beveled (2), pointed (X bevel) (3), V-grooved (4). This character takes into account the general shape of the posterior margin of the dentary when looking at the lateral profile of the lateral surface of the dentary. We used the terminology for the description of edge profile. Dorsally beveled (or top bevel) implies than the pointed posterior edge of the posterior margin of the dentary is located ventrally (e.g., *Gavinia, Laugia*), while ventrally beveled (or bottom bevel) it is the dorsal part that is pointed (e.g., *Libys, Tachymetopon*). In the pointed shape (or X bevel), the pointed part of the posterior margin of the dentary is approximately located at mid-height of the dentary (e.g., *Coelacanthus, Parnaibaia*), while the V-grooved shape describes the pointing part projecting inward the posterior margin (e.g., *Foreyia*). Most coelacanths having a dorsal hook-shape posteriorly oriented on the dentary (Char. 108) have a V-grooved posterior margin. This character does not apply for the out-groups in which a long dentary is known.

112.   **Dentary, orientation of** [Ca37, Cb37]: horizontally straight (0), slightly dipping (1), sharply downturned (2). Lund and Lund (1985)[13] proposed the lack of a distinct angular diastema in the orientation of the dentary (which thus has a relatively continuous occlusal line with the angular) to be the plesiomorphic condition. Cloutier (1991a, b, char. 37)[95,96] suggested that the apomorphic condition corresponds to the presence of a dentary oriented diagonally with the angular. Because of the large disparity of inclination of the dentary we divided the original apomorphic condition into two character-states (slightly dipping and sharply inclined). The three character-states forms a morphocline on the anterior inclination of the dentary. The horizontally straight condition corresponds to the plesiomorphic condition where the dentary is nearly parallel to the main orientation of the lower jaw (e.g., *Miguashaia, Caridosuctor, Coelacanthus*). In a few species, the dentary is slightly dipping or inclined anteroventrally; the angle of inclination could vary between 10 (e.g., *Serenichthys*) and 40 degrees (e.g., *Diplocercides*). The sharply downturned orientation of the dentary corresponds to the condition where the main orientation of the dentary is approximately to a right angle with the main orientation of the lower jaw (e.g., *Allenypterus, Diplurus, Foreyia*). The three character-states form a morphocline.

113.   **Dentary** [Fa29, Fb65, C65, F&C65, Y65, G65, W65, W&W65, Da65, Z65, GR65, WE65, CAa65, C&G65, A&S65, G&C65, Db65, CAb65, R&S65, CAc34, CAd34, T65]: without prominent lateral swelling (0), with prominent lateral swelling (1). Forey (1998, p. 153; char. 65)[12] described the presence a prominent lateral swelling on the dentary of *Mawsonia, Axelrodichthys* and *Lualabaea*, located in front of the depression for the deep pseudomaxillary fold. This protuberance is a smooth dome-shaped protuberance (see Forey, 1998, char. 5.10A, B)[12].

114.   **Dentary, ornament of** [Fa32 in part, Fb63, C63, F&C63, Y63, G63, W63, W&W63, Da63, Z63, GR63, WE63, CAa63, C&G63, A&S63, G&C63, Db63, CAb63, R&S63, T63]: with ornament (0), without ornament (1). Character 114 is linked to character 132.

115.   **Dentary teeth** [new]: present (0), absent (1). Friedman & Coates (2006, char. 54)[47] coded *Allenypterus* as "?" because of its edentulous condition. We used a separate character to take into account the present or absent of teeth on the mandible.

116.   **Dentary teeth** [Fa26, Fb54, C54, F&C54, Y54, G54, W54, W&W54, Da54, Z54, GR54, WE54, CAa54, C&G54, A&S54, G&C54, Db54, CAb54, R&S54, T54]: attached to dentary (0), on separate tooth plates (1). The presence of dentary teeth fused to the dentary or separate from the dentary was

used by Forey (1998, char. 54)[12]. Forey (1998)[12] mentioned that the apomorphic condition takes into account both a condition in which teeth are present on separate tooth plates and the edentulous condition (Character 115). Character 116 is linked with character 115.

117. **Dentary sensory pore** [Fa42, Fb61, C61, F&C61, Y61, G61, W61, W&W61, Da61, Z61, GR61, WE61, CAa61, C&G61, A&S61, G&C61, Db61, CAb61, R&S61, T61]: absent (0), present (1). The dentary sensory pore is generally a single large pore associated with the trigeminal nerve; *Mawsonia soba* differs by the presence of four pores rather than one large pore (Brito et al., 2018)[56]. As defined by Forey (1998, char. 61)[12], this pore is located near the suture between the dentary and the splenial, above the mandibular canal.

118. **Parasymphysial plate** [new]: present (0), absent (1)

119. **Parasymphysial plate** [new]: detachable tooth whorl (0), long sutured to coronoid (1), short not sutured to coronoid (2). Character 119 is linked with character 118.

120. **Parasymphysial tusk** [FR52 in part]: present (0), absent (1). Character 120 is linked with character 118.

121. **Coronoid opposite posterior end of dentary** [Fa28 in part, Fb56, C56, F&C56, Y56, G56, W56, W&W56, Da56, Z56, GR56, WE56, CAa56, C&G56, A&S56, G&C56, Db56, CAb56, R&S56, CAc30, CAd30, T56]: not modified (0), modified (1). Forey (1998, char. 56)[12] described that the fourth coronoid of the anterior series of coronoids is modified in some actinistians. This coronoid is closely associated with the posterior end of the dentary and is modified to bear enlarged tooth/teeth [e.g., *Spermatodus* (Forey, 1998, fig. 5.8A)[12]; *Undina penicillata* (Forey, 1998, fig. 5.12C)[12]] and the lateral edge rolled over [e.g., *Sassenia*; see Forey (1998, fig. 5.8B)[12]]. This coronoid is located anterior to the principal coronoid (char. 122).

122. **Principal coronoid** [new]: present (0), absent (1). An enlarged posterior (principal) coronoid projecting considerably above the occlusal margin of the lower jaw has been recognized by many authors as an actinistian synapomorphy (Schaeffer, 1952; Lund & Lund, 1985; Cloutier, 1991a)[13,35,95]. Cloutier (1991a)[95] recognized the coronoid IV oriented vertically as an actinistian synapomorphy; although we agree that the posteriormost is oriented vertically, the homology of this element with coronoid IV is questioned. The modified coronoid (char. 121) is frequently referred to as Coronoid IV.

123. **Principal coronoid** [Cb68 in part, Fa31 in part, Fb66 in part, C66 in part, F&C66 in part, Y66 in part, G66, W66, W&W66, Da66 in part, Z66 in part, GR66 in part, WE66 in part, CAa66 in part, C&G66 in part, A&S66 in part, G&C66 in part, Db66 in part, CAb66 in part, R&S66 in part, CAc35, CAd35, T66 in part]: lying free (0), sutured to angular (1). Cloutier (1991b)[96] mentioned that in most actinistians, the principal coronoid (his "Coronoid IV") abuts the mesial side of the prearticular. Forey (1998, char. 66)[12] proposed two character-states for the condition of the principal coronoid: lying free (0) and sutured to the angular (1). Forey (1998, p. 163)[12] and Clément (1999, p. 238)[68] mentioned that the principal coronoid does not sutured to the angular in most actinistians with the exception of *Axelrodichthys* and *Mawsonia*. Character 123 is linked with character 122.

124. **Principal coronoid, shape of** [Ca38 in part, Cb38 in part]: subtriangular (0), subquadrilateral (1), saddle-shaped (2), boomerang-shaped (3). Forey (1981, 1998)[12,105] mentioned the difference in the shape of the principal coronoid, but did not defined a character. Cloutier (1991a, char. 38)[95] recognized two shapes relative to the lateral view of the principal coronoid (his "coronoid IV") visible above the angular: subtriangular and subquadrilateral. In addition, Cloutier (1991a)[95] mentioned that these two character-states did not apply to the shape of *Axelrodichthys araripensis*. Yabumoto & Uyeno (2005)[20]

used the shape of the principal coronoid as distinctive for *Mawsonia* [*M. lavocati* (Yabumoto & Uyeno, 2005, figs. 6, 7)[20] and *M. brasiliensis*]. Dutel et al. (2015, fig. 1)[88] described the principal coronoid of *Trachymetopon liassicum* as saddle-shape. Fragoso et al. (2018)[104] qualified the principal coronoid of *Mawsonia*/*Axelrodichthys* complex as saddle shaped displaying a cranial and a caudal process. We added a second apomorphic state to consider this shape. A third apomorphic state, the boomerang-shape, was defined to take into account the curved shape of the principal coronoid of *Macropoma lewesiensis* (Forey, 1998, fig. 5.13)[12]. Character 124 is linked with character 122.

125. **Coronoid fangs** [Fb67, C67, F&C67, Y67, G67, W67, W&W67, Da67, Z67, GR67, WE67, CAa67, C&G67, A&S67, G&C67, Db67, CAb67, R&S67, CAc36, CAd36, T67]: absent (0), present (1). Forey (1998, char. 67)[12] considered the presence of enlarged teeth lying alongside a replacement socket upon at least some of the anterior coronoids as the apomorphic condition. However, based on outgroup comparison with onychodontiforms, the presence would rather correspond to the plesiomorphic condition.

126. **Oral pit line** [Fa43, Fb58, C58, F&C58, Y58, G58, W58, W&W58, Da58, Z58, GR58, WE58, CAa58, C&G58, A&S58, G&C58, Db58, CAb58, R&S58, T58]: short confined to angular (0), long reaching forward to dentary and or splenial (1)

127. **Oral pit line, position of** [Fb59, C59, F&C59, Y59, G59, W59, W&W59, Da59, Z59, GR59, WE59, CAa59, C&G59, A&S59, G&C59, Db59, CAb59, R&S59, CAc32, CAd32, T59]: located at center of ossification of angular (0), removed from the center of ossification (1). Character 127 is in part linked with character 126.

128. **Subopercular branch of mandibular sensory canal** [Fa41, Fb60, C60, F&C60, Y60, G60, W60, W&W60, Da60, Z60, GR60, WE60, CAa60, C&G60, A&S60, G&C60, Db60, CAb60, R&S60, CAc33, CAd33, T60]: absent (0), present (1)

129. **Mandibular canal, trajectory of** [FR68, L&Z31]: not passing through most posterior infradentary (0), passing through most posterior infradentary (1). Zhu & Yu (2002, char. 80)[84], Zhu & Yu (2004)[106] and Friedman (2007, char. 68)[98] used the trajectory of the mandibular canal in relation to the posteriormost infradentary to address the phylogenetic position among sarcopterygians as well as basal forms of actinistians such as *Styloichthys*.

130. **Mandibular canal, trajectory of** [L&Z32]: not passing through the lowermost part of the infradentary series with many tubes (0), passing through the lowermost part of the infradentary series with many tubes (1)

131. **Lower jaw, ornament of** [Fb62, C62, F&C62, Y62, G62, W62, W&W62, Da62, Z62, GR62, WE62, CAa62, C&G62, A&S62, G&C62, Db62, CAb62, R&S62, T62]: ridged (0), tubercular (1), unornamented (2). Forey (1998, char. 62)[12] recognized two character-states to describe the ornamentation of the lower jaw: ridged (0) and granular (1) ornament. We recognize an additional character-state to consider the complete disparity of the lower jaw ornament: unornamented (2). Character 131 is partly linked with characters 133 and 114.

132. **Splenial** [new]: present (0), absent (1)

133. **Splenial, ornament of** [Fa32 in part, Fb64, C64, F&C64, Y64, G64, W64, W&W64, Da64, Z64, GR64, WE64, CAa64, C&G64, A&S64, G&C64, Db64, CAb64, R&S64, T64]: with ornament (0), without ornament (1). Character 133 is linked to character 132.

134. **Posterior margin of splenial** [new]: relatively at right angle with dorsal margin (0), dorsally beveled (1), ventrally believed (2), pointed (X bevel) (3), V-grooved (4). This character considers the general shape of the posterior margin of the splenial when looking at the lateral profile of the lateral surface of the splenial; this character is similar to Character 111 that is relative to the posterior margin of the dentary. We used the terminology for the description of edge profile. Dorsally beveled (or top bevel) implies than the pointed posterior edge of the posterior margin of the splenial is located ventrally (e.g., *Allenypterus*, *Diplocercides*, *Garnbergia*), while ventrally beveled (or bottom bevel) it is the dorsal part that is pointed (e.g., *Parnaibaia*). In the pointed shape (or X bevel), the pointed part of the posterior margin of the splenial is approximately located at mid-height of the splenial (e.g., *Coelacanthus, Holophagus*), while the V-grooved shape describes the pointing part projecting inward the posterior margin (e.g., *Foreyia*). Character 134 is linked to character 132.

135. **Prearticular and/or coronoid teeth** [Fa27 in part, Fb68, C68, F&C68, Y68, G68, W68, W&W68, Da68, Z68, GR68, WE68 modified, CAa68, C&G68, A&S68, G&C68, Db68, CAb68, R&S68, CAc37, CAd37, T68]: pointed and smooth (0), pointed and marked with fine striations (1), rounded and marked with fine striations (2). The definition and order of character-states have been changed from previous uses of this character [Forey (1991, char. 27 in part)[97]; Forey (1998, char. 68)[12]]. Wen et al. (2013, char. 68)[54] added an additional apomorphic character-states (pointed and marked with fine striations). The order of the two apomorphic states are changed to obtain three character-states forming a morphocline.

136. **Extensive dorsal expansion of angular** [Ca]: absent (0), present (1)

137. **Angular, depth of** [new]: posterior half deeper than anterior half of angular (0), deepest at approximately at midway along the length of the angular (1), anterior half deeper than posterior half of angular (2). Cavin et al. (2020, char. 56)[101] defined a character identifying the deepest point of the angular. Two character-states were originally used: approximately midway along length of the bone (0) and near the anterior margin of the bone (1). Since the character-states were primarily defined in order to reflect a difference among derived coelacanths (mainly *Mawsonia* and *Axelrodichthys*), we used another state as "posterior half deeper than anterior half of angular" which is herein considered as the plesiomorphic state because it is observed among basal coelacanths. The three character-states form a morphocline. Character 137 is linked to character 136.

138. **Angular with dentary and splenial, contact of** [new]: linear (0), broad V-shaped (1), fine tapering (2), W-shaped (3), interdigitate (4). Character 138 is linked to characters 111 and 132.

139. **Surangular** [Ca]: present (0), absent (1)

140. **Retroarticular and articular** [Fa25, Fb53, C53, F&C53, Y53, G53, W53, W&W53, Da53, Z53, GR53, WE53, CAa53, C&G53, A&S53, G&C53, Db53, CAb53, R&S53, T53]: coossified (0), separated (1)

141. **Jaw articulation** [new]: anterior to anterior level of operculum (0), posterior to anterior level of operculum (1)

142. **Submandibulars** [Ca, FR71]: absent (0), present (1)

143. **Internasal pits** [FR91]: absent (0), one large pit (1), shallow pits with midline ridge (2), deep pear-shaped pits (3)

144.   Vomers, contact of [Fb81, C81, F&C81, FR77, Y81, G81, W81, W&W81, Da81, Z81, GR81, WE81, CAa81, C&G81, A&S81, G&C81, Db81, CAb81, R&S81, T81]: not meeting in midline (0), meeting medially (1)

145.   Vomerine fangs [FR78]: absent (0), present (1)

146.   Parasphenoid, shape of [L&Z12]: small lozenge shaped (0), broad splint shaped (1)

147.   Parasphenoid, shape of [new]: margin close to parallel or subparallel (0), flared anteriorly (1). Character 147 reflects the broadening of the anterior part of the parasphenoid as spatulate lateral expansion.

148.   Parasphenoid denticle field [Ca34, Cb34, FR169 modified]: denticule field not expanding anterolaterally (0), denticule field expanding anterolaterally (1). Friedman (2007, char. 169)[98] defined a character as the absence or presence of "denticle field of parasphenoid with anteriorly divergent lateral margins." This character reflects if the denticles covered the anterolateral margins of the parasphenoid that flare anteriorly (character 147).

149.   Parasphenoid denticle field [new]: ending at or anterior to level of foramina for internal carotid arteries (0), extending posterior to internal carotid foramina (1)

150.   Parasphenoid [Fa3, Fb61, C79, F&C79, Y79, G79, W79, W&W79, Da79, Z79, GR79, WE79, CAa79, C&G79, A&S79, G&C79, Db79, CAb79, R&S79, CAc39, CAd39, T79]: without ascending laminae anteriorly (0), with ascending laminae anteriorly (1). The anterolateral ascending laminae of the parasphenoid are known in *Macropoma* and *Latimeria* (Forey, 1998)[12]. They also have been referred to as the "prominent lateral wing" (Forey, 1998)[12].

151.   Buccohypophysial canal [Ca35, Cb35, Fa4 polarity, Fb78 polarity, C78 polarity, F&C78 polarity, Y78 polarity, G78, W78, W&W78, Da78 polarity, Z78 polarity, GR78 polarity, WE78 polarity, CAa78 polarity, C&G78 polarity, A&S78 polarity, G&C78 polarity, Db78 polarity, CAb78 polarity, R&S78 polarity, T78 polarity]: open (0), close (1). Khonsari et al. (2013)[107] addressed specifically the evolution of the buccohypophysial foramen with a special interest to coelacanths.

152.   Entopterygoid, shape of [new]: elongated (0), triangular (1)

153.   Ventral swelling of palatoquadrate [Da110, CAa110, C&G110, CAb110, R&S110, CAc47, CAd47, T110]: absent (0), present (1). Dutel et al. (2012, fig. 20)[60] illustrated the ventral swelling of the palatoquadrate (their character 110) as a process located on the ventrolateral margin of the entopterygoid seen in *Latimeria*. According to Dutel et al. (2012)[60], the swelling is only observed in *Holophagus, Latimeria, Libys, Macropoma, Megalocoelacanthus,* and *Undina*. Toriño et al. (2021, p. 14 SI)[14] discussed various codings that have been used in Fragoso's (2014)[108] analysis, and maintained Dutel et al.`s coding.

154.   Linear subparallel ridges of remodeled denticles on dermal bones lining the oral cavity [FR161]: absent (0), present (1). Friedman (2007, char. 161)[98] recognized that a shagreen of denticles is the plesiomorphic conditions in osteichthyans, whereas actinistians share denticles remodeled into long ridges on the oral surface of dermal bones (including the entopterygoids).

155.   Nasal capsule, shape of [new]: round or triangular shaped (0), deep and elongate (1)

156. **Olfactory tracts** [new]: short diverging at the level or anterior to the ethmoid process (0), long diverging posterior to the level of the ethmoid process (closer to the optic foramen) (1)

157. **Hypophysial fossa** [new]: extending posterior to the orbit (0), extending at the level of the orbit or anterior to the orbit (1)

158. **Hypophysial fossa posterior lobe** [new]: absent (0), present (1)

159. **Fenestra ventralis** [FR93 in part, L&Z11]: absent (0), present (1). Zhu & Yu (2002, char. 107)[84] and Friedman (2007, char. 93)[98] used the presence of the fenestra ventralis (or ventrolateralis) as well as the common ventral fenestra for anterior and posterior nostrils to investigate sarcopterygian interrelationships.

160. **Tectum orbitale, size of** [new]: narrow (0), extensive (1)

161. **Ethmoid articulation for palatoquadrate** [FR172]: placed on postnasal wall (0), majority of facet located anterior to postnasal wall (1). Friedman (2007, char. 172)[98] originally used this character by including two apomorphic states. Herein, we are solely using one of the two character-states that is relevant with the taxa analyzed. Actinistians are characterized by greatly expanded depressions marking the ethmoid articulation between the palatoquadrate and the neurocranium (Friedman, 2007)[98].

162. **Eye stalk or unfinished area for similar structure** [FR95 polarity]: present (0), absent (1). Zhu & Yu (2002, char. 109)[84] and Friedman (2007, char. 95)[98] used this character with a different polarity.

163. **Foramen for oculomotor nerve (III) relative, position of** [new]: dorsal and near the optic nerve (II) foramen (0), posterior and at the same height as the optic nerve (II) foramen (1)

164. **Foramen for the facial nerve (VII) relative, position of** [new]: same level as the anterior tip of the processus connectens (0), dorsal to the anterior tip of the processus connectens (1)

165. **Basipterygoid process** [Ca36, Cb36, Fb72 polarity, C72 polarity, F&C72 polarity, Y72 polarity, G72, W72, W&W72, Da72 polarity, Z72 polarity, GR72 polarity, WE72 polarity, CAa72, C&G72 polarity, A&S72 polarity, G&C72 polarity, Db72 polarity, CAb72 polarity, R&S72 polarity, T72 polarity]: present (0), absent (1)

166. **Basipterygoid process, size of** [Fa2]: small knob-like process (0), developed as a broad platform (1). Character 166 is linked with character 165.

167. **Basipterygoid process articular facet** [new]: facing posteriorly (0), facing anteriorly (1). Character 167 is linked with character 165.

168. **Intracranial joint relative to cranial nerves, position of** [new]: through profundus foramen (0), through or behind trigeminal (V) foramen (1)

169. **Vagus nerve (X)** [Fa8]: not bone enclosed (0), bone enclosed (1)

170. **Processus connectens, size of** [new]: knob like not well developed (0), long and well developed (1)

171.   **Vestibular fontanelle** [FR180]: absent (0), present (1). The vestibular fontanelle is a large basicranial fenestra located ventrally to the notochord and that opens into the saccular region of the inner ear. The fenestra ovalis present in tetrapods is derived from the vestibular fontanelle (Clack, 1994)[109].

172.   **Posttemporal fossae** [FR103]: absent (0), present (1)

173.   **Orbitosphenoid and basisphenoid regions** [Fb69, C69, F&C69, Y69, G69, W69, W&W69, Da69, Z69, GR69, WE69, CAa69, C&G69, A&S69, G&C69, Db69, CAb69, R&S69, T69]: coossified (0), separate (1)

174.   **Basisphenoid** [Fb70, C70, F&C70, Y70, G70, W70, W&W70, Da70, Z70, GR70, WE70, CAa70, C&G70, A&S70, G&C70, Db70, CAb70, R&S70, T70]: extending forward to enclose optic foramen (0), optic foramen lying within separate interorbital ossification or cartilage (1). Forey (1998, char. 70)[12] defined a character as the basisphenoid extending forward to enclose the optic foramen (0) or the optic foramen lying within separate interorbital ossification or cartilage (1). Toriño et al. (2021, char. 70)[14] rather used the character relative to the optic foramen which is either enclosed by the basisphenoid extending forward (0) or lying within separate interorbital ossification or cartilage (1). Herein, the character concerns two conditions for the basisphenoid: extending forward to enclose the optic foramen (0) and optic foramen lying within separate interorbital ossification or cartilage (1).

175.   **Basisphenoid base of the lateral wings** [new]: broad (0), constricted (1)

176.   **Processus connectens** [Fb71 polarity, C71 polarity, F&C71 polarity, Y71 polarity, G71 polarity, W71 polarity, W&W71 polarity, Da71 polarity, Z71 polarity, GR71 polarity, WE71 polarity, CAa71 polarity, C&G71 polarity, A&S71 polarity, G&C71 polarity, Db71 polarity, CAb71 polarity, R&S71 polarity, T71 polarity]: not meeting the parasphenoid (0), meeting the parasphenoid (1). Forey (1998, char. 71)[12] considered the processus connectens meeting the parasphenoid as the plesiomorphic state, whereas a processus connectens failing to meet the parasphenoid as the apomorphic state. Cavin & Grădinaru (2014, char. 71)[37] and Toriño et al. (2021, char. 71)[14] mentioned that the original formulation given by Forey (1998, char. 71)[12] is opposite to the character coding observed in Forey's matrix. Cavin & Grădinaru (2014)[37] inverted the original character-states. Therefore, we are using the character-states.

177.   **Antotic process** [new]: absent (0), present (1)

178.   **Antotic process** [Fb73, C73, F&C73, Y73, G73, W73, W&W73, Da73, Z73, GR73, WE73, CAa73, C&G73, A&S73, G&C73, Db73, CAb73, R&S73, T73]: not covered by parietal descending process (0), covered by parietal descending process (1). Character 178 is linked with character 177 (antotic process) and character 31 (descending process of parietal).

179.   **Temporal excavation** [Fb74, C74, F&C74, Y74, G74, W74, W&W74, Da74, Z74, GR74, WE74, CAa74, C&G74, A&S74, G&C74, Db74, CAb74, R&S74, CAc38, CAd38, T74]: lined with bone (0), not lined with bone (1). The prootic presents two roughened areas: an anterior one, the prefacial eminence, that is sutured on the inner side with the postparietal descending (ventral) process, and a posterior one suturing with the tabular descending (ventral) process. The temporal excavation is located between these two areas. Forey (1998, char. 74)[12] defined two character-states for the condition of the temporal excavation (or temporal fossa): lined with bone and not lined with bone. In his list of characters, Forey (1998, p. 192)[12] coded this temporal excavation as lined with bone (1) and not lined with bone (0). Toriño et al. (2021, char. 74)[14] used "0" for lined with bone and "1" for not lined.

180. **Otic region** [new]: mainly ossified (0), mainly cartilaginous (1)

181. **Well-developed posterolateral otic process** [new]: absent (0), present (1)

182. **Jugular process** [new]: absent (0), present (1)

183. **Accessory jugular processes** [new]: absent (0), present (1)

184. **Otico-occipital** [Fa5, Fb75, C75, F&C75, Y75, G75, W75, W&W75, Da75, Z75, GR75, WE75, CAa75, C&G75, A&S75, G&C75, Db75, CAb75, R&S75, T75]: solid (0), separated to prootic and opisthotic (1)

185. **Otico-occipital** [new]: not hypertrophied (0), hypertrophied (1). Cavin et al. (2017)[41] mentioned that the condition of the otico-occipital in *Foreyia* was hypertrophied in comparison to the generalized coelacanth Bauplan. It is suggested that in *Foreyia* that the postparietal, supratemporal (or tabular) and extrascapulars are all fused together. Not only the otico-occipital part of the skull roof forms a single ossified component, but this component is larger than in other coelacanths.

186. **Supraoccipital** [Fb76, C76, F&C76, Y76, G76, W76, W&W76, Da76, Z76, GR76, WE76, CAa76, C&G76, A&S76, G&C76, Db76, CAb76, R&S76, T76]: absent (0), present (1)

187. **Vestibular fontanelle accessory fenestration of otic capsule, size of** [Fb77, C77, F&C77, FR181, Y77, G77, L&Z14, W77, W&W77, Da77 homology, Z77, GR77, WE77, CAa77, C&G77 homology, A&S77 homology, G&C77, Db77, CAb77 homology, R&S77 homology, T77 homology]: small (0), large (1). Forey (1998, char. 77)[12] and subsequent analyses [up to Toriño et al. (2021, char. 80)[14]] coded for the presence or absence of the vestibular fontanelle. Herein, we are redefining the vestibular fontanelle character in terms of its size. We considered a vestibular fontanelle to be large if it occupies 33% or more of the length of the otico-occipital region of the neurocranium; this condition is found in *Macropoma precursor* (Forey, 1998, fig. 6.10)[12]. A vestibular fontanelle is considered to be small if it occupies less than 25% of the length of the otico-occipital region of the neurocranium; this condition is seen in *Laugia groenlandica* (Forey, 1998, fig. 6.7)[12] and *Sassenia groenlandica* (Forey, 1998, fig. 6.8)[12].

188. **Suprapterygoid process** [Fb80, C80, F&C80, Y80, G80, W80, W&W80, Da80, Z80, GR80, WE80, CAa80, C&G80, A&S80, G&C80, Db80, CAb80, R&S80, T80]: absent (0), present (1)

189. **Prominent groove for the jugular vein on the prootic** [new]: present (0), absent (1)

190. **Prootic** [Fa6, Fb82, C82, F&C82, Y82, G82, W82, W&W82, Da82, Z82, GR82, WE82, CAa82, C&G82, A&S82, G&C82, Db82, CAb82, R&S82, T82]: without complex suture with basioccipital region (0), with complex suture with basioccipital region (1)

191. **Prominent ridge on prootic** [new]: present (0), absent (1). A prominent ridge on the prootic is also present in tetrapodomorphs (e.g., *Gogonasus*).

192. **Superficial ophthalmic branch of anterodorsal lateral line nerve** [Fb83, C83, F&C83, Y83, G83, W83, W&W83, Da83, Z83, GR83, WE83, CAa83, C&G83, A&S83, G&C83, Db83, CAb83, R&S83, T83]: not piercing antotic process (0), piercing antotic process (1)

193. **Process on braincase for articulation of infrapharyngobranchial 1 or epibranchial 1** [Fb84, C84, F&C84, Y84, G84, W84, W&W84, Da84, Z84, GR84, WE84, CAa84, C&G84, A&S84, G&C84, Db84, CAb84, R&S84, T84]: absent (0), present (1)

194. **Lateral ethmoids** [Fb85, C85, F&C85, Y85, G85, W85, W&W85, Da85, Z85, GR85, WE85, CAa85, C&G85, A&S85, G&C85, Db85, CAb85, R&S85, T85]: fused (0), separate (1)

195. **Basioccipital** [Fb86, C86, F&C86, Y86, G86, W86, W&W86, Da86, Z86, GR86, WE86, CAa86, C&G86, A&S86, G&C86, Db86, CAb86, R&S86, T86]: fused (0), separate (1)

196. **Dorsum sellae, size of** [Fb87, C87, F&C87, Y87, G87, W87, W&W87, Da87, Z87, GR87, WE87, CAa87, C&G87, A&S87, G&C87, Db87, CAb87, R&S87, T87]: small (0), large and constricting entrance to cranial cavity anterior to intracranial joint (1)

197. **Hypophysial fossa** [new]: with anterior lobe (0), without anterior lobe (1)

198. **Endolymphatic ducts** [new]: open posteriorly (0), open dorsally (1)

199. **Hyomandibular** [new]: ossified (0), cartilaginous (1)

200. **Hyomandibular, orientation of** [new]: almost horizontal (0), almost vertical (1)

201. **Hyomandibular proximal articular facet** [FR84, L&Z13]: single headed (0), double headed (1)

202. **Ceratohyal, size of** [new]: short and stubby (0), long and narrow (1)

203. **Anterior end of urohyal** [new]: unifid (0), bifid (1). Romano et al. (2016)[110] compared the evolutionary morphology of the urohyal among coelacanths. We based our two urohyal characters (characters 203 and 204) on the general trends reflected by this comparison (Romano et al., 2006, fig. 9)[110].

204. **Urohyal, shaft of** [new]: narrow (0), broad (1)

205. **Basibranchial anterior one, shape of** [new]: pointed lateral margins (0), parallel lateral margins (1)

206. **Basibranchial, number of** [new]: two (0), one (1)

207. **Ceratobranchials, shape of** [new]: straight to weakly curved (0), strongly curved (1)

208. **Ceratobranchials, shape of** [new]: expanded distally (0), same width along length (1), expanded proximally (2). The three character-states form a morphocline.

209. **Epibranchials, shape of** [new]: elongate and rod like (0), short and flat (1)

210. **Anocleithrum** [new]: subdermal (0), dermal (1)

211. **Anocleithrum, shape of** [Fb89, C89, F&C89, Y89, G89, W89, W&W89, Da89, Z89, GR89, WE89, CAa89, C&G89, A&S89, G&C89, Db89, CAb89, R&S89, CAc40, CAd40, T89]: ovoid (0), sigmoid (1), forked (2), broad plate like (3), triangular (4). Forey (1998, char. 89)[12] and subsequent

analyses [up to Toriño et al. (2021, char. 89)[14] used solely two shapes [simple (0) and forked (1)] to describe the disparity of the shape of the anocleithrum. We are defining the plesiomorphic shape as ovoid as could be observed in the outgroup *Onychodus jandemarrai* (Andrews et al., 2006, figs. 5b, 21c-e)[4] and *Miguashaia bureaui* (Cloutier, 1996, figs. 13A-B, 14C)[61]. Three apomorphic states are used to cover the disparity of anocleithral shape among coelacanths: sigmoid (1; e.g., *Allenypterus montanus*, *Hadronector donbairdi*), forked (2; e.g., *Caridosuctor populosum*), broad plate-like (3; e.g., *Rhabdoderma elegans*), and triangular (4; e.g., *Coccoderma suevicum*).

212. **Anocleithrum, position of** [new]: at dorsal end of cleithrum (0), at midpoint of cleithrum (1)

213. **Cleithrum** [new]: not covered anteriorly by operculum (0), covered anteriorly by operculum (1)

214. **Dorsal end of cleithrum, shape of** [FR107]: pointed (0), broad and rounded (1)

215. **Cleithrum, articulation of** [Ca39, Cb39]: cleithrum articulates externally with extracleithrum only (0), cleithrum articulates externally with extracleithrum and clavicle (1). Character 215 is linked with character 216.

216. **Extracleithrum** [Ca40, Cb40, Fb88, C88, F&C88, Y88, G88, W88, W&W88, Da88, Z88, GR88, WE88, CAa88, C&G88, A&S88, G&C88, Db88, CAb88, R&S88, T88]: absent (0), present (1)

217. **Extracleithrum** [new]: without anteroventral canal (0), with anteroventral canal (1). Character 217 is linked with character 216.

218. **Extracleithrum and clavicle, dorsal extent of** [new]: extracleithrum extends more dorsally than clavicle (0), extracleithrum and clavicle extend dorsally approximately at the same level (1), clavicle extends more dorsally than the extracleithrum (2). This character is not polarized based on out-group comparison because the out-groups do not have an extracleithrum. However, in basal actinistians both elements extend approximately at the same level (e.g., *Miguashaia bureaui*) or the clavicle extends slightly more dorsally than the extracleithrum (e.g., *Miguashaia grossi*). The three character-states form a morphocline. Character 218 is linked with character 216.

219. **Cleithrum and clavicle** [new]: not forming a prominent postbranchial lamina (0), forming a prominent postbranchial lamina (1)

220. **Clavicle** [new]: not hypertrophied (0), hypertrophied (1). The clavicle is considered to be hypertrophied to take into account the condition in *Foreyia maxkuhni* (Cavin et al., 2017, figs. 1A-C, 2A-B)[41]. With the exception of the postparietal shield, the clavicle is the largest element in *Foreyia*; it is approximately twice the size of the operculum, and represents approximately a fourth of the size of the head.

221. **Facet posterior to glenoid** [new]: absent (0), present (1)

222. **Pectoral lepidotrichia** [Fb99 in part, C99 in part, F&C99 in part, Y99 in part, G99 in part, W99 in part, W&W99 in part, Da99 in part, Z99 in part, GR99 in part, WE99 in part, CAa99 in part, C&G99 in part, A&S99 in part, G&C99 in part, Db99 in part, CAb99 in part, R&S99 in part, T99 in part]: not expanded (0), expanded (1). Forey (1998, char. 99)[12] described the paired fin lepidotrichia either as not expanded or expanded. Four actinistian genera (i.e., *Laugia*, *Coccoderma*, *Holophagus*, and *Libys*) were coded as having expanded paired fin lepidotrichia. However, two different conditions are covered by the expression, expanded lepidotrichia: (1) in *Libys* and *Holophagus*, the pectoral lepidotrichia are broad and relatively longer than in comparative species and (2) in *Laugia* and *Coccoderma*, the pelvic

lepidotrichia are disproportionately long. We are splitting the original expanded condition into two characters to reflect the disparity. Character 222 takes into account solely the condition of the pectoral lepidotrichia.

223. **Pelvic lepidotrichia** [Fb99 in part, C99 in part, F&C99 in part, Y99 in part, G99 in part, W99 in part, W&W99 in part, Da99 in part, Z99 in part, GR99 in part, WE99 in part, CAa99 in part, C&G99 in part, A&S99 in part, G&C99 in part, Db99 in part, CAb99 in part, R&S99 in part, T99 in part]: not expanded (0), expanded (1). Forey (1998, char. 99)[12] described the paired fin lepidotrichia either as not expanded or expanded. Four actinistian genera (i.e., *Laugia*, *Coccoderma*, *Holophagus*, and *Libys*) were coded as having expanded paired fin lepidotrichia. However, two different conditions are covered by the expression, expanded lepidotrichia: (1) in *Libys* and *Holophagus*, the pectoral lepidotrichia are broad and relatively longer than in comparative species and (2) in *Laugia* and *Coccoderma*, the pelvic lepidotrichia are disproportionately long. We are splitting the original expanded condition into two characters to reflect the disparity. Character 223 takes into account solely the condition of the pelvic lepidotrichia.

224. **Pelvic fins, position of** [Ca43, Cb43 and 71, Fa51, Fb100 polarity, C100 polarity, F&C100 polarity, Y100 polarity, G100 polarity, W100 polarity, W&W100 polarity, Da100 polarity, Z100 polarity, GR100, WE100, CAa100, C&G100 polarity, A&S100 polarity, G&C100 polarity, Db100 polarity, CAb100 polarity, R&S100 polarity, T100 polarity]: anterior to level of D1 (0), between level of D1 and D2 (1), posterior to level of D2 (2). The three character-states form a morphocline. The order of character-states has been changed from the original description of the character (Cloutier, 1991a,b, char. 43[95,96]; Forey, 1991, char. 51[97]; Forey, 1998, char. 100[12]).

225. **Pelvic bones on each side** [Fb108, C108, F&C108, Y108, G108, W108, W&W108, Da108, Z108, GR108, WE108, CAa108, C&G108, A&S108, G&C108, Db108, CAb108, R&S108, T108]: separate (0), fused in midline (1)

226. **Anterior process(es) of pelvic plate** [new]: single (0), forked (1). Schaeffer (1941)[111] revised morphology of the pelvic plates in seven coelacanth taxa. The morphology of the pelvic plate was described in terms of three components of the pelvic plates: the anterior division, the posterior division and the medial process. We considered that the "anterior division" is composed between one to three processes: the anteromedial, the anterolateral and the lateral processes. The "posterior division" includes the posterior process; occasionally the lateral process seems to be coalescent with the posterior process. The presence of the anterior processes of the pelvic girdle refers to the presence of the anteromedial and anterolateral processes. If a single anterior process is present (e.g., *Changxingia*, *Libys*) it is assumed that it corresponds generally to the anteromedial process. The forked condition corresponds to the clear presence of an anterior bifurcation, most likely corresponding to the presence of both the anteromedial and anterolateral processes.

227. **Anterior processes of pelvic plate relative, length of** [new]: anteromedial process longer than anterolateral process (0), anteromedial and anterolateral processes approximately the same length (1), anteromedial process shorter than anterolateral process (2). The presence of the anterior processes of the pelvic girdle refers to the presence of the anteromedial and anterolateral processes; character 227 is linked with the forked condition of character 226. These processes correspond in part to the anterior division of the pelvic girdle mentioned by Schaeffer (1941)[111]. The three character-states are organized into a morphocline reflecting the relative length of the anteromedial and anterolateral processes.

228. **Medial process of pelvic plate** [new]: absent (or cartilaginous) (0), present (1)

229. **Lateral process of pelvic plate** [new]: absent (or cartilaginous) (0), present (1)

230.   **Posterior process of pelvic plate** [new]: absent or not clearly differentiated from the main corpus of the pelvic girdle or from the lateral process (0), clearly differentiated as a spatulated process from the main corpus of the pelvic girdle (1)

231.   **Distal radials of basal plates** [Ca]: present (0), absent (1)

232.   **D1 basal plate, ventral margin of** [Ca45, Cb45, Fb101, C101, F&C101, Y101, G101, W101, W&W101, Da101, Z101, GR101, WE101, CAa101, C&G101, A&S101, G&C101, Db101, CAb101, R&S101, T101]: smooth (0), emarginated and accommodating the tips of adjacent neural spines (1)

233.   **D1 basal plate, shape of** [Cb73]: hemispherical or ovoid (0), triangular (1), trapezoidal or pentagonal (2). Schaeffer (1941)[111] reported that in most coelacanth genera the basal plate of the first dorsal fin is triangular with the apex directed anteriorly.

234.   **D1 lepidotrichia** [Cb72, Fa49, Fb98, C98, F&C98, Y98, G98, W98, W&W98, Da98, Z98, GR98, WE98, CAa98, C&G98, A&S98, G&C98, Db98, CAb98, R&S98, CAc43, CAd43, T98]: without denticles (0), with denticles (1)

235.   **D1 lepidotrichia** [new]: same width as the lepidotrichia of the second dorsal and anal fins (0), substantially stouter than the second dorsal and anal fins (1). We considered a lepidotrichia to be substantially stouter when it is from two to three times broader than the lepidotrichia of the second dorsal and anal fins. Occasionally the caudal lepidotrichia could also be as stout as those of the first dorsal fin. This condition is clearly visible in *Undina penicillata* (see Arratia et al., 2001, fig. 31)[112], *Whiteia oishii* (Yabumoto & Brito, 2016, fig. 2b)[92], *Ticinepomis peyeri* (Cavin et al., 2013, fig. 4)[87].

236.   **D2 fin** [G&C113]: without a lobe (0), with a lobe (1)

237.   **D2 basal plate, shape of** [Fb102, C102, F&C102, Y102, G102, W102, W&W102, Da102, Z102, GR102, WE102, CAa102, C&G102, A&S102, G&C102, Db102, CAb102, R&S102, T102]: single anterior process (0), forked anteriorly (1)

238.   **Anterodorsal process of D2 basal plate** [Ca46, Cb46]: absent (0), present (1). Character 238 is linked with character 237.

239.   **Anterodorsal process of D2 basal plate** [new]: narrow on all the length of the process (0), expanded by a dorsal flange on most of the length of the process (1). Character 239 is linked with character 238.

240.   **Anterodorsal process of D2 basal plate, relative size of** [new]: short and stubbier than the anteroventral process of D2 basal plate (0), similar in length and height to anteroventral process of D2 basal plate (1), longer than anteroventral process of D2 basal plate (2). The three character-states form a morphocline in terms of the relative size of the anterodorsal and anteroventral processes of the D2 basal plate. Character 240 is linked with characters 237 and 238.

241.   **Posteroventral process of D2 basal plate** [Ca47, Cb47]: absent (0), present (1)

242.   **Posteroventral process of D2 basal plate** [Ca48, Cb48]: poorly developed (0), well developed (1). Character 242 is linked with character 241.

243. **Anal fin** [G&C112 polarity]: with a lobe (0), without a lobe (1)

244. **Anal fin basal plate** [new]: lacking processes (0), with processes (1)

245. **Anal fin basal plate** [Ca49, Cb49]: single process (0), bifurcated process (1). Character 245 is linked with character 244.

246. **Anterodorsal process of anal fin basal plate** [Ca50, Cb50]: short and broad (0), long and narrow (1). Character 246 is linked with character 244.

247. **Median fin lepidotrichia** [Cb75, Fa51, Fb103, C103, F&C103, Y103, G103, W103, W&W103, Da103, Z103, GR103, WE103, CAa103, C&G103, A&S103, G&C103, Db103, CAb103, R&S103, T103]: not expanded (0), expanded (1)

248. **Caudal fin** [Ca51, Cb51, Fa45 in part, Fb93 in part, C93 in part, F&C93 in part, Y93 in part, G93, W93, W&W93, Da93 in part, Z93 in part, GR93 in part, WE93 in part, CAa93 in part, C&G93 in part, A&S93 in part, G&C93 in part, Db93 in part, CAb93 in part, R&S93 in part, T93 in part]: heterocercal (0), diphycercal (1), triphycercal (2)

249. **Epichordal and hypochordal lobes of caudal fin** [new]: convex (0), concave (1), pointed (2). The convex, concave and pointed conditions only apply to the diphycercal and triphycercal conditions of character 248. The posterior profile of the caudal fin of actinistians varies among taxa. Three character-states are defined based on the curvature provided by the distal extremities of epichordal and hypochordal lepidotrichia of the caudal fin excluding the supplementary lobe. The caudal fin could either be convex (i.e., rounded curvature outward; e.g., *Latimeria*, *Caridosuctor*, *Diplurus*), concave (i.e., rounded curvature inward; e.g., *Rebellatrix*) or pointed (e.g., *Allenypterus*, *Holopterygius*). This character does not apply for actinistians having an heterocercal caudal fin (e.g., *Miguashaia*, *Gavinia*). Character 249 is linked to character 248.

250. **Caudal lobes** [Fa46, Fb97, C97, F&C97, Y97, G97, W97, W&W97, Da97, Z97, GR97, WE97, CAa97, C&G97, A&S97, G&C97, Db97, CAb97, R&S97, T97]: symmetrical (0), asymmetrical (1). The distinction between symmetrical and asymmetrical dorsal and ventral lobes of the caudal fin was not clarified by Forey (1998, char. 97)[12]. Generally, the ventral lobe bears 1 or 2 lepidotrichia less than the dorsal lobe. We considered a condition with a difference of up to two lepidotrichia as symmetrical.

251. **Epichordal lobe of caudal fin** [new]: starting posterior to mid-total length (0), starting anterior to mid-total length (1)

252. **Caudal fin supplementary lobe** [Ca52, Cb52, Fa45 in part]: absent (0), present (1). Character 252 is linked with the triphycercal condition of Character 248.

253. **Caudal fin lepidotrichia** [new]: without denticules (0), with denticules (1)

254. **Caudal fin lepidotrichia** [Ca53, Cb53, Fa47, Fb94, C94, F&C94, Y94, G94, W94, W&W94, Da94, Z94, GR94, WE94, CAa94, C&G94, A&S94, G&C94, Db94, CAb94, R&S94, T94]: more numerous than radials (0), equal in number with radials (1)

255. **Lepidotrichia** [Ca54, Cb54, Fa48, Fb95, C95, F&C95, Y95, G95, W95, W&W95, Da95, Z95, GR95, WE95, CAa95, C&G95, A&S95, G&C95, Db95, CAb95, R&S95, T95]: branched (0), unbranched (1)

256. Lepidotrichial segments [FR187]: without interlocking flanges (0), with interlocking flanges (1). The interlocking articulation pattern of lepidotrichial segments has been originally described for *Miguashaia bureaui* by Cloutier (1996, fig. 16)[61].

257. Vertebrae, alignment of [new]: linear above abdominal cavity (0), strongly arched above abdominal cavity (1)

258. Supraneural [FR125]: presence of "supraneurals" along most of the abdominal-thoracic region of the axial skeleton (0), presence of "supraneurals" limited to 1-5 vertebrae located anteriorly to the insertion of the epichordal lobe of the caudal fin (1), absence of "supraneurals" anteriorly to the insertion of the epichordal lobe of the caudal fin (2). According to Arratia et al. (2001)[112], "supraneurals" are independent, median, elongate, rod-like bones that articulate proximally with the neural spine and distally with the dorsal radial [...], or lack articulation distally with another bone [...]." Arratia et al. (2001)[112] illustrated 'supraneurals' located distally to the neural spines found anteriorly to the insertion of the epichordal lobe of the caudal fin in *Diplurus* (Arratia et al., 2001, fig. 30)[112] and *Undina penicillata* (Arratia et al., 2001, fig. 31)[112]. They mentioned that the caudal fin of *Laugia*, *Diplurus*, and *Holophagus* (likely *Undina*), among others, begins with two or three 'supraneurals'. Friedman (2007, char. 125)[98] considered the presence of supraneural spines (herein referred to as "supraneurals") for the thoracic and abdominal vertebrae [Char. 125(0)] or the absence of such elements or its presence only at the anterior end of the vertebral column [Char. 125(1)]. Herein, we considered the presence or absence of supraneural associated to the vertebrae located anteriorly to the insertion of the caudal fin. Three character-states are recognized: presence of 'supraneurals' along most of the abdominal-thoracic region of the axial skeleton (0), presence of 'supraneurals' limited to 1-5 vertebrae located anterior to the insertion of the epichordal lobe of the caudal fin (1), and absence of 'supraneurals' anteriorly to the insertion of the epichordal lobe of the caudal fin (3). The three character-states form a morphocline.

259. Neural spines [new]: abutting one another (0), not abutting (1)

260. Cervical neural arches, shape of [Fa53, Fb91, C91, F&C91, Y91, G91, W91, W&W91, Da91, Z91, GR91, WE91, CAa91, C&G91, A&S91, G&C91, Db91, CAb91, R&S91, T91]: not expanded (0), expanded (1)

261. Haemal spines [Fb90, C90, F&C90, Y90, G90, W90, W&W90, Da90, Z90, GR90, WE90, CAa90, C&G90, A&S90, G&C90, Db90, CAb90, R&S90, T90]: abutting one another (0), not abutting (1). Forey (1998, char. 90)[12] considered that the plesiomorphic condition was when the posterior neural and haemal spines were abutting with each other as seen in *Miguashaia* and *Diplocercides*; polarized based on the porolepiform condition. It is clearer to mention that the contact between adjacent neural and haemal spines is on the totality of their length. This clarification is given because adjacent spines could abut proximally just dorsal to the arches. In species for which the haemal and neural spines are abutting, the spines are broad on most of their length and the extremities are less club-shaped the remaining actinistian species. We redefined the character to take into account solely the haemal spines because character 259 takes into account the condition of the neural spines.

262. Ossified ribs [Cb69, Fa52, Fb92, C92, F&C92, Y92, G92, W92, W&W92, Da92, Z92, GR92, WE92, CAa92, C&G92, A&S92, G&C92, Db92, CAb92, R&S92, CAc44, CAd44, T92]: absent (0), present (1). Lambers (1992)[31] mentioned that the presence of pleural ribs is rare in coelacanths. Since 1992, a few species with anatomical structures identified as ossified ribs are fairly common. Cloutier (1991b, char. 69)[96] coded for the presence of pleural ribs, whereas Forey (1991, char. 52)[97] coded for the presence of "long, ossified ribs". Lambers (1992, p. 43)[31] suggested that this character should be

coded as three character-states: absence of ossified ribs (0), presence of small, rudimentary ribs (1; as in *Libys* and *Undina*) and large ossified ribs (2; as in *Diplurus*).

263. **Scale ornament** [Fa54, Fb104, C104, F&C104, Y104, G104, W104, W&W104, Da104, Z104, GR104, WE104, CAa104, C&G104, A&S104, G&C104, Db104, CAb104, R&S104, CAc44, CAd44, T104]: not differentiated (0), differentiated (1). Forey (1991, char. 54)[97] first defined this character. He mentioned that the plesiomorphic condition corresponds to a scale with a dense covering of uniform tubercles and/or ridges. The apomorphic condition (i.e., differentiated) as originally defined, corresponds to a scale where "the central tubercles are very much enlarged, hollow and surrounded by much smaller tubercles." Mondéjar-Fernàndez et al. (2021)[113] reviewed scale ornament for all coelacanth species.

264. **Scale ornament** [Fa56 in part, Fb106, C106, F&C106, Y106, G106, W106, W&W106, Da106, Z106, GR106, WE106, CAa106, C&G106, A&S106, G&C106, Db106, CAb106, R&S106, CAc45, CAd45, T106]: longitudinal ridges and tubercules (0), only longitudinal ridges (1), only tubercules (2). Forey (1998, char. 106)[12] defined two character-states to take into account the condition of scale ornament: ridges or tubercles (0) and rugose (1). Since most of the disparity among coelacanths comes from the presence or absence of ridges and tubercles, we used three character-states to describe these conditions. Only three taxa were coded as having rugose ornament (i.e., *Mawsonia*, *Axelrodichthys*, and *Guizhoucoelacanthus*) by Toriño et al. (2021, char. 106)[14]. Mondéjar-Fernàndez et al. (2021, table 1)[113] summarized the type of ornament on the exposed area of the external surface of the scales for numerous coelacanth species.

265. **Scale inner surface** [new]: without bumps (0), with bumps (1). Cloutier (1996, fig. 17D)[61] and Mondéjar-Fernàndez et al. (2021, fig. 2)[113] figured and described the presence of small circular bumps on the inner surface of the scales of *Miguashaia bureaui*.

266. **Lateral line pores per scale** [Ca2, Cb2, Fa55 polarity, Fb105, C105, F&C105, Y105, G105, W105, W&W105, Da105, Z105, GR105, WE105, CAa105, C&G105, A&S105, G&C105, Db105, CAb105, R&S105, T105]: single (0), multiple (1)

267. **Ventral keel scales** [F&C109, G109, W109, W&W109, Da109, Z109, GR109, WE109, CAa109, C&G109, A&S109, G&C109, Db109, CAb109, R&S109, T109]: absent (0), present (1). Friedman & Coates (2006, char. 109)[47] used the absence or presence of ventral keel scales. They coded the presence of ventral keel scales in *Allenypterus* and *Holopterygius*; a polymorphic state was coded for the actinopterygian out-group.

268. **Lung** [Fb107, C107, F&C107, Y107, G107, W107, W&W107, Da107, Z107, GR107, WE107, CAa107, C&G107, A&S107, G&C107, Db107, CAb107, R&S107, CAc46, CAd46, T107]: not ossified (0), ossified (1). Forey (1998, char. 107)[12] referred to the condition of the swimbladder rather than the condition of the lung (Cavin et al., 2019, char. 46)[100]. Brito et al. (2010)[114] and Cupello et al. (2017)[115] investigated the structure identified as the calcified lungs in actinistians and more specifically that of *Axelrodichthys*. These structures have been identified in the literature also as ossified bladders. The ossified organ is located in a ventral position relative to the gut. One as to be aware that the outer wall of the spiral intestine and stomach of *Latimeria* also shows a higher density than surrounding tissues in CT-scan (Schultze & Cloutier, 1991)[116].

1b.ii. Meristic characters

The list of 14 meristic characters provides the reference to character numbers used in previous publications: Ca, Cloutier (1991a)[95], Cb, Cloutier (1991b)[96], Fa, Forey (1991)[97], Fb, Forey (1998)[12], C, Clément (2005)[86], F&C,

Friedman & Coates (2006)[47], Y, Yabumoto (2008)[66], G, Geng et al. (2009)[45], W, Wendruff (2011)[91], W&W, Wendruff & Wilson (2012)[70], Da, Dutel et al. (2012)[60], Z, Zhu et al. (2012)[40], GR, Graf (2012)[71], WE, Wen et al. (2013)[54], CAa, Cavin et al. (2013)[87], C&G, Cavin & Grădinaru (2014)[37], A&S, Arratia & Schultze (2015)[15], G&C, Gess & Coates (2015)[78], Db, Dutel et al. (2015)[99], CAb, Cavin et al. (2017)[41], R&S, Renesto & Stockar (2018)[1], CAc, Cavin et al. (2019)[100], CAd, Cavin et al. (2020)[101], T, Toriño et al. (2021)[14]. Most of the meristic characters have been remove from the discrete matrix to constitute the meristic matrix.

(1) **Number of premaxillae** [Ca4 in part, Cb4 in part, Fb4 in part, C4 in part, F&C4 in part, Y4 in part, G4 in part, W4 in part, W&W4 in part, Da4 in part, Z4 in part, GR4 in part, WE4 in part, CAa4 in part, C&G4 in part, A&S4 in part, G&C4 in part, Db4 in part, CAb4 in part, R&S4 in part, CAc4 in part, CAd4 in part, T4 in part]

(2) **Number of extrascapulars** [Ca21 in part, Cb21 in part, Fa18 in part, Fb17 in part, C17 in part, F&C17 in part, Y17 in part, G17 in part, W17 in part, W&W17 in part, Da17 in part, Z17 in part, GR17 in part, WE17 in part, CAa17 in part, C&G17 in part, A&S17 in part, G&C17 in part, Db17 in part, CAb17 in part, R&S17 in part, CAc10 in part, CAd10 in part, T17 in part]

(3) **Number of supraorbitals** [Fa14 in part, Fb9 in part, C9 in part, F&C9 in part, Y9 in part, G9 in part, W9 in part, W&W9 in part, Da9 in part, Z9 in part, GR9 in part, WE9 in part, CAa9 in part, C&G9 in part, A&S9 in part, G&C9 in part, Db9 in part, CAb9 in part, R&S9 in part, CAc6 in part, Cad6 in part, T9 in part]

(4) **Number of preparietals per row** [Ca21 in part, Cb21 in part, Fa18 in part, Fb17 in part, C17 in part, F&C17 in part, Y17 in part, G17 in part, W17 in part, W&W17 in part, Da17 in part, Z17 in part, GR17 in part, WE17 in part, CAa17 in part, C&G17 in part, A&S17 in part, G&C17 in part, Db17 in part, CAb17 in part, R&S17 in part, CAc10 in part, CAd10 in part, T17 in part]

(5) **Number of anterior coronoids** [Fb55, C55, F&C55 modified, Y55, G55, W55, W&W55, Da55 modified, Z55 modified, GR55 modified, WE55 modified, CAa55, C&G55 modified, A&S55 modified, G&C55 modified, Db55 modified, CAb55 modified, R&S55 modified, T17 modified]

(6) **Number of neural arches** [new]

(7) **Number of pectoral fin lepidotrichia** [Cb70 in part]

(8) **Number of pelvic fin lepidotrichia** [new]

(9) **Number of D1 fin lepidotrichia** [Ca44 in part, Cb44 in part, Fb96 in part, C96 in part, F&C96 in part, Y96 in part, G96 in part, W96 in part, W&W96 in part, Da96 in part, Z96 in part, GR96 in part, WE96 in part, CAa96 in part, C&G96 in part, A&S96 in part, G&C96 in part, Db96 in part, CAb96 in part, R&S96 in part, CAc42, Cad42, T96 in part]

(10) **Number of D2 fin lepidotrichia** [Cb74 in part]

(11) **Number of anal fin lepidotrichia** [new]

(12) **Number of lepidotrichia in epichordal lobe of caudal fin** [new]

(13) **Number of triphycercal fin rays** [new]

(14) **Number of scale rows from D1 to lateral line** [new]

1b.iii. Continuous characters

We selected a total of 88 landmarks (Supplementary Fig. 3) to define 59 linear measurements to evaluate 40 continuous (morphometric) variables. We selected continuous characters to cover the general anatomy of coelacanths

and specifically some relative size (e.g., ethmoid shield length / otico-occipital shield length, lateral extrascapular width / median extrascapular width) and positions (e.g., position of first dorsal fin / body length) between elements and shape of certain elements (e.g., postparietal width / postparietal length) that have been used previously in the literature. With the exception of the total and standard lengths, we define all variables as ratios to be comparable among species which vary in terms of total length. We provide ratios in terms of four categories: (**1**) 'length *versus* length' for proportion between cranial structures and position of fins along the body; (**2**) 'width *versus* length' used as a proxy of the shape of a skull roofing element; (**3**) 'height *versus* length' used as a proxy of the shape of a cheek element; and (**4**) 'height *versus* height' for the relative position or proportion of structures. We took measurements (1) preferably on images of specimens rather than reconstructions and (2) preferably on a single specimen or a single reconstruction rather than multiple specimens. Total and standard lengths correspond to the maximum size recorded from the literature when available; if not available, we measured specimens.

We took measurements (either in mm or pixels) from images using *Fiji* (Schindelin et al., 2012)[117]. To minimize measurement error owing to the manipulator, A. M. Clement did all measurements. We identified outlayers by using either cluster analyses, regression lines and/or principal component analyses (R. Cloutier); we then retook measurements and corrected errors.

SI Table 1.1. The list of continuous characters with the distances defined by landmarks (Supplementary Fig. 3) and the ratios.

Body
Total length (Body size): [1, 2]
Standard length: [1, 8]

Skull roof
Skull length / total body length: [1, 3] / [1, 2]
Skull height / skull length (HL/HD): [19, 55] / [1, 3]
Ethmoid shield length / otico-occipital shield length: [1, 17] / [18, 19]
Ethmoid shield width / ethmoid shield length: [78, 79] / [1, 17]
Otico-occipital shield width / otico-occipital shield length: [80, 81] / [18, 19]
Orbit diameter / ethmoid shield length: [12, 13] / [1, 17]
Posteriormost preparietal length / parietal length: [15, 16] / [16, 17]
Parietal length / postparietal length: [16, 17] / [18, 19]
Postparietal width / postparietal length: [64, 65] / [18, 19]
Lateral extrascapular width / median extrascapular width: [69, 70] / [67, 68]
Median extrascapular width / median extrascapular length: [67, 68] / [19, 66]
Lateral extrascapular width / lateral extrascapular length: [69, 70] / [71, 72]

Cheek and opercular series
Preorbital length / postorbital length: [1, 12] / [13, 14]
Lacrimojugal height (at mid-length) / lacrimojugal length: [82, 83] / [20, 21]
Postorbital height / postorbital length: [22, 23] / [24, 25]
Squamosal height / squamosal length: [28, 29] / [26, 27]
Preoperculum height / preoperculum length: [32, 33] / [30, 31]
Operculum height / operculum length: [35, 36] / [34, 3]
Suboperculum height / suboperculum length: [62, 63] / [76, 77]

Urohyal
Urohyal shaft length / urohyal posterior branches length: [86, 88] / [87, 88]

Palate
Parasphenoid denticulated / Parasphenoid length: [7, 84] / [7, 85]

Mandible
Splenial length / dentary length: [47, 48] / [41, 53]
Dentary length / lower jaw length: [41, 53] / [41, 42]
Splenial length / lower jaw length: [47, 48] / [41, 42]
Angular length / lower jaw length: [43, 44] / [41, 42]
Dentary height / dentary length: [51, 52] / [41, 53]
Splenial height / splenial length: [49, 50] / [47, 48]
Angular height / angular length: [45, 46] / [43, 44]

Postcranial
Cleithrum height / extracleithrum height: [37, 38] / [39, 40]
Pectoral fin height / body height: [9, 58] / [54, 58]
Pectoral fin length / pelvic fin length: [56, 73] / [74, 75]
Position 1st dorsal fin / body length: [1, 4] / [1, 2]
D1 plate height / D1 plate length: [61, 57] / [59, 60]
Position 2nd dorsal fin / body length: [1, 5] / [1, 2]
Position of pelvic fin / body length: [1, 10] / [1, 2]
Position of anal fin / body length: [1, 11] / [1, 2]
Caudal fin length / pre-caudal length: [6, 2] / [1, 6]
Supplementary lobe length / caudal fin length: [8, 2] / [6, 2]

1c. Coding modifications from original matrices and new data

Changes of coding from previously published data and codings are specified in the following list of characters organized by taxa in alphabetical order. Changes to actual scorings for individual taxa are discussed.

List of character coding changes per taxon from original matrices of Forey (1998)[12] and Toriño et al. (2021)[14] with justifications. More than 300 changes have been made to original matrices for 86 taxa (excluding observations on *Ngamugawi*). These changes correspond to either (1) original miscoding, (2) unused information published at the time the matrix was compiled, (3) newly published information, (4) new observation on original material, or (5) transcription error from matrix to matrix.

Institutional abbreviations: **AMNH**, American Museum of Natural History, New York, New York, USA; **BMNH,** The Natural History Museum, London, England; **CM**, Carnegie Museum of Natural History, Pittsburgh, Penssylvania, USA; **FMNH**, Field Museum of Natural History, Chicago, Illinois, USA; **LPV**, Luoping County Vertebrates, Chengdu Institute of Geology and Mineral Resources, Chengdu, China; **MB.f**, Museum für Naturkunde Berlin, Germany; **MHNM**, Musée d'Histoire naturelle de Miguasha, Miguasha, Quebec, Canada; **MNA**, Museum of Northern Arizona, Flagstaff, Arizona, USA; **MV**, University of Montana, Missoula, Montana, USA; **NKMB**, Naturkundemuseum Bamberg, Bamberg, Germany; **PRPRC**, Peace Region Palaeontology Research Center, Tumbler Ridge, British Columbia, Canada; **SM D**, Sunderland Museum, Sunderland, England; **SOS**, Jura Museum Eichstätt, Eichstätt, Germany; **Sto**, Naturhistoriska riksmuseet, Stockholm, Sweden; **YPM PU**, Yale Peabody Museum, Yale University, New Haven, Connecticut, USA

Grossius aragonensis
Based on Schultze (1973)[9]; known only from the holotype; JAL and RC (double-checked by RC, February 27, 2021).

Char. 8: Mondéjar-Fernàndez (2019, char. 120)[118] coded the premaxillae of *Grossius aragonensis* to be present. However, the anterior part of the snout is not preserved, thus it is impossible to code for this character.

Char. 23: The posterior margin of the tabular of *Grossius aragonensis* extends beyond the posterior margin of the postparietal (Schultze, 1973, fig. 6a, b)[9]. Mondéjar-Fernàndez (2019, char. 45)[118] coded *Grossius* as having the posterior margin of the tabular to be anterior to the posterior margin of the postparietal. We are coding *G. aragonensis* according the Schultze's (1973)[9] illustration.

Char. 54: Mondéjar-Fernàndez (2019, char. 30)[118] coded the posterior margin of the skull roof of *Grossius aragonensis* as being convex rather than straight. Although the posterior margin of the postparietals is slightly convex it is not considered as being embayed in comparison to the coelacanth condition.

Char. 65: The element identified as "squamosal 2" by Schultze (1973, fig. 6)[9] in *Grossius aragonensis* is rather identified as the preoperculum as suggested by Mondéjar-Fernàndez (2009, fig. 16a)[118].

Char. 110: The infradentaries of *Grossius aragonensis* are all fused together (or a single elongated infradentary) (Schultze, 1973) rendering it impossible to determine the size of the splenial.

Char. 143: Mondéjar-Fernàndez (2019, char. 49)[118] coded *Grossius aragonensis* has deep pear-shaped internasal pits being absent. However, we consider the condition as unclear based on the cross-section available in Schultze (1973, fig. 6)[9].

Onychodus jandemarrai

Based on Andrews et al. (2006)[4] plus observations on all known Gogo specimens (JAL); JAL (double-checked by RC, February 26, 2021; neurocranial characters double-checked by AMC September 6th, 2021).

Char. 2: Long (2001, fig. 1c)[119] reconstructed the trajectory of the ethmoid commissure of *Onychodus* sp. (which subsequently was named *O. jandemarai*) as going through the center of the premaxillae. However, the trajectory of the ethmoid commissure in *Onychodus jandemarrai* goes through the most dorsal part of the premaxillae (Andrews et al. 2006, figs. 5, 8)[4] as well as the median rostral (Andrews et al. 2006, fig. 4a)[4].

Char. 30: The parietal of *Onychodus jandemarrai* has a posterolateral extension (Andrews et al., 2006, fig. 4a)[4] that resembles the lateral process observed in actinistians. Although we are coding this process to be present in *Onychodus*, it is unlikely that it is homologous.

Char. 40: In *Onychodus,* the postparietal narrows very weakly, not as pronounced as in stem-tetrapods like *Osteolepis* or in other stem sarcopterygians (e.g., rhizodontids).

Char. 47: The middle and posterior pit lines of *Onychodus jandemarrai* are located at mid-length of the postparietal (Andrews et al., 2006, figs. 2a, 4a)[4]. We are coding the condition as being within the posterior half since it is closer to this condition than being located in the anterior third of the postparietal.

Char. 51: The condition of the extrascapulars of *Onychodus jandemarrai* is coded as both the plesiomorphic and apomorphic conditions. The median extrascapular is located behind the level of the neurocranium, whereas the lateral extrascapulars are part of the skull roof because they are located laterally to the postparietals (Andrews et al., 2006, figs. 2b, 4a, b, 5a, c, d)[4].

Char. 76: In the outgroups the lacrimal and jugal are not fused; thus, we decided to code this character as "-" in *Onychodus*.

Char. 93: Although pit lines on the cheek region of *Onychodus jandemarrai* have not been figured in reconstitution (Long, 2001, fig. 1B; Andrews et al., 2006, fig. 4b)[4,119], the squamosal of *O. jandemarrai* carries a curved pit line that runs posteroventrally from the growth center of the squamosal (Andrews et al., 2006, p. 203)[4].

Char. 144: Andrews et al. (2006, p. 228, 231)[4] argued that the vomers of *Onychodus jandemarrai* are lost. Andrews et al. (2006, p. 206, figs. 16, 17)[4] labeled the anterior tooth bearing palatal bone as the "predermopalatine" but admitted that the evidence is weak. This element could alternatively be

interpreted as a "vomer". We accept the latter, which is a more parsimonious view that this anterior element is a vomer.

Char. 155: The overall shape of the nasal capsules was strongly laterally compressed to make room for the enormous internasal fossae (Andrews et al. 2006, p. 224)[4].

Char. 158: Based on unpublished data of CT scan 3D model of the holotype of *Onychodus jandemarrai*, the ethmosphenoid is cut in half to reveal the shape of the hypophysial fossa (J.A. Long, pers. observ.).

Char. 159: Zhu & Yu (2002, char. 107)[84] and Friedman (2007, char. 93)[98] coded the condition of the fenestra ovalis of *Onychodus* as unknown.

Char. 170: We examined the basipterygoid area of *Onychodus* and decided the unfinished area around the basipterygoid process was not strong evidence enough for coding the presence of a basipterygoid process. We refer to the braincase of *Latimeria* where this area is covered by cartilage and there is no basipterygoid process. We reinterpret the basipterygoid area of *Onychodus* being part of the larger cartilage covered processes connectens.

Char. 173: The anterior margin of the lateral portion of the basisphenoid of *Onychodus jandemarrai* consists entirely of unfinished bone, suturing with the lateral ethmoid ossification (Andrews et al., 2006, p. 223)[4].

Char. 188: Dorsal to the posterior margin of the optic nerve foramen, immediately below the curving ridge, sits a small but prominent suprapterygoid process (Andrews et al., 2006, fig. 56a)[4].

Char. 189: Andrews et al. (2006, p. 220)[4] mentioned that "Anterior to the dorsal part of the vestibular fontanelle, a well-defined groove runs horizontally along the side wall of the otic capsule, becoming more deeply incised towards the anterior. This must have housed the jugular vein."

Char. 206: Andrews et al. (2006, p. 209, figs. 24, 25)[4] mentioned that the basibranchial of *O. jandemarrai* is a fused element composed of an anterior and posterior basibranchials. However, the organization of bone structure and the homogenous bony ventral surface rather suggest the presence of a single basibranchial.

Qingmenodus yui

Based on Lu & Zhu (2009)[8] and Lu et al. (2016)[120]; JAL (double-checked by RC, March 12, 2021; neurocranial characters double-checked by AMC September 6th, 2021).

Char. 155: Lu et al. (2016, p. 3)[120] mentioned that the laterodorsally positioned nasal capsules are large, elongate, and oblong. However, Lu et al. (2016, fig. 2)[120] figured them as triangular.

Char. 171: A putative vestibular fontanelle is found in *Qingmenodus* (Lu & Zhu, 2009, p. 294)[8].

Char. 176: The processus connectens of *Qingmenodus* is anteroventrally elongated, reaching the level of the basipterygoid process, similar to that of Devonian coelacanths (Lu et al., 2016, p. 5)[120].

Strunius rolandi

Based on Jessen (1966)[7], Gross (1956; *O. rolandi*)[121], and personal observations on Swedish Museum material (JAL); JAL (double-checked by RC, March 12, 2021).

Char. 76: In the outgroups the lacrimal and jugal are not fused; thus, we decided to code this character as "-" in *Strunius*.

Char. 110: The infradentaries of *Strunius rolandi* are fused together (Jessen, 1966, pl. 16, fig. 9)[7] rendering it impossible to determine the size of the splenial.

Strunius walteri

Based on Jessen (1966)[7]; JAL (double-checked by RC, March 12, 2021).

Char. 32: Based on the plates provided by Jessen (1966, pl. 11, 12, 13)[7], it seems that the ornamentation of the postparietals varies among specimens and according to the region of the postparietal. Thus, char. 32 is coded as polymorphic for *Strunius walteri*.

Char. 68: Upeniece (1995, fig. 1G)[122] showed two cheek elements present: the preopercular and the squamosal (unlabeled in his figure).

Char. 99: The ornament of *Strunius walteri* cheek bones (Jessen, 1966, pl. 11, 12)[7] is composed of both fine ridges and tubercles. Thus, we coded char. 99 as polymorphic.

Char. 110: The infradentaries of *Strunius walteri* are fused together into two elongated infradentaries (Jessen, 1966, pl. 15, fig. 5)[7] rendering it impossible to determine the size of the splenial.

Alcoveria brevis
Based on Beltan (1972, 1984)[10,11], Cloutier (1991b)[96], and Forey (1998)[12] and images from holotype (part and counterpart); RC (double-checked by RC, January 15, 2021).

Char. 253: In contrast to Forey (1998)[12], the supplementary lobe of *Alcoveria* is present on the holotype.

Allenypterus montanus
Based on Lund & Lund (1985)[13], Cloutier (1991a)[95], and Forey (1998)[12]; and original material (R. Cloutier, pers. observ.; RC (double-checked by RC).

Char. 5: In *Allenypterus*, Lund & Lund (1985, figs. 60-61)[13] illustrated premaxillae without anterior pores while rostrals located dorsally to the premaxillae are perforated with pores that could either be anterior pores of the rostral organ or pores from the ethmoid commissure. None of the observed specimens show clear anterior pores.

Char. 8: Forey (1998)[12] mentioned that Cloutier (1991a)[95] coded the condition of *Allenypterus* as fragmented premaxillae, while in fact Cloutier (1991a, b)[95,96] coded as paired.

Char. 9: Forey (1998, char. 5)[12] coded the condition of the dorsal lamina of the premaxilla of *Allenypterus* as unknown. However, *Allenypterus montanus* has a reduced dorsal lamina of the premaxilla.

Char. 13: Forey (1998, char. 3)[12] and subsequent analyses (up to Toriño et al., 2021, char. 3)[14] coded character 3 for *Allenypterus* as unknown. Lund & Lund (1985, figs. 61, 65, 66)[13] and observed specimens show the presence of one larger median rostral and a few smaller rostrals.

Char. 62: Cloutier (1991a, char. 23)[95] coded *Allenypterus* as having cheek bones in contact. However, Forey (1998, char. 29)[12] and subsequent analyses [up to Toriño et al. (2021, char. 29)[14]] coded *Allenypterus* as having cheek bones separated from one another. Lund & Lund (1985)[13] illustrated the cheek bones of *A. montanus* as being in contact. Furthermore, observation on specimen FMNH PF 10939 (R. Cloutier, pers. observ.) confirmed this condition based on the matching of the intricate suture between the squamosal and preoperculum.

Char. 64: Lund & Lund (1985, figs. 60-61)[13] illustrated a dermal element located in the postero-dorsal part of the cheek. However, Forey (1998, fig. 4.6)[12] did not figure such element; personal observation did not reveal such bone either (a fractured operculum might have been interpreted as a separate bone on FMNH PF 10939).

Char. 76: Lund & Lund (1985, fig. 57)[13] illustrated the anterior end of the lacrimojugal as not expanded anteriorly, while Lund & Lund (1985, figs. 54, 60)[13] showed a slight expansion anteriorly. Forey (1998, fig. 4.6)[12] rather shows a slight anterior tapering of the lacrimojugal which corroborated our observations on specimens.

Char. 91: Forey (1998, char. 46)[12] and subsequent analyses [up to Toriño et al. (2021, char. 46)[14]] coded the condition of *Allenypterus* as unknown. However, specimens FMNH PF 10939 of *Allenypterus montanus* shows that the jugal canal is simple having only a few pores aligned with the main canal.

Char. 100: Forey (1998, char. 50)[12] and subsequent analyses [up to Toriño et al. (2021, char. 50)[14]] coded for the presence of a few large pores forming the infraorbital, jugal and preopercular canal of *Allenypterus*. Although cheek sensory pores are not clearly visible on many specimens of *A. montanus*, specimen FMNH PF10939 displays small pores on the postorbital.

Char. 116: Toriño et al. (2021b, char. 54)[14] coded the condition of the dentary teeth of *Allenypterus* as "?" in contrast to Forey (1998)[12]. They justify this modification based on "the arguments of Friedman & Coates (2006)[47] ", without providing additional information. Friedman & Coates (2006, SI)[47] mentioned

that the mandible of *Allenypterus* is edentulous; thus, they coded *Allenypterus* as "?". Lund & Lund (1985, p. 44)[13] reported the presence of fine teeth on one or more very thin plates lining the dentary, whereas Forey (1998, p. 136)[12] and observation on original material (FMNH PF 10940; R. Cloutier, pers. observ.) suggest that the dentary lacks teeth.

Char. 138: The suture is described as a broad V-shape, as represented in Forey (1998)[12] rather than Lund & Lund (1985)[13].

Char. 150: Forey (1998, char. 79)[12] and subsequent analyses [up to Toriño et al. (2021, char. 79)[14]] coded the condition of the ascending laminae of the parasphenoid in *Allenypterus* as unknown. Specimen FMNH PF 10940 of *A. montanus* shows that the parasphenoid lacks the ascending laminae (R. Cloutier, pers. observ.).

Char. 151: Forey (1998, char. 78)[12] and subsequent analyses [up to Toriño et al. (2021, char.78)[14]] coded the condition of the buccohypophysial canal in *Allenypterus* as unknown. Cloutier (1991a, p. 407)[95] mentioned that the buccohypophysial foramen of *A. montanus* is open based on specimens CM 27284, CM 40900, FMNH PF 8666. However, Cloutier (1991a, char. 35)[95] erroneously coded for the absence of the buccohypophysial foramen of *A. montanus*. The three cited specimens of *A. montanus* as well as specimen FMNH PF 10940 show parasphenoid with an open buccohypophysial foramen (R. Cloutier, pers. observ.).

Char. 211: Forey (1998, char. 89)[12] and subsequent analyses [up to Toriño et al. (2021, char. 89)[14]] coded the shape of the anocleithrum of *Allenypterus* as simple. Specimens CM 27285ab, CM 37699ab, and CM 46078 clearly shows the sigmoid shape of the anocleithrum of *A. montanus* (R. Cloutier, pers. observ.).

Char. 258: Lund & Lund (1985, fig. 57)[13] illustrated solely caudal "supraneurals" associated to epichordal lepidotrichia of *Allenypterus montanus*. However, numerous specimens (e.g., FMNH PF 10939, CM 27285) show clearly that there are two "supraneurals" located anteriorly to the insertion of the epichordal lobe of the caudal fin.

Char. 268: Forey (1998, char. 107)[12] and subsequent analyses up to Gess & Coates (2015, char. 107)[78] coded the swimbladder of *Allenypterus* as not ossified. Dutel et al. (2012, char. 107)[60] and subsequent analyses [up to Toriño et al. (2021, char. 107)[14]] coded *Allenypterus* as having an ossified lung. Based on Lund & Lund (1985)[13] and our observation of the original material (R. Cloutier, pers. observ.), the lung of *A. montanus* is not ossified.

Atacamaia solitaria
Based on Arratia & Schultze (2015)[15]; known only from holotype; RC (double-checked by RC).

Char. 1: In contrast to Arratia & Schultze (2015)[15], we are coding Character 1 as "?" because the snout is unknown in the sole specimen of *Atacamaia*.

Char. 22: The single bone located along the posterolateral margin of the postparietal of *Atacamaia* is interpreted as the tabular, whereas Arratia & Schultze (2015)[15] identified it as a supratemporal.

Char. 32: Arratia & Schultze (2015, char. 27)[15] coded *Atacamaia* as a polymorphic condition.

Char. 37: Arratia & Schultze (2015)[15] coded the margin of the dermal intracranial joint of *Atacamaia* as undulated or excavated (their char. 1[2]).

Char. 50: Arratia & Schultze (2015, char. 15)[15] and subsequent analyses [up to Toriño et al. (2012, char. 15)[14]] coded the extrascapulars of *Atacamaia* as being free from the postparietal. Arratia & Schultze (2015, figs. 2, 3, 4)[15] mentioned that a few pieces of bones posteroventral to the tabular (their "supratemporal") and postparietal are interpreted as remnants of extrascapulars. The condition of the extrascapulars is too ambiguous to be coded.

Char. 66: All characters related to the preoperculum are coded with a question mark for *Atacamaia*. Arratia & Schultze (2015)[15] mentioned that the absence of preoperculum may be a correct prediction because no remnant is found in the studied specimen of *Atacamaia*.

Char. 76: Arratia & Schultze (2015)[15] coded the lacrimojugal of *Atacamaia* as expanded anteriorly; they included this condition in the generic diagnosis. However, we do not consider the condition to be expanded since it rather slightly tapers anteriorly.

Char. 77: Arratia & Schultze (2015)[15] mentioned that the condition of the infraorbital canal and its pores is poorly known because of the state of preservation of the lacrimojugal; most of the outer surface of the bone has been damaged. Although *Atacamaia solitaria* is coded as "?", it is likely that the apomorphic condition is present since we can see a slight expansion of the canal towards the anterior tip of the lacrimojugal (Arratia & Schultze, 2015, figs. 1, 3)[15].

Char. 87: Arratia & Schultze (1995)[15] coded *Atacamaia* as "2" without defining the apomorphic condition; based on their data matrix it is the only species with this character-state. We are coding the postorbital of *Atacamaia* as having a plate-like shape.

Char. 88: We consider that the postorbital is spanning the intracranial joint level. Arratia & Schultze (2015)[15] mentioned that it is mainly located in front of this level.

Char. 267: In contrast to Arratia & Schultze (2015)[15], we coded *Atacamaia* with a "?" because the postcranial condition remains unknown.

Axelia robusta
Based on Stensiö (1921)[16], Schaeffer (1941)[111], Forey (1998)[12]; JAL (double-checked by RC, November 11th, 2020).

Char. 4: Forey (1998, p. 69)[12] confirms that the rostral organ pores are likely present in the so-called tectal-preorbital.

Char. 5: Premaxilla are unknown in *A. robusta*.

Char. 6: The two openings on the antorbital of *Axelia robusta* identified as the nares by Stensiö (1921, figs. 39, 40)[16] rather corresponds to the posterior openings of the rostral organ.

Char. 13: Forey (1998, char. 3)[12] and subsequent analyses [up to Toriño et al. (2021, char. 3)] coded the condition of *Axelia* as "?". Stensiö (1921, fig. 2)[16] figured a series of at least two rostrals (and potentially two small median elements referred to as interrostrals) anterior to the nasals (his "postrostral") in *A. robusta* which we considered herein to be multiple rostrals.

Char. 57: Forey (1998, p. 69)[12] confirmed the presence of the preorbital (his "antorbital") illustrated by Stensiö's (1921, fig. 53; his "nasalo-antorbital")[16].

Char. 109: Forey (1998, char. 57)[12] and subsequent analyses [up to Toriño et al. (2021, char. 57)[14]] coded *Axelia* as lacking the hook-shaped process on the dentary. However, Forey (1998, p. 147)[12] mentioned that the condition of the dentary is very incompletely known. None of the plates in Stensiö (1921)[16] shows the condition of the dentary. Thus, we are coding *A. robusta* as unknown.

Char. 112: Based on Stensiö (1921, pl. 15a, b)[16], the dentary seems to be slightly inclined.

Char. 150: Forey (1998, char. 79)[12] and subsequent analyses [up to Toriño et al. (2021, char. 79)[14]] coded the condition of the ascending laminae of the parasphenoid of *Axelia* as unknown. Stensiö (1921, pl. 16, fig. 1; text-fig. 42)[16] figured a parasphenoid of *A. robusta* lacking the ascending laminae.

Char. 151: Cloutier (1991a, b, char. 35)[95,96] coded for the absence of a buccohypophysial foramen in *Axelia robusta*. Forey (1998, char. 78)[12] and subsequent analyses [up to Toriño et al. (2021, char. 78)[14]] coded the condition of the buccohypophysial foramen of *Axelia* as unknown. Stensiö (1921, text fig. 42)[16] illustrated the parasphenoid of *A. robusta* without an open buccohypophysial foramen.

Char. 247: Forey (1998, char. 103)[12] and subsequent analyses [up to Toriño et al. (2021, char. 103)[14]] coded the condition of the median fin lepidotrichia of *Axelia* as unknown. However, Stensiö (1921, pl. 16, fig. 3)[16] figured the caudal fin of *A. robusta* with not expanded lepidotrichia.

Axelrodichthys araripensis
Based on Maisey (1986, 1991)[18,123], Forey (1998)[12], Fragoso et al. (2018)[104], Barbosa et al. (2019)[124] and observations on original material (RC); JAL (double-checked by RC, November 5th, 2020).

Char. 1: Forey (1998, char. 2)[12] and subsequent analyses coded *Axelrodichthys* as snout bones being separated from one another; in 1998, only *A. araripensis* was recognized. Toriño et al. (2021)[14] considered the condition to be too difficult to perceive if the bones are consolidated or not, thus they coded *Axelrodichthys* as "?". The condition of the snout of *Axelrodichthys araripensis* as illustrated by

Fragoso et al. (2018, fig. 3)[104] still suggests that the snout bones are separated although some of these elements are fragmented during fossilization.

Char. 13: Maisey (1986)[18] mentioned that at least one pair of internasals was present in *Axelrodichthys araripensis*. However, the condition of the snout region is better preserved in the specimens described by Fragoso et al. (2018)[104]. Fragoso et al. (2018, fig. 3a)[104] illustrated that there was a single median rostral (their internasal); the elements identified as rostral ossicles are not considered as rostrals.

Char. 28: Forey (1998, char. 21)[12] and subsequent analyses [up to Toriño et al. (2021, char. 21)[14]] coded *Axelrodichthys* as having the otic canal joining the supratemporal canal in the tabular (their "supratemporal"). However, Fragoso et al. (2018, fig. 2B)[104] has illustrated that the connection of both canals is located in the lateral extrascapular.

Char. 37: Forey (1998, char. 1)[12] considered the margin of the dermal intracranial joint of *Axelrodichthys araripensis* to be deeply interdigitate. However, we considered the margin to be straight based on the illustrations of the skull roof of *A. araripensis* provided by Maisey (1986, figs. 13B, C, 18A, 20A, 22A; 1991, p. 307, 308, 310)[18,123] and Fragoso et al. (2018, figs. 1A, 2A, B, 15A)[104].

Char. 41: The dermal bone identified by Maisey (1986)[18] as the dermosphenotic in *Axelrodichthys araripensis* is herein considered as the postorbital.

Char. 50: We are re-interpreting the posterior and median postparietals of Maisey (1986, figs. 20, 26)[18] as the lateral and median extrascapulars.

Char. 66: Forey (1998, char. 38)[12] and subsequent analyses [up to Toriño et al. (2021, char. 38)[14]] coded the preoperculum of *Axelrodichthys* as reduced to a narrow tube. However, Forey (1998, fig. 4.17)[12] and Maisey (1986, fig. 26)[18] figured a preoperculum smaller than the squamosal, but still not reduced to a narrow tube.

Char. 72: Forey (1998, char. 37)[12] coded *Axelrodichthys* as having a squamosal reduced to a narrow tube. However, the size of the squamosal in *A. araripensis* is not reduced to a narrow tube as illustrated by Maisey (1986, figs. 14, 26)[18], Forey (1998, fig. 4.17)[12] and Fragoso et al. (2018, fig. 2)[104].

Char. 86: The similarity with *Mawsonia* is more about the anterior extent, spanning the intracranial joint. *Axelrodichthys* does not have an anterior process as in *Mawsonia*.

Char. 123: The coding of the articulation of the principal coronoid in *Axelrodichthys* follows the comments provided by Toriño et al. (2021b, p. SI 20)[14].

Char. 126: The oral pit line is absent in *Axelrodichthys araripensis* (Forey, 1998, fig. 5.10[12]; Fragoso et al., 2018, fig. 1)[104].

Char. 150: Maisey (1991)[123] mentioned that the parasphenoid of *Axelrodichthys araripensis* has ascending laminae. However, Fragoso et al. (2018)[104] and Toriño et al. (2021b, char. 79)[14] demonstrate that the parasphenoid of *A. araripensis* lacks ascending laminae.

Char. 153: Toriño et al. (2021b)[14] mentioned that Fragoso et al. (2018)[104] documented the ventral swelling of the palatoquadrate in new specimens of *Axelrodichthys araripensis*, although Dutel et al. (2012, char. 110)[60] considered it to be absent in the original material figured by Maisey (1986)[18]. We are coding this character as polymorphic since there is variation among specimens.

Char. 174: Forey (1998, char. 70)[12] and subsequent analyses [up to Toriño et al. (2021, char. 70)[14]] coded the condition of the optic nerve of *Axelrodichthys* as enclosed by the basisphenoid extending forward. However, in *A. araripensis*, the optic nerve is not enclosed by the basisphenoid but by the interorbital cartilage (H. Dutel, pers. observ.).

Char. 176: Toriño et al. (2021)[14] coded *Axelrodichthys* as the processus connectens failing to meet the parasphenoid. Maisey (1986, figs. 17, 18)[18] figured clearly the neurocranium showing that the processus connectens meets the parasphenoid of *A. araripensis*.

Char. 202: The condition of the ceratohyal in *Axelrodichthys araripensis* is coded based on the ceratohyal figured by Fragoso et al. (2018, figs. S7, S21)[104]; a similar stubby condition was also figured by Forey (1998, fig. 4.7)[12].

Char. 211: Forey (1998, char. 89)[12] coded the shape of the anocleithrum of *Axelrodichthys* as unknown. Fragoso (2014)[108], Fragoso et al. (2018)[104] and Toriño et al (2021, char. 89)[14] coded the

shape of the anocleithrum of *A. araripensis* as simple. Fragoso et al. (2018, p. 9, fig. S24)[104] described and figured a sigmoid anocleithrum in *A. araripensis*.

Char. 232: Forey (1998, char. 101)[12] coded the ventral margin of the basal plate of the first dorsal fin of *Axelrodichthys* as smooth. However, Fragoso (2014)[108] and Toriño et al. (2021b)[14] coded for an emarginated ventral margin. We are coding the ventral margin of the basal plate of the first dorsal fin of *A. araripensis* as smooth based on observation of specimen FMNH PF12839 (R. Cloutier, pers. observ.).

Char. 250: Forey (1998, char. 97)[12] and subsequent analyses [up to Toriño et al. (2021, char. 97)[14]] coded the caudal lobes of *Axelrodichthys* as symmetrical. In the diagnosis of *A. araripensis*, Forey (1998, p. 303)[12] reported the presence of 15 lepidotrichia in both the dorsal and ventral lobes of the caudal fin, whereas Forey (1998, fig. 11.3)[12] reconstructed the caudal fin of *A. araripensis* with 18 lepidotrichia in the dorsal lobe and 15 lepidotrichia in the ventral lobe [based on Maisey (1991)[123] and specimen FMNH PF11856]. Maisey (1986, fig. 12)[18] figured the holotype of *A. araripensis* (AMNH 11759) with 18 lepidotrichia in the dorsal lobe and 15 lepidotrichia in the ventral lobe); this asymmetry was also represented in the reconstruction (Maisey, 1986, fig. 14)[18]. High-resolution image of specimen MB.f. 12607 also displays an asymmetry [also figured by Brito & Yabumoto (2011, fig. 32)[125]].

Char. 258: The postcranial anatomy of *Axelrodichthys araripensis* is poorly described. Maisey (1991, p. 303)[123] figured a reconstruction of the postcranial skeleton in which the neural spines located anterior to the insertion of the caudal fin are not associated with "supraneural". Therefore, we code *A. araripensis* as "2".

Char. 263: Forey (1991, char. 54)[97] coded *Axelrodichthys araripensis* as having undifferentiated ornament, whereas Dutel et al. (2015, char. 104)[88] and Forey (1998, char. 104)[12] considered that the condition is differentiated. Based on the illustration of the scale of *A. araripensis* (Forey, 1998, fig. 11.7)[12] and Fragoso et al. (2018, fig. 12)[104], the central ridges are more developed than the lateral ridges and tubercles.

Axelrodichthys lavocati

Based on Yabumoto & Uyeno (2005)[20], Fragoso et al. (2018)[104]; HD & RC (double-checked by RC, February 3rd, 2021).

Char. 1: Forey (1998, char. 2)[12] and subsequent analyses coded *Axelrodichthys* as snout bones being separated from one another. However, Toriño et al. (2021)[14] considered the condition to be too difficult to perceive if the bones are consolidated or not, thus they coded *Axelrodichthys* as "?". The condition of the snout of *Axelrodichthys lavocati* (Yabumoto & Uyeno, 2005, fig. 1a)[20] is unknown.

Char. 16: The relative length of the posterior preparietal in relation to the parietal varies among specimens as figured by Cavin et al. (2016)[24] based on published drawings (see Yabumoto & Uyeno (2005)[20] and Cavin & Forey (2004)[126].

Char. 36: Cavin et al. (2020, char. 51)[101] coded *Axelrodichthys lavocati* has having three supraorbitals articulating with the parietal. However, Yabumoto & Uyeno (2005, fig. 1a, b)[20] illustrated bilateral difference: on the right side, three supraorbitals articulate with the right parietal, whereas two supraorbitals articulate with the left parietal. Therefore, this character is coded as polymorphic in *A. lavocati*.

Char. 174: Forey (1998, char. 70)[12] and subsequent analyses [up to Toriño et al. (2021, char. 70)[14]] coded the condition of the optic nerve of *Axelrodichthys* as enclosed by the basisphenoid extending forward. However, in *A. lavocati*, the optic nerve is not enclosed by the basisphenoid but by the interorbital cartilage (H. Dutel, pers. observ.).

Char. 176: Toriño et al. (2021, char. 71, p. SI 11)[14] mentioned that one of the specimens referred as cf. *Mawsonia lavocati* by Cavin & Forey (2004)[126] indicates that the processus connectens meets the parasphenoid.

Axelrodichthys maiseyi

Based on de Carvalho et al. (2013)[23], Cavin et al. (2016)[24], Fragoso et al. (2018)[104]; HD (double-checked by RC, November 11th, 2020).

Char. 1: Forey (1998, char. 2)[12] and subsequent analyses coded *Axelrodichthys* as snout bones being separated from one another. However, Toriño et al. (2021)[14] considered the condition to be too difficult to perceive if the bones are consolidated or not, thus they coded *Axelrodichthys* as "?". The condition of the snout of *Axelrodichthys mayseyi* (de Carvalho et al., 2013, fig. 3)[23] is unknown on the holotype.

Char. 15: Fragoso et al. (2018, p. 12)[104] mentioned that the profile of the parietal shield of *Axelrodichthys maiseyi* was less pronounced than that of *A. araripensis* and *A. lavocati*. However, this subtle distinction is not reflected in the definition of our character.

Char. 123: The coding of the articulation of the principal coronoid in *Axelrodichthys* follows the comments provided by Toriño et al. (2021b, p. SI 20)[14].

Char. 126: The oral pit line is absent in *Axelrodichthys araripensis* (Forey, 1998, fig. 5.10[12]; Fragoso et al., 2018, fig. 1[104]).

Axelrodichthys megadromos

Based on Cavin et al. (2016, 2020)[24,101]; RC (double-checked by RC, February 3rd 2021).

Char. 16: The relative length of the parietal and posterior preparietal varies bilaterally in the specimen represented by Cavin et al. (2016, fig. 4A)[24].

Char. 26: The otic canal passes through the tabular of *Axelrodichthys megadromos*, but it is unclear if it passes in the postparietal (Cavin et al., 2020)[101].

Char. 28: The condition of the supratemporal commissure of *Axelrodichthys megadromos* is clearly visible in Cavin et al. (2020, fig. 2C)[101].

Char. 78: Cavin et al. (2020, fig. 2F)[101] illustrated the lacrimojugal of *Axelrodichthys megadromos* showing that the anterior end was not angled. Toriño et al. (2021, char. 36)[14] coded *Axelrodichthys* based on the condition of the angled lacrimojugal observed in *A. araripensis*. However, *A. megadromos* is coded as not angled anteriorly which differs from the condition of *A. araripensis*.

Char. 123: The coding of the articulation of the principal coronoid in *Axelrodichthys* follows the comments provided by Toriño et al. (2021b, p. SI 20)[14].

Char. 126: The oral pit line is absent in *Axelrodichthys araripensis* (Forey, 1998, fig. 5.10[12]; Fragoso et al., 2018, fig. 1[104]).

Belemnocerca prolata

Based on Wendruff & Wilson (2013)[25]; known only from the holotype; RC (double-checked by RC).

Caridosuctor populosum

Based on Lund & Lund (1985)[13], Cloutier (1991a)[95] and Forey (1998)[12] and original material (R. Cloutier, pers. observ.); RC (double-checked by RC).

Char. 20: Lund & Lund (1985)[13] reconstructed two elements (tabular and supratemporal) located laterally to the postparietal, whereas Forey (1998, fig. 3.3C)[12] reconstructed a single element (tabular). Cloutier (1991a)[95] and our new observations confirm the presence of two elements.

Char. 22: Lund & Lund (1985)[13] reconstructed the presence of a supratemporal located anterolaterally to the postparietal, whereas Forey (1998, fig. 3.3C)[12] reconstructed solely the presence of a tabular. Cloutier (1991a)[95] and our new observations confirm the presence of a supratemporal in *Caridosuctor populosum*.

Char. 27: Forey (1998, char. 20)[12] and subsequent analyses [up to Toriño et al. (2021, char. 20)[14]] coded *Caridosuctor* as having a medial branch of the otic canal. Lund & Lund (1985)[13] discussed and illustrated a large pore located on the anterior part of the postparietal of *Caridosuctor populosum*. As mentioned by Cloutier (1991a, char. 16, p. 401)[95], this single pore on the postparietal of *C. populosum* (e.g., CM 27315 A) is variable among individuals; it is either present on one side only (e.g., CM 35529

A), or absent (e.g., CM 27299 B, CM 27317 B, CM 30674). Thus, character 27 is coded as polymorphic as done by Cloutier (1991a, char. 16)[95].

Char. 37: Forey (1998, char. 1)[12] coded the margin of the dermal intracranial joint of *Caridosuctor populosum* as strongly interdigitate. However, based on Lund & Lund (1985, figs. 23, 24)[13] and observation on numerous specimens (R. Cloutier, pers. observ.) we considered the margin to be relatively straight rather than strongly interdigitate.

Char. 38: Cloutier (1991a)[95] coded for the presence of the descending process of the postparietal, whereas Forey (1998)[12] coded for its absence. Internal impressions of postparietals suggest that it is absent.

Char. 103: Lund & Lund (1985)[13] mentioned that the subopercumum might be lost in *Caridosuctor*; however, we agree with Cloutier (1991a, b)[95,96] and Forey (1998)[12] that the subopercumum is present.

Char. 150: Forey (1998, char. 79)[12] and subsequent analyses [up to Toriño et al. (2021, char. 79)[14]] coded the condition of the ascending laminae of the parasphenoid in *Caridosuctor* as unknown. One of the specimens of *C. populosum* housed in the collections the Field Museum of Natural (field number 87-803) shows that the parasphenoid lacks the ascending laminae (R. Cloutier, pers. observ.).

Char. 151: Forey (1998, char. 78)[12] and subsequent analyses [up to Toriño et al. (2021, char. 78)[14]] coded the condition of the buccohypophysial canal in *Caridosuctor* as unknown. Cloutier (1991a, char. 35)[95] coded the buccohypophysial foramen of *C. populosum* as present. One of the specimens of *C. populosum* housed in the collections the Field Museum of Natural (field number 87-803) shows a complete parasphenoid with an open small, drop-shaped buccohypophysial foramen (R. Cloutier, pers. observ.).

Char. 153: Dutel et al. (2012, char. 110)[60] and subsequent analyses [up to Toriño et al. (2021, char. 110)[14]] coded the condition of the ventral swelling of the palatoquadrate of *Caridosuctor* as unknown. Specimen in the FMNH (PF) collections (Field number 87-803 and 82-80302B) of *C. populosum* show clearly the condition in which the ventral swelling of the palatoquadrate is absent (R. Cloutier, pers. observ.).

Char. 225: One specimen of *Caridosuctor populosum* (CM 37693B; R. Cloutier, pers. observ.) seems to show a partial fusion of the distal end of the medial processes of both pelvic girdles.

Char. 229: The complex morphology of the pelvic girdle of *Caridosuctor populosum* shows an additional short process between the anterolateral and lateral processes (Lund & Lund, 1985, figs 19, 30[13]; R. Cloutier, pers. observ. on CM 35535, CM 35203).

Char. 237: *Caridosuctor* is coded as having a basal plate of the second dorsal fin as forked anteriorly. However, we have to mention than the anteroventral process is clearly developed, whereas a short expansion anterodorsally is interpreted as another process (CM 35535, CM 37693).

Char. 244: A single specimen of *Caridosuctor* displays a partial anal fin basal plate (CM 37693a) (R. Cloutier, pers. observ.). This information was not available on Lund & Lund's (1985)[13] reconstruction.

Char. 258: Although "supraneural" are lacking from the reconstruction of *Caridosuctor populosum* given by Lund & Lund (1985, fig. 19)[13], a few specimens show the presence of one independent "supraneural".

Char. 260: Lund & Lund (1985, fig. 19)[13] illustrated broad and stubby cervical neural arches in *Caridosuctor populosum*; thus, we are coding *C. populosum* as having expanded cervical neural arches. However, Forey (1998, char. 91)[12] coded *Caridosuctor* as "?".

Char. 262: Lund & Lund (1985, p. 25)[13] mentioned that *Caridosuctor* possessed strong rib bases in the thoracic region of the axial skeleton, but that ribs are absent.

Changxingia aspratilis
Based on Wang & Liu (1981)[26]; known only from the holotype; RC (double-checked by RC).
Char. 52: Based on Wang & Liu's (1981)[26] drawing and image, it seems that there is no median extrascapular but a series of four lateral extrascapulars. But because of the uncertainty of the condition, we are coding *Changxingia aspratilis* as "?".

Char. 222: Only the condition of the pelvic fins of *Changxingia* is known from the original drawing (Wang & Liu, 1981)[26].

Changxingia weii
Based on Jin (1997)[28]; known only from the holotype; RC (double-checked by RC).
Char. 52: Based on Jin's (1997)[28] drawing and images, it seems that there is no median extrascapular but a series of four lateral extrascapulars. But because of the uncertainty of the condition, we are coding *Changxingia weii* as "?".

Chaohuichthys majiashanensis
Based on Tong et al. (2006)[29] and Benton et al. (2013)[127]; JAL, December 5th 2019 (double-checked by RC).
Char. 21: Tong et al. (2006)[29] and Benton et al. (2013)[127] identified the most posterior dermal bone composing the skull roof of *Chaohuichthys* as the parieto-intertemporal. We identified this element as the postparietal; it is unlikely that the intertemporal is fused with this large bone.
Char. 68: Tong et al. (2006, fig. 12.2)[29] and Benton et al. (2013, fig. 16B)[127] identified a large triangular bone in the cheek region of *Chaohuichthys* as the metapterygoid. We rather identified this element as the squamosal; the triangular pterygoid is found anteriorly to the squamosal.
Char. 72: The bone identified as the metapterygoid by Tong et al. (2006, fig. 12)[29] in *Chaohuichthys majiashanensis* is most likely the squamosal.

Chinlea sorenseni
Coded; based on Schaeffer (1967)[30], Elliott (1987)[128], Forey (1998)[12], Martz et al. (2017)[129] and Fragoso et al. (2018)[104], and radiograph of original material MNA V5470; RC (double-checked by RC).
Char. 9: Forey (1998, char. 5)[12] coded the dorsal laminae of the premaxillae of *Chinlea* to be absent. However, the dorsal laminae of the premaxilla of *Chinlea sorenseni* is present but reduced (Elliot, 1987, fig. 3)[128].
Char. 53: The extrascapular series of *Chinlea sorenseni* is composed of four elements (Elliott, 1987)[128]: paired median extrascapulars and one lateral extrascapular per side. Thus, the comparison of size between the median extrascapular and the lateral extrascapular is difficult with that of the remaining taxa.
Char. 54: Forey (1998, char. 18)[12] coded *Chinlea* a having an embayed posterior margin of the skull roof. Although the posterior margin of the skull roof including the extrascapulars is straight, the posterior margin in relation of the relationship between the tabulars and postparietals is embayed.
Char. 62: Forey (1998, char. 29)[12] coded *Chinlea* as having the cheek bones not in contact. However, Schaeffer (1967, fig. 14)[30] and Elliott (1987, fig. 2A, C)[128] showed the contact among the postorbital, squamosal and preoperculum of *C. sorenseni*.
Char. 64: Elliott (1987)[128] illustrated and identified a small cheek element as a postspiracular (referred herein as the spiracular). However, Forey (1998, p. 305)[12] mentioned that the spiracular bone was probably absent in the emended diagnosis of *Chinlea*.
Char. 70: We are coding *Chinlea sorenseni* as a polymorphic condition because the condition is intermediate between a completely ventral and completely posterior position of the squamosal in relation to the squamosal.
Char. 116: Forey (1998, char. 54)[12] and subsequent analyses [up to Toriño et al. (2021, char. 54)[14]] coded the condition of the dentary teeth of *Chinlea* as unknown. Planar X-ray of specimen MNA V5470 reveals the presence of separated tooth plates on the dentary.
Char. 146: The general condition of the parasphenoid of *Chinlea sorenseni* is coded from planar X-ray that have been done on the specimen described by Elliott (1987)[128].
Char. 147: The general condition of the parasphenoid of *Chinlea sorenseni* is coded from planar X-ray that have been done on the specimen described by Elliott (1987)[128].

Char. 148: The general condition of the parasphenoid of *Chinlea sorenseni* is coded from planar X-ray that have been done on the specimen described by Elliott (1987)[128].

Char. 152: Only the general shape of the entopterygoid of *Chinlea sorenseni* can be coded from the planar X-ray that have been done on the specimen described by Elliott (1987)[128].

Char. 260: This character was coded as "?" by Forey (1998, char. 91)[12] and subsequent phylogenetic analyses. An X-ray of specimen MNA V5470 of *Chinlea sorenseni* (provided by David Elliott) shows clearly that the cervical neural arches are not expanded; thus, we are coding *C. sorenseni* as not expanded.

Char. 263: Forey (1991, char. 54)[12] coded the ornamentation of the scales of *Chinlea* as undifferentiated, whereas Forey (1998, char. 104)[12], Dutel et al. (2015, char. 104)[88] and Toriño et al. (2021, char. 104)[14] coded *Chinlea* as having differentiated ornamentation on the scales. However, Schaeffer (1967, pl. 26.3)[30] and Yabumoto (2008, fig. 4D)[66] illustrated an isolated scale that is covered by fine longitudinal ridges without a prominent one.

Coccoderma suevicum

Based on Lambers (1991, 1992)[31,130] and Forey (1998)[12] and images of specimens; RC (double-checked by RC).

Char. 1: Lambers (1991, p. 175; 1992, p. 11)[31,130] mentioned that anterior to the parietals (frontals) a mass of bone is visible that consists of a rostral complex and that no separate bones can be recognized.

Char. 13: A median rostral cannot be identified since a rostral complex is present (Lambers, 1991, 1992)[31,130].

Char. 14: A median rostral cannot be identified since a rostral complex is present (Lambers, 1991, 1992)[31,130].

Char. 16: Lambers (1991, 1992)[31,130] suggested that the preparietal (anterior frontal) was fused with the rostral complex.

Char. 29: Lambers (1991, fig. 3; 1992, fig. 3)[31,130] illustrated a skull of *Coccoderma suevicum* (holotype of *Coelacanthus harlemensis*) in which the right tabular if partly fused with the postparietal. The character is coded as "separated" because the anterior suture is clear.

Char. 32: The skull roof is considered to be unornamented because Lambers (1991, p. 177; 1992, p. 12)[31,130] mentioned that these "bones do not show any tubercular ornamentation." Furthermore, he mentioned that the postparietal (parietal) is "only a little wrinkled."

Char. 37: Forey (1998, char. 1)[12] considered the margin of the dermal intracranial joint of *Coccoderma* as strongly interdigitate. However, based on illustrations of the skull roof of *Coccoderma suevicum* provided by Lambers (1991, fig. 3; 1992, fig. 3)[31,130] and Forey (1998, fig. 3.10)[12] the margin is fairly straight. The narrowing of the anterior part of the postparietals might have been interpreted as digitate; however, we are coding this character as straight.

Char. 53: The precise condition cannot be coded based on Lambers (1991, fig. 3; 1992, fig. 3)[31,130]; however, the lateral extrascapular does not form a series of small ossicles.

Char. 57: Forey (1998, p. 64)[12] mentioned that a preorbital may be absent.

Char. 66: Forey (1998, char. 38)[12] and subsequent analyses [up to Toriño et al. (2021, char. 38)[14]] coded the preoperculum of *Coccoderma* as being reduced to a narrow tube. Lambers (1991, fig. 3; 1992, fig. 3)[31,130] and Forey (1998, fig. 4.12B)[12] showed an elongated preoperculum that is larger than the infraorbital canal itself; thus, we decided to code it as large.

Char. 101: Lambers (1991, fig. 3; 1992, fig. 3)[31,130] and Forey (1998, fig. 5.7)[12] illustrated the lateral side of the skull of *Coccoderma suevicum* showing a distinct squamosal and preoperculum, but no quadratojugal. Thus, we are coding *C. suevicum* as "-".

Char. 266: Lambers (1991, fig. 11; 1992, fig. 11)[31,130] illustrated the presence of two pores per scale.

Char. 268: Forey (1998, char. 107)[12] and subsequent analyses [up to Toriño et al. (2021, char. 107)[14]] coded the lung (his "swimbladder") of *Coccoderma* as ossified. However, photographs of original specimens show no indication of an ossified lung. Lambers (1991, 1992)[31,130] does not mentioned the

condition of the lung in his redescription of *Coccoderma*; thus, we are coding *Coccoderma suevicum* as lung not ossified.

Coelacanthus granulatus

Based on Moy-Thomas & Westoll (1935)[131], Schaumberg (1978)[34], Cloutier (1991a)[95] and Forey (1998)[12] and original images of specimens; RC (double-checked by RC)

Char. 8: Schaumberg (1978)[34] illustrated and described the premaxillae of *Coelacanthus granulatus* as being fragmented; however, Forey (1998)[12] mentioned that he cannot validate this condition. Nevertheless, we are coding the premaxillae as fragmented.

Char. 28: Forey (1998, fig. 3.7)[12] illustrated a postparietal shield of *Coelacanthus granulatus* (BMNH P.3340) showing the left side with the lateral extrascapular separated from the supratemporal, whereas on the right side the lateral extrascapular is fused with the supratemporal. However, the reconstruction of the skull roof provided by Schaumberg (1978, figs. 5, 6)[34] does not show fusion. Thus, character 28 is coded as polymorphic.

Char. 38: Forey (1998, p. 60)[12] mentioned that there is no evidence of descending process of the postparietal in *Coelacanthus granulatus*.

Char. 54: Forey (1998, char. 18)[12] coded for an embayment of the posterior margin of the skull roof, although he mentioned that the margin is not markedly embayed (p. 307). Forey (1998, p. 91)[12] mentioned that the fusion of the lateral extrascapular with the tabular (his "extratemporal") results in the posterior profile of the skull roof being embayed with the remaining extrascapulars lying in between. However, we do not consider the lateral extrascapular being fused with the tabular. The posterior margin of the postparietals are approximately at the same level as the posterior margin of the tabulars (Schaumberg, 1978, fig. 5)[34]; thus, we are coding the posterior margin of the skull roof of *C. granulatus* as being straight.

Char. 63: Schaumberg (1978, fig. 6)[34] reconstructed the skull of *Coelacanthus granulatus* showing a single contact between the lacrimojugal and the lateral rostral. However, Schaumberg (1978, fig. 9)[34] illustrated a contact between the preorbital (his "Tectalplatte") and the lacrimojugal. Thus, we are coding *C. granulatus* as having a contact between the lacrimojugal and the preorbital.

Char. 66: Forey (1998, char. 38)[12] and subsequent analyses [up to Toriño et al. (2021, char. 38)[14]] coded the condition of the preoperculum of *Coelacanthus* as unknown. However, Schaumberg (1978, figs. 2, 6)[34] figured a preoperculum reduced to a narrow tube.

Char. 78: Schaumberg (1978, fig. 6)[34] illustrated the lacrimojugal with an angle anteriorly, whereas Forey (1998, p. 111)[12] reexamined the same specimen (HM 926.52) without observing an obvious angle anteriorly.

Char. 90: Schaumberg (1978, fig. 6)[34] reconstructed the postorbital of *Coelacanthus granulatus* with the infraorbital running through the center of the bone. However, Forey (1998, fig. 5.4)[12] provided a detailed drawing of the cheek region of a specimen of *C. granulatus* illustrating a couple sensory pores being located close to the anterior margin of the postorbital.

Char. 91: Forey (1998, char. 46)[12] and subsequent analyses [up to Toriño et al. (2021, char. 46)[14]] coded *Coelacanthus* as unknown. Schaumberg (1978, fig. 6)[34] reconstructed the jugal canal of *C. granulatus* as a simple canal.

Char. 92: Schaumberg (1978, fig. 6)[34] and Forey (1998, fig. 5.4)[12] illustrated the squamosal of *Coelacanthus granulatus*. In both cases, the squamosal is narrow only slightly broader than the infraorbital canal tube. However, Schaumberg (1978)[34] reconstructed a long squamosal, in contrast to Forey (1998, fig. 5.4A)[12] who provided a camera lucida drawing of specimen SM D.435 showing a short squamosal. Based on both drawings, we considered that the canal runs through the center of the squamosal, although this bone is reduced.

Char. 93: Forey (1998, char. 48)[12] and subsequent analyses [up to Toriño et al. (2021, char. 48)[14]] coded the condition of the pit lines on the cheek region of *Coelacanthus* to be unknown. The reduced condition of the cheek bones of *C. granulatus* are most likely related with the absence of pit line marking on these elements.

Char. 150: Forey (1998, char. 79)[12] and subsequent analyses [up to Toriño et al. (2021, char. 79)[14]] coded the condition of the ascending laminae of the parasphenoid of *Coelacanthus* as unknown. However, isolated parasphenoids identified as *C. granulatus* show that the parasphenoid lacks the ascending laminae (Brandt, 2007, figs. 4, 6, 11)[132].

Char. 151: Forey (1998, char. 78)[12] and subsequent analyses [up to Toriño et al. (2021, char. 78)[14]] coded the condition of the buccohypophysial foramen of *Coelacanthus* as unknown. However, isolated parasphenoids identified as *C. granulatus* show that the buccohypophysial foramen is open (Brandt, 2007, figs. 4, 6, 11)[132].

Char. 207: Schaumberg (1978, figs. 2, 14)[34] figured the branchial arches of *Coelacanthus granulatus*.

Char. 230: It is likely that the lateral and posterior processes have merged in *Coelacanthus granulatus* because of the shape and size of the posterior division of the pelvic plate (Moy-Thomas & Westoll, 1935, fig. 9[131]; Schaeffer, 1941, fig. 6C)[111]; thus, both processes are coded as present.

Char. 233: The D1 basal plate of *Coelacanthus granulatus* has been figured by Schaumberg (1978, fig. 19)[34] and reconstructed by Forey (1998, fig. 11.4)[12]. We considered the shape of D1 basal plate to be hemispherical although the ventral margin is slightly convex.

Char. 250: Forey (1998, char. 97)[12] and subsequent analyses [up to Toriño et al. (2021, char. 97)[14]] coded the caudal lobes of *Coelacanthus* as asymmetrical. The ventral lobe of the caudal fin of *C. granulatus* bears 1-2 less lepidotrichia than the dorsal lobe (Forey, 1998, p. 308)[12]; the condition is closer to symmetrical lobes than asymmetrical lobes.

Diplocercides heiligenstockiensis
Based on Jessen (1966, 1973)[5,7], Cloutier (1991a)[95], Forey (1998)[12] and observation on original material (R. Cloutier, pers. observ.); JAL (October 2020) (double-checked by RC, November 2020).

Char. 42: A contact between the postparietal and the lateral extrascapular of *Diplocercides heiligenstockiensis* is clearly visible in Jessen (1966, Tafel 22-2)[7].

Char. 53: The median extrascapular is unknown in *Diplocercides heiligenstockiensis*. Nevertheless, Jessen (1966, plate 22.2)[7] figured the complete right lateral extrascapular as well as the right postparietal and tabular. Taking into account the width of the lateral extrascapular and the distance between the posteromedian corner of the postparietal and the medialmost limit of the lateral extrascapular, we can estimate that the median extrascapular would have been approximately twice the width of the lateral extrascapular.

Char. 64: Jessen (1973, fig. 3A)[5] reconstructed the presence of a spiracular bone in *Diplocercides heiligenstockiensis*, whereas Cloutier (1991a, fig. 3)[95] did not represented such an element in the camera lucida drawing of the holotype.

Char. 66: Based on Forey's (1998, p. 103-104)[12] and Cloutier's (1991a)[95] interpretations rather than that of Jessen (1973, fig. 3A)[5].

Char. 79: Cloutier (1991a, fig. 3)[95] provided a camera lucida drawing of the skull of *Diplocercides heiligenstockiensis* (specimen Sto. P7775a) where there is a triangular bony fragment located posterior to the lacrimojugal and anteroventral to the preoperculum (his "quadratojugal"). Based on the published figure, it is still unclear if this fragment belongs to the lacrimojugal (in which case it could corresponds to the ventral extension) or to the preoperculum (in which case it would complete the anteroventral margin of the preoperculum which is unclear). Observation of the original drawing and photo (R. Cloutier, pers. observ.) suggests that it is part of the lacrimojugal.

Char. 88: Forey (1998, char. 43)[12] coded *Diplocercides* as having the postorbital entirely lying behind the intracranial joint. The condition of *D. heiligenstockiensis* differs from that of *D. kayseri*. In *D. heiligenstockiensis*, the postorbital spanned the intracranial joint (Jessen, 1973[5]; Cloutier, 1991a, fig. 3[95]).

Char. 93: Forey (1998, char. 48)[12] and subsequent analyses [up to Toriño et al. (2021, char. 48)[14]] coded *Diplocercides* as having pit lines marking the cheek bones. However, the condition differs between *D. heiligenstockiensis* and *D. kayseri*. Cloutier (1991a, fig. 3)[95] figured a detailed camera

lucida drawing of the cheek of *D. heiligenstockiensis* showing the ornamentation as well as the position of the sensory pores. However, pit lines are absent from the cheek region.

Char. 101: Jessen (1973, fig. 3A)[5] figured a subtriangular bone articulating posteriorly with the operculum as the suboperculum of *Diplocercides heiligenstockiensis*. However, Cloutier (1991a, fig. 3)[95] reinterpreted the holotype and identified two different elements in the original position of the operculum represented by Jessen. These two elements were identified as the operculum itself and a subtriangular bone abutting to the operculum as the preoperculum. This interpretation was questioned by Forey (1998, p. 103-104)[12]. Based on Forey's (1998)[12] comments and a reinterpretation of the original camera lucida drawing (R. Cloutier, pers. observ.), it is suggested that the element identified by Cloutier (1991a)[95] as the preoperculum is part of the operculum. Therefore, the quadrilateral bone identified by Jessen (1973)[5] and Cloutier (1991a)[95] as the quadratojugal is reinterpreted as the preoperculum; in addition, this element is carrying a vertical segment of the preopercular canal.

Char. 127: Forey (1998, char. 59)[12] and subsequent analyses [up to Toriño et al. (2021, char. 59)[14]] coded the condition of the oral pit line of *Diplocercides* to be located at the center of ossification of the angular. Although the condition of *D. kayseri* corresponds to this plesiomorphic condition, the condition in *D. heiligenstockiensis* differs. The oral pit line in *D. heiligenstockiensis* is located in the anterior third of the length of the angular.

Char. 258: Although only a few thoracic-abdominal vertebrae are known in *Diplocercides heiligenstockiensis*, we agree with the description of Jessen (1973)[5] as well as the coding of Friedman (2007, char. 125)[98] that supraneural spines are absent.

Diplocercides kayseri

Based on Stensiö (1922, 1937)[133,134], Szrek (2007)[135], Cloutier (1991a)[95] and Forey (1998)[12] and observation on original material; RC (double-checked by RC; neurocranial characters double-checked by AMC, September 6th, 2021).

Char. 47: The middle and posterior pit lines of *Diplocercides kayseri* are located at mid-length (Forey, 1998, fig. 3.4)[12]. We are coding *D. kayseri* as having middle and posterior pit lines in the anterior third as it is closer to this condition and clearly not located in the posterior half of the postparietal.

Char. 51: Forey (1998, char. 16)[12] and subsequent analyses coded *Diplocercides* as having extrascapulars behind the level of the neurocranium. The condition of the extrascapulars of *Diplocercides kayseri* is similar to the condition reported in *Onychodus jandemarrai*. Based on Stensiö's illustration (1922, fig. 1)[133], it is suggested that the median extrascapular would be located above the neurocranium, whereas the lateral extrascapular would be posterior to the neurocranium. Thus, we are coding *D. kayseri* as a polymorphic condition.

Char. 79: Cloutier (1991a, fig. 2a)[95] illustrated the posterior part of the lacrimojugal of *Diplocercides kayseri* (based on a latex peel of the holotype). The shape could correspond to the ventral extension.

Char. 99: Forey (1998, char. 49)[12] coded *Diplocercides* as having ornament of the cheek bones as being absent or as coarse superficial rugosity. However, the ornament of *Diplocercides kayseri* cheek bones is composed of both fine ridges and tubercles (Cloutier, 1991a, fig. 2a)[95]. Thus, we coded character 99 as polymorphic.

Char. 101: Cloutier (1991a, fig. 2)[95] identified the presence of a postorbital, squamosal, quadratojugal and preopercular in *Diplocercides kayseri* (ex. *Nesides schmidti*). The element interpreted as the quadratojugal is reidentified as the preopercular, whereas the element identified as the preopercular is reidentified as the subopercular; this reinterpretation of the cheek bones of *D. kayseri* agrees with that of Forey (1998, fig. 4.5)[12].

Char. 116: Forey (1998, char. 54)[12] and subsequent analyses [up to Toriño et al. (2021, char. 54)[14]] coded *Diplocercides* as having teeth attached to the dentary. However, the condition figured by Stensiö (1922, pl. III, fig. 1, pl. V, fig. 1)[133], Forey (1998, fig. 5.2)[12], and Szrek (2007, figs. 2, 3)[135] suggests the presence of separate plates with teeth rather than teeth attached to the dentary.

Char. 171: Forey (1998, fig. 6.2, p. 171)[12] reported the presence of a vestibular fontanelle in *Diplocercides kayseri*.

Char. 176: Stensiö (1922, fig. 1, pl. III, fig. 2; 1937, text-fig. 8)[133,134] and Forey (1998, fig. 6.2)[12] figured the neurocranium of *Diplocercides kayseri*. Stensiö identified the processus annectens without showing a clear connection with the parasphenoid. On the other hand, Forey (1998, fig. 6.2A)[12] did not figured a clear limit of the parasphenoid. In Toriño et al. (2021, char. 71)[14], *Diplocercides* is coded as a processus annectens meeting the parasphenoid. New observation on the holotype of *D. kayseri* confirms that the processus connectens does not meet the parasphenoid (J.A. Long, pers. observ.).

Diplurus newarki
Based on Bryant (1934)[136], Schaeffer (1952)[35], Cloutier (1991b)[96] and Forey (1998)[12] and observation of original material (R. Cloutier, pers. observ.); RC (double-checked by RC).
Char. 13: Forey (1998, char. 3)[12] coded *Diplurus* as having a single median rostral. However, the median snout region of *Diplurus newarki* is composed of multiple elements as figured by Schaeffer (1952, pl. 8)[35] and seen on specimens YPM PU 14945 and YPM PU 14918.
Char. 36: Cavin et al. (2020, char. 51)[101] coded *Diplurus* has having three supraorbitals articulating with the parietal. However, Schaeffer (1952, figs. 4a, 5a)[35] illustrated bilateral difference: on the right side, four supraorbitals articulate with the right parietal, whereas three supraorbitals articulate with the left parietal. Therefore, this character is coded as polymorphic in *D. newarki*.
Char. 54: Forey (1998, char. 18)[12] coded *Diplurus* has having an embayed posterior margin of the skull roof. However, based on Schaeffer (1952, figs. 4, 5, pl. 7, 9)[35], the posterior margin is straight with the exception of a small posterior process extending posteriorly to the tabulars. Thus, *D. nerwarki* is coded as a straight posterior margin of the skull roof.
Char. 62: Forey (1998, char. 29)[12] coded *Diplurus* as having cheek bones not in contact. However, Schaeffer (1952, fig. 4, pl. 9, 12)[35] and numerous specimens (R. Cloutier, pers. observ.) show contact among most of the cheek bones.
Char. 90: Forey (1998, char. 45)[12] and subsequent analyses [up to Toriño et al. (2021, char. 45)[14]] coded the trajectory of the infraorbital canal of *Diplurus* as running along the anterior margin of the postorbital. However, Schaeffer (1952, fig. 4, plate 9.2)[35] and Forey (1998, fig. 4.16A)[12] showed the presence of 1-3 sensory pores either close to the center of the postorbital or close to the anterior margin [best visible in Schaeffer (1952, pl. 9.2)[35]]. We keep the coding as "1" although the reconstruction could have been misleading.
Char. 91: Forey (1998, char. 46)[12] and subsequent analyses [up to Toriño et al. (2021, char. 46)[14]] coded the jugal canal of *Diplurus* as having prominent branches. However, Schaeffer (1952, fig. 4B)[35] illustrated the squamosal of *D. newarki* with a single sensory jugal pore. Observed specimens of *D. newarki* have a reduced number of aligned jugal pores indicating that the jugal canal is simple rather than having prominent branches.
Char. 92: Forey (1998, char. 47)[12] and subsequent analyses [up to Toriño et al. (2021, char. 47)[14]] coded the trajectory of the jugal canal of *Spermatodus* as running along the ventral margin of the squamosal. However, Schaeffer (1952, fig. 4)[35] figured a sensory jugal pore in the center of the squamosal.
Char. 99: Forey (1998, char. 49)[12] and subsequent analyses [up to Toriño et al. (2021, char. 49)[14]] coded the cheek bone ornament to be absent in *Diplurus*. However, Schaeffer (1952, fig. 4, pl. 9, 11)[35] illustrated the cheek bones of *Diplurus newarki* are either smooth or ornamented with coarse rugosity. Thus, we are coding *D. newarki* as polymorphic.
Char. 108: In contrast to Schwimmer et al. (1994, tab. 2)[59] who considered to operculum to be quadrilateral, we considered the shape of the operculum of *Diplurus newarki* to be triangular (Schaeffer, 1952, fig. 4, pl. 9, 10, 13)[35].
Char. 126: Forey (1998, char. 58)[12] and subsequent analyses [up to Toriño et al. (2021, char. 57)[14]] coded *Diplurus* has having a short oral pit line on the angular. However, Forey (1998, p. 150)[12] mentioned that the angular of *Diplurus* is smooth without a pit line; this comment corresponds to our observation of numerous specimens. Thus, we are coding *Diplurus newarki* as "-" because the oral pit line is absent.

Char. 127: Forey (1998, char. 59)[12] and subsequent analyses [up to Toriño et al. (2021, char. 59)[14]] coded the condition of the oral pit line of *Diplurus* to be located at the center of ossification of the angular. However, Schaeffer (1952, fig. 7, pl. 7-9)[35] did not report the presence of an oral pit line. Forey (1998, p. 150)[12] mentioned that the angular is smooth, without ornament or a pit line. Thus, we are coding character 127 as "-" since the oral pit line is absent.

Char. 137: Cavin et al. (2020, char 56)[101] coded *Diplurus* as "?". We keep this coding since the depth of the angular is relatively uniform throughout the length of the angular in *D. newarki* (Schaeffer, 1952, fig. 7)[35].

Char. 176: Forey (1998, char. 71)[12] coded the processus connectens of *Diplurus* as meeting the parasphenoid, whereas Toriño et al. (2021, char. 71)[14] coded *Diplurus* as the processus connectens failing to meet the parasphenoid. We keep the coding proposed by Forey (1998, char. 71)[12].

Char. 263: Forey (1991, char. 54)[12] coded the ornamentation of the scales of *Diplurus* as undifferentiated, whereas Forey (1998, char. 104)[12] and Dutel et al. (2015, char. 104)[88] coded it as differentiated. The median ridges are more developed than the lateral ones as illustrated by Schaeffer (1952, fig. 12)[35].

Dobrogeria aegyssensis
Based on Cavin & Grădinaru (2014)[37]; known only from the holotype; JAL, December 5th 2019 (double-checked by RC, November 10, 2020).

Char. 21: Cavin & Grădinaru (2014, char. 12)[37] coded for the absence of intertemporal in *Dobrogeria aegyssensis*; however, since this region of the skull in unknown in the specimens we rather coded it as "?".

Char. 22: Cavin & Grădinaru (2014)[37] refered to the supratemporal, whereas we identify this element as the tabular.

Char. 23: The dermal bone suturing with the posterolateral margin of the postparietal of *Dobrogeria aegyssensis* is identified by Cavin & Grădinaru (2014)[37] as the supratemporal. Herein, we considered this element to be homologous with the tabular.

Char. 30: Cavin & Grădinaru (2014, text-fig. 2)[37] referred to this process in *Dobrogeria aegyssensis* as the ventral process of the parietal.

Char. 38: Cavin & Grădinaru (2014, text-fig. 3)[37] referred to the descending process of the postparietal of *Dobrogeria aegyssensis* as the ventral process of the postparietal.

Char. 50: Cavin & Grădinaru (2014, char. 15)[37] coded the extrascapulars of *Dobrogeria aegyssensis* to be free from the postparietals. Since these elements are unknown in the material described by Dobrogeria and that the posterior margin of the postparietals and tabulars could suggested the presence of sutures with the extrascapulars we rather code this character as "?".

Char. 62: Cavin & Grădinaru (2014, char. 15)[37] wrote that the cheek bones did not suture to each other.

Char. 78: Cavin & Grădinaru (2014, char. 36)[37] considered that the lacrimojugal of *Dobrogeria aegyssensis* is angled anteriorly. However, based on their illustrated lacrimojugal (Cavin & Grădinaru, 2014, fig. 13)[37] we considered that the anterior part of the lacrimojugal is too unclear to code properly the condition.

Char. 81: Based on the shape of the lacrimojugal figured by Cavin & Grădinaru (2014, text-fig. 13 A1, A2)[37], the margin seems to go well beyond the orbital notch anteriorly.

Eoactinistia foreyi
Based on Johanson et al. (2006)[38] and observation of the original dentary (JAL); known only from the holotype; JAL (double-checked by RC, February 3rd, 2021).

Euporosteus eifeliensis

Based on Stensiö (1937)[134], Jaekel (1927)[137], Cloutier (1991a)[95], Forey (1998)[12], Zhu et al. (2012)[40], and observation on the original specimen; known only from the holotype; JAL (double-checked by RC, February 3rd 2021; neurocranial characters double-checked by AMC, September 6th, 2021).

Char. 16: Zhu et al. (2012, char. 8)[40] coded the parietals and preparietals to be of similar size; however, the parietal is approximately twice the length of the preparietal (R. Cloutier, pers. observ.; Forey, 1998, fig. 6.3A[12]).

Char. 31: Zhu et al. (2012, p. 4)[40] mentioned the presence of a weakly developed descending process of the parietal in *Euporosteus eifeliensis*. However, they coded *Euporosteus* as lacking a descending process. Herein, we coded the parietal of *Euporosteus eifeliensis* as having a descending process, even though the process is poorly developed.

Char. 32: Zhu et al. (2012)[40] mentioned that the surface of the parietonasal shield is smooth and not ornamented with tubercles in *Euporosteus eifeliensis*.

Char. 50: Forey (1998, char. 15)[12] as well as Zhu et al. (2012, char. 15)[40] coded the condition of *Euporosteus* as "?". Dutel et al. (2012, char. 15)[60] and subsequent analysis [up to Toriño et al. (2021, char. 15)[14]] coded *Euporosteus* as having free extrascapulars. However, the condition of the otico-occipital part of *E. eifeliensis* are unknown.

Char. 57: Cloutier (1991a, char. 22)[95] coded for the presence of a preorbital (his "tectal") in *Euporosteus eifeliensis*. Zhu et al. (2002, char. 10)[40] coded *Euporosteus* as having a preorbital. Forey (1998, fig. 6.3B)[12] illustrated the preorbital forming the anterior part of the left orbit that is carrying the two posterior rostral openings.

Char. 147: The parasphenoid does flair anteriorly, as shown in our personal photos of the holotype (J.A. Long, pers. observ.) and in Friedman (2007, fig. 7B)[98].

Char. 151: Forey (1998, char. 78)[12] and subsequent analyses [up to Toriño et al. (2021, char. 78)] coded *Euporosteus* as having a close buccohypophysial foramen. Cloutier (1991a, b, char. 35)[95,96] coded *E. eifeliensis* with an open buccohypophysial foramen. Cloutier (1996, fig. 10C)[61] illustrated (camera lucida drawing) the parasphenoid of *E. eifeliensis* with an open buccohypophysial foramen. Herein, *E. eifeliensis* is coded with an open foramen.

Char. 163: The condition of the foramen for the oculomotor nerve of *Euporosteus eifeliensis* is coded as polymorphic as it is somewhat dorsal and posterior to n.II (A.M. Clement, pers. observ. from scan data).

Char. 176: Forey (1998, char. 71)[12] coded the condition of the processus connectens of *Euporosteus* as failing to meet the parasphenoid. Toriño et al. (2021, char. 71)[14] coded the processus connectens as meeting the parasphenoid. Forey's (1998, fig. 6.3)[12] reconstruction suggests that there is no contact. New CT-scan analysis of the holotype of *E. eifeliensis* shows unambiguously that the processus connectens fails to meet the parasphenoid (A.M. Clement, pers. observ.).

Char. 263: Cavin & Grădinaru (2014, p. 176)[37] mentioned that they added character-states for *Euporosteus* from Zhu et al. (2012)[40]. Since the scales are unknown in *E. eifeliensis* as well as in *E. yunnanensis*, Zhu et al. (2012, char. 104)[40] coded the condition of the scales of *Euporosteus* as "?". However, Cavin & Grădinaru (2014, char. 104)[37] and subsequent analyses [up to Toriño et al. (2021, char. 104)[14]] coded the scale ornament of *Euporosteus* as differentiated. We are coding *E. eifeliensis* as "?".

Char. 267: Dutel et al. (2012, 2015; char. 109)[60,88] and some subsequent analyses up to Cavin et al. (2013, 2017, char. 109)[41,87] coded the condition of the ventral keel scales of *Euporosteus* as unknown. Cavin & Grădinaru (2014, char. 109)[37] and some subsequent analyses [up to Toriño et al. (2021, char. 109)[14]] coded for the presence of ventral keel scales in *Euporosteus*. However, *E. eifeliensis* is solely known from part of a skull (Stensiö, 1937[134]; Forey, 1998[12]).

Euporosteus yunnanensis

Based on Zhu et al. (2012)[40] and personal observation by JAL; JAL (double-checked by RC, February 3rd, 2021).

Char. 26: The otic canal of *Euporosteus yunnanensis* follows a simple trajectory that most likely passes through the postparietals (Zhu et al., 2012, fig. 3)[40]; however, since the condition of the lateral series of bones is unclear, it is not possible to code this character unambiguously.

Char. 28: Forey (1998, char. 21)[12] coded *Euporosteus* (in reference to *E. eifeliensis*) as "?" in reference to character 28. Zhu et al (2012, char. 21)[40] and subsequent analyses [including Cavin & Grădinaru (2014)[37] up to Toriño et al. (2021, char. 21)[14]] coded *Euporosteus* as having the otic canal joining the supratemporal canal in the lateral extrascapular. However, the limits of skull roofing bones of *Euporosteus yunnanensis* are unknown as well as the condition of the extrascapulars. Thus, we are coding character 28 as "?" because the extrascapulars are unknown.

Char. 32: Zhu et al. (2012, p. 4)[40] mentioned that the surface of the postparietal shield is smooth and is not ornamented with tubercles in *Euporosteus yunnanensis*.

Char. 37: Although Zhu et al. (2012, p. 4)[40] wrote that the anterior margin of the postparietal shield is not straight, in reference to the presence of two small anterior protrusions, they coded *Euporosteus* as having a straight margin (Zhu et al., 2012, char. 1)[40]. We considered the condition to be straight in comparison to the disparity observed in actinistians.

Char. 50: Forey (1998, char. 15)[12] as well as Zhu et al. (2012, char. 15)[40] coded the condition of *Euporosteus* as "?". Dutel et al. (2012, char. 15)[60] and subsequent analysis [up to Toriño et al. (2021, char. 15)[14]] coded *Euporosteus* as having free extrascapulars. However, the condition of the dermatocranium is poorly known in *E. yunnanensis* (Zhu et al., 2012)[40] and the extrascapulars are unknown.

Char. 263: Cavin & Grădinaru (2014, p. 176)[37] mentioned that they added character-states for *Euporosteus* from Zhu et al. (2012)[40]. Since the scales are unknown in *E. yunnanensis*, Zhu et al. (2012, char. 104)[40] coded the condition of the scales of *Euporosteus* as "?". However, Cavin & Grădinaru (2014, char. 104)[37] and subsequent analyses [up to Toriño et al. (2021, char. 104)[14]] coded the scale ornament of *Euporosteus* as differentiated. We are coding *E. yunnanensis* as "?".

Char. 267: Dutel et al. (2012, 2015; char. 109)[60,88] and some subsequent analyses up to Cavin et al. (2013, 2017, char. 109)[41,87] coded the condition of the ventral keel scales of *Euporosteus* as unknown. Cavin & Grădinaru (2014, char. 109)[37] and some subsequent analyses [up to Toriño et al. (2021, char. 109)[14]] coded for the presence of ventral keel scales in *Euporosteus*. However, *E. yunnanensis* is solely known from partial cranial material (Zhu et al., 2012)[40].

Foreyia maxkuhni

Based on Cavin et al. (2017)[41]; known only from the holotype; RC (double-checked by RC).

Char. 2: Cavin et al. (2017, fig. S4)[41] illustrated the position of sensory pores in the rostral region. A pore (identified as a foramen of the supraorbital sensory canal) is located at the suture of nasal 2 (left), tectal 2 and tectal 3. There is another unidentified pore at the anterior margin of nasal 2 (right) which is considered herein as being a pore of the ethmoid commissure.

Char. 14: *Foreyia* has a series of rostral ossicles which lack teeth (Cavin et al., 2017, fig. S4)[41].

Char. 20: A single bone is interpreted as a fusion of the postparietal, supratemporal (or tabular according to the homology suggested herein) and extrascapulars by Cavin et al. (2017)[41].

Char. 42: According to Cavin et al. (2017)[41], the postparietal is fused with the extrascapulars. Thus, *Foreyia* is coded as "-".

Char. 44: Cavin et al. (2017, char. 24)[41] coded *Foreyia* as a condition unknown for the anterior pit lines. However, we considered that the anterior pit lines are absent since the excellent preservation of the surface of the skull roofing bones does not show any indication of the presence of pit lines.

Char. 55: Cavin et al. (2017, char. 22)[41] coded *Foreyia* as a condition unknown for the presence of the anterior branches of the occipital commissure. However, we considered that the anterior branches of the occipital commissure are absent since the excellent preservation of the surface of the skull roofing bones does not show any indication of its presence.

Char. 68: Cavin et al. (2017)[41] considered that the squamosal is fused to the lacrimojugal in *Foreyia*. Thus, we coded the squamosal to be absent.

Char. 72: Cavin et al. (2017, supplementary information)[41] suggested that the squamosal of *Foreyia* is fused to the lacrimojugal; thus, we are coding the condition of the squamosal as irrelevant "-".

Char. 88: Cavin et al. (2017, char. 43)[41] and subsequent analyses [up to Toriño et al. (2021, char. 43)[14]] coded the postorbital of *Foreyia* as spanning the intracranial joint. We are coding the condition as "?" since the precise morphology of the postorbital is unclear.

Char. 101: Based on Cavin et al. (2017)[41], the squamosal is fused to the lacrimojugal and the quadratojugal is absent. Cavin et al. (2017, fig. S2)[41] illustrated a small element ventroposteriorly to the preopercular that might represent a quadratojugal; however, his identification is dubious. Thus, we are coding *Foreyia* as "-" since the condition is unique to this species.

Char. 126: The oral pit line seems to be absent in *Foreyia maxkuhni* (Cavin et al., 2017, supplementary information)[41].

Char. 247: Cavin et al. (2017, char. 103)[41] and subsequent analyses [up to Toriño et al. (2021, char. 103)[14]] coded the median fin lepidotrichia of *Foreyia* as expanded. However, comparing species in which the lepidotrichia are clearly expanded, the condition figured by Cavin et al. (2017, figs. 1, S2)[41] is not indicative of expanded lepidotrichia.

Char. 257: Although the vertebrae slightly bent upward anteriorly in *Foreyia*, we do not consider that the condition is strongly arched as in *Allenypterus*.

Char. 258: Cavin et al. (2017, fig. 1C)[41] reconstructed the axial skeleton of *Foreyia maxkuhni* without "supraneural". However, based on the photography of the holotype (Cavin et al., 2017, fig. S2A)[41], a single "supraneural" is present anteriorly to the first radial supporting lepidotrichia in the epichordal lobe of the caudal fin.

Char. 263: Cavin et al. (2017, char. 104)[41] coded the scale ornamentation of *Foreyia* as differentiated. Cavin et al. (2017, fig. 2C)[41] figured different ornament pattern for scales coming from various body localization. Some of the scales show a prominent short median ridge, other a unique ornament pattern, whereas others are undifferentiated. We are coding *F. maxkuhni* as polymorphic.

Garnbergia ommata

Based on Martin & Wenz (1984)[43]; known only from holotype; RC (double-checked by RC).

Char. 9: Forey (1995, char. 5)[12] coded the condition of the dorsal laminae of the premaxillae of *Garnbergia* as "?". However, Martin & Wenz (1984)[43] described and illustrated the premaxillae of *Garnbergia ommata* as having the shape of a "courte baguette transversale." Thus, the dorsal laminae are present but reduced.

Char. 21: Martin & Wenz (1984, fig. 1)[43] reconstructed the skull of *Garnbergia* in lateral view. They illustrated a small dermal bone articulating anteriorly with a supraorbital, ventrally with the postorbital, and dorsally with the lateral process of the parietal. Topographically this element could be an intertemporal but it is rather interpreted as a supraorbital although we do not have information concerning the trajectory of the sensory canal.

Char. 23: Although the precise posterior limit of the postparietal in unclear in *Garnbergia*, we considered that the tabular extends posterior to the posterior limit of the postparietal based on the reconstruction given by Martin & Wenz (1985, fig. 1)[43] and the photography of the dorsal view of the skull roof (Planche 1.3).

Char. 62: Forey (1998, char. 29)[12] and subsequent analyses [up to Toriño et al. (2021, char. 29)[14]] coded *Garnbergia* as having separated cheek bones. Martin & Wenz (1984, fig. 1, pl. 1)[43] and reexamination of a high resolution of the holotype (SMNS 51035) show that the cheek bones of *G. ommata* are in contact.

Char. 72: The cheek bone identified by Martin & Wenz (1984, fig. 1)[43] as the "préopercule dorsal" is herein identified as the squamosal.

Char. 83: In *Garnbergia*, the postorbital limb of the lacrimojugal extends almost to mid-height of the orbit (Martin & Wenz, 1984, fig. 1)[43]; we coded it as below mid-orbit height although it is very close to it.

Char. 99: Forey (1998, char. 49)[12] and subsequent analyses [up to Toriño et al. (2021, char. 49)[14]] coded the cheek bone ornamentation of *Garnbergia* as tubercular. The condition of the ornamentation of the cheek bones is poorly known on the sole specimen of *G. ommata* (see Martin & Wenz, 1984, pl. 1, fig. 1)[43]. Thus, we are coding character 49 as unknown.

Char. 103: According to both Martin & Wenz (1984)[43] and Forey (1998)[12] the suboperculum is most likely absent in *Garnbergia*.

Char. 109: Forey (1998, char. 57)[12] and subsequent analyses [up to Toriño et al. (2021, char. 57)[14]] coded the condition of the hook-shaped dentary of *Garnbergia* as unknown. Martin & Wenz (1984, p. 2)[43] mentioned in the diagnosis of *G. ommata* that "dentaire en forme de baguette non recourbée et à bord postérieur présentant une forte encoche" [straight, tube-shaped dentary with a strong hook-shaped notch on the posterior margin].

Gavinia syntrips

Based on Long (1999)[44] and observation on the original specimens (JAL); known only from two specimens; JAL (double-checked by RC, February 3rd, 2021).

Char. 91: Gess & Coates (2015, char. 46)[78] and subsequent analyses [up to Toriño et al. (2021, char. 46)[14]] coded the condition of the jugal canal of *Gavinia* as unknown. However, Long (1999, fig. 3)[44] clearly illustrated a simple jugal canal (his "preopercular sensory-line").

Char. 107: Long (1999, p. 47)[44] reported the presence of three small pits on the operculum of *Gavinia syntrips* near the contact with the cheek; similar pores found in the dipnoans *Howidipterus* and *Barwickia* were suggested as sensory pit clusters (Long, 1992)[138].

Char. 113: Gess & Coates (2015, char. 65)[78] and subsequent analyses [up to Toriño et al. (2021, char. 65)[14]] coded the condition of the dentary of *Gavinia* as unknown. However, Long (1999, figs. 3, 5[44]; and pers. observ.) did not reported the presence of a prominent lateral swelling of the dentary.

Char. 117: Gess & Coates (2015, char. 61)[78] and subsequent analyses [up to Toriño et al. (2021, char. 61)[14]] coded the condition of the dentary pore of *Gavinia* as unknown. However, the dentary of specimen NMV P160710 of *G. syntrips* shows no indication of the presence of a dentary pore (Long, 1999)[44].

Char. 131: Gess & Coates (2015, char. 62)[78] and subsequent analyses [up to Toriño et al. (2021, char. 62)[14]] coded the condition of the lower jaw ornament of *Gavinia* as tubercular. The ornamentation of the lower jaw of *G. syntrips* includes both the tubercular type (for the dentary and dorsal part of the posterior part of the angular) and the ridged type (for the ventral part of the posterior part of the angular) (Long, 1999, figs. 3-6)[44]. Thus, character 131 is coded as polymorphic.

Char. 201: Friedman (2007, char. 84)[98] coded *Gavinia* as double headed. However, the articular facet of the proximal extremity of the hyomandibular is single headed as well as the facet for hyomandibular articulation on the neurocranium as illustrated by Long (1999, fig. 3)[44].

Guizhoucoelacanthus guanlingensis

Based on Geng et al. (2009)[45]; known only from two specimens; JAL, December 5th, 2019 (double-checked by RC, January 29th, 2021).

Char. 41: Restoring the slightly moved postparietal shield back to normal articulation shows it would laterally contact the postorbital (Geng et al., 2009, fig. 2)[45].

Char. 51: Geng et al. (2009, char. 16)[45] and Wen et al. (2013, char. 16)[54] and subsequent analyses coded *Guizhoucoelacanthus* as having extrascapulars located behind the neurocranium. However, based on Geng et al. (2009, figs. 1A-B, 2A-B)[45], the extrascapulars are clearly part of the skull roof.

Char. 62: Geng et al. (2009, fig. 29)[45] and subsequent analyses [up to Toriño et al. (2021, char. 29)[14]] coded *Guizhoucoelacanthus* as having separated cheek bones. However, based on Geng et al. (2009, fig. 2)[45], there is a clear contact between the postorbital and the squamosal and a separation between the squamosal and preoperculum. Thus, we are coding *G. guanlingensis* as polymorphic.

Char. 78: Geng et al. (2009, char. 36)[45] and subsequent analyses [up to Toriño et al. (2021, char. 36)[14]] coded the lacrimojugal of *Guizhoucoelacanthus* as angled anteriorly. However, there is no clear anterior angle on the lacrimojugal of *G. guanlingensis* as figured by Geng et al. (2009, fig. 2)[45].

Char. 90: Geng et al. (2009, char. 45)[45], Dutel et al. (2012, 2015, char. 45)[60,88], Wen et al. (2013, char. 45)[54], and Cavin et al. (2013, char. 45)[87] coded properly the trajectory of the infraorbital canal of *Guizhoucoelacanthus* as running through the center of the postorbital (Geng et al., 2009, fig. 2)[45]. However, Cavin & Grădinaru (2014, char. 45)[37], Cavin et al. (2017, char. 45)[41], and Toriño et al. (2021, char. 45)[14] coded the condition of the trajectory of the infraorbital canal as passing along the anterior margin of the postorbital. We agree with the original coding of Geng et al. (2009)[45].

Char. 91: Geng et al. (2009, char. 46)[45] and subsequent analyses [up to Toriño et al. (2021, char. 46)[14]] coded the condition of the jugal canal of *Guizhoucoelacanthus* as unknown. However, Geng et al. (2009, fig. 2B)[45] figured only two pores in the squamosal associated to the jugal canal which suggests that the jugal canal is simple.

Char. 134: Geng et al. (2009)[45] figured the lower jaw of *Guizhoucoelacanthus guanlingensis*. They figured the condition splenial of the sole specimen on the drawing of the specimen (figs. 1B, 2) as well as the reconstruction (fig. 1C). According to their reconstruction, the lateral gular would articulate with the posterior margin of the dentary and splenial which is most unlikely. Thus, the preservation of the specimen does not allow us to code for this character.

Char. 264: Geng et al. (2009, char. 106)[45] and subsequent analyses [up to Toriño et al. (2021, char. 106)[14]] coded the condition of the scale ornament in *Guizhoucoelacanthus* as rugose [based on the character-states used by Forey (1998, char. 106)[12]]. However, Geng et al. (2009, fig. 3)[45] figured scales from three different body positions, each one of them showing only longitudinal ridges.

Hadronector donbairdi
Based on Lund & Lund (1985)[13], Cloutier (1991a)[95] and Forey (1998)[12] and observations on original material (R. Cloutier, pers. observ.); RC (double-checked by RC).

Char. 19: Forey (1998, char. 23)[12] coded *Hadronector* as having bifurcating pores for the supraorbital sensory canals. However, Cloutier (1991a, fig. 4)[95] illustrated the presence of two or three tiny pores located in each supraorbital.

Char. 22: We recognized the presence of a tubular in *Hadronector donbairdi* as shown by Lund & Lund (1985, figs. 43-44)[13] and Cloutier (1991a, fig. 4)[95]; the same element was identified as a supratemporal by Forey (1998, fig. 3.3B)[12]. Lund & Lund (1985, figs. 43, 44)[13] identified the presence of a supratemporal as well as a tabular; also using specimen CM 27307, Cloutier (1991a)[95] did not to observe the presence of a separate supratemporal.

Char. 69: Forey (1998, char. 34)[12] and subsequent analyses [up to Toriño et al. (2021, char. 34)[14]] coded the squamosal of *Hadronector* as being limited to the mid-level of the cheek. However, Cloutier (1991a, fig. 4)[95] illustrated the cheek region of specimen CM 27307B of *H. donbairdi* showing a contact between the dorsal margin of the squamosal and the skull roof.

Char. 90: Forey et al. (1998, char. 45)[12] and subsequent analyses [up to Toriño et al. (2021, char. 45)[14]] coded the trajectory of the infraorbital canal as passing along the anterior margin of the postorbital. However, Lund & Lund (1985, figs. 37, 43)[13], Cloutier (1991a, fig. 4)[95], and Forey (1998, fig. 4.7B)[12] showed sensory pores located near the center of the postorbital.

Char. 91: Forey (1998, char. 46)[12] and subsequent analyses [up to Toriño et al. (2021, char. 46)[14]] coded the condition of *Hadronector* as unknown. However, specimens CM 30712A of *Hadronector donbairdi* clearly shows that the jugal canal is simple having only a few pores aligned with the main canal.

Char. 93: Forey (1998, char. 48)[12] and subsequent analyses [up to Toriño et al. (2021, char. 48)[14]] coded the condition of the cheek pit lines of *Hadronector* as unknown. However, Lund & Lund (1985, fig. 43)[13] and Cloutier (1991a, fig. 4)[95] illustrated the presence of a vertical pit line on the preoperculum (their "quadratojugal") of *H. donbairdi*.

Char. 99: Forey (1998, char. 49)[12] coded *Hadronector* as having ornament of the cheek bones as being absent or as coarse superficial rugosity. However, the ornament of *Hadronector donbairdi* cheek bones is composed of both fine ridges and tubercles (Cloutier, 1991a, fig. 4[95]; Lund & Lund, 1985, figs. 38, 40[13]). Thus, we coded character 99 as polymorphic.

Char. 103: Lund & Lund (1985, p. 61)[13] suggested that the plesiomorphic condition among actinistians is to have both an operculum and subopercum. Lund & Lund (1985, fig. 43)[13] identified the presence of a quadrilateral subopercum in *Hadronector*. On the other hand, Cloutier (1991a, fig. 4)[95] illustrated two elements in the same position as the single element represented by Lund & Lund (1985)[13]; the dotted-line separating the dorsal and ventral parts might correspond to a fracture. Forey (1998)[12] suggested that these two elements represented by Cloutier (1991a)[95] might correspond to two scales that have been move anteriorly. In contrast to Forey (1998)[12], we recognize the presence of a subopercum in *Hadronector donbairdi*.

Char. 116: Forey (1998, char. 54)[12] and subsequent analyses [up to Toriño et al. (2021, char. 54)[14]] coded the condition of dentary teeth in *Hadronector* as unknown. Lund & Lund (1985, p. 31, fig. 45)[13] mentioned and illustrated the dentary of *Hadronector donbairdi* bearing a series of small teeth along the oral margin.

Char. 258: Lund & Lund (1985, fig. 35)[13] illustrated solely caudal "supraneurals" associated to epichordal lepidotrichia of *Hadronector donbairdi*. However, numerous specimens show clearly that there are two "supraneurals" located anteriorly to the insertion of the epichordal lobe of the caudal fin.

Char. 260: Lund & Lund (1985, fig. 35)[13] illustrated the anteriormost cervical neural arches of *Hadronector donbairdi* as stubby and thicker; thus, we are coding *H. donbairdi* as having expanded cervical neural arches. However, Forey (1998, char. 91)[12] coded *Hadronector* as "?".

Char. 263: According to Forey (1991, char. 54)[97], Forey (1998, char. 104)[12] and Dutel et al. (2015, char. 104)[88] the condition of the ornamentation of the scales of *Hadronector* is unknown. However, based on Lund & Lund (1985, fig. 38)[13] and observation on specimens (CM 30713, CM 37697), the ornamentation of the scales of *Hadronector* is composed of longitudinal ridges without a prominent central one.

Hainbergia granulata
Based on Schweizer (1966)[46] and Forey (1998)[12]; known only from the holotype; JAL, September 11th 2020 (double-checked by RC, January 25, 2021).

Char. 22: The dermal bone identified by Schweizer (1966)[46] in *Hainbergia granulata* is identified herein as the tabular.

Char. 234: Schweizer (1966)[46] mentioned in the diagnosis of *Hainbergia granulata* that the anterior lepidotrichia of the first dorsal fin have "nodular tubercles" (knotige Tuberkeln); these denticles were not figured by Schweizer (1966, fig. 1)[46].

Char. 253: Schweizer (1966)[46] mentioned in the diagnosis of *Hainbergia granulata* that the anterior lepidotrichia of the caudal fin most likely have "knotige tubercles" (knotige Tuberkeln). These denticles were not figured by Schweizer (1966, fig. 1)[46] and they do not show on the photography of the holotype (Schweizer, 1966, pl. 22, fig. 1)[46]. Thus, we are coding *H. granulata* as lacking denticles on the caudal lepidotrichia.

Heptanema paradoxum
Based on Renesto & Stockar (2018)[1]; JAL, September 11th 2020 (double-checked by RC, January 29th, 2021).

Char. 39: The shape of the postparietal of *Heptanema* sp. of Renesto & Stockar (2018, fig. 4)[1] is intermediate between pentagonal and the "inverted L"; thus, among our descriptors it fits best the "inverted L".

Char. 77: Most of the lacrimojugal is preserved in *Heptanema* sp. of Renesto & Stockar (2018, fig. 4)[1]; however, the reconstruction of the specimen as well as the resolution of the photography do not allow us to code for the condition.

Char. 78: Forey (1998, char. 36)[12] and subsequent analyses [up to Toriño et al. (2021, char. 36)[14]] coded the condition of the anterior end of the lacrimojugal of *Heptanema* as "?". However, using the condition figured by Renesto & Stockar (2018, figs. 3, 4)[1] for *Heptanema* sp., we considered that the anterior end of the lacrimojugal is angled.

Char. 109: Cavin et al. (2017, char. 57)[41], Renesto & Stockar (2018, char. 57)[1] and Toriño et al. (2021, char. 57)[14] coded the condition of the hook-shaped process of the dentary of *Heptanema* as unknown. We are using the condition figured by Renesto & Stockar (2018, fig. 4)[1] in *Heptanema* sp. to code for the presence of a hook-shaped process on the dentary of *H. paradoxum*.

Char. 113: Renesto & Stockar (2018, char. 60)[1] and Toriño et al. (2021, char. 60)[14] coded the condition of the dentary of *Heptanema* as unknown. However, the left dentary of *Heptanema* sp. illustrated by Renesto & Stockar (2018, figs. 3, 4)[1] does not show sign of a prominent lateral swelling; we assume that the juvenile condition did not change in the adults.

Char. 114: Renesto & Stockar (2018, char. 63)[1] and Toriño et al. (2021, char. 63)[14] coded the condition of the dentary ornament of *Heptanema* as unknown. However, the dentary of *Heptanema* sp. figured by Renesto & Stockar (2018, fig. 4A)[1] does not indicate the presence of ornament.

Char. 137: We code *Heptanema paradoxum* as "?" because the depth of the angular is relatively uniform throughout the length of the angular (Renesto & Stockar, 2018, fig. 7; *Heptanema* sp.)[1].

Char. 211: Renesto & Stockar (2018, char. 89)[1] and subsequent analyses [up to Toriño et al. (2021, char. 89)[14]] coded the condition of the anocleithrum of *Heptanema* as unknown. However, Renesto & Stockar (2018, figs. 3, 4)[1] clearly figured narrow sigmoid anocleithra in a specimen of *Heptanema* sp.; we are coding *H. paradoxum* based on this condition observed in *H.* sp. of Renesto & Stockar (2018)[1].

Char. 232: Renesto & Stockar (2018, char. 101)[1] and Toriño et al. (2021, char. 101)[14] coded the ventral margin of the basal plate of the first dorsal fin as smooth; however, Renesto & Stockar (2018, p. 644)[1] mentioned that the basal plate of the first dorsal fin is not visible. Nevertheless, we are coding the condition as smooth since a high-resolution image of the holotype of *H. paradoxum* shows the smooth ventral margin of the basal plate of the first dorsal fin.

Char. 263: Renesto & Stockar (2018, fig. 8)[1] illustrated and described the scales of *Heptanema* sp. indicating clearly that the central ridge is stout and prominent.

Holophagus gulo

Based on Gardiner (1960)[139] and Forey (1998)[12]; JAL, November 2020 (double-checked by RC, January 27th, 2021).

Char. 50: Forey (1998, char. 15)[12] coded for the presence of free extrascapulars in *Holophagus*. However, Forey (1998, fig. 11.8)[12] figured extrascapulars sutured to the posterior margin of the postparietals in the complete restoration of the species.

Char. 62: Forey (1998, char. 29)[12] coded *Holophagus* as having cheek bones not in contact. However, Forey (1998, p. 122)[12] mentioned that although the cheek bones do not overlap each other they closely abut one another with matching margins, thus we are coding *H. gulo* as having cheek bones in contact.

Char. 78: Gardiner (1960, fig. 55)[139] figured the lacrimojugal of *Holophagus gulo* in which the anterior part does not form a pronounced angle.

Char. 88: Forey (1998, char. 43)[12] and subsequent analyses [up to Toriño et al. (2021, char. 43)[14]] coded the postorbital of *Holophagus* as lying wholly behind the intracranial joint. However, Forey (1998, fig. 11.8)[12] reconstructed the cheek region of *H. gulo* showing that the postorbital spans the intracranial joint.

Char. 108: In contrast to Schwimmer et al. (1994, tab. 2)[59] who considered to operculum to be quadrilateral, we considered the shape of the operculum of *Holophagus gulo* to be triangular (Forey, 1998, fig. 11.8)[12].

Char. 211: Forey (1998, char. 89)[12] and subsequent analyses [up to Toriño et al. (2021, char. 89)[14]] coded the condition of the shape of the anocleithrum of *Holophagus* as unknown. Nevertheless, Forey (1998, fig. 11.8)[12] reconstructed the complete morphology of *H. gulo* based on specimens BMNH P.7795, P.2022 and P.3344, including a sigmoid anocleithrum.

Char. 250: Forey (1998, char. 97)[12] and subsequent analyses [up to Toriño et al. (2021, char. 97)[14]] coded the condition of the caudal lobes of *Holophagus* as unknown. However, the reconstruction of *H. gulo* by Forey (1998, fig. 11.8)[12] as well as the diagnosis (18 dorsal lepidotrichia and 17 ventral lepidotrichia) suggest that the lobes are symmetrical.

Holopterygius nudus

Based on Friedman & Coates (2006)[47] and Jessen (1973)[5]; known only from the holotype; RC (double-checked by RC).

Char. 116: Friedman & Coates (2006, char. 54)[47] coded *Holopterygius* as having teeth attached to the dentary. However, Toriño et al. (2021, char. 54)[14] coded the condition of *Holopterygius* as unknown. Herein, we code *H. nudus* as having teeth attached to the dentary based on the description provided by Friedman & Coates (2006, p. 247-248)[47].

Char. 127: Friedman & Coates (2006, char. 59)[47] coded the condition of the position of the oral pit line of *Holopterygius* as unknown. Toriño et al. (2021, char. 59)[14] coded that the oral pit line of *Holopterygius* was located at the center of ossification of the angular. However, the condition of the oral pit line of *H. nudus* is unknown.

Char. 188: Toriño et al. (2021, char. 80)[14] coded *Holopterygius* as lacking a suprapterygoid process, mentioning that it was based on Friedman & Coates (2006, char. 80)[47]. However, Friedman & Coates (2006, char. 80)[47] coded the condition as unknown. The poor preservation of the neurocranium of *H. nudus* does not allow to code for this character.

Char. 211: Friedman & Coates (2006, char. 89)[47] coded *Holopterygius* as having a simple anocleithrum, while Toriño et al. (2021, char. 89)[14] coded the condition of the anocleithrum as unknown. Although the shape of the anocleithrum of *H. nudus* does not seem to be forked, the precise shape cannot be determined because of its fragmentary nature (Friedman & Coates, 2006, p. 248, figs. 1, A1)[47]. Thus, we are coding this character as unknown.

Char. 222: Friedman & Coates (2006, char. 99)[47] coded the condition of the lepidotrichia of the paired fins as "?", because the condition of the paired lepidotrichia is unknown; the condition illustrated in their reconstruction is based on *Allenypterus*. Wendruff & Wilson (2012, char. 99)[70] and subsequent phylogenetic analyses [e.g., Dutel et al. (2012)[60], Cavin & Grădinaru (2014)[37], Toriño et al. (2021)] coded incorrectly the lepidotrichia of the paired fins of *Holopterygius nudus* as expanded. Therefore, we are coding *Holopterygius nudus* as "?".

Char. 247: Friedman & Coates (2006, char. 103)[47] coded the condition of the median fin lepidotrichia of *Holopterygius* as not expanded. However, Toriño et al. (2021, char. 103)[14] coded the condition as unknown. Although the condition of the dorsal and anal fins is unknown in *Holopterygius*, it is clear that the lepidotrichia are not expanded as visible in the caudal fin (Friedman & Coates, 2006, figs. 1, A3)[47].

Char. 258: Although most of the abdominal-thoracic neural spines of *Holopterygius nudus* are not associated with supraneural spines, five elements located anteriorly to the insertion of the epichordal lobe of the caudal fin have being reconstructed by Friedman & Coates (2006, fig. 1c)[47]. These elements might be interpreted as supraneural spines or radials associated to the caudal fin. We are tentatively coding the supraneural spines of *Holopterygius* as present.

Char. 266: In redescribing *Holopterygius* as a coelacanth, Friedman & Coates (2006, char. 105)[47] and Gess & Coates (2015, char. 105)[78] coded the coding of the lateral line pores of the scale as unknown. Dutel et al. (2012, char. 105)[60] and subsequent analyses [up to Toriño et al. (2021, char. 105)[14]] coded the condition of *Holopterygius* as having single pore per scale.

Indocoelacanthus robustus

Based on Jain (1974)[49] and new images of the specimens provided by Dhurjati Sengupta [Geological Studies Unit, Indian Statistical Institute (Calcutta-35)]; RC (double-checked by RC).

Char. 62: Forey (1998, char. 29)[12] and subsequent analyses [up to Toriño et al. (2021, char. 29)[14]] coded *Indocoelacanthus* as having separated cheek bones. Although Jain (1974, fig. 5)[49] reconstructed

the cheek bones as separated, Jain (1974, pl. 1, fig. 2)[49] shows that the margins of the postorbital, squamosal and preoperculum match, suggesting that these elements articulate.

Char. 64: Jain (1974, text-fig. 5)[49] identified a small quadrilateral dermal bone as a postspiracular in *Indocoelacanthus robustus*. It is unlikely that this element be unambiguously identified as a postspiracular or spiracular.

Char. 65: Jain (1974, p. 53)[49] identified a cheek element located posteroventrally to the squamosal of *Indocoelacanthus robustus* as the "preoperculo-quadratojugal". This element most likely corresponds to the preoperculum.

Char. 100: Forey (1998, char. 50)[12] and subsequent analyses [up to Toriño et al. (2021, char. 50)[14]] coded for the presence of tiny pores forming the infraorbital, jugal and preopercular sensory canals of *Indocoelacanthus*. However, Jain (1974)[49] did not figure nor describe the condition of the pores of these sensory canals in *I. robustus*. Thus, we coded the condition of *I. robustus* as unknown because of the lack of information.

Char. 153: Dutel et al. (2012, char. 110)[60] and subsequent analyses [up to Toriño et al. (2021, char. 110)[14]] coded the condition of the ventral swelling of the palatoquadrate of *Indocoelacanthus* as unknown. Jain (1974, text-fig. 3)[49] figured the condition of the palatoquadrate of *I. robustus* that does not indicate the presence of the ventral swelling.

Char. 225: Forey (1998, char. 108)[12] and subsequent analyses [up to Toriño et al. (2021, char. 108)[14]] coded the condition of the pelvic girdle of *Indocoelacanthus* as unknown. However, Jain (1974, text-fig. 6A-B)[49] figured the separated pelvic bones of *I. robustus*.

Char. 228: The spatulated shape of the pelvic girdle of *Indocoelacanthus* shows an additional process between the anteromedial and medial processes (Jain, 1974, text-fig. 6A)[49].

Char. 232: Forey (1998, char. 101)[12] and subsequent analyses [up to Toriño et al, (2021, char. 101)[14]] coded the condition of the ventral margin of the basal plate of the first dorsal fin of *Indocoelacanthus* as unknown. However, Jain (1974, text-fig. 6C)[49] figured the basal plate of the first dorsal fin of *I. robustus* with a smooth ventral margin.

Char. 247: Forey (1998, char. 103)[12] and subsequent analyses [up to Toriño et al. (2021, char. 103)[14]] coded the condition of the median fin lepidotrichia in *Indocoelacanthus*. However, Jain (1974, text-fig. 7E)[49] figured not expanded lepidotrichia of the caudal fin.

Latimeria chalumnae

Based on Millot & Anthony (1958)[140], Jarvik (1980)[141], Schultze (1991)[142], Forey (1998)[12], Dutel et al. (2013, 2015, 2019)[143-145], Mansuit et al. (2020, 2021)[146,147], Mondéjar-Fernàndez et al. (2021)[113]; RC (double-checked by RC, January 27th, 2021).

Char. 79: Gess & Coates (2015, char. 110)[78] coded the lacrimojugal of *Latimeria* as lacking a posteroventral extension. Although it is not as clearly defined as the condition in *Diplocercides kayseri* (Forey, 1998, fig. 4.5)[12] and *Serenichthys kowiensis* (Gess & Coates, 2015, fig. 2)[78], the posteroventral part of the lacrimojugal of *L. chalumnae* is expanded (Forey, 1998, fig. 4.1)[12].

Char. 99: Forey (1998, char. 49)[12] and subsequent analyses [up to Toriño et al., 2021, char. 49)[14]] coded *Latimeria* as having cheek bones ornamented with tubercles. However, the cheek bones of *L. chalumnae* are ornamented with a coarse rugosity; most likely the condition of *L. menadoensis* is similar.

Char. 127: Forey (1998, char. 59)[12] and subsequent analyses [up to Toriño et al. (2021, char. 59)[14]] coded the position of the oral pit line of *Latimeria* to be removed from the center of ossification of the angular. Forey (1998, fig. 5.1A)[12] figured the oral pit line of *L. chalumnae* as being only located slightly anterior to the center of ossification of the angular. Thus, we are coding the position of the oral pit line of *L. chalumnae* as being located at the center of ossification of the angular.

Char. 131: Forey (1998, char. 62)[12] and subsequent analyses [up to Toriño et al. (2021, char. 62)[14]] coded the condition of the ornament of the lower jaw of *Latimeria* as "?". However, the condition of *L. chalumnae* is rather unornamented.

Char. 151: Cloutier (1991b, char. 35)[96] and Forey (1998, char. 78)[12] and subsequent analyses [up to Toriño et al. (2021, char. 78)[14]] coded for a closed buccohypophysial foramen in *Latimeria* chalumnae. Most representations of the palate of *L. chalumnae* do not figure the presence of the buccohypophysial foramen (e.g., Dutel et al., 2013, fig. 1c[144]; Meunier et al., 2019, fig. 4[148]) with the exception of Schultze (1991)[142]. Schultze (1991, fig. 3A)[142] figured an open buccohypophysial foramen in the posterior part of the denticulated field of the parasphenoid; this interpretation was made based on the first CT-scan of *Latimeria* (Schultze, 1991, fig. 2)[142] where the resolution was fairly poor compared to recent CT-scan. Khonsari et al. (2013)[107] addressed specifically the evolution of the buccohypophysial foramen with a special interest to coelacanths, mentioning that the buccohypophysial foramen is closed in *Latimeria chalumnae*.

Char. 174: Forey (1998, char. 70)[12] and subsequent analyses [up to Toriño et al. (2021, char. 70)[14]] coded the condition of the optic nerve of *Latimeria* as enclosed by the basisphenoid extending forward. However, in *L. chalumnae*, the optic nerve is not enclosed by the basisphenoid but by the interorbital cartilage (H. Dutel, pers. observ.).

Char. 199: Forey (1998)[12] mentioned that the hyoid arch of *Latimeria chalumnae* includes the hyomandibular, interhyal, ceratohyal, hypohyal and a symplectic, and that only the ceratohyal and symplectic are ossified.

Char. 211: Forey (1998, char. 89)[12] and subsequent analyses [up to Toriño et al. (2021, char. 89)[14]] coded for the presence of a simple anocleithrum in *Latimeria chalumnae*. Mansuit et al. (2020)[146] provided a detailed anatomical description of the pectoral girdle of *L. chalumnae* including the ontogeny of the anocleithrum. Mansuit et al. (2020, figs. 2A-B, 3, 4A-B, 5) figured unambiguously the sigmoid shape of the anocleithrum both in juvenile and adult specimens of *L. chalumnae*.

Char. 225: Mansuit et al. (2020)[146] described in great details the anatomy and ontogeny of the pelvic girdle of *Latimeria chalumnae*.

Char. 241: The posteroventral process of the D2 basal plate of *Latimeria chalumnae* is cartilaginous and well-developed.

Char. 258: Arratia et al. (2001, p. 136)[112] mentioned that they have not observed the presence of independent "supraneural" in *Latimeria chalumnae*. However, Forey (1998, fig. 8.1)[12] illustrated the presence of three independent "supraneurals" anterior to the insertion of the caudal fin.

Char. 263: Forey (1991, char. 54)[12] coded the scales of *Latimeria chalumnae* as differentiated, whereas Forey (1998, char. 104)[12] and Dutel et al. (2015, char. 104)[88] coded it as undifferentiated. The scales of *Latimeria chalumnae* do not have a large central ridge, and therefore are coded as undifferentiated.

Latimeria menadoensis
Based on Watanabe & Koie (2009)[149], Meunier et al. (2019)[148], and Saruwatari et al. (2019); RC (double-checked by RC, January 27, 2021).

Char. 146: The condition of the parasphenoid of *Latimeria menadoensis* are coded based on a 3D CT-scan reconstruction provided by Watanabe & Koie (2009, fig. 2)[149].

Char. 207: The condition of the branchial arches of *Latimeria menadoensis* are coded based on a 3D CT-scan reconstruction provided by Watanabe & Koie (2009, fig. 2)[149].

Char. 208: The condition of the branchial arches of *Latimeria menadoensis* are coded based on a 3D CT-scan reconstruction provided by Watanabe & Koie (2009, fig. 2)[149].

Char. 210: The condition of the pectoral girdle of *Latimeria menadoensis* are coded based on a 3D CT-scan reconstruction provided by Watanabe & Koie (2009, fig. 2)[149].

Char. 225: The condition of the pelvic plate of *Latimeria menadoensis* are coded based on a 3D CT-scan reconstruction provided by Watanabe & Koie (2009, fig. 2)[149].

Char. 232: The condition of the basal plate of the first dorsal fin of *Latimeria menadoensis* are coded based on a 3D CT-scan reconstruction provided by Watanabe & Koie (2009, figs. 2, 3)[149].

Char. 237: The condition of the basal plate of the second dorsal fin of *Latimeria menadoensis* are coded based on a 3D CT-scan reconstruction provided by Watanabe & Koie (2009, fig. 3)[149].

Char. 238: The anterodorsal process of the D2 basal plate of *Latimeria menadoensis* is well-developed based on the sagittal CT-scan section figured in Watanabe & Koie (2007, fig. 3)[149].

Char. 239: The anterodorsal process of the D2 basal plate of *Latimeria menadoensis* is well-developed based on the sagittal CT-scan section figured in Watanabe & Koie (2007, fig. 3)[149]. The rendering of the CT-scan image is not clear however, the anterodorsal process of the D2 basal plate seems to be narrow on all its length.

Char. 240: The anterodorsal and anteroventral processes of the D2 basal plate of *Latimeria menadoensis* are well-developed based on the sagittal CT-scan section figured in Watanabe & Koie (2007, fig. 3)[149].

Char. 241: The posteroventral process of the D2 basal plate of *Latimeria menadoensis* is cartilaginous and well-developed based on the sagittal CT-scan section figured in Watanabe & Koie (2007, fig. 3)[149].

Char. 257: The conditions of the axial skeleton of *Latimeria menadoensis* are coded based on a 3D CT-scan reconstruction provided by Watanabe & Koie (2009, figs. 2, 3)[149].

Laugia groenlandica
Based on Stensiö (1932)[150] and Forey (1998)[12]; JAL November 2020 (double-checked by RC, January 26th, 2021).

Char. 1: Stensiö (1932)[150] considered that the snout was consolidated in *Laugia groenlandica*. Forey (1998, p. 62)[12] noted that the consolidated toothed bone of the snout might be composed of several smaller bones. Nevertheless, Forey (1998, fig. 3.8A)[12] figured a consolidated snout. In contrast to Forey (1998, char. 2)[12] and subsequent modifications of the original matrix, we are coding *L. groenlandica* as having a consolidate toothed snout.

Char. 5: Forey (1998, char. 6)[12] coded the condition of the anterior opening of the rostral organ as unknown. However, Forey (1998, fig. 3.8)[12] illustrated the consolidated snout bones with large pores some of which are associated with the ethmoid commissure plus the rostral organ. Although the snout is formed by fused premaxillae and rostrals, we considered that the anterior openings of the rostral organ are located in this fused element, and are coding the it to be present in the premaxilla.

Char. 8: Forey (1998)[12] doubted Stensiö's interpretation[150] of a single fused premaxilla, but until this is disproved it must be coded according to the literature.

Char. 9: Forey (1998, char. 5)[12] coded *Laugia* as "?" as for other species in which the snout is consolidated. We consider that the dorsal lamina of the premaxilla is present in the consolidated snout.

Char. 13: The rostral of *Laugia groenlandica* are assumed to be fused to the premaxillae (Forey, 1998, fig. 3.8)[12].

Char. 16: Although preparietals are missing from the restorations (Forey 1998, fig. 3.8)[12], it is clear that there is no space for preparietals to be longer than the parietals. Thus, we are coding character 15, as the preparietals shorter than the parietals.

Char. 51: Forey (1998, char. 16)[12] coded *Laugia* as having extrascapulars located behind the neurocranium. However, Forey (1998, figs. 3.9, 4.10)[12] figured the skull of *L. groenlandica* showing that the extrascapulars are clearly part of the skull roof with interdigitated sutures with the postparietals and tabulars.

Char. 90: Forey (1998, char. 45)[12] and subsequent analyses [up to Toriño et al. (2021, char. 45)[14]] coded the infraorbital canal of *Laugia* as passing through the center of the postorbital. However, Forey (1998, figs. 4.10, 4.12A)[12] showed clearly that the infraorbital canal of *L. groenlandica* runs along the anteriormost margin of the postorbital.

Char. 116: Forey (1998, char. 54)[12] and subsequent analyses [up to Toriño et al. (2021, char. 54)[14]] coded the dentary teeth of *Laugia* as being on separate plates. However, the detailed illustration of Forey (1998, fig. 5.5)[12] shows no other dental plate associated with the dentary (or the medial side of the lower jaw) than the anterior coronoids. Thus, *L. groenlandica* is coded as lacking dentary teeth.

Char. 176: The connection between the processus connectens and the parasphenoid has been illustrated by Forey (1998, fig. 6.6B)[12].

Char. 188: Forey (1998, char. 80)[12] and subsequent analyses [up to Toriño et al. (2021, char. 80)[14]] coded the condition of the suprapterygoid process of *Laugia* as unknown. Although, the lateral view of the neurocranium of *L. groenlandica* figured by Forey (1998, fig. 6.7)[12] does not show a suprapterygoid process which could suggest that it is absent, this information is unknown in the original material figured by Forey (1998, fig. 6.6)[12]. Thus, we keep the condition as unknown.

Char. 199: Forey (1998, p. 198)[12] mentioned that the hyomandibular of *Laugia* is partly ossified.

Char. 211: Forey (1998, char. 89)[12] and subsequent analyses [up to Toriño et al. (2021, char. 89)[14]] coded the shape of the anocleithrum of *Whiteia* as simple. We considered the shape of the anocleithrum of *L. groenlandica* as being a broad plate-like based of the reconstruction of the anocleithrum by Forey (1998, fig. 4.10)[12] where a rounded dorsal process protrudes from a large plate located medially to the dorsal part of the cleithrum.

Char. 266: Forey (1998, char. 105)[12] and subsequent analyses [up to Toriño et al. (2021, char. 105)[14]] coded the condition of the lateral line pores per scale of *Laugia* as unknown. However, Stensiö (1932, text-fig. 22)[150] figured the lateral line scales of *L. groenlandica* with a single pore per scale.

Libys polypterus

Based on Forey (1998)[12] and Lambers (1992)[31] and original images of specimens in collections; RC (double-checked by RC, November 12, 2020).

Char. 9: Dutel et al. (2015)[88] coded for the presence of premaxilla without dorsal lamina in *Libys*; however, the condition of the premaxilla is not described in the literature, thus we are coding this character as "6".

Char. 18: Dutel et al. (2015, char. 19)[88] coded *Libys* with the supraorbital sensory canal following the sutural course. We coded this character as Dutel et al. (2015)[88] since the condition of the canal is located close to the suture on the postparietals (Forey, 1998, fig. 3.17)[12] and supraorbitals (Lambers, 1992, fig. 7)[31], however the position of the few large pores seems to be more centrally located on the tabular (Forey, 1998, fig. 3.17)[12].

Char. 31: Dutel et al. (2015; char. 11)[88] coded for the presence of the descending process of the parietal in *Libys*.

Char. 50: Dutel et al. (2015, char. 15)[88] coded for the presence of extrascapulars free from the postparietals in *Libys*.

Char. 56: Lambers (1992)[31] and Forey (1998)[12] notices that the sensory pores of *Libys* are extremely large among all actinistian species.

Char. 57: Forey (1998, char. 10)[12] coded *Libys* as "?". Based on Lambers (1992, fig. 7)[31] and specimen BMNH PV P.3337), the preorbital is absent in *Libys polypterus*.

Char. 67: Dutel et al. (2015, char. 39)[88] coded the preoperculum of *Libys* to be developed as a posterior-like canal-bearing portion and an anterior blade-like portion.

Char. 131: Forey (1998, char. 62)[12] and subsequent analyses [up to Toriño et al. (2021, char. 62)[14]] coded the condition of the ornamentation of the lower jaw of *Libys* as unknown. Lambers (1992, p. 28)[31] modified the diagnosis of the genus *Libys* including a comment on the ornamentation on the dermal skull bones.

Char. 211: Forey (1998, char. 89)[12] and subsequent analyses [up to Toriño et al. (2021, char. 89)[14]] coded the anocleithrum of *Libys* at forked in contrast to simple. Based on the illustration of Lambers (1992, fig. 1)[31], the anocleithrum of *L. polypterus* is clearly sigmoid.

Char. 262: Dutel et al. (2015, char. 92)[88] coded for the absence of ossified ribs in *Libys*. Lambers (1992, fig. 1)[31] illustrated the presence of a few short ossified ribs located in the portion region of the thoracic region of *Libys*.

Char. 264: Mondéjar-Fernàndez et al. (2021, table 1)[113] reported that the scale ornament of *Libys polypterus* is composed of short ridges. However, Lambers (1992, fig. 4)[31] figured three distinct types of ornaments in *L. polypterus*. Thus, we are coding *L. polypterus* as polymorphic.

Lochmocercus aciculodontus

Based on Lund & Lund (1985)[13] and original images of the specimens; RC (double-checked by RC).

Char. 9: Forey (1998, char. 5)[12] coded the condition of the dorsal lamina of the premaxilla of *Lochmocercus* as unknown. However, *Lochmocercus aciculodontus* has a reduced dorsal lamina of the premaxilla.

Char. 19: Forey (1998, char. 23)[12] and subsequent analyses [up to Toriño (2021, char. 23)[14]] coded *Lochmocercus* as having single large pores forming the supraorbital sensory canals. However, the coding of the supraorbital canal is unknown (Lund & Lund, 1985)[13] or at best unclear (based on R. Cloutier, pers. observ.).

Char. 22: Lund & Lund (1985)[13] illustrated the presence of a potential supratemporal in Figure 68-69 in addition to the presence of a tabular; however, while the presence of a tabular is clear, the presence of a supratemporal is not dubious (R. Cloutier, pers. observ.).

Char. 28: Forey (1998, char. 20)[12] and subsequent analyses [up to Toriño et al. (2021, char. 20)[14]] coded *Lochmocercus* as having the otic canal joining the supratemporal canal in the tabular (their "supratemporal"). However, the preservation is too poor to determine unambiguously the condition for character 28.

Char. 54: Forey (1998, char. 18)[12] coded *Lochmocercus* as "?". However, Lund & Lund (1985, fig. 69)[13] have illustrated the posterior margin of the tabular and postparietal has being straight.

Char. 57: Forey (1998, char. 10)[12] coded *Lochmocercus* as "?". Lund & Lund (1985, fig. 69)[13] figured a preorbital in *Lochmocercus aciculodontus*.

Char. 78: Forey (1998, char. 36)[12] and subsequent analyses [up to Toriño et al. (2021, char. 36)[14]] coded the lacrimojugal of *Lochmocercus* as not ending anteriorly with an angle. However, Lund & Lund (1985, fig. 69)[13] clearly showed the lacrimojugal of *L. aciculodontus* to be angled anteriorly.

Char. 93: Forey (1998, char. 48)[12] and subsequent analyses [up to Toriño et al. (2021, char. 48)[14]] coded for the presence of pit lines marking the cheek bones of *Lochmocercus*. However, we considered the preservation condition of *Lochmocercus* to be poor to allow us to code for this character.

Char. 99: Forey (1998, char. 49)[12] and subsequent analyses [up to Toriño et al. (2021, char. 49)[14]] have coded the condition of cheek bones ornament of *Lochmocercus* as unknown. However, the cheek bones of the holotype of *Lochmocercus aciculodontus* (specimen MV 6044) show tubercular ornamentation.

Char. 211: Forey (1998, char. 89)[12] and subsequent analyses [up to Toriño et al. (2021, char. 89)[14]] coded the shape of the anocleithrum of *Lochmocercus* as simple. Specimen MV 6044 shows the sigmoid shape of the anocleithrum of *L. aciculodontus* (R. Cloutier, pers. observ.). Lund & Lund (1985, fig. 69)[13] figured the pectoral girdle of specimen MV 6044; the element identified by Lund & Lund (1985)[13] as the supracleithrum is re-identified as the anocleithrum.

Char. 216: Lund & Lund (1985, p. 47)[13] mentioned that *Lochmocercus* seems to have a large extracleithrum; it is illustrated in their figure 69 but not on their figure 68.

Char. 260: Lund & Lund (1985, fig. 68)[13] illustrated the anteriormost cervical neural arches of *Lochmocercus aciculodontus* as narrow and thin; thus, we are coding *L. aciculodontus* as lacking expanded cervical neural arches. However, Forey (1998, char. 91)[12] coded *Lochmocercus* as "?".

Char. 263: Forey (1991, char. 54[97]; 1998, char. 104[12]) and Dutel et al. (2015, char. 104)[88] coded as "?" the condition of the ornamentation of the scales of *Lochmocercus*. Based on the observation of specimen (MV 6044), the ornamentation is clearly composed of longitudinal ridges without a prominent central one.

Char. 268: Forey (1998, char. 107)[12] and subsequent analyses [up to Toriño et al. (2021, char. 107)[14]] coded the condition of the swimbladder (lung) of *Lochmocercus* as unknown. Based on Lund & Lund (1985)[13] and our observation of the original material (R. Cloutier, pers. observ.), the lung of *L. aciculodontus* is not ossified.

Lualabaea lerichei

Based on Forey (1998)[12], Brito et al. (2018)[56], Fragoso et al. (2018)[104], Cavin et al. (2019)[100]; RC (double-checked by RC).

Luopingcoelacanthus eurylacrimalis

Based on Wen et al. (2013)[54] and high-resolution images provided by W. Wen; RC (double-checked by RC).

Char. 9: Wen et al. (2013, char. 5)[54] and Toriño et al. (2021, char. 5)[14] coded *Luopingcoelacanthus* has lacking a dorsal lamina of the premaxillae, however, Wen et al. (2013, fig. 2)[54] clearly illustrated a dorsal lamina on the left premaxillae.

Char. 10: We are coding the dorsal lamina of *Luopingcoelacanthus eurylacrimalis* as complete based on the adult condition figured by Wen et al. (2013, fig. 2)[54]. However, it seems that the embryonic condition corresponds to the invaginated lamina (Wen et al., 2013, fig. 5B)[54].

Char. 91: Wen et al. (2013, char. 46)[54] and subsequent analyses [up to Toriño et al. (2021, char. 46)[14]] coded the condition of the jugal canal of *Luopingcoelacanthus* as simple. However, based on Wen et al. (2013, fig. 2A, p. 178)[54], the condition of the squamosal is unclear and therefore does not allow us to code for the condition of the jugal canal.

Char. 99: Wen et al. (2013, char. 49)[54] and subsequent analyses [up to Toriño et al. (2021, char. 49)[14]] coded *Luopingcoelacanthus* as having tubercular cheek bone ornamentation. However, Wen et al. (2013, p. 178)[54] wrote that the ornamentation of the cheek region is not visible on the specimens. Thus, we are coding the condition of the cheek bone ornamentation of *L. eurylacrimalis* as unknown.

Char. 100: Wen et al. (2013, char. 50)[54] and subsequent analyses [up to Toriño et al. (2021, char. 50)[14]] coded for the presence of tiny sensory pores forming the infraorbital, jugal and preopercular canals of *Luopingcoelacanthus*. The condition cannot be validated based on figured specimens (Wen et al., 2013, figs. 1a, 2a)[54], therefore we coded the condition of *L. eurylacrimalis* as unknown.

Char. 117: Wen et al (2013, char. 61)[54] and subsequent analyses [up to Toriño et al. (2021, char. 61)[14]] coded for the presence of a dentary pore in *Luopingcoelacanthus*. However, the condition of the margin between the dentary and splenial of specimens LPV-10575 and LPV-10146 of *L. eurylacrimalis* is too poorly known to allow the identification of such pore. Thus, we are coding the condition of character 61 as unknown.

Char. 150: Wen et al. (2013, char. 79)[54] and subsequent analyses [up to Toriño et al. (2021, char. 79)[14]] coded for the presence of ascending laminae on the parasphenoid of *Luopingcoelacanthus*. The parasphenoid of *L. eurylacrimalis* figured by Wen et al. (2013, fig. 3A, C)[54] does not show evidence of the presence of ascending laminae, therefore, we are coding this structure as absent.

Char. 151: Wen et al. (2013, char. 78)[54] and subsequent analyses [up to Toriño et al. (2021, char. 78)[14]] coded the condition of the buccohypophysial foramen of *Luopingcoelacanthus* as unknown. However, Wen et al. (2013, fig. 3C)[54] illustrated a complete parasphenoid without a foramen.

Char. 174: Wen et al. (2013, char. 70)[54] and subsequent analyses [up to Toriño et al. (2021, char. 70)[14]] coded the condition of the optic foramen in *Luopingcoelacanthus* as being enclosed by the basisphenoid extending forward. Wen et al. (2013, fig. 3A, B)[54] figure the basisphenoid of *L. eurylacrimalis*, however, its relationships with the optic foramen is not documented. Therefore, we are coding the condition as unknown.

Char. 176: Wen et al. (2013, char. 71)[54] and subsequent analyses [up to Toriño et al. (2021, char. 71)[14]] coded the condition of *Luopingcoelacanthus* as having a processus connectens failing to meet the parasphenoid. However, the lateral view of the skull figured by Wen et al. (2013, fig. 2)[54] do not show the posterior limit of the parasphenoid nor the condition of the processus connectens. Therefore, we are coding the condition of *L. eurylacrimalis* as unknown.

Char. 211: Wen et al. (2013, char. 89)[54] and subsequent analyses [up to Toriño et al. (2021, char. 89)[14]] coded for a simple shape of the anocleithrum of *Luopingcoelacanthus*. Wen et al. (2013, fig. 2)[54] identified an elongated, slightly sigmoid element located dorsally to the cleithrum as the supracleithrum; this element is reidentified as a sigmoid anocleithrum of *L. eurylacrimalis*.

Char. 250: Wen et al. (2013, char. 97)[54] and subsequent analyses [up to Toriño et al. (2021, char. 97)[14]] coded the caudal lobes of *Luopingcoelacanthus* as symmetrical. However, Wen et al. (2013, p. 181)[54] wrote that the ventral lobe of *L. eurylacrimalis* contains 19-20 lepidotrichia, whereas the dorsal lobe

contains 15-16 lepidotrichia. Thus, the meristic count supports to consider the caudal lobes as asymmetrical.

Char. 263: Wen et al. (2013, char. 104)[54] and subsequent analyses [up to Toriño et al. (2021, char. 104)[14]] coded the scale ornament of *Luopingcoelacanthus* as differentiated. However, Wen et al. (2013)[54] described and figured the scales of *L. eurylacrimalis*. One of the two scales reconstructed by Wen et al. (2013, fig. 6B)[54] shows a median longitudinal ridge that is not prominent. Furthermore, scales of *L. eurylacrimalis* visible along the flank of the body show variation in terms of ridge pattern without a prominent median ridge (see Wen et al., 2013, fig. 5A, B)[54].

Char. 264: Wen et al. (2013, fig. 6)[54] reconstructed scales from the lateral region ("normal scale") (Wen et al., 2013, fig. 5)[54] and from the anteroventral region of the body of *Luopingcoelacanthus eurylacrimalis* (Wen et al., 2013, fig. 1)[54]. The generalized condition is composed of ridges, whereas the anteroventral scales are ornamented solely with tubercles. Thus, character 278 is coded as polymorphic.

Macropoma lewesiensis

Based on Woodward (1911; *Macropoma mantelli*)[151] and Forey (1998)[12] and on photographs of the original material from the Natural History Museum (London); HD (double-checked by RC, January 26, 2021).

Char. 30: In *Macropoma lewesiensis*, the poorly-developed posterolateral process of the parietal is present, but a supraorbital fit in between this process and the postorbital (Forey, 1998, figs. 3.19A, 4.19)[12]. The process is less developed than in *Macropoma precursor* (Forey, 1998, fig. 3.19B)[12].

Char. 50: Forey (1998, char. 15)[12] and subsequent analyses [up to Toriño et al. (2021, char. 15)[14]] coded *Macropoma* as having free extrascapulars. However, Forey (1998, fig. 4.19)[12] figured the extrascapulars of *M. lewesiensis* articulating with the posterior margin of the tabular and postparietal.

Char. 114: Forey (1998, fig. 5.13)[12] figured rare tubercles on the angular, splenial and dentary of *Macropoma lewesiensis*. We coded *M. lewesiensis* as having an unornamented dentary because most of the surface is without ornament.

Char. 116: Forey (1998, char. 54)[12] and subsequent analysis coded the dentary teeth of *Macropoma* as being on separate plates. However, the detailed illustration of Forey (1998, fig. 5.13)[12] shows no other dental plate associated with the dentary (or the medial side of the lower jaw) than the anterior coronoids. Thus, *M. lewesiensis* is coded as lacking dentary teeth.

Char. 171: The condition of the vestibular fontanelle is unknown in *Macropoma lewesiensis* because most of the otic region of the neurocranium was cartilaginous (Forey, 1998, fig. 6.10)[12].

Char. 174: Forey (1998, char. 70)[12] and subsequent analyses [up to Toriño et al. (2021, char. 70)[14]] coded the condition of the optic nerve of *Macropoma* as enclosed by the basisphenoid extending forward. However, in *Macropoma*, the optic nerve is not enclosed by the basisphenoid but by the interorbital cartilage (H. Dutel, pers. observ.).

Char. 211: Forey (1998, char. 89)[12] and subsequent analyses [up to Toriño et al. (2021, char. 89)[14]] coded for the presence of a forked anocleithrum. Based on our new definition of character-states as well as the reconstruction of the anocleithrum provided by Forey (1998, fig. 4.19)[12] we considered that the anocleithrum of *M. lewesiensis* is a broad plate-like shape.

Char. 225: Forey (1998, char. 108)[12] and subsequent analyses [up to Toriño et al. (2021, char. 108)[14]] coded the pelvic bones of *Macropoma* as separated. The pelvic girdle is well preserved on specimen BMNH 4256 of the Mantell Collection (originally identified as *M. mantelli* and figured by Agassiz (1835, vol. II, pt. II, pl. LXVC, fig. I); high resolution image available on www.gbif.org). The posterior median processes are fused on this specimen.

Char. 263: Forey (1998, fig. 11.12A, B)[12] illustrates scale of *Macropoma lewesiensis* with and without the more prominent median ridge. Forey (1998, char. 104)[12] and subsequent analyses [up to Toriño et al. (2021, char. 104)[14]] coded *Macropoma* as having differentiated scales. We code *M. lewesiensis* as polymorphic because flank scales are not differentiated, whereas caudal peduncle scale are differentiated.

Macropoma precursor
Based on Woodward (1909)[152] and Forey (1998)[12] and photographs of MHNM specimens on the Data Portal of The Natural History Museum (BMNH P.3353, P10916, P10917, P.35700, P.49828, P.10810, P.10816); JAL (double-checked by RC, January 26, 2021). Although Forey (1998)[12] said that most of the cheek and lower jaw are identical with *M. lewesiensis, M. precursor* has been coded based on the specimens listed above.

Char. 50: Forey (1998, char. 15)[12] and subsequent analyses [up to Toriño et al. (2021, char. 15)[14]] coded *Macropoma* as having free extrascapulars. However, Forey (1998, fig. 3.21A)[12] figured the extrascapulars of *M. precursor* articulating with the posterior margin of postparietal and the posteromedial margin of the tabular.

Char. 99: Forey (1998, char. 49)[12] and subsequent analyses [up to Toriño et al. (2021, char. 49)[14]] coded *Macropoma* as having a tubercular ornamentation on cheek bones. While *M. lewesiensis* effectively has a tubercular ornamentation, the cheek bones of *M. precursor* are fairly smooth with numerous pores (BMNH P.3353, P.10916). Thus, *M. precursor* is coded as lacking cheek bones ornament.

Char. 116: Forey (1998, char. 54)[12] and subsequent analyses [up to Toriño et al. (2021, char. 49)[14]] coded the dentary teeth of *Macropoma* as being on separate plates. However, specimens BMNH P.10916 and BMNH P.3353 of *M. precursor* show no dental plate associated with the dentary with the exception of the medial anterior coronoids. Thus, *M. precursor* is coded as lacking dentary teeth.

Char. 131: Forey (1998, char. 62)[12] and subsequent analyses [up to Toriño et al. (2021, char. 62)[14]] coded the lower jaw ornament of *Macropoma* as being tubercular. The condition of the lower jaw ornament in *M. lewesiensis* is effectively tubercular, however the condition of *M. precursor* differs. The lower jaws of specimens BMNH P.10916, P.10917 and P.3353 of *M. precursor* show an unornamented condition.

Char. 174: Forey (1998, char. 70)[12] and subsequent analyses [up to Toriño et al. (2021, char. 70)[14]] coded the condition of the optic nerve of *Macropoma* as enclosed by the basisphenoid extending forward. However, in *Macropoma*, the optic nerve is not enclosed by the basisphenoid but by the interorbital cartilage (H. Dutel, pers. observ.).

Char. 263: Forey (1998, char. 104)[12] coded the scale of *Macropoma* as being differentiated. However, based on scale ornamentation of specimens BMNH P.10810 and P.10816 of *M. precursor* the ornamentation is not differentiated.

Macropoma willemoesii
Based on Forey (1998)[12] and images of specimens SOS 2190, 2192, 2203, 2204, and 2207 from Jura Museum Eichstätt available from the BiNHum from the Humboldt-Ring; RC (double-checked by RC, January 26th, 2021).

Macropomoides orientalis
Based on Forey (1998)[12] and images from Khalaf-Sakerfalke von Jaffa (2019); RC (double-checked by RC, December 9, 2020).
Char. 72: Forey (1998, p. 353)[12] mentioned in the diagnosis of *Macropomoides* that the squamosal is very small.

Mawsonia brasiliensis
Based on Yabumoto (2002)[55]; JAL, November 2020 (double-checked by RC, January 22nd, 2021); Toriño et al. (2021) considered *Mawsonia brasiliensis* as a junior synonym of *Mawsonia gigas*.
Char. 13: Forey (1998, char. 3)[12] and subsequent analyses [up to Toriño et al. (2021, char. 3)[14]] coded the condition of *Mawsonia* as "?". Yabumoto (2002, fig. 2)[55] figured a series of four rostrals (his "rostral ossicles") in *M. brasiliensis* which we considered herein to be multiple rostrals.

Char. 62: Forey (1998, char. 29)[12] and Toriño et al. (2021, char. 29)[14] coded *Mawsonia* as having separated cheek bones. Yabumoto (2002, fig. 3)[55] showed the contact among the postorbital, squamosal and preoperculum of *M. brasiliensis*.

Char. 63: Toriño et al. (2021, char. 51)[14] corrected the coding of Cavin et al. (2017, char. 51)[41] suggesting that in *Mawsonia* there is a gap between the lacrimojugal and the supraorbital series (the preorbital being absent). However, Yabumoto (2002, fig. 4)[55] illustrated a contact between the lacrimojugal and the tectal.

Char. 230: The posterior section of the pelvic girdle of *Mawsonia brasiliensis* is only partly preserved (Yabumoto, 2002, fig. 1)[55]; however, the shape of the posterior fragment suggests that a posterior process is present.

Char. 232: Forey (1998, char. 101)[12] and most subsequent analyses coded the ventral margin of the basal plate of the first dorsal fin of *Mawsonia* as smooth. However, this coding was not assigned to a specific species and as far as we known the postcranium of most *Mawsonia* species is unknown. The ventral margin of the basal plate of the first dorsal fin of *Mawsonia brasiliensis* is coded as emarginated based on the coding by Fragoso (2014, char. 101)[108]. Toriño et al. (2021, char. 101)[14] coded *Mawsonia* as polymorphic.

Char. 234: The coding of the denticles on the lepidotrichia of the first dorsal fin of *Mawsonia brasiliensis* is based on the comments of Fragoso (2014)[108] and Toriño et al. (2021b, char. 96)[14].

Char. 250: Yabumoto (2002)[55] described the presence of 23 lepidotrichia in the dorsal lobe of the caudal fin (his third dorsal fin) and 25 lepidotrichia in the ventral lobe (his second anal fin).

Char. 263: Yabumoto (2002)[55] mentioned the ornamentation of the scales of *Mawsonia brasiliensis* is not typical coelacanth tubercle or ridges; however, the condition is not illustrated. Thus, we are coding this taxon as "?".

Mawsonia gigas
Based on Toriño et al. (2021)[14] and Maisey (1986)[18]; HD & RC (double-checked by RC, January 20, 2021).

Char. 62: Forey (1998, char. 29)[12] and Toriño et al. (2021, char. 29)[14] coded *Mawsonia* as having separated cheek bones. Toriño et al. (2021, fig. 3)[14] showed the contact and overlap between of the postorbital and squamosal, and the partial contact between the squamosal and preoperculum of *M. gigas*.

Char. 63: The anterior tip of the lacrimojugal of *Mawsonia gigas* is unknown (Toriño et al., 2021a, fig. 3)[14]; thus, it is unclear if there is a contact or not.

Char. 117: Forey (1998, char. 61)[12] and subsequent analyses [up to Toriño et al. (2021, char. 61)[14]] coded for the presence of a dentary pore in *Mawsonia*. However, the detailed images of the dentary and splenial of *M. gigas* provided by Toriño et al. (2021, fig. 12)[14] do not show indication of the presence of the dentary pore. Therefore, we are coding the dentary pore of *M. gigas* as absent.

Char. 123: Character 123 is coded as polymorphic based on Toriño et al. (2021, char. 66)[14].

Char. 135: Toriño et al. (2021b, char. 68)[14] coded the presence of pointed teeth with fine striations as well as rounded teeth with fine striations radiating from the crown in *Mawsonia gigas*. Thus, in reference to the character-states as defined herein, *M. gigas* has both apomorphic states.

Char. 171: The condition of the vestibular fontanelle is unknown in *Mawsonia gigas* because most of the otic region of the neurocranium was cartilaginous (Maisey, 1986, fig. 1)[18].

Char. 186: Toriño et al. (2021b, char. 76)[14] coded the supraoccipital of *Mawsonia* as present based on the illustration and description of this structure in *M.* sp. cf. *M. gigas* (Maisey, 1986, fig. 6)[18].

Char. 216: The extracleithrum is interpreted to be present in *Mawsonia gigas* owing to the description of an articular surface located on the cleithrum (Toriño et al., 2021)[14].

Char. 234: The coding of condition of the lepidotrichia of the first dorsal fin of *Mawsonia gigas* is based on the comments of Toriño et al. (2021b, char. 96)[14].

Char. 263: Forey (1991, char. 54)[12] coded *Mawsonia* as "?" while Forey (1998, char. 104)[12] and Dutel et al. (2015, char. 104)[88] coded it as differentiated.

Mawsonia soba

Based on Brito et al. (2018)[56]; RC (double-checked by RC).

Char. 13: Forey (1998, char. 3)[12] and subsequent analyses [up to Toriño et al. (2021, char. 3)[14]] coded the condition of *Mawsonia* as "?". Brito et al. (2018, fig. 2A-B)[56] figured a series of at least three rostrals in *M. soba* which we considered herein to be multiple rostrals.

Char. 117: Brito et al. (2018)[56] mentioned that *Mawsonia soba* differs from the other *Mawsonia* species by the presence of four dentary pores rather than a single one.

Mawsonia tegamensis

Based on Wenz (1975)[57], Forey (1998)[12], Fragoso et al. (2018)[104], Cavin et al. (2016)[24], de Carvalho & Maisey (2008)[153]; HD & RC (double-checked by RC, February 2nd, 2021).

Char. 13: Forey (1998, char. 3)[12] and subsequent analyses [up to Toriño et al. (2021, char. 3)[14]] coded the condition of *Mawsonia* as "?". Wenz (1975, fig. 1; her "postrostral")[57] and Fragoso et al. (2018, fig. 15)[104] reported the presence of a single median rostral that was said to be "a small element between the anterior nasals".

Char. 62: Forey (1998, char. 29)[12] and Toriño et al. (2021, char. 29)[14] coded *Mawsonia* as having separated cheek bones. Wenz (1975, fig. 1)[57] and Fragoso et al. (2018, fig. 15)[104] showed the contact among the postorbital and squamosal and the separation between the squamosal and preoperculum of *M. tegamensis*. Thus, we are coding *M. tegamensis* as polymorphic.

Megalocoelacanthus dobiei

Based on Schwimmer et al. (1994)[59] and Dutel et al. (2012)[60]; RC & HD (double-checked by RC, January 22, 2021).

Char. 150: Forey (1998, char. 79)[12] and subsequent analyses [up to Toriño et al. (2021, char. 79)[14]] coded the condition of the ascending laminae of the parasphenoid of *Megalocoelacanthus* as unknown. However, Dutel et al. (2012, 2015; char. 79)[60,88] coded the presence of the ascending laminae in *M. dobiei*. Dutel et al. (2012, fig. 2)[60] figured the ascending laminae (their "ascending wing") of the parasphenoid of *M. dobiei*.

Char. 151: Dutel et al. (2012, fig. 11B)[60] figured the parasphenoid of *Megalocoelacanthus* without a buccohypophysial foramen. Although Toriño et al. (2021, char. 78)[14] mentioned that they followed Dutel et al. (2012)[60] coding for *Megalocoelacanthus*, the buccohypophysial foramen is coded as present in their published matrix.

Char. 176: Dutel et al. (2012, char. 71)[60] coded the condition of *Megalocoelacanthus* as the processus connectens meeting the parasphenoid. However, Toriño et al. (2021, char. 71)[14] coded the condition of *Megalocoelacanthus* as the processus connectens failing to meet the parasphenoid. Dutel et al. (2012, fig. 3)[60] figured the connection between the processus connectens and the parasphenoid.

Miguashaia bureaui

Based on Cloutier (1991a, 1996)[61,95], Forey (1998)[12] and Forey et al. (2000)[63] and observations of new material (R. Cloutier, pers. observ.); RC (double-checked by RC).

Char. 16: The preparietals are absent in *Miguashaia bureaui*.

Char. 38: Forey (1998, char. 13)[12] and subsequent authors coded for the condition of the descending process of the postparietal as unknown. However, Cloutier (1996, fig. 4)[61] illustrated the internal view of the postparietals not revealing the presence of descending process.

Char. 57: Forey (1998, char. 10)[12] coded *Miguashaia* as "?". The preorbital is clearly visible on new specimens of *Miguashaia bureaui* (R. Cloutier, pers. observ.).

Char. 59: A small portion of the anterior part of the orbit of *Miguashaia bureaui* incorporates part of the lateral rostral as indicated by specimen MHNM 06-1236A (R. Cloutier, pers. observ.).

Char. 69: The condition of the squamosal of *Miguashaia bureaui* is unique since it occupies a large part of the cheek region, thus not only restricted to the mid-level since it forms part of the ventral

margin of the cheek. However, the squamosal does not reach the skull roof as reconstructed by Cloutier (1996, fig. 5)[61].

Char. 76: The condition of the anterior part of the lacrimojugal was unknown in previous matrices. Specimen MHNM 06-1236 shows clearly that the anterior part of the lacrimojugal is not expanded anteriorly (R. Cloutier, pers. observ.).

Char. 83: Specimen MHNM 06-1236 of *Miguashaia bureaui* shows that the postorbital limb of the lacrimojugal ends at mid-orbit (R. Cloutier, pers. observ.).

Char. 93: Forey (1998, char. 93)[12] and subsequent analyses [up to Toriño et al. (2021, char. 93)[14]] coded the condition of the cheek pit lines in *Miguashaia* as unknown. Cloutier (1996, figs. 4-8)[61] did not reported the presence of cheek pit lines in *M. bureaui* while pit lines on the skull roof and lower jaw were clearly identified. New cranial material of *M. bureaui* (e.g., MHNM 06-1236) do not reveal the presence of cheek pit lines either (R. Cloutier, pers. observ.).

Char. 99: Forey (1998, char. 49)[12] and subsequent analyses [up to Toriño et al. (2021, char. 49)[14]] coded the ornament of the cheek bones of *Miguashaia* as tubercular. However, specimens of *M. bureaui* showing cheek bones (MHNM 06-494, 06-1809, 06-1236) in external view display a smooth condition (R. Cloutier, pers. observ.). Thus, *M. bureaui* is coded as lacking ornament on cheek bones.

Char. 114: Forey (1998, char. 63)[12] and subsequent analyses [up to Toriño et al. (2021, char. 63)[14]] coded the condition of the dentary ornament in *Miguashaia* to be unknown. Specimen MHNM 06-1236 of *M. bureaui* shows a fine ornamentation on the dentary similar to the ornament present on the angular and splenial (R. Cloutier, pers. observ.).

Char. 117: Forey (1998, char. 61)[12] and subsequent analysis [up to Toriño et al. (2021, char. 61)[14]] coded the condition of the dentary pore of *Miguashaia* as unknown. New observation on the lower jaw of *M. bureaui* on specimen MHNM 06-1236 show no indication of the dentary pore (R. Cloutier, pers. observ.).

Char. 121: Forey (1998, char. 56)[12] and subsequent analyses [up to Toriño et al. (2021, char. 56)[14]] coded the condition of the coronoid opposite to the posterior end of the dentary of *Miguashaia* as unknown. However, the condition of the anterior series of coronoids (Cloutier, 1996, fig. 12)[61] in specimens MHNM 06-494, 06-1236, and BMNH P.58693 does not show enlarged teeth.

Char. 127: Forey (1998, char. 59)[12] and subsequent analyses [up to Toriño et al. (2021, char. 59)[14]] coded the position of the oral pit line of *Miguashaia* as being removed from the center of ossification of the angular. Cloutier (1996, p. 237, fig. 5) mentioned that the oral pit line (his "angular pit line") is located slightly posterior to mid-length of the angular based on specimen BMNH P.58693). Although the pit line is located slightly posterior to mid-length of the angular, it is still located near the center of ossification of the angular and not removed from it.

Char. 131: The ornament of the lower jaw of *Miguashaia bureaui* had not been previously observed. Specimens MHNM 06-1236B and MHNM 06-1809B show small regions of the ornament on the angular that is composed solely of small tubercles (R. Cloutier, pers. observ.).

Char. 133: Forey (1998, char. 64)[12] and subsequent analyses [up to Toriño et al. (2021, char. 64)[14]] coded the condition of the splenial ornament in *Miguashaia* to be unknown. Specimen MHNM 06-1236 of *M. bureaui* shows a fine ornamentation on the splenial similar to the ornament present on the angular and dentary (R. Cloutier, pers. observ.).

Char. 150: Forey (1998, char. 79)[12] and subsequent analyses [up to Toriño et al. (2021, char. 79)[14]] coded the condition of the ascending laminae of the parasphenoid of *Miguashaia* as unknown. Cloutier (1996, fig. 10A)[61] figured the parasphenoid of *M. bureaui* lacking the ascending laminae.

Char. 151: Forey (1998, char. 78)[12] and subsequent analyses [up to Toriño et al. (2021, char. 78)[14]] coded the condition of the buccohypophysial foramen of *Miguashaia* as unknown. Cloutier (1991a, b, char. 35) coded the presence of an open buccohypophysial foramen in *M. bureaui*; this condition was subsequently figured by Cloutier (1996, fig. 10A)[61].

Char. 153: Dutel et al. (2012, char. 110)[60] and subsequent analyses [up to Toriño et al. (2021, char. 110)[14]] coded the condition of the ventral swelling of the palatoquadrate of *Miguashaia* as unknown.

Cloutier (1996, figs. 4, 11)[61] figured specimens of *M. bureaui* showing that the ventral swelling of the palatoquadrate is absent.

Char. 211: Forey (1998, char. 89)[12] and subsequent analyses [up to Toriño et al. (2021, char. 89)[14]] coded the condition of the shape of the anocleithrum of *Miguashaia* as unknown. However, Cloutier (1996, figs. 13A-B, 14C)[61] figured an ovoid anocleithrum in *M. bureaui*.

Char. 218: In *Miguashaia bureaui*, the extracleithrum and clavicle extend dorsally to approximately the same height (Cloutier, 1996, fig. 13)[61] as seen in specimen MHNM 06-41, in contrast to Forey's (1998, fig. 4.4)[12] reconstruction.

Char. 225: Only specimen MHNM 06-1236 of *Miguashaia bureaui* shows part pelvic girdle (R. Cloutier, pers. observ.). The size of the plate suggests that there is a single fused element.

Char. 231: Based on specimen MHNM 06-1809, the second dorsal fin of *Miguashaia bureaui* has at least one distal radial associated with the basal plate (R. Cloutier, pers. observ.); it is likely that a second distal radial that was also present because of the distal margin of the basal plate.

Char. 243: In *Miguashaia*, the lobe is present but poorly developed.

Char. 250: Forey (1998, char. 97)[12] and subsequent analyses [up to Toriño et al. (2021, char. 97)[14]] coded the condition of the caudal lobes of *Miguashaia* as unknown. *Miguashaia bureaui* has an heterocercal caudal fin (Schultze, 1973[9]; Cloutier, 1996, figs. 1, 2, 15[61]). The ventral lobe is approximately twice as long as the dorsal lobe.

Char. 257: New information on the general condition of the vertebral column of *Miguashaia bureaui* is available on specimens MHNM 06-1236 and 06-1237 (R. Cloutier, pers. observ.). Although vertebral elements are covered by scales, neural arches and spines form a bas relief showing that the vertebrae alignment is linear and horizontal.

Char. 264: Mondéjar-Fernàndez et al. (2021)[113] described the different types of ornament observed on the scales of *Miguashaia bureaui*. The ornamentation pattern of *M. bureaui* varies according to the position of the scales on the body as well as during ontogeny (Mondéjar-Fernàndez et al., 2021, fig. 2)[113]. Five types of ornamentation were reported: (1) coarse tubercles, (2), coarse and short longitudinal ridges, (3) fine leaf-or spoon-shaped tubercles, (4) fine, parallel, longitudinal, low-profile ridges, and (5) smooth, thinly and regularly pitted enamel surface. Thus, *M. bureaui* is coded as polymorphic.

Char. 266: Forey (1998, char. 105)[12] and subsequent phylogenetic analyses [up to Toriño et al. (2021, char. 105)[14]] coded *Miguashaia* as having single lateral line pore per scale. However, specimens MHNM 06-494 and 06-1236 of *Miguashaia bureaui* show clearly that there are multiple pores per scales (R. Cloutier, pers. observ.); the condition has been properly described by Cloutier (1996)[61] and Mondéjar-Fernàndez et al. (2021)[113].

Char. 268: Forey (1998, char. 107)[12] and subsequent analyses [up to Toriño et al. (2021, char. 107)[14]] coded the condition of the lung (or swimbladder) of *Miguashaia* as unknown. Observation of all known specimens of *Miguashaia bureaui* permits us to code the lung as not ossified.

Miguashaia grossi
Based on Forey et al. (2000)[63]; RC (double-checked by RC).

Moenkopia wellesi
Based on Schaeffer & Gregory (1961)[154]; JAL, September 11th 2020 (double-checked by RC, January 22th, 2021).

Ngamugawi wirngarri
Based on original material; AMC, JAL, and RC (neurocranial characters double-checked by AMC, September 6th, 2021).

Char. 73: The shape of the squamosal of *Ngamugawi* shows a clear linear ventral margin (parallel to the dorsal margin of the preoperculum), a posterior margin (almost parallel to the anterior margin of the operculum), an oblique dorsal margin, and the anterior part is divided into two segments (a ventral linear margin and a dorsal inwardly curved margin).

Char. 99: The ornament of *Ngamugawi wirngarri* cheek bones is composed of both fine ridges and tubercles. Thus, we coded char. 99 as polymorphic.

Char. 122: The principal coronoid of *Ngamugawi* is visible in an early photo of the specimen, despite not being able to identify it from scan data.

Char. 131: The ornamentation of the lower jaw of *Ngamugawi wirngarri* is primarily composed of ridges. However, tuberculated areas are present on the dentary, part of the splenial and sporadically on the posterior part of the angular. Thus, character 131 is coded as polymorphic.

Char. 157: The hypophyseal fossa is posterior to the orbit in *Ngamugawi* whereas it projects ventrally to the orbit in *Latimeria*.

Parnaibaia maranhaoensis

Based on Yabumoto (2008)[66] and Barbosa et al. (2019)[124]; BK (double-checked by RC, December 9, 2020).

Char. 1: Yabumoto (2008, char. 2)[66] coded *Parnaibaia maranhaoensis* as having consolidated snout bones, however, Yabumoto (2008, fig. 6)[66] illustrated clearly that the snout bones were separated from one another. This coding was also corrected by Toriño et al. (2021, char. 2)[14].

Char. 9: Yabumoto (2008, char. 5)[66] coded the condition of the dorsal lamina of the premaxillae of *Parnaibaia maranhaoensis* as unknown. However, Yabumoto (2008, fig. 6)[66] illustrated the fragmented premaxillae with a highly reduced dorsal lamina.

Char. 32: The parietals and postparietals of *Parnaibaia maranhaoensis* are ornamented by coarse tuberosities as originally suggested by Yabumoto (2008, char. 27)[66] and corroborated by Cavin et al. (2019)[100] and Toriño et al. (2021)[14].

Char. 44: *Parnaibaia maranhaoensis* lacks anterior pit-lines in agreement with Fragoso (2014)[108] and Toriño et al. (2021, char. 24)[14] in contrast to Yabumoto (2008)[66] who coded it as "?".

Char. 47: In contrast to Yabumoto (2008, char. 25)[66] and subsequent authors that coded *Parnaibaia maranhaoensis* as "?", we agree with Fragoso (2014, char. 25)[108] and Toriño et al. (2021, char. 25)[14] that the posterior and middle pit-lines are located in the posterior half of the postparietal as illustrated by Yabumoto (2008, fig. 3)[66].

Char. 50: In the diagnosis of *Parnaibaia maranhaoensis*, Yabumoto (2008, p. 329)[66] mentioned that the extrascapulars and the tabular (his supratemporal) are not fused. Yabumoto (2008, char. 15)[66] coded the extrascapulars of *P. maranhaoensis* as sutured with the postparietals; this condition is well illustrated in Yabumoto (2008, figs. 2, 3)[66]. Fragoso (2014, char. 15)[108] and Toriño et al. (2021, char. 15)[14] coded *Parnaibaia* as having free extrascapulars arguing that Yabumoto's (2008)[66] coding was incongruent with the diagnosis. However, the diagnosis only refers that the extrascapulars are not fused to the postparietals which is different from the position of the extrascapulars relative to the postparietals. Thus, we are keeping the coding as "sutured with the postparietals" which does not imply that the extrascapulars are fused to the postparietals.

Char. 109: Yabumoto (2008, char. 57)[66] and subsequent analyses [up to Toriño et al. (2021, char. 57)[14]] coded *Parnaibaia* as having a hook-shaped process posteriorly oriented on the dentary. However, Yabumoto (2008, fig. 3, p. 330)[66] did not figured not described the presence of the hook-shaped process. Therefore, based on the condition observed in Figure 3 of Yabumoto (2008)[66] we coded *P. maranhaoensis* as lacking the hook-shaped process of the dentary.

Char. 131: Yabumoto (2008)[66] indicated that the ornament of the lower jaw of *Parnaibaia maranhaoensis* is granular, while Fragoso (2014, char. 62)[108] coded for the presence of ridged ornamentation. Toriño et al. (2021, char. 62)[14] followed the original coding by Yabumoto (2008)[66].

Char. 151: The buccohypophysial foramen opens through the parasphenoid of *Parnaibaia maranhaoensis* as documented by Fragoso (2014, fig. 137)[108] and Toriño et al. (2021b, char. 78)[14].

Char. 262: The ribs of *Parnaibaia* are long (Yabumoto, 2008, fig. 2)[66].

Char. 263: The scales of *Parnaibaia* have a clearly prominent central ridge (Yabumoto, 2008, fig. 4A, B)[66].

Piveteauia madagascariensis

Based on Clément (1999)[68], Forey (1998)[12], Cloutier (1991b; *Rhabdoderma madagascariensis*)[96], and image of specimen P1130491 from Senckenberg Naturmuseum Frankfurt; RC (double-checked by RC).

Char. 54: Geng et al. (2009, char. 18)[45] and subsequent analyses [up to Toriño et al. (2021, char. 18)[14]] coded the posterior margin of the skull roof with an embayement. However, Clément (1999, fig. 5A)[68] figured the posterior part of the skull roof of the holotype of *P. madagascariensis* which shows a straight condition.

Char. 55: Geng et al. (2009, char. 22)[45] and Dutel et al. (2012, 2015, char. 22)[60,88] coded *Piveteauia* as "?". However, Wendruff & Wilson (2012)[70] and some subsequent analyses [including Toriño et al. (2021, char. 22)] coded *Piveteauia* as having anterior branches of occipital commissure. Herein, we are coding *P. madagascariensis* as "?". Clément (1999)[68] did not report or illustrate the presence of anterior branches of the occipital commissure on the postparietals.

Char. 103: Geng et al. (2009, char. 32)[45] and subsequent analyses [up to Toriño et al. (2021, char. 32) coded the condition of the suboperculum of *Piveteauia* as unknown. Clément (1999, p. 236)[68] mentioned that the suboperculum has not been seen, and the condition of preservation of the cheek bones suggests that if a suboperculum would have been present it would have been preserved. Thus, we are coding character 103 in *P. madagascariensis* as absent.

Char. 114: Forey (1998, char. 63)[12] and subsequent analyses [up to Toriño et al. (2021, char. 63)[14] coded the condition of the dentary ornament in *Piveteauia* to be unknown. Clément (1999, fig. 2)[68] did not figure ornamentation on the dentary while ornamentation on various dermal bones of *P. madagascariensis* was reported and figured.

Char. 116: Clément (1999, fig. 2)[68] figured the condition of the dentary of *Piveteauia* lacking any indication of teeth. However, Toriño et al. (2021, char. 54)[14] coded the condition of *Piveteauia* as having separated tooth plates. Herein, we consider the condition of the dentary dentition as unknown for *P. madagascariensis*.

Char. 131: Geng et al. (2009, char. 63)[45] and subsequent analyses [up to Toriño et al. (2021, char. 63)[14]] coded the condition of the lower jaw ornamentation of *Piveteauia* as unknown. However, the lower jaw of *P. madagascariensis* is unornamented (see Clément, 1999)[68].

Char. 263: Forey (1991, char. 54)[12] coded the scales of *Piveteauia* as not differentiated, whereas Dutel et al. (2015, char. 104)[88] coded it as '6'. Based on the illustration of Clément (1999, figs. 1, 2)[68], the scales are clearly not differentiated.

Polyosteorhynchus simplex

Based on Lund & Lund (1985)[13] and personal observation on original material (R. Cloutier, pers. observ.); RC (double-checked by RC).

Char. 13: Forey (1998, char. 3)[12] and subsequent analyses [up to Toriño et al. (2021, char. 3)[14]] coded character 3 for *Polyosteorhynchus* as unknown. Lund & Lund (1985, figs. 50, 53, 55)[13] and observed specimens show the presence of multiple rostrals.

Char. 26: In *Polyosteorhynchus*, the condition of the otic canal is coded as "0" thus, running through the tabular and supratemporal, but the intertemporal is absent.

Char. 28: Forey (1998, char. 21)[12] coded *Polyosteorhynchus* as having the otic canal joining the supratemporal canal in the tabular (his "supratemporal"). However, the condition is unclear on the specimens; in addition, the condition has not been figured by Lund & Lund (1985, figs. 49, 51-54)[13]. Furthermore, it would be unlikely that the connection between the two canals be located in the tabular because the posterior margin of the tabular is in line with the posterior margin of the postparietal, while the lateral extrascapular would provide the best support.

Char. 53: Lund & Lund (1985, figs. 54-56)[13] illustrated part of the extrascapular series of *Polyosteorhynchus simplex*. Lund & Lund (1985, fig. 54)[13] figured an extrascapular broader than the posterior margin of the tabular, whereas in their figure 55, the lateral extrascapular is narrower than the tabular. In specimen MV 6042, the median extrascapular is clearly broader than the lateral extrascapular.

Char. 91: Forey (1998, char. 46)[12] and subsequent analyses [up to Toriño et al. (2021, char. 46)[14]] coded the condition of the jugal canal of *Polyosteorhynchus* as unknown. We are coding *P. simplex*, as a simple jugal canal, based on the condition illustrated by Lund & Lund (1985, figs. 49, 54)[13].

Char. 100: Forey (1998, char. 50)[12] and subsequent analyses [up to Toriño et al. (2021, char. 50)[14]] coded for the presence of tiny pores forming the infraorbital, jugal and preopercular canal of *Polyosteorhynchus*. However, Lund & Lund (1985, fig. 54)[13] figured solely the presence of a couple of large pores on the trajectory of the infraorbital canal as well as a pore that could be associated with the jugal canal of *P. simplex*.

Char. 116: Forey (1998, char. 54)[12] and subsequent analyses [up to Toriño et al. (2021, char. 54)[14]] coded *Polyosteorhynchus* as having dentary teeth attached to separate plates. However, Forey (1998, p. 137)[12] mentioned that "it is unknown if the dentary teeth are fused or separate from the supporting bone." Observation on original material (R. Cloutier, pers. observ.) does not allow to clearly seen the dentary teeth condition.

Char. 117: Forey (1998, char. 61)[12] coded for the presence of the dentary pore of *Polyosteorhynchus*. The presence of the dentary pore was based on Lund & Lund's (1985, fig. 46)[13] reconstruction (Forey, 1998, p. 137)[12]. However, it is not clear if such a pore was reconstructed in the original drawing. Specific drawings of the lower jaw of *P. simplex* by Lund & Lund (1985, figs. 54a, b, 56)[13] do not represent such pore. Thus, we are coding the dentary pore of *P. simplex* as absent.

Char. 127: Based on the drawing of Lund & Lund (1985, fig. 56B)[13], the oral pit line of *Polyosteorhynchus* is located on the anterior third of the angular.

Char. 146: Specimens CM 30714ab (R. Cloutier, pers. observ.) and CM 27283 (Lund & Lund, 1985, fig. 52)[13] show the condition of the parasphenoid of *Polyosteorhynchus simplex*.

Char. 150: Forey (1998, char. 79)[12] and subsequent analyses [up to Toriño et al. (2021, char. 79)[14]] coded the condition of the ascending laminae of the parasphenoid in *Polyosteorhynchus* as unknown. Lund & Lund (1985, fig. 52)[13] figured a specimen of *P. simplex* (CM 27283) showing that the parasphenoid lacks the ascending laminae.

Char. 151: Forey (1998, char. 78)[12] and subsequent analyses [up to Toriño et al. (2021, char. 78)[14]] coded the condition of the buccohypophysial canal in *Polyosteorhynchus* as unknown. Cloutier (1991a, char. 35)[95] coded the buccohypophysial foramen of *P. simplex* as absent. Specimen CM 27283A of *P. simplex* shows a parasphenoid with a closed buccohypophysial foramen (R. Cloutier, pers. observ.).

Char. 203: The condition of the urohyal of *Polyosteorhynchus simplex* is visible on specimen CM 30714ab (R. Cloutier, pers. observ.).

Char. 204: The condition of the urohyal of *Polyosteorhynchus simplex* is visible on specimen CM 30714ab (R. Cloutier, pers. observ.).

Char. 207: The condition of the ceratobranchials of *Polyosteorhynchus simplex* are visible on specimen CM 30714ab (R. Cloutier, pers. observ.).

Char. 211: Forey (1998, char. 89)[12] and subsequent analyses [up to Toriño et al. (2021, char. 89)[14]] coded the condition of the shape of the anocleithrum of *Polyosteorhynchus* as unknown. Although Lund & Lund (1985, p. 37 and fig. 51)[13] described the anocleithrum of *P. simplex* as bearing "a stout spike-like vertical process", the global shape of the anocleithrum remains unclear. Thus, we are also coding the condition as unknown.

Char. 250: Forey (1998, char. 97)[12] and subsequent analyses [up to Toriño et al. (2021, char. 97)[14]] coded the caudal lobes of *Polyosteorhynchus* as asymmetrical. Lund & Lund (1985, fig. 46)[13] reconstructed the caudal fin of *P. simplex* with a dorsal lobe slightly longer than the ventral lobe in which some distal radials did not support lepidotrichia. However, in the diagnosis of *P. simplex*, Lund & Lund (1985, p. 32)[13] provided meristic counts for the dorsal (3-4 unsegmented lepidotrichia plus 14-15 segmented lepidotrichia) and ventral lobes (3-4 unsegmented lepidotrichia plus 14-16 segmented lepidotrichia) of the caudal fin supporting the symmetry of these lobes.

Char. 268: Forey (1998, char. 107)[12] and subsequent analyses up to Gess & Coates (2015, char. 107)[78] coded the swimbladder of *Polyosteorhynchus* as not ossified. Dutel et al. (2012, char. 107)[60] and subsequent analyses [up to Toriño et al. (2021, char. 107)[14]] coded *Polyosteorhynchus* as having an

ossified lung. Based on Lund & Lund (1985)[13] and our observation of the original material (R. Cloutier, pers. observ.), the lung of *P. simplex* is not ossified.

Rebellatrix divaricerca
Based on Wendruff & Wilson (2012)[70]; RC (double-checked by RC).
Char. 99: Wendruff & Wilson (2012, char. 49)[70] coded the ornamentation of the cheek bones of Rebellatrix as being absent. However, Wendruff & Wilson (2012, p. 200, fig. 1)[70] figured only a small patch of tubercular ornament on the dorsal part of the operculum, whereas all cheek bones are not preserved. Thus, we are coding the condition of *R. divaricerca* as unknown.
Char. 140: Toriño et al. (2021, char. 53)[14] coded the condition of the retroarticular and articular of *Rebellatrix* as unknown. Herein, we follow the coding presented by Wendruff & Wilson (2012, char. 53; fig. 1E-F)[70] in which both elements are separated.
Char. 212: Although the anocleithrum is displaced on specimen PRPRC 2006.10.001, Wendruff & Wilson (2012, p. 504)[70] mentioned that it articulates with the dorsal end of the cleithrum, wrapping around the curved dorsal margin of the operculum (based on the articular facets). Thus, we are coding *Rebellatrix* with the plesiomorphic condition.

Reidus hilli
Based on Graf (2012)[71]; known only from the holotype; JAL (double-checked by RC, December 11, 2020).
Char. 62: Graf (2012, char. 29)[71] coded *Reidus* as having cheekbones separated. However, because of the poor state of preservation of the specimen (with the exception of the lower jaw), the condition of the contact among cheek bones is unclear and we coded it as "?".
Char. 65: Graf (2012)[71] identified a large rectangular element as the preoperculum in *Reidus hilli*. We coded the preoperculum to be present based on the identification made by Graf (2012)[71]. Nevertheless, this identification remains questionable based on Graf's (2012, fig. 2F) drawing.
Char. 69: Graf (2012, char. 34)[71] coded the squamosal of *Reidus hilli* as reaching the skull roof. Since skull roof bones of *R. hilli* are unknown as well as the poor state of preservation of the cheek region we prefer coding this character as "?".
Char. 99: Graf (2012)[71] and subsequent analyses [up to Toriño et al. (2021, char. 49)[14]] coded the condition of the cheek bone ornament in *Reidus* as unknown. However, the condition of the squamosal and preoperculum figured by Graf (2012, fig. 2)[71] indicates that the surface is unornamented; furthermore, Graf (2012)[71] mentioned that the surface of the opercula, dentaries, and gulars is unornamented. Thus, we are coding the condition of the cheek bone ornamentation of *R. hilli* as absent.

Rhabdoderma elegans
Based on Forey (1981, 1998)[12,105] and Lund & Lund (1985)[13] and observations on original material (R. Cloutier, pers. observ.); RC (double-checked by RC; neurocranial characters double-checked by AMC, September 6th, 2021).
Char. 20: Forey (1981, 1998)[12,105] recognized the presence of a single bone lateral to the postparietal of *Rhabdoderma elegans*; Forey (1981, 1998)[12,105] identified this element as the supratemporal, whereas we identify this element as the tabular. Lund & Lund (1985, fig. 4)[13] identified the presence of two lateral dermal bones; they identified the anterior narrow bone as a supratemporal, whereas the larger posterior element as the tabular. We coded *R. elegans* as having a single element located laterally to the postparietal, that we identified as the tabular.
Char. 27: Forey (1998, char. 20)[12] coded *Rhabdoderma* as Forey (1998, p. 58)[12] mentioned, but did not figured (Forey, 1998, fig. 3.3D)[12], the potential presence of a sensory pore, sometimes double, located anteriorly to the middle pit-lines on the postparietal of *Rhabdoderma elegans*. Most observed specimens lack the median branch of the otic canal. Thus, we are coding character 27 as polymorphic to reflect this variation.

Char. 47: The middle pit lines of *Rhabdoderma elegans* are located in the anterior fourth of the postparietal. The posterior pit lines extend from the middle pit lines posteriorly to the posterior third of the length of the postparietal. Thus, we coded char. 45 as polymorphic while both conditions are observed on the specimens.

Char. 99: The ornament of *Rhabdoderma elegans* cheek bones is composed of both fine ridges and tubercles (Forey, 1998, fig. 4.8)[12].

Char. 114: Forey (1998, fig. 5.3)[12] illustrated a very small patch of ornament in the lowermost part of the dentary near the contact between the splenial and angular.

Char. 131: Forey (1998, char. 62)[12] and subsequent analyses [up to Toriño et al. (2021, char. 62)[14]] coded the ornament of the lower jaw of *Rhabdoderma* as being ridged. Both types of ornamentation are present on the angular of *Rhabdoderma elegans* (Forey. 1998, fig. 5.3C)[12] where the ridged one are found primarily dorsally and the tuberculated one more ventrally. Thus, character 131 is coded as polymorphic.

Char. 169: The vagus foramen is shown in figure 6.4 of Forey (1998)[12].

Char. 258: Forey (1981, text-fig. 9)[105] and Forey (1998, fig. 11.14)[12] did not reconstructed the presence of "supraneurals" in *Rhabdoderma elegans*. However, Lund & Lund (1985, figs. 2, 3)[13] figured a specimen showing the presence of at least one 'supraneural" located anteriorly to the insertion of the epichordal lobe of the caudal fin.

Rhabdoderma exiguum
Based on numerous specimens from Peabody Museum (Yale University) and Field Museum of Natural History (R. Cloutier, pers. observ.); RC (double-checked by RC, February 19, 2021).

Char. 9: The premaxillae of *Rhabdoderma exiguum* is fairly well-preserved in specimen FMNH PF 5521.

Char. 24: Cloutier (1991a, char. 19)[95] coded *Rhabdoderma exiguum* as not available. New observations on specimens permits us to code this process to be present.

Char. 38: The condition of the internal imprint of the postparietal of *Rhabdoderma exiguum* is well-preserved in the yolk-sac embryo specimen FMNH PF 5494.

Char. 57: The preorbital of *Rhabdoderma* exiguum is preserved in specimen FMNH PF 5760.

Char. 80: The condition of the lacrimojugal of *Rhabdoderma exiguum* is fairly well-preserved in specimen FMNH PF 5760.

Char. 86: The condition of the postorbital of *Rhabdoderma exiguum* is preserved in specimen FMNH PF 5760.

Char. 114: The absence of ornamentation on the dentary of *Rhabdoderma exiguum* is most likely associated with the embryonic, larval, and juvenile stages of the specimens.

Char. 124: Forey (1998, p. 336)[12] mentioned that the principal coronoid of *Rhabdoderma exiguum* is triangular. However, the shape of the principal coronoid on specimens YPM 2022 and FMNH PF 7528 is clearly subquadrilateral.

Char. 130: The trajectory of the mandibular canal in the angular is visible in specimen FMNH PF.8667 (R. Cloutier, pers. observ.); large incomplete pores are present on the ventral margin of the angular.

Char. 151: The open buccohypophysial foramen of the parasphenoid of *Rhabdoderma exiguum* is visible in specimen FMNH PF 6270 and YPM-2024-350.

Char. 237: Most of the specimens of *Rhabdoderma exiguum* are larvae or juveniles. It seems that the basal plates of the median fins are among the last postcranial elements to ossify (R. Cloutier, pers. observ.). The first basal plate to ossify is the one associated with the second dorsal fin where only the anteroventral process is formed (FMNH PF.7529).

Char. 258: Some of the specimens of *Rhabdoderma exiguum* (e.g., FMNH PF 3779, PF 6270, PF 7338, PF 8673) show the presence of one or two "supraneurals" anterior to the insertion of the caudal fin.

Rhabdoderma (?) *newelli*

Based on Echols (1963)[75] and observation on original material (R. Cloutier, pers. observ.); RC (double-checked by RC; neurocranial characters double-checked by AMC, September, 6th, 2021. Originally *Synaptotylus newelli*, synonymized by Forey (1998, p. 335)[12].

Char. 20: Echols (1963, fig. 3)[75] identified a single bone located posterolaterally to the postparietal (his "intertemporal") as the supratemporal; we identify this element as the tabular.

Char. 21: The element identified as an intertemporal by Echols (1963, fig. 3)[75] in *Rhabdoderma* (?) *newelli* corresponds to the postparietal.

Char. 131: Based on Echols (1963)[75], both types of ornamentation are present on the angular of *Rhabdoderma* (?) *newelli*, where the ridged one are found primarily ventrally and the tuberculated one more dorsally. Thus, character 131 is coded as polymorphic.

Char. 216: The posteroventral element of the pectoral girdle identified by Echols (1963, fig. 6a)[75] is an extracleithrum rather than a clavicle.

Char. 218: In the original description Echols (1963, fig. 6A)[75] illustrated the pectoral girdle of *Rhabdoderma* (?) *newelli*, and mislabeled the extracleithrum for the clavicle. Most likely the extracleithrum extends more dorsally than the clavicle, however, the clavicle is not represented. Nevertheless, we are coding this character as "?".

Char. 228: The pelvic girdle of *Rhabdoderma* (?) *newelli* shows a short process between the anteromedial and medial processes (Echols, 1963, fig. 6B)[75].

Sassenia groenlandica

Based on Forey (1998)[12]; JAL, September 2020 (double-checked by RC, January 22, 2021).

Char. 6: Forey (1991, char. 35)[97] coded *Sassenia* has having confluent posterior pores of the rostral organ. Forey (1998, fig. 4.13)[12] illustrated clearly the presence of both pores separated by a narrow bony bridge.

Char. 51: Forey (1998, char. 16)[12] coded *Sassenia* as having extrascapulars located behind the neurocranium. However, Forey (1998, fig. 3.11)[12] illustrated the posterior part of the skull of *S. groenlandica* showing that the left extrascapular is clearly part of the skull roof and located above the neurocranium.

Char. 62: Forey (1998, char. 29)[12] coded the cheek bone of *Sassenia* as being separated. However, Forey (1998, fig. 4.13)[12] illustrated the cheek elements of *S. groenlandica* with little space among some of the cheek bones. However, the margins of these elements suggested that there was a contact among them.

Char. 69: Forey (1998, char. 34)[12] and subsequent analyses [up to Toriño et al. (2021, char. 34)[14]] coded the squamosal of *Sassenia* as reaching the skull roof. However, Forey (1998, fig. 4.13)[12] illustrated a deep squamosal that does not reach the skull roof because of the presence of the spiracular. Thus, we are coding the squamosal of *S. groenlandica* as limited to the mid-level of the cheek.

Char. 90: Forey (1998, char. 45)[12] and subsequent analyses [up to Toriño et al. (2021, char. 45)[14]] coded the infraorbital canal of *Sassenia* as passing along the anterior margin of the postorbital. However, Forey (1998, fig. 4.13)[12] did not illustrated the trajectory of the infraorbital canal and he mentioned (p. 115) the canal "appears to lie close to the anterior margin, although the exact course is difficult to trace and there are no prominent anterior and posterior branches." Because of the uncertainty, we are coding *L. groenlandica* as "?".

Char. 91: Forey (1998, char. 46)[12] and subsequent analyses [up to Toriño et al. (2021, char. 46)[14]] coded *Sassenia* as having a simple jugal canal. However, Forey (1998, fig. 4.13)[12] illustrated the presence of a large jugal canal leading to numerous ventral branches. Thus, we are coding *Sassenia groenlandica* as having a prominent jugal canal.

Char. 176: Toriño et al. (2021, char. 71)[14] coded the condition of the processus annectens of *Sassenia* as meeting the parasphenoid. However, based on the condition figured by Forey (1998, fig. 6.8)[12], the processus connectens does not meet the parasphenoid in *S. groenlandica*.

Char. 264: The ornamentation of the scales of *Sassenia groenlandica* is composed of abutting tubercles covering the complete field (Forey, 1998, fig. 11.17)[12] similar to the condition of *Spermatodus*.

Sassenia tuberculata
Based on Stensiö (1921)[16] and Forey (1998)[12]; JAL, September 11, 2020 (double-checked by RC, January 21st, 2021).
Char. 54: Forey (1998, char. 18)[12] coded *Sassenia* as having a straight posterior margin of the skull roof. However, the condition of *S. tuberculata* is clearly with an embayed margin (Stensiö, 1921, fig. 35)[16].

Serenichthys kowiensis
Based on Gess & Coates (2015)[78]; JAL (double-checked by RC).
Char. 91: Gess & Coates (2015, char. 46)[78] and subsequent analyses [up to Toriño et al. (2021, char. 46)[14]] coded the condition of the jugal canal of *Serenichthys* as unknown. However, Gess & Coates (2015, fig 2)[78] illustrated a simple jugal canal; we assume that the juvenile condition observed remains similar in adults.
Char. 93: Gess & Coates (2015, char. 48)[78] coded *Serenichthys* as having pit lines marking the bones; however, they did not precise if this character referred to cheek pit lines. Subsequent analyses [up to Toriño et al. (2021, char. 48)[14]] used the same coding while these analyses used the original definition of the characters provided by Forey (1998)[12] which was in reference to the cheek pit-lines. Gess & Coates (2015)[78] did not mention or figure cheek pit-lines, while they reported the presence of the gular pit-lines. Thus, we are coding *S. kowiensis* as pit-lines not marking the cheek; we assume that this juvenile condition reflects the adult condition.
Char. 99: Gess & Coates (2015, char. 49)[78] changed the description of the character-states for the condition of the ornament on cheek bones as absent (0) or present (1). They coded *Serenichthys* as having ornament on the cheek bones without coding for the condition of the ornamentation itself. Toriño et al. (2021, char. 49)[14] coded *Serenichthys* as having tubercular ornament on the cheek bones; this miscoding might come from the change in the character-states used by Gess & Coates (2015)[78] in comparison to the original coding used by Forey (1998)[12]. Gess & Coates (2015)[78] mentioned the linear ornamentation on the cheek of *S. kowiensis*.
Char. 113: Gess & Coates (2015, char. 65)[78] and subsequent analyses [up to Toriño et al. (2021, char. 65)[14]] coded the condition of the dentary of *Serenichthys* as unknown. However, Gess & Coates (2015, figs. 1, 2)[78] did not figure the presence of a prominent lateral swelling of the dentary.
Char. 117: Gess & Coates (2015, char. 61)[78] and subsequent analyses [up to Toriño et al. (2021, char. 61)[14]] coded the condition of the dentary pore of *Serenichthys* as unknown. All the lower jaws of *S. kowiensis* figured by Gess & Coates (2015, figs. 1, 2, 4)[78] show no indication of a dentary pore; thus, we are coding character 117 as absent.
Char. 134: The condition of the posterior margin of the splenial of *Serenichthys kowiensis* is based on the drawing of the holotype represented by Gess & Coates (2015, figs. 1, 2C, 5D)[78]; their reconstruction of the head of *S. kowiensis* (Gess & Coates, 2015, fig. 2D)[78] did not include the splenial.
Char. 211: Gess & Coates (2015, char. 89)[78] and subsequent analyses [up to Toriño et al. (2021, char. 89)[14]] coded for the presence of a simple anocleithrum in *Serenichthys*. Based on Gess & Coates (2015, figs. 1C, 2, 4C)[78], the anocleithrum is fairly elongated and ovoid; it is not considered as a broad plate-like since it is not broader that the dorsal extremity of the cleithrum.
Char. 268: Gess & Coates (2015, char. 107)[78] and subsequent analyses [up to Toriño et al. (2021, char. 107)[14]] coded the condition of the lung of *Serenichthys* as unknown. Although specimens of *Serenichthys* are considered as juveniles and the taphonomic conditions only revealed replacement of the organic matter (Gess & Coates, 2015)[78], none of the specimens of *S. kowiensis* show signs of ossified lung.

Shoshonia arctopteryx
Based on Friedman et al. (2007)[79]; JAL (double-checked by RC).

Sinocoelacanthus fengshanensis
Based on Liu (1964)[80]; RC (double-checked by RC).

Spermatodus pustulosus
Based on Westoll (1939)[155] and Forey (1998)[12]; JAL (double-checked by RC; neurocranial characters double-checked by AMC, September 6th, 2021).
Char. 4: Posterior rostral organ pores open through the preorbital bone, not the lateral rostral (Forey, 1998, p. 339)[12].
Char. 6: Forey (1991, char. 35)[97] coded *Spermatodus* as having confluent posterior pores of the rostral organ. Forey (1998, fig. 3.12)[12] illustrated the presence of two pores closely spaced on the preorbital.
Char. 50: Forey (1998, char. 15)[12] and subsequent analyses [up to Toriño et al. (2021, char. 15)[14]] coded for the presence of free extrascapulars in *Spermatodus*. However, Forey (1998, p. 68-69)[12] mentioned that the extrascapular series of *Spermatodus* remains virtually unknown. Based on one specimen, he suggested that there was probably a large median extrascapular and many small ossicles appear to be present on either side of the median element. Because of the uncertainty, we are coding *Spermatodus pustulosus* as "?".
Char. 54: The condition of the posterior margin of the tabulars and postparietals shows a smooth and continuous embayment (Forey, 1998, fig. 3.14)[12].
Char. 58: Forey (1998, fig. 3.12)[12] figured the lateral rostral with a ventral process.
Char. 62: Forey (1998, char. 29)[12] and subsequent analyses [up to Toriño et al. (2021, char. 29)[14]] coded *Spermatodus* as having separated cheek bones. Westoll (1939, fig. 2a)[155] clearly shows the contact among the postorbital, squamosal and preoperculum.
Char. 75: Based on specimen BMNH P338 figured by Forey (1998, fig. 3.12)[12], a few ossicles are present between the premaxilla and the anterior tectal.
Char. 91: Forey (1998, char. 46)[12] and subsequent analyses [up to Toriño et al. (2021, char. 46)[14]] coded the condition of the jugal canal of *Spermatodus* as unknown. However, Westoll (1939, fig. 2a)[155] figured a simple jugal canal in *Spermatodus pustulosus* and he described it (p. 15) as narrow and shallow.
Char. 92: Forey (1998, char. 47)[12] coded the condition of the trajectory of the jugal canal of *Spermatodus* as unknown. However, Westoll (1939, fig. 2a)[155] figured the left cheek of *S. pustulosus* where the jugal canal passes through the center of the squamosal.
Char. 176: Forey (1998, char. 71)[12] coded the processus annectens as failing to meet the parasphenoid of *Spermatodus*, whereas Toriño et al. (2021, char. 71)[14] coded the processus connectens as meeting the parasphenoid. Since the illustration of the neurocranium of *S. pustulosus* by (Westoll, 1939, fig. 1)[155] are not detailed the relationships between the processus connectens and the parasphenoid is unclear; thus, we are coding the condition of the processus annectens as unknown.
Char. 214: The shape of the dorsal end of the cleithrum of *Spermatodus pustulosus* is based on the figured specimen presented by May (2012, fig. 2)[156].

Styloichthys changae
Based on Zhu & Yu (2002)[84], Friedman (2007)[79]; JAL, November 10, 2020 (double-checked by RC, January 5, 2021; neurocranial characters double-checked by AMC, September 6th, 2021).
Char. 12: Lu & Zhu (2009, char. 19)[8] coded *Styloichthys* as having anteriorly arched premaxillae based on the zone of articulation of the premaxillae.
Char. 32: The surface of the skull roofing bones of *Styloichthys* is covered by large-pore cosmine (Zhu & Yu, 2002)[84]. Thus, we coded character 31 as unornamented.
Char. 35: Zhu & Yu (2002, char. 14)[84] coded *Styloichthys* as having the anterior margin of the parietal between or in front of the orbits. However, Friedman (2007)[79] pointed out that Zhu & Yu (2002, p.

767)[84] indicate that the anterior margin of the parietals is at the level of the pineal foramen, which lies posterior to the orbits in *Styloichthys*. Thus, in agreement with Friedman (2007, char. 13)[79], we are coding this taxon as having the anterior limit of the parietal slightly posterior to the orbit.

Char. 42: Zhu and Yu (2002, fig. 1b)[84] showed distinct overlapped areas on both postparietals for the lateral extrascapulars.

Char. 91: Gess & Coates (2015, char. 46)[78] and subsequent analyses [up to Toriño et al. (2021, char. 46)[14]] coded the condition of the jugal canal of *Styloichthys* as unknown. However, Zhu & Yu (2002, fig. 2e)[84] and Friedman (2007, fig. 4C)[79] clearly illustrated a simple jugal canal showing an aligned series of small pores.

Char. 99: Toriño et al. (2021, char. 49)[14] coded the condition of the cheek bone ornamentation of *Styloichthys* as tubercular. However, Zhu & Yu (2002, fig. 2e)[84] figured the compound cheek bone of *Styloichthys* showing clearly the smooth cosmine surface on this dermal bone.

Char. 117: Gess & Coates (2015, char. 61)[78] and subsequent analyses [up to Toriño et al. (2021, char. 61)[14]] coded the condition of the dentary pore of *Styloichthys* as unknown. Zhu & Yu (2004, fig. 5)[106] reported only the presence of three small infradentary pores but not a dentary pore (unless the anterior infradentary pore corresponds to the dentary pore). Thus, we are coding the dentary pore absent in *S. changae*.

Char. 122: Friedman (2007, p. 297)[79] mentioned that it is unsurprising that the principal coronoid has not been reported in *Styloichthys* partly owing to the entirely ligamentous connection of this element with the angular in coelacanths. However, CT-scan analysis revealed the presence of a small triangular principal coronoid that has been moved from its original position within the lower jaw (Sam Giles, pers. comm.).

Char. 123: The CT-scan analysis of *Styloichthys* by Sam Giles revealed the presence of a small triangular principal coronoid that has been displaced from its original position within the lower jaw (Sam Giles, pers. comm.). It suggests that the principal coronoid was lying free and simply felt when the ligamentous connection decayed.

Char. 126: Gess & Coates (2015, char. 57)[78] and Toriño et al. (2021, char. 57)[14] coded *Styloichthys* as having a long oral pit-line reaching forward to the dentary and/or the splenial. However, in *Styloichthys*, the oral pit line is a short canal located at mid-length of the lower jaw most likely at the level of the dentary (Zhu & Yu, 2004, fig. 5A, B, K[106]; Friedman, 2007, fig. 5A)[79]. Thus, we are coding *Styloichthys* as "?" because the character-states do not take into account the condition observed in *Styloichthys*.

Char. 127: Gess & Coates (2015, char. 59)[78] and subsequent analyses [up to Toriño et al. (2021, char. 59)[14]] coded the position of the oral pit line of *Styloichthys* to be located at the center of ossification of the angular. As figured by Zhu & Yu (2004, fig. 5A-B)[106], the oral pit line is located slightly posteriorly to mid-length of the lower jaw; however, the limits of the angular are not visible and therefore it is impossible to code the relative position of the oral pit line with respect to the center of ossification of the angular. Thus, we are coding character 127 as unknown.

Char. 131: Gess & Coates (2015, char. 62)[78] and subsequent analyses [up to Toriño et al. (2021, char. 62)[14]] coded the condition of the lower jaw ornament of *Styloichthys* as tubercular. However, Zhu & Yu (2004, fig. 5)[106] figured numerous lower jaws of *Styloichthys* showing clearly that the surface is not covered by tubercular ornament but rather a smooth cosmine surface. Thus, we are coding the lower jaw of *Styloichthys* as unornamented.

Char. 143: Zhu & Yu (2002, fig. 1c)[84] showed shallow pits separated by midline ridge in *Styloichthys*.

Char. 151: Gess & Coates (2015, char. 78)[78] and subsequent analyses [up to Toriño et al. (2021, char. 78)[14]] coded the condition of the buccohypophysial foramen of *Styloichthys* as unknown. However, Zhu & Yu (2002, fig. 1c)[84] and Friedman (2007, fig. 6A)[79] figured an open buccohypophysial foramen in *S. changae*.

Char. 190: Gess & Coates (2015, char. 82)[78] and Toriño et al. (2021, char. 82)[14] coded *Styloichthys* as having a prootic without complex suture with the basioccipital. However, the condition of the prootic and basioccipital is not described by Zhu & Yu (2002)[84] nor Friedman (2007)[79]. The otico-occipital

region of the neurocranium of *S. changae* appears to be a single fused unit (Zhu & Yu, 2002, fig. 1d, f, h)[84]. Thus, this character is coded as unknown.

Swenzia latimerae

Based on Clément (2005)[86]; HD (double-checked by RC, December 11, 2020).

Char. 27: Clément (2005, char. 20)[86] coded the condition of the median branch of the otic canal of *Swenzia latimerae* as "?". Although we are coding *S. latimerae* as "?", it is noteworthy to mention that Clément (2005, p. 483)[86] reported that the condition of the sensory pores on the anterior part of the postparietal is unusual because sensory pores are distributed all over the surface. Thus, some of these pores could potential belong to the median branch of the otic canal.

Char. 28: Clément (2005, char. 21)[86] and subsequent analyses [up to Toriño et al. (2021, char. 21)[14]] coded for the otic canal joining the supratemporal canal of *Swenzia latimerae* in the tabular (his "supratemporal") rather than the extrascapular. The otic canal passes through the tabular, however, extrascapulars are not preserved in *Swenzia* and there is no indication for the trajectory of the supratemporal canal. Therefore, we coded *Swenzia* as "?".

Char. 34: Clément (2005, char. 28)[86] coded *Swenzia latimerae* as having the parietals and postparietals with raised areas. Although this condition is mentioned as a derived feature in the abstract, Clément (2005, fig. 2)[86] illustrated an anterior depression at the anteromedian region of the postparietals.

Char. 62: Clément (2005, char. 29)[86] and subsequent analyses [up to Toriño et al. (2021, char. 29)[14]] coded the cheek bones of *Swenzia latimerae* as separated from one another. However, Clément (2005, fig. 3)[86] illustrated a tight contact between the postorbital and squamosal. Furthermore, the undulating ventral margin of the squamosal matches the shape of the dorsal margin of the preoperculum. We are coding Character 62 in *Swenzia* as the cheek bones sutured to one another.

Char. 127: Clément (2005, char. 59)[86] considered the oral pit line (his "angular pit line") of *Swenzia latimerae* to be removed from the center of ossification of the angular. Although the exact limits of the extent of the angular are poorly identified (Clément, 2005, fig. 3)[86], the oral pit line seems to be removed from the center of the angular; we consider this localization of the oral pit line to be more accurate than the one represented in the reconstruction of *S. latimerae* (Clément, 2005, fig. 9B)[86].

Char. 131: Clément (2005, char. 62)[86] coded the condition of the lower jaw ornament of *Swenzia* as non-applicable (meaning the ornament is not ridged nor tubercular). Analyses subsequent to Clément (2005)[86] coded the condition as "?" without mentioning that the condition was non-applicable. The lower jaw of *S. latimerae* is unornamented.

Char. 137: We code *Swenzia latimerae* as "?" because the depth of the angular is relatively uniform throughout the length of the bone in *S. latimerae* (Clément, 2005, fig. 3)[86].

Char. 224: Clément (2005, char. 100)[86] coded the pelvic fins of *Swenzia latimerae* to be in abdominal position. Since, the precise information about the insertion of the dorsal fins and pelvic fins remains unclear, we are coding *Swenzia* as "?".

Char. 250: Clément (2005, char. 97)[86] considered the caudal fin of *Swenzia latimerae* to be symmetrical. However, the posterior part of the epichordal and hypochordal lobes are missing (Clément, 2005, fig. 6, p. 486)[86]; thus, we are coding *Swenzia* as "?".

Char. 263: Clément (2005, fig. 6B)[86] showed the undifferentiated ornamentation of the scales of *Swenzia*.

Char. 268: Clément (2005)[86] called this structure the calcified bladder (p. 487), we interpret it as an ossified lung.

Ticinepomis peyeri

Based on Rieppel (1980)[157], Forey (1998)[12] and Cavin et al. (2013)[87]; RC (double-checked by RC).

Char. 9: Forey (1998, char. 5)[12] coded the condition of the dorsal laminae of the premaxillae of *Ticinepomis* as "?". However, Cavin et al. (2013, figs. 3b, 4, 5)[87] clearly figured a well-developed dorsal lamina of the premaxillae.

Char. 50: Cavin et al. (2013, char. 15)[87] coded the condition of the extrascapulars in *Ticinepomis* as "?". Although the skull of the holotype of *T. peyeri* is partly disarticulated, Rieppel (1980, fig. 2)[157] figured an extrascapular articulating with the posterior margin of the postparietal, while in the skull reconstruction the extrascapular is figured as being free from the postparietal and tabular. Thus, we are coding *T. peyeri* as "?".

Char. 72: Forey (1998, char. 37)[12] and Cavin et al. (2013, char. 37)[87] coded the condition of the squamosal of *Ticinepomis* as unknown. Cavin et al. (2017, char. 37)[41] and Toriño et al. (2021, char. 37)[14] coded the squamosal of *Ticinepomis* as large. Based on Rieppel (1980, fig. 2)[157], we considered that the squamosal of *T. peyeri* is reduced to a narrow tube.

Char. 73: Although the exact shape of the squamosal is unclear in *Ticinepomis* (Rieppel, 1980, fig. 3[157]; Forey, 1998, fig. 4.16[12]), the general condition is similar to a rectangular shape (Rieppel, 1980, fig. 2)[157].

Char. 78: Forey (1998, char. 36)[12], Cavin et al. (2013, char. 36)[87] and subsequent analyses [up to Toriño et al. (2021, char. 36)[14]] coded the condition of the anterior angle of the lacrimojugal of *Ticinepomis* as "?". However, based mainly on the new images of the holotype of *T. peyeri* (Cavin et al., 2013, fig. 3b)[87] and also the reconstruction by Rieppel (1980, fig. 3)[157], the ventral margin of the lacrimojugal shows an anterior angle.

Char. 99: Forey (1998, char. 49)[12], Cavin et al. (2013, char. 49)[87] and subsequent analyses [up to Toriño et al. (2021, char. 49)[14]] coded the condition of the cheek bone ornamentation of *Ticinepomis* as unknown. However, Rieppel (1980, figs. 2, 3)[157] illustrated a smooth condition on the postorbital and squamosal of *T. peyeri*.

Char. 109: Forey (1998, char. 57)[12] coded *Ticinepomis* as lacking a hook-shaped process on the dentary, while Cavin et al. (2013, char. 57)[87] coded for the presence of the process. Toriño et al. (2021, char. 57)[14] coded the condition as unknown. The condition of the posterior margin of the dentary of *Ticinepomis* is slightly atypical for coelacanths where a thin splint-like angled ossification (or process) borders the dorso-posterior margin of the dentary (Cavin et al., 2013, p. 170)[87]. Thus, we considered that a modified hook-shaped process is present in *T. peyeri*.

Char. 116: The description of the dentary and anterior coronoids of *Ticinepomis peyeri* provided by Cavin et al. (2013)[87] suggests that dentary teeth as absent.

Char. 117: The coding of the dentary pore of *Ticinepomis* sp. cf. *T. peyeri* is based on the description and illustration by Cavin et al. (2013, fig. 5)[87].

Char. 126: Forey (1998, char. 58)[12] coded for the presence of a short oral pit line on the angular of *Ticinepomis*. However, the oral pit line is never illustrated not described (Rieppel, 1980[157]; Forey, 1998, p. 151[12]; Cavin et al. 2013[87]).

Char. 131: Forey (1998, char. 62)[12] coded the ornamentation of the lower jaw of *Ticinepomis* as being tubercular. While describing new material identified as *T.* sp. cf. *T. peyeri*, Cavin et al. (2013, char. 62)[87] coded *Ticinepomis* as polymorphic. On the other hand, Toriño et al. (2021, char. 62) coded the condition of the lower jaw ornament of *Ticinepomis* as "?". Herein, we follow the coding provided by Cavin et a. (2013, char. 62)[87]; the tubular ornament of the angular is clear on the holotype (Cavin et al., 2013, fig. 3)[87], while ridged area of the angular is visible on the posterior part of the angular of *T.* sp. cf. *T. peyeri* (Cavin et al., 2013, fig. 4)[87].

Char. 140: Cavin et al. (2013, char. 53)[87] and subsequent analyses (up to Toriño et al., 2021, char. 53)[14] coded the condition of the retroarticular and articular as unknown. However, Cavin et al. (2013, fig. 5, p. 171)[87] described the articular and retroarticular of *Ticinepomis* sp. cf. *T. peyeri* as being two separated elements.

Char. 230: Because of the size, shape and topography of the pelvic girdle of *Ticinepomis* sp. cf. *T. peyeri* (Cavin et al., 2013, fig. 4)[87], the posterior and medial processes seem to be merged.

Trachymetopon liassicum
Based on Dutel et al. (2015)[88]; BK (double-checked by RC, January 20, 2021).

Char. 116: Dutel et al. (2015, char. 54)[88] and subsequent analyses [up to Toriño et al. (2021, char. 54)[14]] coded *Trachymetopon* as having dentary teeth attached to separate plate. However, the figured specimen (Dutel et al., 2015, fig. 1B)[88] does not show any indication of dentition associated with the dentary; thus, we considered that is preferable to code *T. liassicum* as "?".

Char. 263: Dutel et al. (2015, char. 104, p. 8)[88] described the scale ornament of *Trachymetopon liassicum* as composed of longitudinal ridges, and they coded as differentiated.

Undina cirinensis

Based on Saint-Seine (1949)[158], Schaeffer (1952)[35], and Forey (1998)[12]; JAL & HD (doubled-checked by RC, January 18, 2021).

Char. 10: Both Saint-Seine (1949, fig. 34)[158] and Schaeffer (1952, fig. 14I)[35] illustrated the lateral view of the premaxillae. Saint-Seine (1949, p. 86)[158] wrote that both the dentigenous part and the external surface of the dorsal laminae of the premaxillae bear numerous conical teeth. Considering the illustrations and the description, the condition of the dorsal laminae is unclear; this it is coded as "?".

Char. 13: Forey (1998, char. 3)[12] and subsequent analyses [up to Toriño et al. (2021, char. 3)[14]] coded the condition concerning the number of median rostral in *Undina* as unknown. Saint-Seine (1949)[158] figured the holotype of *U. cirinensis* suggesting that there is a single median rostral.

Char. 47: Based on Saint-Seine`s (1949)[158] drawing, it seems that the middle pit-line is located in the anterior third of the postparietal whereas the posterior pit line is located in the posterior half of *Undina cirinensis*. Thus, *U. cirinensis* is coded as polymorphic for character 47.

Char. 50: Forey (1998, char. 15)[12] coded for the presence of free extrascapulars in *Undina*. However, Saint-Seine (1949, fig. 34, pl. V-VI)[158] figured the left lateral extrascapulars sutured to the posterior margin of the postparietals of *Undina cirinensis*.

Char. 54: Forey (1998, char. 18)[12] coded *Undina* as having an embayed posterior margin of the skull roof. However, based on Saint-Seine (1949)[158] and Schaeffer (1952)[35], the posterior margin of the skull roof of *U. cirinensis* is fairly straight.

Char. 62: Forey (1998, char. 29)[12] coded *Undina* as having cheek bones not in contact. However, Forey (1998, p. 122)[12] mentioned that although the cheek bones do not overlap each other they closely abut one another with matching margins, thus we are coding *U. cirinensis* as having cheek bones in contact.

Char. 85: Forey (1998, char. 40)[12] coded *Undina* as lacking an anterodorsal excavation on the postorbital. We code *U. cirinensis* as lacking this anterodorsal excavation although the margin of the anterodorsal corner of the postorbital is slightly curved inward where the posteriormost supraorbital articulates (Saint-Seine, 1949, fig. 34[158]; Schaeffer, 1952, fig. 14I[35]).

Char. 147: Saint-Seine (1949, p. 77)[158] mentioned that the parasphenoid of *Undina cirinensis* forms is spatulated anteriorly.

Undina penicillata

Based on Clack (1996)[159], Forey (1998)[12], Arratia et al. (2001)[112], Mäuser (2018)[160] and images from collections specimens; JAL, November 11, 2020 (double-checked by RC, May 18, 2021); link.springer.com/chapter/10.1007/978-3-319-77401-5_3; Naturkundemuseum Bamberg's new complete specimen allowed much coding to be done (NKMB-P-Watt 08.212).

Char. 42: The left lateral extrascapulars articulates with the postparietal on specimen NKMB-P-Watt 08/212 of *Undina penicillata* figured by Mäuser (2018, fig. 3.2)[160].

Char. 50: Forey (1998, char. 15)[12] coded for the presence of free extrascapulars in *Undina*. However, on specimen NKMB-P-Watt 08/212 of *Undina penicillata* figured by Mäuser (2018, fig. 3.2)[160] the left lateral extrascapulars suture to the posterior margin of the postparietals.

Char. 116: Forey (1998, char. 54)[12] and subsequent analyses [up to Toriño et al. (2021, char. 54)[14]] coded the condition of dentary teeth of *Undina* as unknown. However, Forey (1998, fig. 5.12c)[12] figured patches of small teeth dorsal to the dentary of *U. penicillata* which we considered herein as separated tooth plates.

Char. 176: Forey (1998, char. 71)[12] coded the processus connectens of *Undina* as meeting the parasphenoid, whereas Toriño et al. (1998, char. 71)[14] coded *Undina* as the processus connectens as failing to meet the parasphenoid. We keep the coding proposed by Forey (1998, char. 71)[12].

Char. 260: Clack (1996, fig. 1)[159] and Arratia et al. (2001, fig. 31 as "*Holophagus penicillate*")[112] figured cervical neural arches of *Undina penicillata*; these elements are not expanded. Forey (1998, char. 91)[12] coded *Undina* as "?".

Whiteia durabilis
Based on Wendruff (2011)[91]; RC, March 30, 2021 (double-checked by RC).

Whiteia lepta
Based on Wendruff (2011)[91]; RC, March 30, 2021 (double-checked by RC).

Char. 13: Forey (1998, char. 3)[12] and subsequent analyses [up to Toriño et al. (2021, char. 3)[14]] coded the condition concerning the number of median rostral in *Whiteia* as unknown. Some of the small dermal bones of *W. lepta* identified by Wendruff (2011, fig. 3.2)[91] as nasals as well as smaller bones located anteriorly to the nasals are identified herein as multiple median rostral.

Char. 211: Forey (1998, char. 89)[12] and subsequent analyses [up to Toriño et al. (2021, char. 89)[14]] coded the condition of the shape of the anocleithrum of *Whiteia* as unknown. The broad plate-like shape of the anocleithrum of *W. lepta* is figured by Wendruff (2011, fig. 3.1C-D)[91].

Whiteia nielseni
Based on Nielsen (1936)[52], Forey (1998)[12], and Wendruff (2011)[91]; RC & JAL (double-checked by RC, March 30th, 2021).

Char. 13: Forey (1998, char. 3)[12] and subsequent analyses [up to Toriño et al. (2021, char. 3)[14]] coded the condition concerning the number of median rostral in Whiteia as unknown. Some of the small dermal bones of *W. nielseni* identified by Nielsen [1936, figs. 8, 9, 10[52]; specimens originally identified as undetermined coelacanthid but subsequently attributed to *W. nielseni* by Forey (1998)[12]] as interrostrals and rostrals are identified herein as multiple median rostral.

Char. 64: Forey (1998, fig. 3.16B)[12] figured a spiracular in *W. nielseni*.

Char. 95: Nielsen (1936, fig. 9)[52] identified a fragmentary element located anteriorly to the lateral rostral as a "perhaps remains of maxillary" in *Whiteia nielseni*. This identification is erroneous.

Whiteia oishoii
Based on Yabumoto & Brito (2016)[92]; RC (double-checked by RC).

Char. 8: The premaxillae is present in *Whiteia oishoii* as figured by Yabumoto & Brito (2016, fig. 3)[92]. However, the condition of the premaxillae is unclear from the photography and illustration. Thus, we prefer to code this character as unknown.

Char. 16: Based on the figured holotype of *Whiteia oishii* (Yabumoto & Brito, 2016, fig. 3)[92], we coded the preparietal to be longer than the parietal; the authors mentioned (p. 234) that the preparietal (their "anterior parietal") and parietal (their "posterior parietals") are almost the same length.

Char. 211: Forey (1998, char. 89)[12] and subsequent analyses [up to Toriño et al. (2021, char. 89)[14]] coded the condition of the shape of the anocleithrum of *Whiteia* as unknown. The sigmoid shape of the anocleithrum of *W. oishoii* is figured by Yabumoto & Brito (2016, fig. 12)[92].

Char. 230: It is likely that the lateral and posterior processes have merged in *Whiteia oishii* because of the shape and size of the posterior division of the pelvic plate (Yabumoto & Brito, 2016, fig. 7)[92]; thus, both processes are coded as present.

Whiteia uyenoteruyai
Based on Yabumoto et al. (2019)[161]; JAL, September 2020 (double-checked by RC, December 18th, 2020).

Whiteia woodwardi

Based on Forey (1998)[12] and Yabumoto et al. (2019)[161]; JAL, November 2020 (double-checked by RC, January 12th, 2021).

Char. 91: Forey (1998, char. 46)[12] and subsequent analyses [up to Toriño et al. (2021, char. 46)[14]] coded *Whiteia* as having prominent branches of the jugal canal. However, the alignment of the sensory pores on the squamosal of *Whiteia woodwardi* illustrated by Forey (1998, figs. 4.14, 4.15)[12] do not suggest the presence of prominent branches associated to the main canal.

Char. 176: Forey (1998, char. 71)[12] coded the processus connectens of *Whiteia* as meeting the parasphenoid, whereas Toriño et al. (2021, char. 71)[14] coded the processus connectens as failing to meeting the parasphenoid. Since we have not additional information on the actual condition of *Whiteia woodwardi*, we are coding the condition of the processus annectens as unknown.

Char. 268: Forey (1998, char. 107)[12] coded *Whiteia* as having a lung (his "swimbladder") not ossified.

Wimania sinuosa

Based on Stensiö (1921, 1932)[16,150] and Forey (1998)[12]; JAL, September, 2020 (double-checked by RC, January 12th, 2021).

Char. 54: Forey (1998, char. 18)[12] coded *Wimania* as "?". However, based on Stensiö (1921, text figs. 19, 21)[16], the tabular extends posteriorly to the posterior margin of the postparietal forming an embayed posterior margin of the skull roof.

Char. 95: Stensiö (1921, text fig. 25)[16] figured a splint like bone that he identified as a maxilla in the reconstruction of the skull of *Wimania sinuosa*; this element most likely corresponds to a palatal bone. We are coding the maxilla of *W. sinuosa* as absent.

Char. 151: Cloutier (1991a, b, char. 35)[95,96] coded for the absence of a buccohypophysial foramen in *Wimania sinuosa*. Forey (1998, char. 78)[12] and subsequent analyses [up to Toriño et al. (2021)[14]] coded the condition of the buccohypophysial foramen of *Wimania* as unknown. Stensiö (1921, text fig. 23)[16] illustrated the parasphenoid of *W. sinuosa* without an open buccohypophysial foramen.

Youngichthys xinghuainsis

Based on Wang & Liu (1981)[26]; JAL, September 2020 (double-checked by RC).

Yunnancoelacanthus acrotuberculatus

Based on Wen et al. (2013)[54]; JAL (double-checked by RC).

Char. 21: Wen et al. (2013, fig. 7C)[54] identified a skull roof element located between the anterior part of the postparietal, the posterior part of the parietal, medially to the postorbital and posteriorly to the supraorbital as a supratemporal. However, because of the topographic position we suggest that this element corresponds to an intertemporal, although it is unlikely that this element be homologous with the intertemporal for in the out-groups.

Char. 39: We coded the shape of the postparietal of *Yunnancoelacanthus* as rectangular. However, the shape is rather a C-shape because the postparietal extends lateroposteriorly and lateroanteriorly to the tabular. This coding was done in order to keep the three character-states of the postparietal shape as a morphocline.

Char. 50: Wen et al. (2013, char. 15)[54] and subsequent analyses [up to Toriño et al. (2021, char. 15)[14]] coded the extrascapulars of *Yunnancoelacanthus* as suturing with the postparietals. However, Wen et al. (2013, p. 184, 186)[54] mentioned that the extrascapulars of *Y. acrotuberculatus* cannot be observed because they have lost some information.

Char. 51: Wen et al. (2013, char. 16)[54] and subsequent analyses coded *Yunnancoelacanthus* as having extrascapulars as part of the skull roof. However, the condition of the extrascapulars in *Y. acrotuberculatus* is poorly known, thus we are coding as "?".

Char. 62: Wen et al. (2013)[54] and subsequent analyses [up to Toriño et al. (2021, char. 29)[14]] coded *Yunnancoelacanthus* as having separated cheek bones. As illustrated by Wen et al. (2013, fig. 7B, C)[54] the ventral margin of the postorbital matches the dorsal margin of the squamosal, however the contact

between the squamosal and preoperculum is unclear. We are coding *Y. acrotuberculatus* as having cheek bones in contact based on the clear condition between the postorbital and squamosal.

Char. 69: Wen et al. (2013, fig. 7B-C)[54] showed the left squamosal of *Yunnancoelacanthus* adjacent to to the tabular (their "supratemporal").

Char. 90: Wen et al. (2013, char. 45)[54] and subsequent analyses [up to Toriño et al. (2021, char. 45)[14]] coded the condition of *Yunnancoelacanthus* as unknown. However, Wen et al. (2013, fig. 7)[54] illustrated both postorbitals as having sensory pores located near the center of the bones.

Char. 99: Wen et al. (2013)[54] and subsequent analyses [up to Toriño et al. (2021, char. 49)[14]] coded *Yunnancoelacanthus* as having tubercular ornament on cheek bones. Because of the size of the ornamentation illustrated on the cheek bones of *Y. acrotuberculatus* by Wen et al. (2013, fig. 7a)[54] we rather considered that the condition corresponds to coarse rugosity.

Char. 113: Wen et al. (2013, char. 65)[54] and subsequent analyses [up to Toriño et al. (2021, char. 65)[14]] coded the condition of the dentary of *Yunnancoelacanthus* as unknown. However, the dentaries of *Y. acrotuberculatus* do not show indication of a prominent lateral swelling (Wen et al., 2013, fig. 7)[54].

Char. 116: Wen et al. (2013, char. 54)[54] and subsequent analyses [up to Toriño et al. (2021, char, 54)[14]] coded the *Yunnancoelacanthus* as having teeth attached to the dentary. However, new high-resolution photography of specimen LPV-12748 of *Y. acrotuberculatus* (provided by Wen Wen, 2020) shows clearly that the dentary dentition is composed of separated tooth plates siting on the dentaries.

Char. 121: Wen et al. (2013, char. 56)[54] and subsequent analyses [up to Toriño et al. (2021, char. 56)[14]] coded the condition of the coronoid opposite to the posterior end of the dentary of *Yunnancoelacanthus* as unknown. However, new high-resolution photography of specimen LPV-12748 of *Y. acrotuberculatus* (provided by W. Wen, 2020) shows a coronoid opposite to the posterior end of the dentary with enlarged teeth.

2. Disparity and geometric morphometrics

Morphological disparity of coelacanths was analyzed with 2-D geometric-morphometrics on body shape, cheek region, and lower jaw. We digitized 2-D landmarks with tpsDig2 v.2.32 on reconstructions of coelacanths previously; each reconstruction was validated for accuracy and corrected when needed. We digitized 14 2-D landmarks on 35 species to describe the lateral body outline and relative positions of the fins, 17 2-D landmarks on 34 species to capture the shape of the cheek, and seven 2-D landmarks on 38 species to describe the shape of the lower jaw. The 38 landmarks are described in Supplementary Table 2.1 and illustrated in Supplementary Figure 7.

Supplementary Table 2.1. Description of landmarks for the body shape, cheek region, and lower jaw analyses respectively.

No.	Description of the landmark
Body shape	
1	Most anterior edge of the extrascapular
2	Insertion of the first ray of the first dorsal fin
3	Insertion of the last ray of the first dorsal fin
4	Insertion of the first ray of the second dorsal fin
5	Insertion of the last ray of the second dorsal fin
6	Insertion of the first ray of the dorsal lobe of the caudal fin
7	Most posterior tip of the caudal peduncle
8	Insertion of the last ray of the ventral lobe of the caudal fin
9	Insertion of the first ray of the ventral lobe of the caudal fin
10	Insertion of the first ray of the anal fin
11	Insertion of the last ray of the anal fin
12	Insertion of the first ray of the pelvic fin
13	Insertion of the most dorsal ray of pectoral fin
14	Most ventral extremity of the pectoral girdle

Cheek region

1	Most anterior-ventral margin of the lacrimojugal
2	Most posterior-ventral margin of the lacrimojugal
3	Most posterior-dorsal margin of the lacrimojugal
4	Most anterior-ventral margin of the lacrimojugal
5	Most dorsal tip of the anterior margin of the posterior-most supraorbital
6	Most ventral tip of the anterior margin of the posterior-most supraorbital
7	Tip of the anterior-dorsal angle of the postorbital
8	Tip of the posterior-dorsal angle of the postorbital
9	Tip of the posterior-dorsal angle of the squamosal
10	Tip of the anterior-ventral angle of the squamosal
11	Tip of the posterior-ventral angle of the squamosal
12	Tip of the anterior-dorsal angle of the operculum
13	Posterior extremity of the operculum
14	Tip of the anterior-ventral angle extremity of the operculum
15	Tip of the anterior-ventral angle of the preopercular
16	Tip of the posterior-dorsal angle of the preopercular
17	Tip of the anterior-dorsal angle of the preopercular

Lower jaw

1	Most anterior extremity of the dorsal occlusal margin of the dentary
2	Most posterior extremity of the dorsal occlusal margin of the dentary
3	Most anterior extremity of the angular
4	Most posterior extremity of the angular
5	Most anterior extremity of the splenial
6	Most posterior extremity of the splenial
7	Dorsal tip of the coronoid

3. Correlation analyses

3a. Data collecting

We used six palaeoenvironmental parameters (dissolved O_2, atmospheric CO_2, sea surface temperature, continental flooded area, and subduction area flux) to characterize globally the Phanerozoic to determine if there was a correlation with the evolutionary rates associated to each one of the 82 coelacanth species. We selected these putative environmental drivers because most coelacanth species have been found in marine and estuarine palaeoenvironments (see main text for hypotheses and justification). A description of source data for each driver follows:

- **Dissolved O_2** (μM) is an important factor that regulates respiration for aquatic organisms as well as activity rate. We used the 90% confidence interval from Song et al. (2019, fig. 5)[162].
- **Atmospheric CO_2** (pCO_2; μatm) provides a global image of the climate. Witkowski et al. (2021)[163] evaluated pCO_2 based on the $\delta^{13}C_{phytane}$. We used the 68% confidence intervals by Witkowski et al. (2021, fig. 3)[163]; the original graphic is plotted using a logarithmic scale.
- **Sea surface temperature** (SST; $^{\circ}$C) is the ocean temperature close to the surface which is between 1 mm and 20 m below the sea surface. We obtain oxygen isotope values from fossil phosphatic and calcareous shells to measure sea surface temperature (Song et al., 2019)[162], using the 90% confidence interval provided by Marcilly et al. (2021, fig. 5)[164].
- **Continental flooded area** (million km^2) is defined by Marcilly et al. (2022)[165] as the difference between the area of the continental crust and the area of exposed land through time. Marcilly et al.'s (2022)[165] evaluation was based on palaeogeographic maps of Scotese (2021)[166]. We used the values provided by the model of Marcilly et al. (2022, fig. 3A). Since confidence interval and

variance were not provided by the original authors, we used the values calculated from Kocsis & Scotese's (2020)[167] model extracted from the curve illustrated by Marcilly et al. (2022, fig. 3A)[165].

- **Subduction area flux** (km^2/yr) is a proxy of plate tectonic activity. Marcilly et al. (2021)[164] evaluated subduction area flux using the zircon age-frequency distributions, which they presented as a subduction flux proxy. We used the values provided by the models of Domeier & Torsvik (2014)[168] and Torsvik et al. (2019)[169] (Marcilly et al., 2021, fig. 6)[164] as the upper and lower limits for each temporal window.

To obtain the values of the palaeoenvironmental parameters for each last and first appearance date, we used PlotDigitizer software (plotdigitizer.com/app) to retrieve the data.

4. Supplementary figures
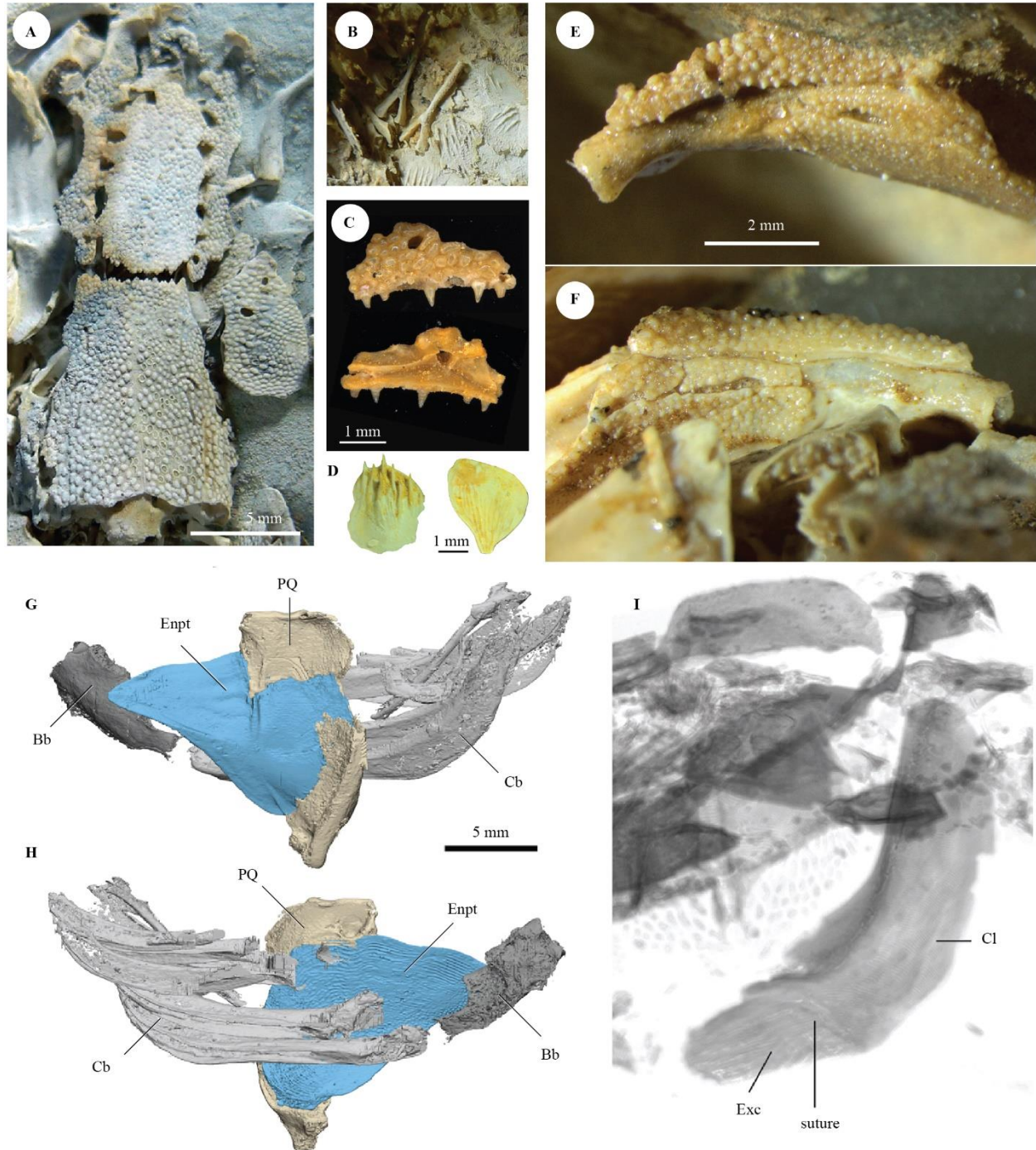
Supplementary Figure 1. Material and volume renderings of *Ngamugawi wirngarri* gen. et sp. nov. WAM 09.6.148 (holotype). (**A**) skull roof shown in dorsal view; (**B**) triradiate epibranchials; (**C**) isolated premaxilla shown in lateral and mesial view; (**D**) isolated scales shown in lateral and mesial view; (**E, F**) anterior portion of left lower jaw ramus showing arrangement of parasymphyseal bone and coronoids (first coronoid missing); (**G, H**) volume renderings from CT data of visceral skeleton; (**I**) volume rendering of pectoral girdle showing suture between the cleithrum and extracleithrum. Abbreviations: Bb, basibranchial; Cb, ceratobranchial; Enpt, entopterygoid; Exc, extracleithrum; PQ, palatoquadrate. All CT data/ models available via: www.morphosource.org/projects/000485769?locale=en.
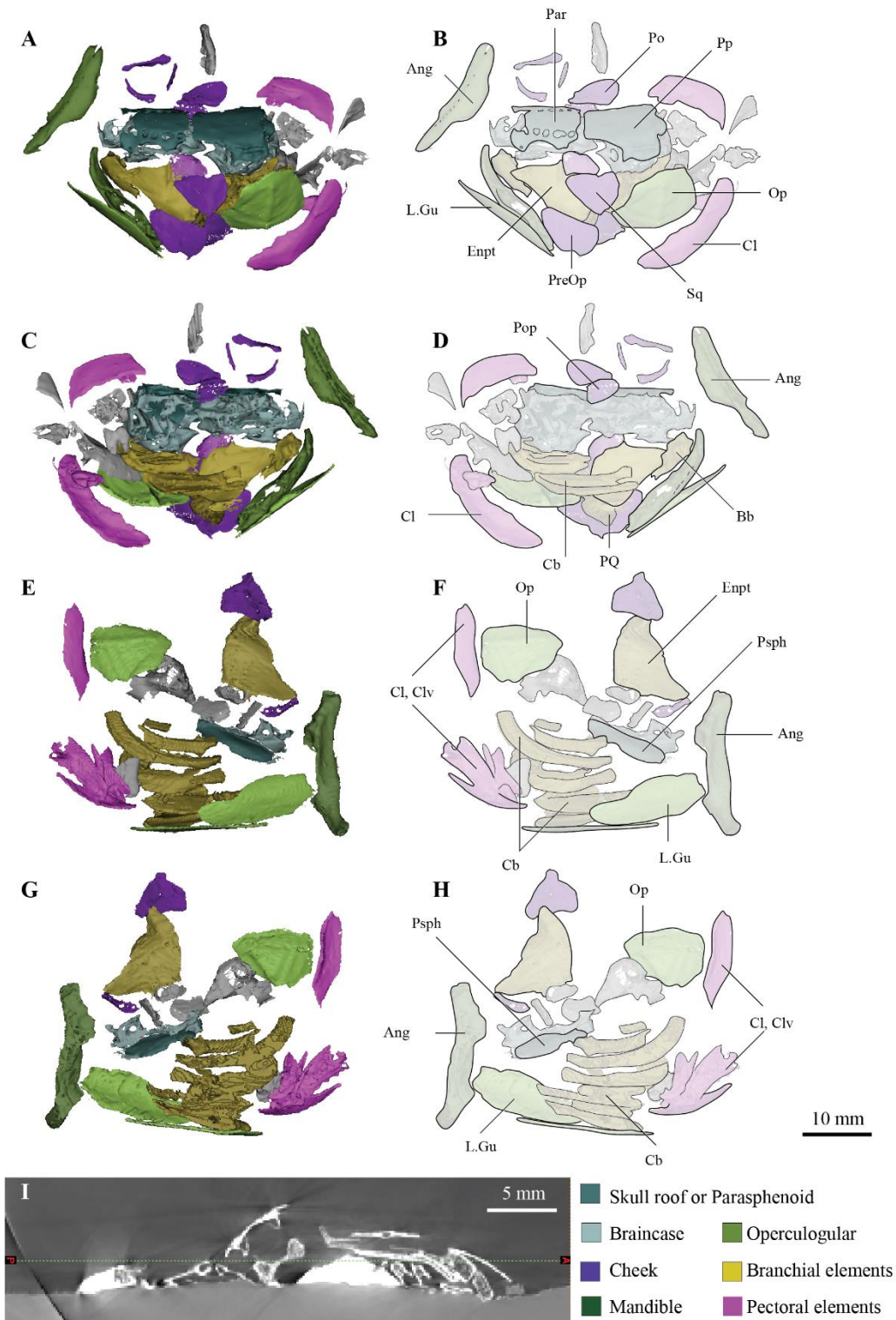
**Supplementary Figure 2. Volume renderings of all elements from part (A-D) and counterpart (E-H) of**
Ngamugawi wirngarri **gen. et sp. nov. WAM 09.6.148 (holotype), with representative low-res scan slice shown**
in I. Abbreviations: Ang, angular; Cb, ceratobranchial; Cl, cleithrum; Clv, clavicle; Enpt, entopterygoid; L.Gu,
lateral gular; Op, operculum; Par, Parietal; Po, postorbital; Pop, preoperculum; Pp, postparietal, Sq, squamosal. All
CT data/ models available via: www.morphosource.org/projects/000485769?locale=en.

a

total length
standard length
pre-caudal length
caudal length
head length
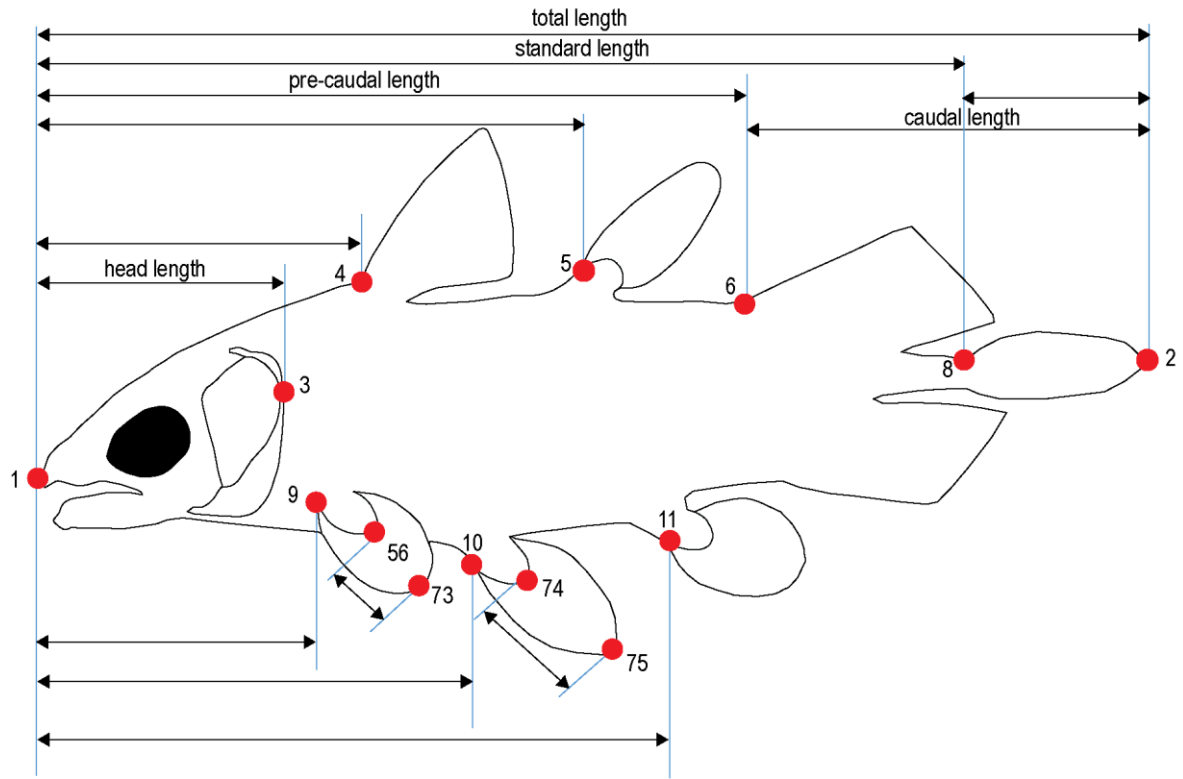
b
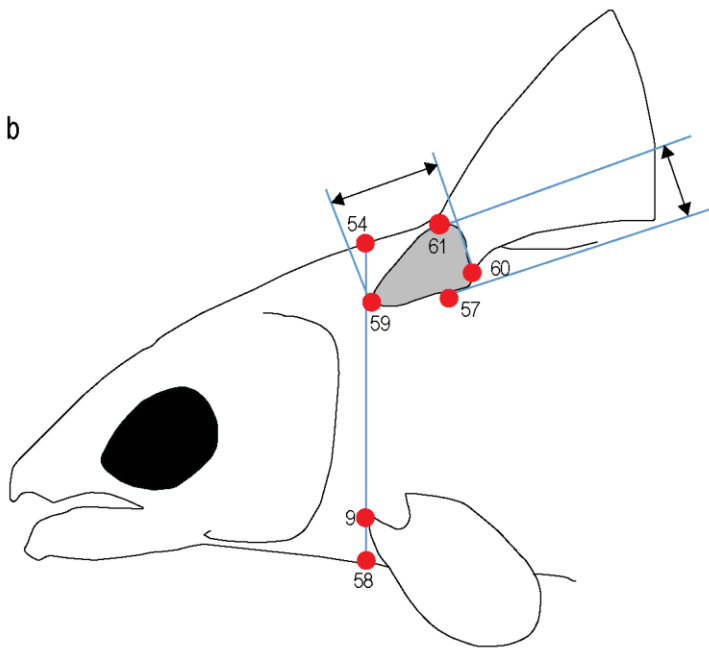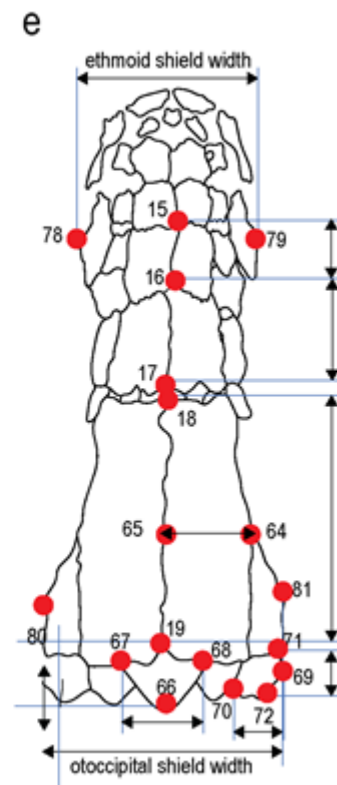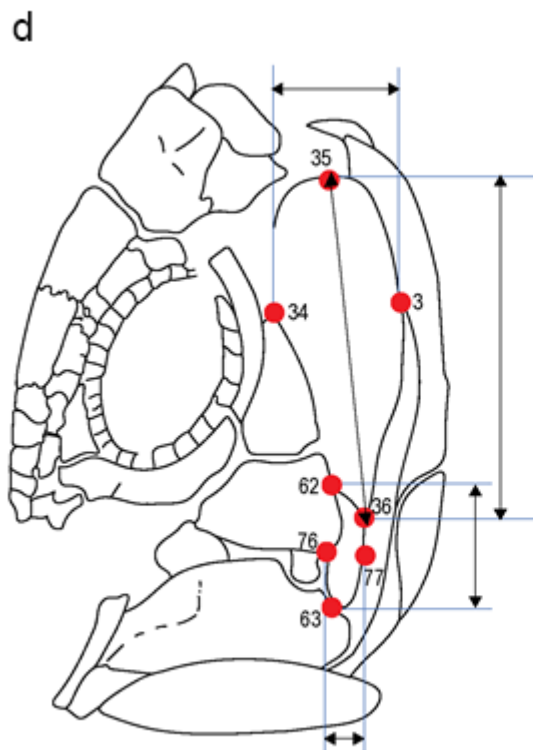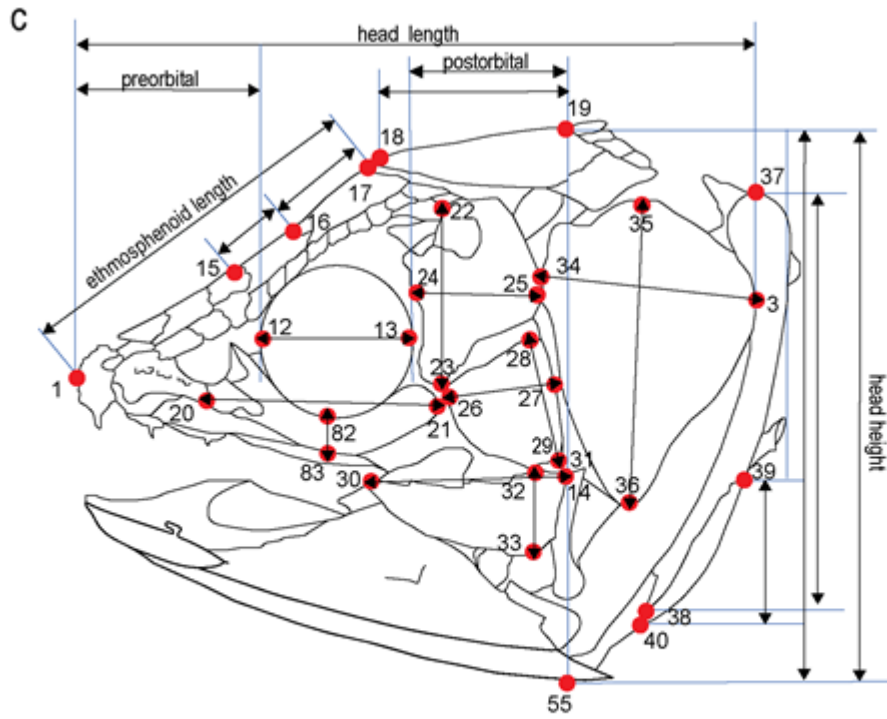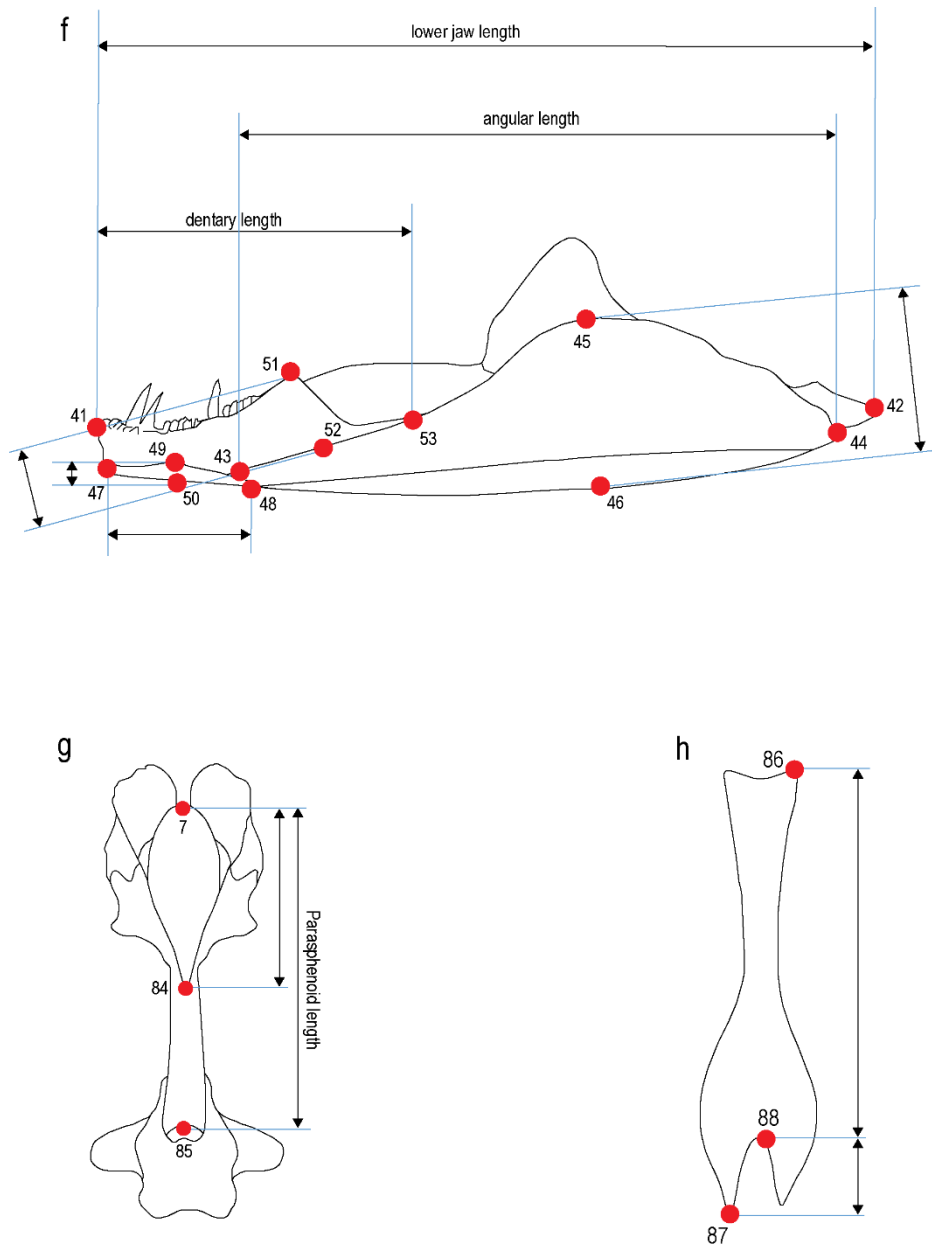
Supplementary Figure 3. Position of 88 landmarks for the 40 continuous characters used in the phylogenetic analysis of coelacanths. The list of the continuous characters with the distances defined by landmarks is provided in SI Table 1.1. (**a**) Landmarks for the body distances. (**b**) Landmarks for the distances associated to the basal plate of the first dorsal fin as well as for the height of the pectoral fin. (**c**) Landmarks for the lateral view of the skull and pectoral girdle. (**d**) Landmarks for the opercular series. (**e**) Landmarks for the skull roof distances. (**f**) Landmarks for the lower jaw. (**g**) Landmarks for the parasphenoid. (**h**) Landmarks for the urohyal. Each image is redrawn from the literature for various species: (**a**) *Diplurus newarki* redrawn from Forey (1998, fig. 11.6)[12], (**b**) *Diplurus newarki* redrawn from Forey (1998, fig. 11.6)[12], (**c**) *Macropoma lewesiensis* redrawn from Forey (1998, fig. 4.19)[12], (**d**) *Allenypterus montanus* redraw from Forey (1998, fig. 4.6), (**e**) *Rhabdoderma elegans* redrawn from Forey (1998, fig. 3.3D)[12], (**f**) *Rhabdoderma elegans* redraw from Forey (1998, fig. 5.3C)[12], (**g**) *Macropoma lewesiensis* redrawn from Forey (1998, fig. 6.10B)[12], (**h**) *Latimeria chalumnae* redrawn from Forey (1998, fig. 7.6B)[12].
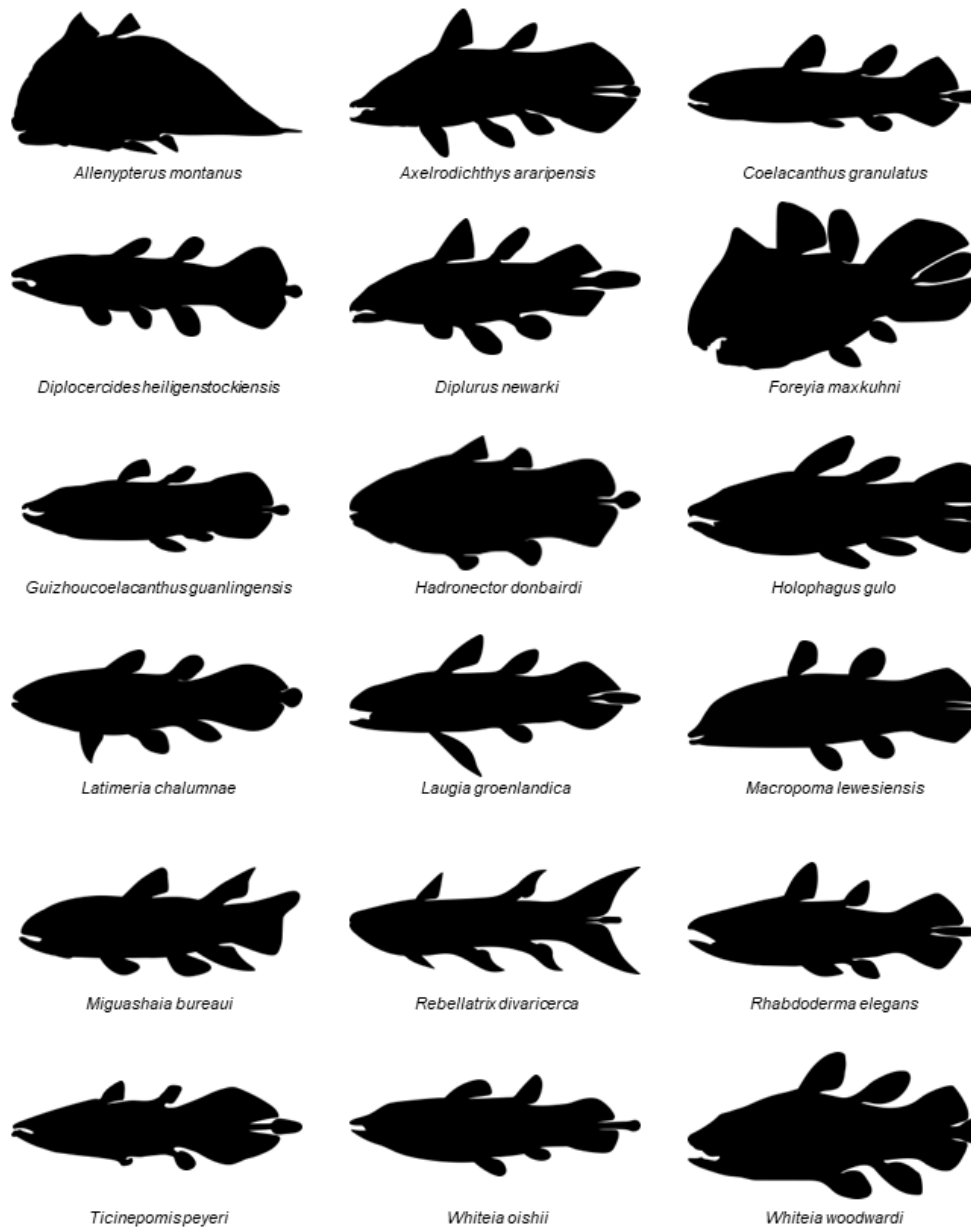
Supplementary Figure 4. **Body silhouettes of coelacanths**. *Allenypterus montanus* (based on Forey (1998, fig. 11.2)[12]), *Axelrodichthys araripensis* (based on Forey (1998, fig. 11.3)[12]), *Coelacanthus granulatus* (based on Forey (1998, fig. 11.4)[12]), *Diplurus newarki* (based on Forey (1998, fig. 11.6)[12]), *Foreyia maxkuhni* (based on Cavin et al. (2017, fig. 1)[41]), *Guizhoucoelacanthus guanlingensis* (based on Wen et al., 2013, fig. 6A)[54]), *Hadronector donbairdi* (based on Lund & Lund (1985, fig. 35)[13] and personal observation (RC)), *Holophagus gulo* (based on Forey (1998, fig. 11.18)[12]), *Latimeria chalumnae* (based on Forey (1998, fig. 8.1)[12]), *Laugia groenlandica* (based on Forey (1998, fig. 11.10)[12]), *Macropoma lewesiensis* (based on Forey (1998, fig. 11.11)[12]), *Miguashaia bureaui* (based on Cloutier (1996, fig. 1)[61]), *Rebellatrix divaricerca* (based on Wendruff & Wilson (2012, fig. 4)[70]), *Rhabdoderma elegans* (based on Forey (1998, fig. 11.14)[12]), *Ticinepomis peyeri* (based on Rieppel (1980, fig. 6)[157]), *Whiteia oishii* (reconstructed based on Yabumoto & Brito, 2016, fig. 2, 10)[92]), and *Whiteia woodwardi* (based on Forey (1998, fig. 11.18)[12]).
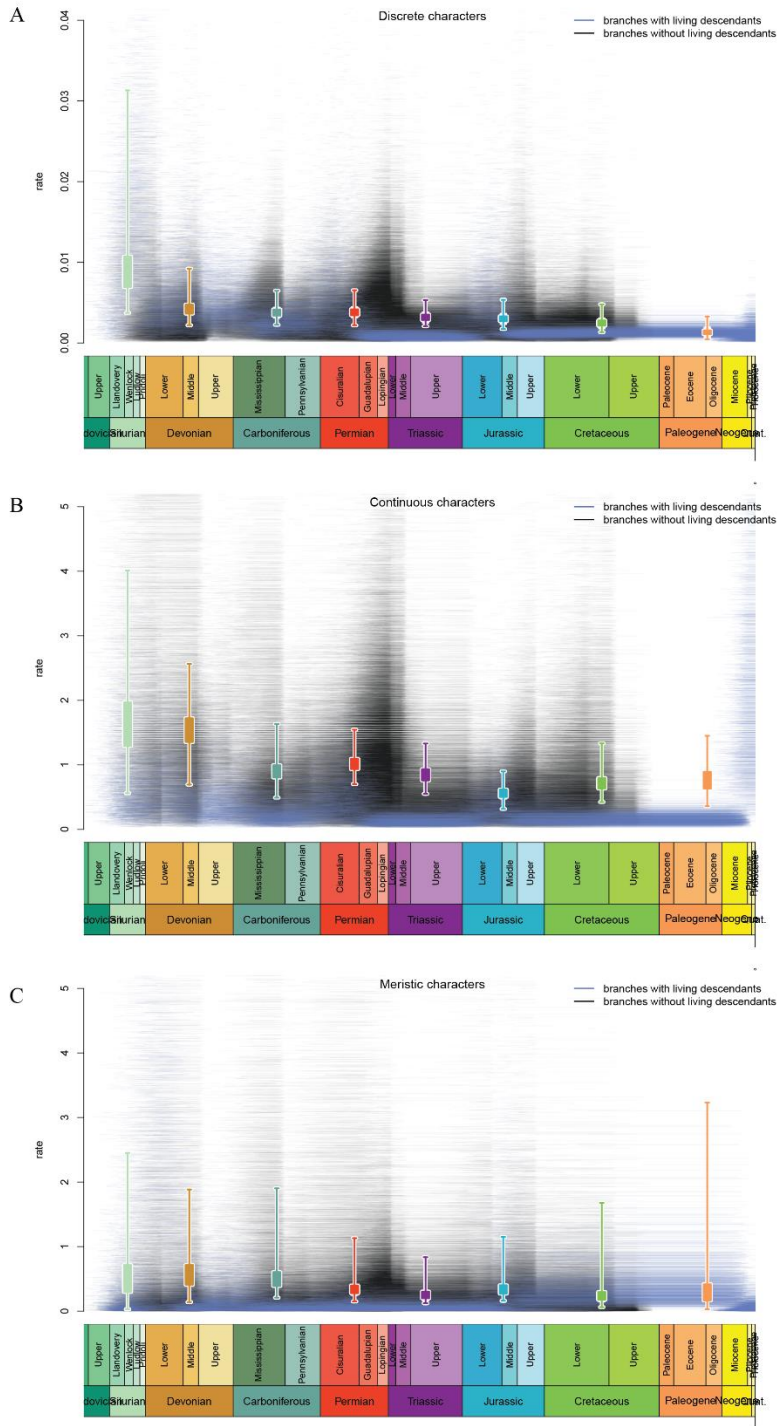
Supplementary Figure 5. Rates of evolution in coelacanths based on Bayesian total-evidence tip dating under the uncorrelated lognormal clock (corresponding dated tree is shown in main Fig. 3A). (**A**) discrete; (**B**) continuous; and (**C**) meristic characters. There is a sharp slowdown in discrete character evolution in the most recent time bin, but no such slowdown for continuous and meristic characters. Rates across all sampled trees are plotted, and each horizontal line represents the duration of a single sample of a single branch.
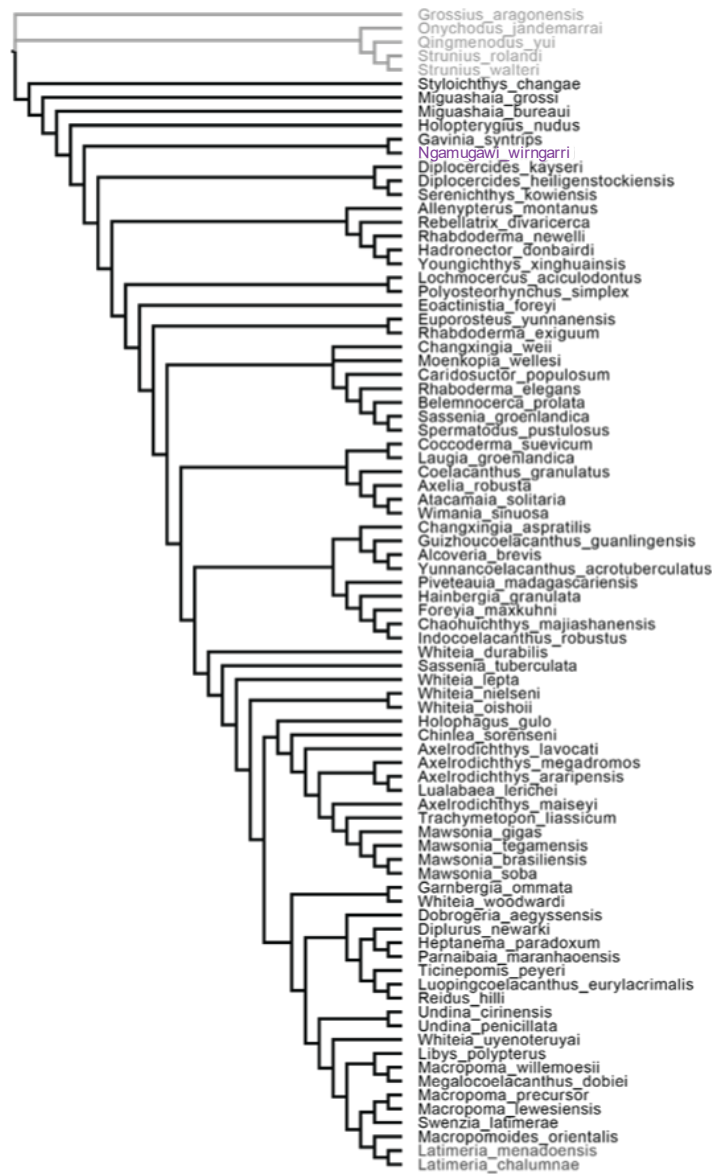
Supplementary Figure 6. **Phylogenetic tree for coelacanths based on parsimony analysis of 268 discrete, 14 meristic and 40 continuous characters, showing position of *Ngamugawi wirngarri*.** This is the strict consensus tree of 280 trees of length 1503.407 found by TNT, after pruning of three most unstable taxa (*Shosania artopteryx, Sinocoelacanthus fengshanesis* and *Euporosteus eifeliensis)* as identified by RogueNaRok.
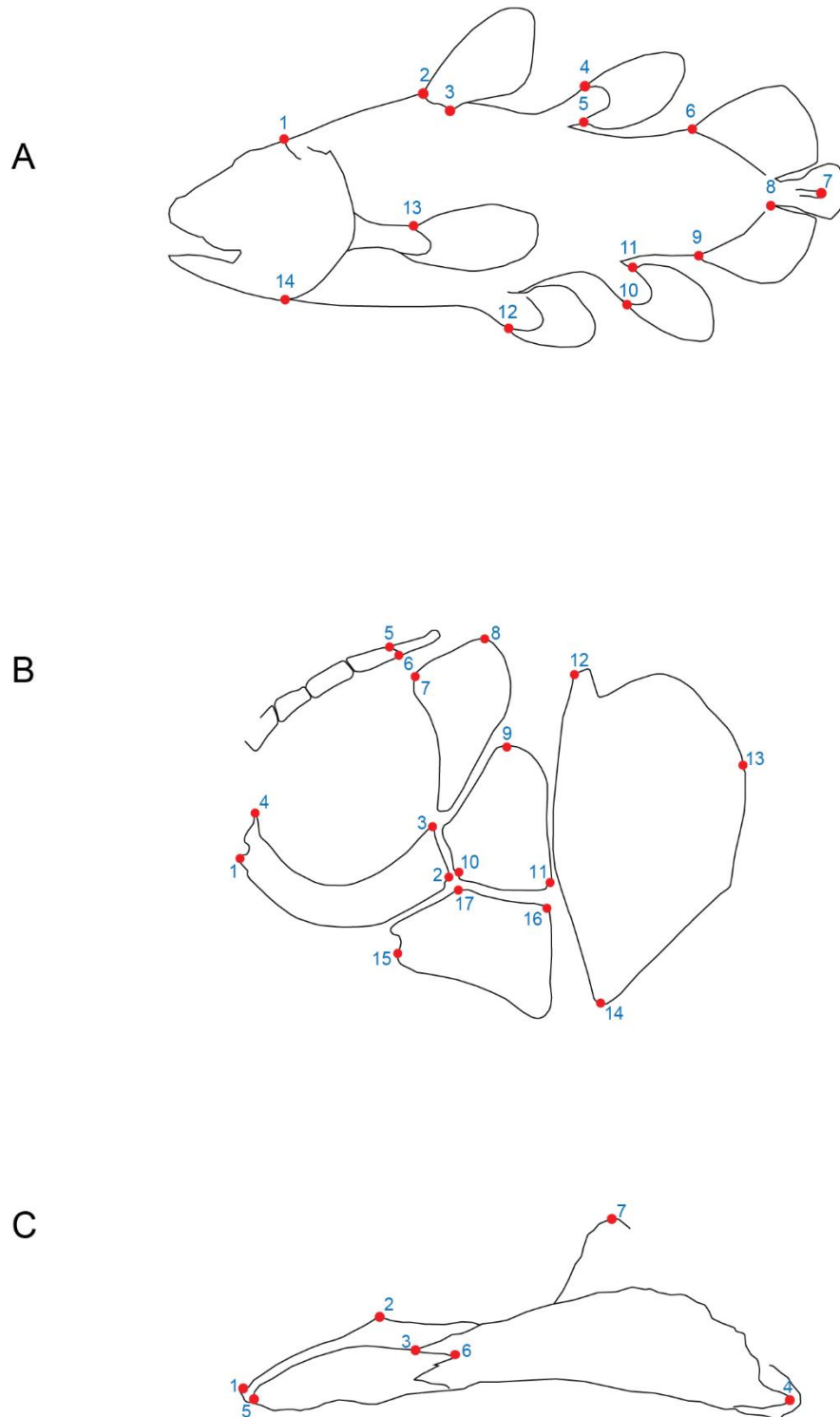
Supplementary Figure 7. Landmarks for the 2-D geometric-morphometrics on body shape, cheek region, and lower jaw. The list of the 38 landmarks defined by landmarks is provided in SI Table 2.1. **a**) Landmarks for the body shape. **b**) Landmarks for the cheek region. **c**) Landmarks for the lower jaw. Landmarks are positioned on *Holophagus gulo* based on Forey (1998, figs. 11.18, 5.12B)[12].
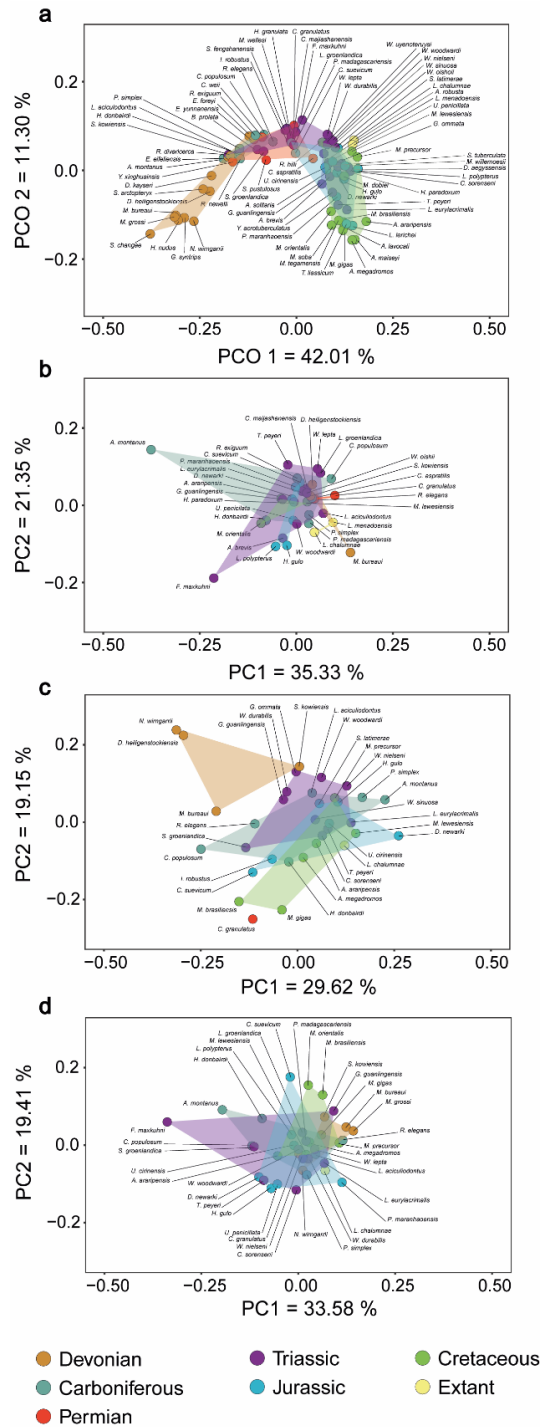
Supplementary Figure 8. Coelacanth morphological disparity. (**A**) Principal coordinates analysis (PCo) applied to 268 discrete characters (i.e., the phylogenetic matrix) (*n* = 82 species); (**B**) principal component analysis (PCA) using 2-D geometric morphometrics of body shape (*n* = 35 species); (**C**) cheek shape (*n* = 34 species); and (**D**) lower jaw shape of coelacanths (*n* = 38 species). *Latimeria* remains near its closest, Mesozoic relatives for discrete characters (**A**) and cheek shape (**C**) but is quite distantly separated from Mesozoic forms for overall body shape (**B**) and lower jaw shape (**D**). The percentage of variation is provided for each axis.
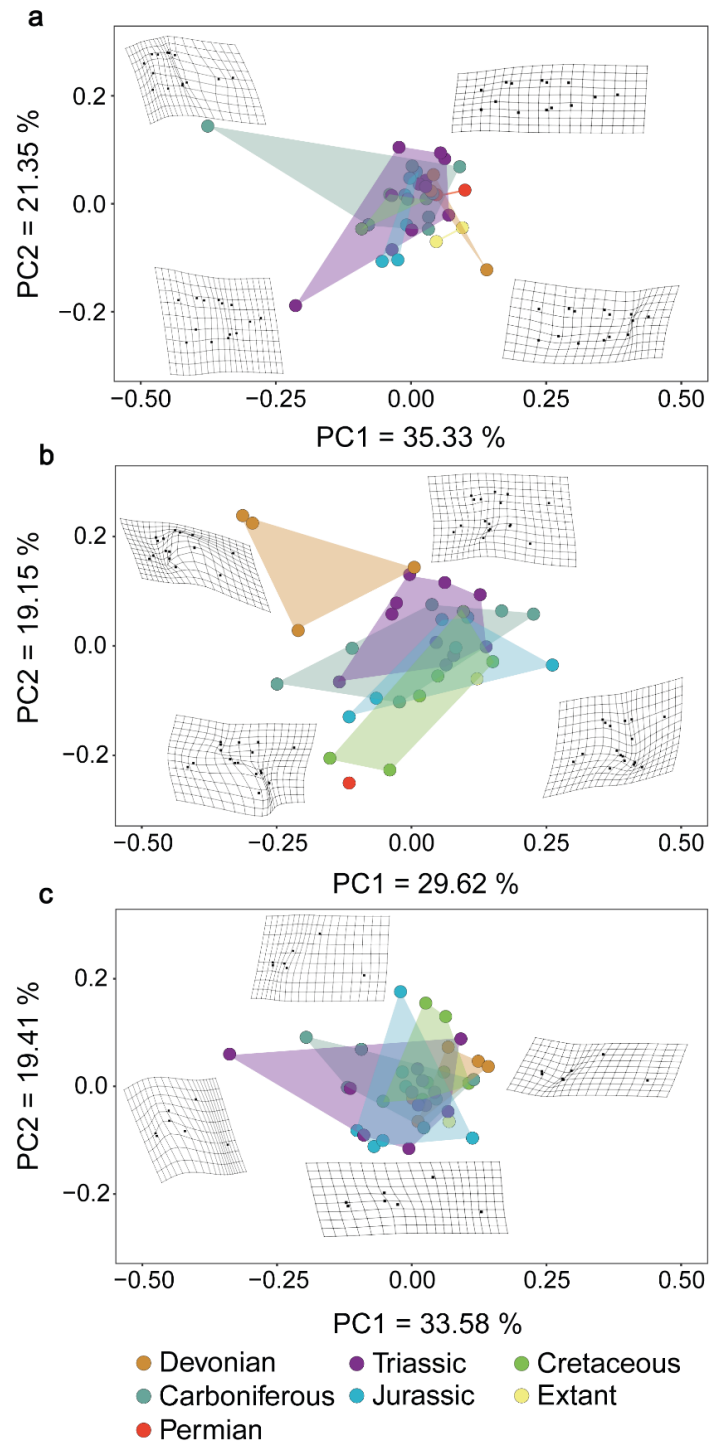
Supplementary Figure 9. **Coelacanth morphological disparity warp grids.** (**A**) based on 2-D geometric morphometrics of body shape (*n* = 35 species); (**B**) cheek shape (*n* = 34 species); (**C**) lower jaw shape of coelacanths (*n* = 38 species). The anterior of the fish is to the left for all grids. See Supplementary Figure 7 for the position of the landmarks and Supplementary Table 2 for the description of the landmarks. The percentage of variation is provided for each axis.
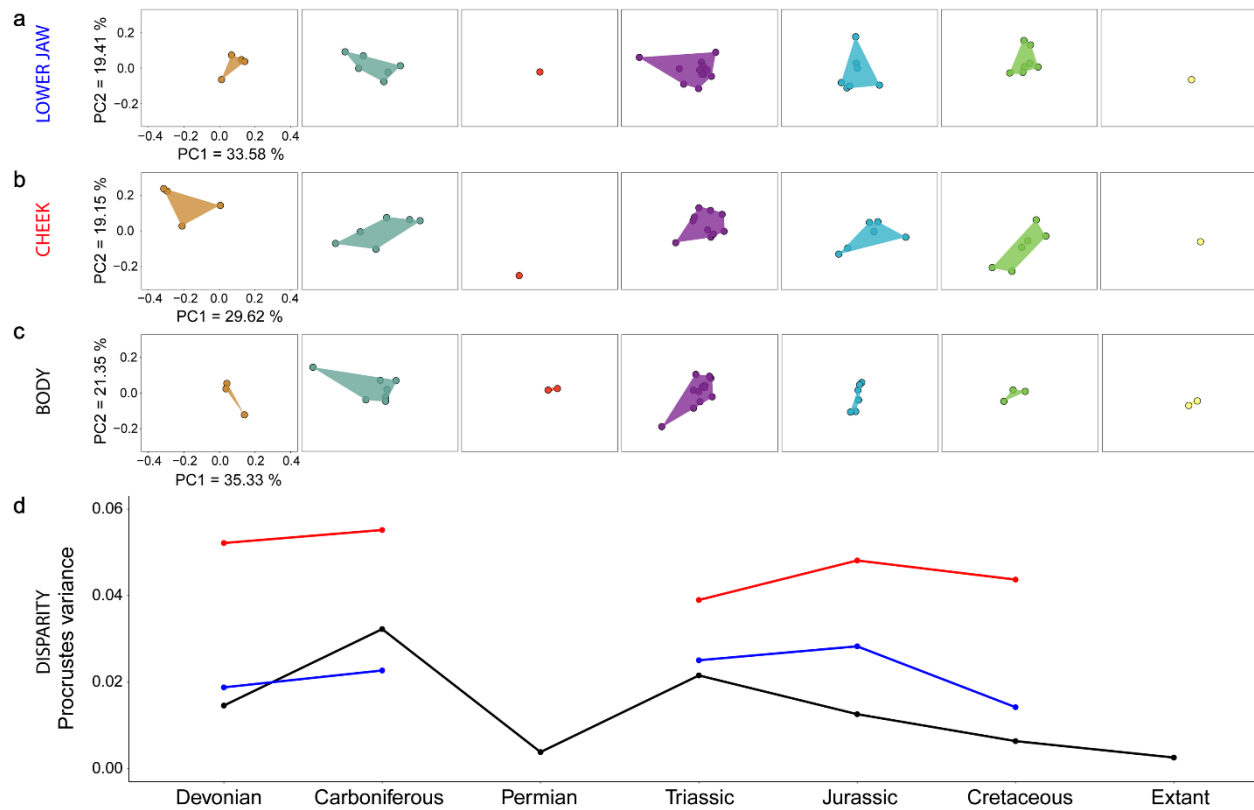
Supplementary Figure 10. **Morphospaces and Procrustes variance for coelacanth disparity per time bin.** (**A-C**) Principal component 1 *versus* principal component 2 per time bin based on 2-D geometric morphometrics (all graphics using the same scale): (**A**) lower jaw; (**B**) cheek; (**C**) body shape. (**D**) Procrustes variance for each time bin as a measure of disparity for cheek (red line), lower jaw (blue line), and body shape (black line). Time bins without Procrustes variance values (Permian and Extant) correspond to periods for which a variance could not be calculated. The percentage of variation is provided for each axis.

Supplementary Figure 11. **Cheek and lower jaw silhouettes of coelacanths.** Species are listed in alphabetical order and scaled to the same width (except *Allenypterus montanus*). Cheek region silhouettes include solely the bones surrounding the orbit, covering the cheek region as such and the opercular series. *Allenypterus montanus* (based on Forey (1998, fig. 4.6)[12]), *Axelrodichthys araripensis* (based on Maisey (1986, fig. 26A)[18]), *Chinlea sorenseni* (based on Schaeffer (1967, fig. 14)[30]), *Coelacanthus granulatus* (based on Schaumberg (1978, fig. 6)[34]), *Diplurus newarki* (based on Forey (1998, fig. 4.16A)[12]), *Foreyia maxkuhni* (based on Cavin et al. (2017, fig. S6)[41]), *Holophagus gulo* (based on Forey (1998, fig. 11.18)[12]), *Latimeria chalumnae* (based on Forey (1998, fig. 2.5B)[12]), *Mawsonia gigas* (based on Toriño et al. (2021, fig. 3B)[170]), *Miguashaia bureaui* (based on Cloutier (1996, fig. 5)[61] and new observation (RC)), *Ngamugawi wirngarri* (this study), and *Rhabdoderma elegans* (based on Forey (1998, fig. 4.8; 1981, text-fig. 6)[12]). Lower jaw silhouettes exclude the lateral gular and articular region. *Allenypterus montanus* (based on Forey (1998, fig. 4.6)[12]), *Axelrodichthys araripensis* (based on Forey (1998, fig. 5.10)[12]), *Chinlea sorenseni* (based on Schaeffer (1967, fig. 14)[30]), *Coelacanthus granulatus* (based on Schaumberg (1978, fig. 6)[34]), *Diplurus newarki* (based on Forey (1998, fig. 4.16)[12]), *Foreyia maxkuhni* (based on Cavin et al. (2017, fig. S6)[41]), *Holophagus gulo* (based on Forey (1998, fig. 11.18)[12]), *Latimeria chalumnae* (based on Forey (1998, fig.

5.1)[12]), *Miguashaia grossi* (based on Forey et al. (2000, fig. 3)[63]), *Ngamugawi wirngarri* (this study), *Rhabdoderma elegans* (based on Forey (1998, fig. 5.3C)[12]), and *Styloichthys changae* (based on Friedman (2007, fig. 5A)[98]).

Supplementary References

1. Renesto, S. & Stockar, R. First record of a coelacanth fish from the Middle Triassic Meride Limestone of Monte San Giorgio (Canton Ticino, Switzerland). *Rivista Italiana di Paleontologia e Stratigrafia* **124**, 639-653, doi:10.13130/2039-4942/10771 (2018).

2. Brownstein, C. D. & Bissell, I. C. Species delimitation and coexistence in an ancient, depauperate vertebrate clade. *BMC Ecology and Evolution* **22**, e90, doi:10.1186/s12862-022-02043-4 (2022).

3. Cohen, K. M., Finney, S. C., Gibbard, P. L. & Fan, J.-X. The ICS international chronostratigraphic chart. *Episodes* **36**, 199-204 ((2013; updated 2022 version 02)).

4. Andrews, S. M., Long, J., Ahlberg, P., Barwick, R. & Campbell, K. The structure of the sarcopterygian *Onychodus jandemarrai* n. sp. from Gogo, Western Australia: With a functional interpretation of the skeleton. *Transactions of the Royal Society of Edinburgh-Earth Sciences* **96**, 197-307 (2006).

5. Jessen, H. Weitere Fischreste aus dem Oberen Plattenkalk der Bergisch-Gladbach-Paffrather Mulde (Oberdevon, Rheinisches Schiefergebirge). *Palaeontographica A* **143**, 159-187 (1973).

6. Schultze, H.-P. & Cloutier, R. in *Devonian Fishes and Plants of Miguasha, Quebec, Canada* (eds H.-P. Schultze & R. Cloutier) 348-368 (Verlag Dr. Friedrich Pfeil, 1996).

7. Jessen, H. Die Crossopterygier des Oberen Plattenkalkes (Devon) der Bergisch-Gladbach-Paffrather Mulde (Rheinisches Schiefergebirge) unter Berücksichtigung von amerikanischem und europäischem *Onychodus*-Material. *Arkiv för Zoologi* **18**, 306-389 (1966).

8. Lu, J. & Zhu, M. An onychodont fish (Osteichthyes, Sarcopterygii) from the Early Devonian of China, and the evolution of the Onychodontiformes. *Proceedings of the Royal Society B-Biological Sciences* **277**, 293-299, doi:10.1098/rspb.2009.0708 (2009).

9. Schultze, H.-P. Crossopterygier mit heterozerker Schwanzflosse aus dem Oberdevon Kanadas, nebst einer Beschreibung von Onychodontida-Resten aus dem Mitteldevon Spaniens und aus dem Karbon der USA. *Palaeontographica Abt. A* **143**, 188-208 (1973).

10. Beltan, L. L. La faune ichthyologique du Muschelkalk de la Catalogne. *Memorias de la Real Academia de Ciencias y Artes de Barcelona* **41**, 281-323 (1972).

11. Beltan, L. Quelques poissons du Muschelkalk supérieur d'Espagne. *Acta Geológica Hispánica* **19**, 117-127 (1984).

12. Forey, P. L. *History of the Coelacanth Fishes*. (Chapman & Hall, 1998).

13. Lund, R. & Lund, W. L. Coelacanths from the Bear Gulch Limestone (Namurian) of Montana and the evolution of the Coelacanthiformes. *Bulletin of Carnegie Museum of Natural History* **25**, 1-74 (1985).

14. Toriño, P., Soto, M. & Perea, D. A comprehensive phylogenetic analysis of coelacanth fishes (Sarcopterygii, Actinistia) with comments on the composition of the Mawsoniidae and Latimeriidae: Evaluating old and new methodological challenges and constraints. *Historical Biology* **33**, 3423-3443, doi:10.1080/08912963.2020.1867982 (2021).

15. Arratia, G. & Schultze, H. P. A new fossil actinistian from the Early Jurassic of Chile and its bearing on the phylogeny of Actinistia. *Journal of Vertebrate Paleontology* **35**, e983524, doi:10.1080/02724634.2015.983524 (2015).

16. Stensiö, E. A. *Triassic fishes from Spitzbergen. Part I. A*. (Holzhausen, 1921).

17. Mørk, A. *et al.* The type section of the Vikinghøgda Formation: a new Lower Triassic unit in central and eastern Svalbard. *Polar Research* **18**, 51-82, doi:10.1111/j.1751-8369.1999.tb00277.x (1999).

18   Maisey, J. G. Coelacanths from the Lower Cretaceous of Brazil. *American Museum Novitates*, 1-30 (1986).

19   Arai, M. & Assine, M. L. Chronostratigraphic constraints and paleoenvironmental interpretation of the Romualdo Formation (Santana Group, Araripe Basin, Northeastern Brazil) based on palynology. *Cretaceous Research* **116**, e104610, doi:10.1016/j.cretres.2020.104610 (2020).

20   Yabumoto, Y. & Uyeno, T. New materials of the Cretaceous coelacanth, *Mawsonia lavocati* Tabaste from Morocco. *Bulletin of the National Science Museum, Tokyo, Series C: Geology & Paleontology* **31**, 39-49 (2005).

21   Tabaste, N. Étude de restes de poissons du Crétacé saharien. *Mémoires de l'Institut français d'Afrique Noire* **68**, 437-485 (1963).

22   Ibrahim, N. *et al.* Geology and paleontology of the Upper Cretaceous Kem Kem Group of eastern Morocco. *Zookeys*, 1-216, doi:10.3897/zookeys.928.47517 (2020).

23   de Carvalho, M. S. S., Gallo, V. & Santos, H. R. S. New species of coelacanth fish from the Lower Cretaceous (Albian) of the Grajau Basin, NE Brazil. *Cretaceous Research* **46**, 80-89, doi:10.1016/j.cretres.2013.09.006 (2013).

24   Cavin, L., Valentin, X. & Garcia, G. A new mawsoniid coelacanth (Actinistia) from the Upper Cretaceous of Southern France. *Cretaceous Research* **62**, 65-73, doi:10.1016/j.cretres.2016.02.002 (2016).

25   Wendruff, A. J. & Wilson, M. V. H. New Early Triassic coelacanth in the family Laugiidae (Sarcopterygii: Actinistia) from the Sulphur Mountain Formation near Wapiti Lake, British Columbia, Canada. *Canadian Journal of Earth Sciences* **50**, 904-910, doi:10.1139/cjes-2013-0010 (2013).

26   Wang, N. & Liu, H. Coelacanth fishes from the marine Permian of Zhejiang, South China. *Vertebrata PalAsiatica* **10**, 305-312 (1981).

27   Shen, S. Z. *et al.* Permian integrative stratigraphy and timescale of China. *Science China-Earth Sciences* **62**, 154-188, doi:10.1007/s11430-017-9228-4 (2019).

28   Jin, X. S. New species of coelacanth from Changxing Formation of Zhejiang. *Bulletin of Science and Technology* **13**, 143-147 (1997).

29   Tong, J. N., Zhou, X. J., Erwin, D. H., Zuo, J. X. & Zhao, L. S. Fossil fishes from the Lower Triassic of Majiashan, Chaohu, Anhui Province, China. *Journal of Paleontology* **80**, 146-161, doi:10.1666/0022-3360(2006)080[0146:Ffftlt]2.0.Co;2 (2006).

30   Schaeffer, B. Late Triassic fishes from the Western United States. *Bulletin of the American Museum of Natural History* **135**, 1-18 (1967).

31   Lambers, P. H. *On the ichthyofauna of the Solnhofen lithographic limestone (Upper Jurassic, Germany)* Ph.D. thesis, Rijkuniversiteit Groningen, (1992).

32   Dietl, G. & Schweigert, G. The Nusplingen lithographic limestone - A "fossil lagerstaette" of Late Kimmeridgian age from the Swabian Alb (Germany). *Rivista Italiana di Paleontologia E Stratigrafia* **110**, 303-309 (2004).

33   Schmid, D. U., Leinfelder, R. R. & Schweigert, G. Stratigraphy and palaeoenvironments of the Upper Jurassic of Southern Germany–a review. *Zitteliana* **B 26**, 31-41 (2005).

34   Schaumberg, G. Neubeschreibung von *Coelacanthus granulatus* Agassiz (Actinistia, Pisces) aus dem Kupferschiefer von Richelsdorf (Perm, W.-Deutschland). *Paläontologische Zeitschrift* **52**, 169-197 (1978).

35   Schaeffer, B. The Triassic coelacanth fish *Diplurus*, with observations on the evolution of the Coelacanthini. *Bulletin of the American Museum of Natural History* **99**, 29-78 (1952).

36   Kent, D. V., Olsen, P. E. & Muttoni, G. Astrochronostratigraphic polarity time scale (APTS) for the Late Triassic and Early Jurassic from continental sediments and correlation with standard marine stages. *Earth-Science Reviews* **166**, 153-180 (2017).

37   Cavin, L. & Grădinaru, E. *Dobrogeria aegyssensis*, a new early Spathian (Early Triassic) coelacanth from North Dobrogea (Romania). *Acta Geologica Polonica* **64**, 161-187, doi:10.2478/agp-2014-0010 (2014).

38   Johanson, Z., Long, J. A., Talent, J. A., Janvier, P. & Warren, J. W. Oldest coelacanth, from the Early Devonian of Australia. *Biology Letters* **2**, 443-446, doi:10.1098/rsbl.2006.0470 (2006).

39   Gross, W. Die paläontologische und stratigraphische Bedeutung der Wirbeltierfaunen des Old Reds und der marinen altpaläozoischen Schichten. *Abhandlungen der deutschen Akademie der Wissenschaften zu Berlin, Mathematisch-Naturwissenschaftliche Klasse* **1949**, 1-130 (1950).

40   Zhu, M. *et al.* Earliest known coelacanth skull extends the range of anatomically modern coelacanths to the Early Devonian. *Nature Communications* **3**, ncomms1764, doi:10.1038/ncomms1764 (2012).

41   Cavin, L., Mennecart, B., Obrist, C., Costeur, L. & Furrer, H. Heterochronic evolution explains novel body shape in a Triassic coelacanth from Switzerland. *Scientific Reports* **7**, e13695, doi:10.1038/s41598-017-13796-0 (2017).

42   Hagdorn, H. & Mutter, R. J. The vertebrate fauna of the Lower Keuper Albertibank (Erfurt Formation, Middle Triassic) in the vicinity of Schwäbisch Hall (Baden-Württemberg, Germany). *Palaeodiversity* **4**, 223-243 (2011).

43   Martin, M. & Wenz, S. Découverte d'un nouveau Coelacanthidé, *Garnbergia ommata* n.g., n.sp., dans le Muschelkalk supérieur du Baden-Württemberg. *Stuttgarter Beiträge zur Naturkunde, Serie B (Geologie und Paläontologie)* **105**, 1-17 (1984).

44   Long, J. A. A new genus of fossil coelacanth (Osteichthyes: Coelacanthiformes) from the Middle Devonian of southeastern Australia. *Records of the Western Australian Museum, Supplement*, 37-53 (1999).

45   Geng, B.-H., Zhu, M. & Jin, F. A revision and phylogenetic analysis of *Guizhoucoelacanthus* (Sarcopterygii, Actinistia) from the Triassic of China. *Vertebrata PalAsiatica* **47**, 165-177 (2009).

46   Schweizer, R. Ein Coelacanthide aus dem Oberen Muschelkalk Göttingens. *Neues Jahrbuch für Geologie und Paläontologie, Abhandlungen* **125**, 216-226 (1966).

47   Friedman, M. & Coates, M. I. A newly recognized fossil coelacanth highlights the early morphological diversification of the clade. *Proceedings of the Royal Society B-Biological Sciences* **273**, 245-250, doi:10.1098/rspb.2005.3316 (2006).

48   Hartkopf-Fröder, C., Jux, U., Knapp, G. & Piecha, M. The Late Devonian of the Bergisch Gladbach-Paffrath Syncline (Ardennes-Rhenish Massif, Germany): An overview. *Courier Forschungsinstitut Senckenberg* **251**, 7-18 (2004).

49   Jain, S. L. *Indocoelacanthus robustus* n. gen., n. sp. (Coelacanthidae, Lower Jurassic), the first fossil coelacanth from India. *Journal of Paleontology* **48**, 49-62 (1974).

50   Gradstein, F. M. *et al.* in *Geochronology, Time Scales and Global Stratigraphic Correlation* (eds W. A. Berggren, D. V. Kent, M.-P. Aubry, & J. Hardenbol) 95-128 (SEPM Special Publication, 1995).

51   Kadarusman *et al.* A thirteen-million-year divergence between two lineages of Indonesian coelacanths. *Scientific Reports* **10**, e192, doi:10.1038/s41598-019-57042-1 (2020).

52   Nielsen, E. Some few preliminary remarks on Triassic fishes from East Greenland. *Meddelelser om Grønland* **112**, 1-55 (1936).

53   Surlyk, F., Bjerager, M., Piasecki, S. & Stemmerik, L. Stratigraphy of the marine Lower Triassic succession at Kap Stosch, Hold with Hope, North- East Greenland. *Bulletin of the Geological Society of Denmark* **65**, 87-123 (2017).

54   Wen, W. *et al.* Coelacanths from the Middle Triassic Luoping Biota, Yunnan, South China, with the earliest evidence of ovoviviparity. *Acta Palaeontologica Polonica* **58**, 175-193, doi:10.4202/app.2011.0066 (2013).

55   Yabumoto, Y. A new coelacanth from the Early Cretaceous of Brazil (Sarcopterygii, Actinistia). *Paleontological Research* **6**, 343-350 (2002).

56 Brito, P. M. *et al.* First occurrence of a mawsoniid (Sarcopterygii: Actinistia), *Mawsonia soba* sp nov., in pre-Aptian Cretaceous deposits from Cameroon. *Cretaceous Research* **86**, 91-96, doi:10.1016/j.cretres.2017.12.014 (2018).

57 Wenz, S. in *Colloques Internationaux du Centre National de la Recherche Scientifique* Vol. 218 175-190 (Centre National de la Recherche Scientifique, 1975).

58 Taquet, P. Géologie et paléontologie du gisement de Gadoufaoua (Aptien du Niger). *Cahiers de paléontologie*, 1-191 (1976).

59 Schwimmer, D. R., Stewart, J. D. & Williams, G. D. Giant fossil coelacanths of the Late Cretaceous in the eastern United-States. *Geology* **22**, 503-506, doi:10.1130/0091-7613(1994)022<0503:Gfcotl>2.3.Co;2 (1994).

60 Dutel, H. *et al.* The giant Cretaceous coelacanth (Actinistia, Sarcopterygii) *Megalocoelacanthus dobiei* Schwimmer, Stewart & Williams, 1994, and its bearing on Latimerioidei interrelationships. *PLoS One* **7**, e49911, doi:10.1371/journal.pone.0049911 (2012).

61 Cloutier, R. in *Devonian Fishes and Plants of Miguasha, Quebec, Canada* (eds H.-P. Schultze & R. Cloutier) 227-247 (Verlag Dr. Friedrich Pfeil, 1996).

62 Cloutier, R., Loboziak, S., Candilier, A.-M. & Blieck, A. Biostratigraphy of the Upper Devonian Escuminac Formation, eastern Quebec, Canada: A comparative study based on miospores and fishes. *Review of Palaeobotany and Palynology* **93**, 191-215 (1996).

63 Forey, P. L., Ahlberg, P. E., Luksevics, E. & Zupins, I. A new coelacanth from the Middle Devonian of Latvia. *Journal of Vertebrate Paleontology* **20**, 243-252 (2000).

64 Heckert, A. B., Lucas, S. G. & Hunt, A. P. in *Vertebrate Paleontology in Arizona* Vol. 29 (eds A. B. Heckert & S. G. Lucas) 16-44 (New Mexico Museum of Natural History and Science Bulletin, 2005).

65 Long, J. A. & Trinajstic, K. A review of recent discoveries of exceptionally preserved fossil fishes from the Gogo sites (Late Devonian, Western Australia). *Earth and Environmental Science Transactions of the Royal Society of Edinburgh* **108**, 111-117 (2018).

66 Yabumoto, Y. A new Mesozoic coelacanth from Brazil (Sarcopterygii, Actinistia). *Paleontological Research* **12**, 329-343 (2008).

67 Montefeltro, F. C., Larsson, H. C. E., de Franca, M. A. G. & Langer, M. C. A new neosuchian with Asian affinities from the Jurassic of northeastern Brazil. *Naturwissenschaften* **100**, 835-841, doi:10.1007/s00114-013-1083-9 (2013).

68 Clément, G. The actinistian (Sarcopterygii) *Piveteauia madagascariensis* Lehman from the Lower Triassic of northwestern Madagascar: A redescription on the basis of new material. *Journal of Vertebrate Paleontology* **19**, 234-242 (1999).

69 Nowak, H., Schneebeli-Hermann, E. & Kustatscher, E. Correlation of Lopingian to Middle Triassic Palynozones. *Journal of Earth Science* **29**, 755-777, doi:10.1007/s12583-018-0790-8 (2018).

70 Wendruff, A. J. & Wilson, M. V. H. A fork-tailed coelacanth, *Rebellatrix divaricerca*, gen. et sp. nov. (Actinistia, Rebellatricidae, fam. nov.), from the Lower Triassic of western Canada. *Journal of Vertebrate Paleontology* **32**, 499-511, doi:10.1080/02724634.2012.657317 (2012).

71 Graf, J. A new Early Cretaceous coelacanth from Texas. *Historical Biology* **24**, 441-452, doi:10.1080/08912963.2012.696636 (2012).

72 Cloutier, R. & Candilier, A.-M. Palaeozoic vertebrates of northern France and Belgium: Part III - Sarcopterygii (Devonian to Carboniferous). *Geobios, mémoire spécial* **19**, 335-342 (1995).

73 Menning, M., Weyer, D., Drozdzewski, G., van Amerom, H. W. & Wendt, I. in *Karbon: Zeitskala und Sequenzstratigraphie* Vol. 156 (eds M. Menning *et al.*) 3-44 (Geologisches Jahrbuch Reihe A, 2000).

74 Clements, T., Purnell, M. & Gabbott, S. The Mazon Creek Lagerstatte: A diverse Late Paleozoic ecosystem entombed within siderite concretions. *Journal of the Geological Society* **176**, 1-11, doi:10.1144/jgs2018-088 (2019).

75   Echols, J. A new genus of Pennsylvanian fish (Crossopterygii, Coelacanthiformes) from Kansas. *University of Kansas Publications. Museum of Natural History, Lawrence* **12**, 475-501 (1963).

76   Schultze, H.-P. Terrestrial biota in coastal marine deposits: Fossil-Lagerstatten in the Pennsylvanian of Kansas, USA. *Palaeogeography Palaeoclimatology Palaeoecology* **119**, 255-273, doi:10.1016/0031-0182(95)00011-9 (1996).

77   Mork, A. *et al.* The type section of the Vikinghogda Formation: a new Lower Triassic unit in central and eastern Svalbard. *Polar Research* **18**, 51-82, doi:10.1111/j.1751-8369.1999.tb00277.x (1999).

78   Gess, R. W. & Coates, M. I. Fossil juvenile coelacanths from the Devonian of South Africa shed light on the order of character acquisition in actinistians. *Zoological Journal of the Linnean Society* **175**, 360-383, doi:10.1111/zoj.12276 (2015).

79   Friedman, M., Coates, M. I. & Anderson, P. First discovery of a primitive coelacanth fin fills a major gap in the evolution of lobed fins and limbs. *Evolution & Development* **9**, 329-337 (2007).

80   Liu, H.-T. A new coelacanth from the marine Lower Triassic of N.W. Kwangsi, China. *Vertebrata Palasiatica* **8**, 211-214 (1964).

81   Tong, J. & Yin, H. The Lower Triassic of South China. *Journal of Asian Earth Sciences* **20**, 803-815 (2002).

82   Galfetti, T. *et al.* Evolution of Early Triassic outer platform paleoenvironments in the Nanpanjiang Basin (South China) and their significance for the biotic recovery. *Sedimentary Geology* **204**, 36-60, doi:10.1016/j.sedgeo.2007.12.008 (2008).

83   Lucas, S. G. Global Permian tetrapod biostratigraphy and biochronology. *Geological Society, London, Special Publications* **265**, 65-93 (2006).

84   Zhu, M. & Yu, X. B. A primitive fish close to the common ancestor of tetrapods and lungfish. *Nature* **418**, 767-770 (2002).

85   Zhao, W.-J. & Zhu, M. Siluro-Devonian vertebrate biostratigraphy and biogeography of China. *Palaeoworld* **19**, 4–26 (2010).

86   Clément, G. A new coelacanth (Actinistia, Sarcopterygii) from the Jurassic of France, and the question of the closest relative fossil to Latimeria. *Journal of Vertebrate Paleontology* **25**, 481-491 (2005).

87   Cavin, L., Furrer, H. & Obrist, C. New coelacanth material from the Middle Triassic of eastern Switzerland, and comments on the taxic diversity of actinistans. *Swiss Journal of Geosciences* **106**, 161-177, doi:10.1007/s00015-013-0143-7 (2013).

88   Dutel, H., Herbin, M. & Clément, G. First occurrence of a mawsoniid coelacanth in the Early Jurassic of Europe. *Journal of Vertebrate Paleontology* **35**, e929581-929582, doi:10.1080/02724634.2014.929581 (2015).

89   Dutel, H., Pennetier, E. & Pennetier, G. A giant marine coelacanth from the Jurassic of Normandy, France. *Journal of Vertebrate Paleontology* **34**, 1239-1242, doi:10.1080/02724634.2014.838176 (2014).

90   Bernier, P. *et al.* The lithographic limestones of Cerin (southern Jura Mountains, France). A synthetic approach and environmental interpretation. *Comptes Rendus Palevol* **13**, 383-402, doi:10.1016/j.crpv.2014.01.006 (2014).

91   Wendruff, A. J. *Lower Triassic Coelacanths of the Sulphur Mountain Formation (Wapiti Lake) in British Columbia, Canada* M.Sc. thesis thesis, University of Alberta, (2011).

92   Yabumoto, Y. & Brito, P. M. A new Triassic coelacanth, *Whiteia oishii* (Sarcopterygii, Actinistia) from West Timor, Indonesia. *Paleontological Research* **20**, 233-246 (2016).

93   Wescott, W. A. & Diggens, J. N. Depositional history and stratigraphical evolution of the Sakamena Group (Middle Karoo Supergroup) in the southern Morondava Basin, Madagascar. *Journal of African Earth Sciences* **27**, 461-479, doi:10.1016/s0899-5362(98)00073-6 (1998).

94   Simões, T. R., Caldwell, M. W., Palci, A. & Nydam, R. L. Giant taxon-character matrices: Quality of character constructions remains critical regardless of size. *Cladistics* **33** 198-219 (2017).

95   Cloutier, R. in *Early Vertebrates and Related Problems of Evolutionary Biology* (eds M.-M. Chang, Y.-H. Liu, & G.-R. Zhang) 379–428 (Science Press, 1991).

96   Cloutier, R. Patterns, trends, and rates of evolution within the Actinistia. *Environmental Biology of Fishes* **32**, 23-58 (1991).

97   Forey, P. L. *Latimeria chalumnae* and its pedigree. *Environmental Biology of Fishes* **32**, 75-97 (1991).

98   Friedman, M. *Styloichthys* as the oldest coelacanth: Implications for early osteichthyan interrelationships. *Journal of Systematic Palaeontology* **5**, 289-343 (2007).

99   Dutel, H., Herbin, M. & Clement, G. First occurrence of a mawsoniid coelacanth in the Early Jurassic of Europe. *Journal of Vertebrate Paleontology* **35**, doi:10.1080/02724634.2014.929581 (2015).

100   Cavin, L. *et al.* Phylogeny and evolutionary history of mawsoniid coelacanths. *Bulletin of the Kitakyushu Museum of Natural History and Human History, Series A (Natural History)* **17**, 3-13 (2019).

101   Cavin, L. *et al.* The last known freshwater coelacanths: New Late Cretaceous mawsoniid remains (Osteichthyes: Actinistia) from Southern France. *PLoS One* **15**, e0234183, doi:10.1371/journal.pone.0234183 (2020).

102   O'Leary, M. A. & Kaufman, S. MorphoBank: phylophenomics in the "cloud". *Cladistics* **27**, 529-537 (2011).

103   Forey, P. L. *Latimeria*: A paradoxical fish. *Proceedings of the Royal Society B-Biological Sciences* **208**, 369-384 (1980).

104   Fragoso, L. G. C., Brito, P. & Yabumoto, Y. *Axelrodichthys araripensis* Maisey, 1986 revisited. *Historical Biology* **31**, 1350-1372, doi:10.1080/08912963.2018.1454443 (2018).

105   Forey, P. L. The coelacanth *Rhabdoderma* in the Carboniferous of the British Isles. *Palaeontology* **24**, 203-229 (1981).

106   Zhu, M. & Yu, X. B. in *Recent Advances in the Origin and Early Radiation of Vertebrates* (eds G. Arratia, M. V. H. Wilson, & R. Cloutier) 271-286 (Verlag Dr. Friedrich Pfeil, 2004).

107   Khonsari, R. H. *et al.* The buccohypophyseal canal is an ancestral vertebrate trait maintained by modulation in sonic hedgehog signaling. *BMC Biology* **11**, e27, doi:10.1186/1741-7007-11-27 (2013).

108   Fragoso, L. G. C. *Revisão do ramo gondwánico da familia Mawsoniidae (Sarcopterygii, Actinistia, Coelacanthiformes)* Ph.D. thesis, Universidade do Estado de Rio de Janeiro, (2014).

109   Clack, J. A. Earliest known tetrapod braincase and the evolution of the stapes and febestra ovalis. *Nature* **369**, 392-394, doi:10.1038/369392a0 (1994).

110   Romano, C., Ware, D., Brühwiler, T., Bucher, H. & Brinkmann, W. Marine Early Triassic Osteichthyes from Spiti, Indian Himalayas. *Swiss Journal of Palaeontology* **135**, 275-294 (2016).

111   Schaeffer, B. A revision of *Coelacanthus newarki* and notes on the evolution of the girdles and basal plates of the median fins in the Coelacanthini. *American Museum Novitates*, 1-17 (1941).

112   Arratia, G., Schultze, H.-P. & Casciotta, J. Vertebral column and associated elements in dipnoans and comparison with other fishes: Development and homology. *Journal of Morphology* **250**, 101-172 (2001).

113   Mondéjar-Fernández, J., Meunier, F. J., Cloutier, R., Clément, G. & Laurin, M. A microanatomical and histological study of the scales of the Devonian sarcopterygian *Miguashaia bureaui* and the evolution of the squamation in coelacanths. *Journal of Anatomy* **239**, 451-478, doi:10.1111/joa.13428 (2021).

114   Brito, P. M., Meunier, F. J., Clément, G. & Geffard-Kuriyama, D. The histological structure of the calcified lung of the fossil coelacanth *Axelrodichthys araripensis* (Actinistia: Mawsoniidae). *Palaeontology* **53**, 1281-1290, doi:10.1111/j.1475-4983.2010.01015.x (2010).

115   Cupello, C. *et al.* The homology and function of the lung plates in extant and fossil coelacanths. *Scientific Reports* **7**, e9244, doi:10.1038/s41598-017-09327-6 (2017).

116   Schultze, H.-P. & Cloutier, R. Computed-tomography and magnetic-resonance-imaging studies of *Latimeria chalumnae*. *Environmental Biology of Fishes* **32**, 159-181 (1991).

117   Schindelin, J. *et al.* Fiji: an open-source platform for biological-image analysis. *Nature Methods* **9**, 676-682, doi:10.1038/nmeth.2019 (2012).

118   Mondéjar-Fernández, J. A new onychodont (Osteichthyes; Sarcopterygii) from the Middle Devonian of Morocco and its bearing on early osteichthyan evolution. *Journal of Systematic Palaeontology* **18**, 573-606, doi:10.1080/14772019.2019.1655495 (2019).

119   Long, J. A. On the relationships of *Psarolepis* and the onychodontiform fishes. *Journal of Vertebrate Paleontology* **21**, 815-820 (2001).

120   Lu, J. *et al.* A Devonian predatory fish provides insights into the early evolution of modern sarcopterygians. *Science Advances* **2**, e1600154, doi:10.1126/sciadv.1600154 (2016).

121   Gross, W. Über Crossopterygier und Dipnoer aus dem baltischen Oberdevon im Zusammenhang einer vergleichenden untersuchung des Porenkanal-systems paläozoischer Agnathen und Fische. *Kungliga Svenska Vetenskapsakademiens Handlingar, serie 4* **5**, 1-140 (1956).

122   Upeniece, I. New species of *Strunius* (Sarcopterygii, Onychodontida) from Latvia, Lode quarry (Upper Devonian). *Geobios, Mémoire Spécial* **19**, 281-284 (1995).

123   Maisey, J. G. *Santana Fossils: An Illustrated Atlas*. 459 (T.F.H. Publications, 1991).

124   Barbosa, R. E. S., da Silva, M. C., Duque, R. R. C. & Barreto, A. M. F. Os Mawsoniídeos das bacias sedimentares do nordest do Brasil: Revisão bibliográfica. *Estudos Geológicos* **29**, 94-119 (2019).

125   Brito, P. M. & Yabumoto, Y. An updated review of the fish faunas from the Crato and Santana formations in Brazil, a close relationship to the Tethys fauna. *Bulletin of the Kitakyushu Museum of Natural History and Human History, Series A (Natural History)* **9**, 107-136 (2011).

126   Cavin, L. & Forey, P. L. in *Mesozoic Fishes 3 - Systematics, Paleoenvironments and Biodiversity* (eds G. Arratia & A. Tintori) 493-506 (Verlag Dr. Friedrich Pfeil, 2004).

127   Benton, M. J. *et al.* Exceptional vertebrate biotas from the Triassic of China, and the expansion of marine ecosystems after the Permo-Triassic mass extinction. *Earth-Science Reviews* **125**, 199-243, doi:10.1016/j.earscirev.2013.05.014 (2013).

128   Elliott, D. K. A new specimen of *Chinlea sorenseni* from the Chinle Formation, Dolores River, Colorado. *Journal of the Arizona-Nevada Academy of Science* **22**, 47-52 (1987).

129   Martz, J., Kirkland, J., Milner, A., Parker, W. & Santucci, V. Upper Triassic lithostratigraphy, depositional systems, and vertebrate paleontology across southern Utah. *Geology of the Intermountain West* **4**, 99-180 (2017).

130   Lambers, P. H. The identity of the type specimen of *Coelacanthus harlemensis* WINKLER (Pisces, Actinistia) from the lithographic limestone of Solnhofen (Tithonian), Bavaria. *Paläontologische Zeitschrift* **65**, 173-189 (1991).

131   Moy-Thomas, J. A. & Westoll, T. S. On the Permian coelacanth, *Coelacanthus granulatus,* Ag. *Geological Magazine* **72**, 446-457 (1935).

132   Brandt, S. Über isolierte Knochenfunde von Quastenflossern aus dem Ober-Perm von Thüringen und Hessen - Ein Beitrag zur Anatomie von *Coelacanthus granulatus* AGASSIZ. *Veröffentlichungen Naturhistorisches Museum Schloss Bertholdsburg Schleusingen* **22**, 69-78 (2007).

133   Stensiö, E. A. Über zwei Coelacanthiden aus dem Oberdevon von Wildungen. *Paläontologische Zeitschrift* **4**, 167-210 (1922).

134   Stensiö, E. A. On the Devonian coelacanthids of Germany with special reference to the dermal skeleton. *Kungliga Svenska vetenskapsakademiens handlingar* **16**, 1-56 (1937).

135   Szrek, P. Coelacanths (Actinistia, Sarcopterygii) from the Famennian (Upper Devonian) of the Holy Cross Mountains, Poland. *Acta Geologica Polonica* **57**, 403-413 (2007).

136   Bryant, W. L. New fishes from the Triassic of Pennsylvania. *Proceedings of the American Philosophical Society* **73**, 319-326 (1934).

137   Jaekel, O. Der Kopf der Wirbeltiere. *Ergebnisse der Anatomie und Entwickelungsgeschichte* **27**, 815-897 (1927).

138   Long, J. A. Cranial anatomy of two new Late Devonian lungfishes (Pisces: Dipnoi) from Mount Howitt, Victoria. *Records of the Australian Museum* **44**, 299-318 (1992).

139   Gardiner, B. G. A revision of certain actinopterygian and coelacanth fishes, chiefly from the Lower Lias. *Bulletin of the British Museum (Natural History) (Geology)* **4**, 239-384 (1960).

140   Millot, J. & Anthony, T. *Anatomie de Latimera chalumnae. Squelette, muscles et formations de soutien*. Vol. Tome I 122 (Centre National de la Recherche Scientifique, 1958).

141   Jarvik, E. *Basic structure and evolution of vertebrates*. Vol. 1 (Academic Press, 1980).

142   Schultze, H.-P. CT scan reconstruction of the palate region of *Latimeria chalumnae*. *Environmental Biology of Fishes* **32**, 183-192 (1991).

143   Dutel, H. *et al.* Neurocranial development of the coelacanth and the evolution of the sarcopterygian head. *Nature* **569**, 556-+, doi:10.1038/s41586-019-1117-3 (2019).

144   Dutel, H., Herrel, A., Clément, G. & Herbin, M. A reevaluation of the anatomy of the jaw-closing system in the extant coelacanth *Latimeria chalumnae*. *Naturwissenschaften* **100**, 1007-1022, doi:10.1007/s00114-013-1104-8 (2013).

145   Dutel, H., Herrel, A., Clément, G. & Herbin, M. Redescription of the hyoid apparatus and associated musculature in the extant coelacanth *Latimeria chalumnae*: Functional implications for feeding. *Anatomical Record* **298**, 579-601, doi:10.1002/ar.23103 (2015).

146   Mansuit, R. *et al.* Development and growth of the pectoral girdle and fin skeleton in the extant coelacanth *Latimeria chalumnae*. *Journal of Anatomy* **236**, 493-509, doi:10.1111/joa.13115 (2020).

147   Mansuit, R. *et al.* Development and growth of the pelvic fin in the extant coelacanth *Latimeria chalumnae*. *Anatomical Record* **304**, 541-558, doi:10.1002/ar.24452 (2021).

148   Meunier, F. J., Cupello, C. & Clément, G. The skeleton and the mineralized tissues of the living coelacanths. *Bulletin of Kitakyushu Museum of Natural History and Human History* **17**, 37–48 (2019).

149   Watanabe, J. & Koie, H. in *Part III: Pioneering Studies on Coelacanth*   51-53 (2009).

150   Stensiö, E. A. Triassic fishes from East Greenland: Collected by the Danish Expeditions in 1929-31. *Meddelelser om Grønland* **83**, 1-305 (1932).

151   Woodward, A. S. The Fossil Fishes of the English Chalk. Part VI. *Monographs of the Palaeontographical Society* **64**, 185–224 (1911).

152   Woodward, A. S.   153-184 (Palaeontographical Society, 1909).

153   de Carvalho, M. S. S. & Maisey, J. G. in *Fishes and the Break-up of Pangaea* Vol. 295 (eds L. Cavin, A. Longbottom, & M. Richter) 109–144 (The Geological Society of London, 2008).

154   Schaeffer, B. & Gregory, J. T. Coelacanth fishes from the continental Triassic of the Western United States. *American Museum Novitates* **2036**, 1-18 (1961).

155   Westoll, T. S. On *Spermatodus pustulosus* Cope, a coelacanth from the "Permian" of Texas. *American Museum Novitates*, 1-23 (1939).

156   May, W. J. First report of coelacanth and hybodont remains from the Lower Permian Wellington Formation of Oklahoma. *Transactions of the Kansas Academy of Science* **115**, 134-138 (2012).

157   Rieppel, O. A new coelacanth from the Middle Triassic of Monte San Giorgio, Switzerland. *Eclogae Geologicae Helvetiae* **73**, 921-939 (1980).

158   Saint-Seine, P. D. Les poissons des calcaires lithographiques de Cerin (Ain). *Publications du musée des Confluences* **2**, 3-79 (1949).

159   Clack, J. A. Otoliths in fossil coelacanths. *Journal of Vertebrate Paleontology* **16**, 168-171 (1996).

160   Mäuser, M. in *Paleontological collections of Germany, Austria and Switzerland. The History of Life of Fossil Organisms at Museums and Universities Natural History Collections* (eds L. A. Beck & U. Joger) 23–26 (Springer Cham, 2018).

161   Yabumoto, Y., Brito, P. M., Iwata, M. & Abe, Y. A new Triassic coelacanth, *Whiteia uyenoteruyai* (Sarcopterygii, Actinistia) from Madagascar and paleobiogeography of the family Whiteiidae.

Bulletin of the Kitakyushu Museum of Natural History and Human History, Series A (Natural History) **17**, 15-27 (2019).

162 Song, H. J., Wignall, P. B., Song, H. Y., Dai, X. & Chu, D. L. Seawater temperature and dissolved oxygen over the past 500 million years. *Journal of Earth Science* **30**, 236-243, doi:10.1007/s12583-018-1002-2 (2019).

163 Witkowski, C. R., Weijers, J. W. H., Blais, B., Schouten, S. & Damsté, J. S. S. Molecular fossils from phytoplankton reveal secular Pco^2 trend over the Phanerozoic. *Science Advances* **4**, eaat4556, doi:10.1126/sciadv.aat4556 (2018).

164 Marcilly, C. M., Torsvik, T. H., Domeier, M. & Royer, D. L. New paleogeographic and degassing parameters for long-term carbon cycle models. *Gondwana Research* **97**, 176-203, doi:10.1016/j.gr.2021.05.016 (2021).

165 Marcilly, C. M., Torsvik, T. H. & Conrad, C. P. Global Phanerozoic sea levels from paleogeographic flooding maps. *Gondwana Research* **110**, 128-142 (2022).

166 Scotese, C. R. An atlas of Phanerozoic paleogeographic maps: The seas come in and the seas go out. *Annual Review of Earth and Planetary Sciences* **49**, 679-728, doi:10.1146/annurev-earth-081320-064052 (2021).

167 Kocsis, A. T. & Scotese, C. R. Mapping paleocoastlines and continental flooding during the Phanerozoic. *Earth-Science Reviews* **213**, e103463, doi:10.1016/j.earscirev.2020.103463 (2021).

168 Domeier, M. & Torsvik, T. H. Plate tectonics in the Late Paleozoic. *Geoscience Frontiers* **5**, 303-350, doi:10.1016/j.gsf.2014.01.002 (2014).

169 Torsvik, T. H. *et al.* Pacific-Panthalassic reconstructions: Overview, errata and the way forward. *Geochemistry Geophysics Geosystems* **20**, 3659-3689, doi:10.1029/2019gc008402 (2019).

170 Toriño, P., Soto, M., Perea, D. & de Carvalho, M. S. S. New findings of the coelacanth *Mawsonia* Woodward (Actinistia, Latimerioidei) from the Late Jurassic ? Early Cretaceous of Uruguay: Novel anatomical and taxonomic considerations and an emended diagnosis for the genus. *Journal of South American Earth Sciences* **107**, e103054, doi:10.1016/j.jsames.2020.103054 (2021).